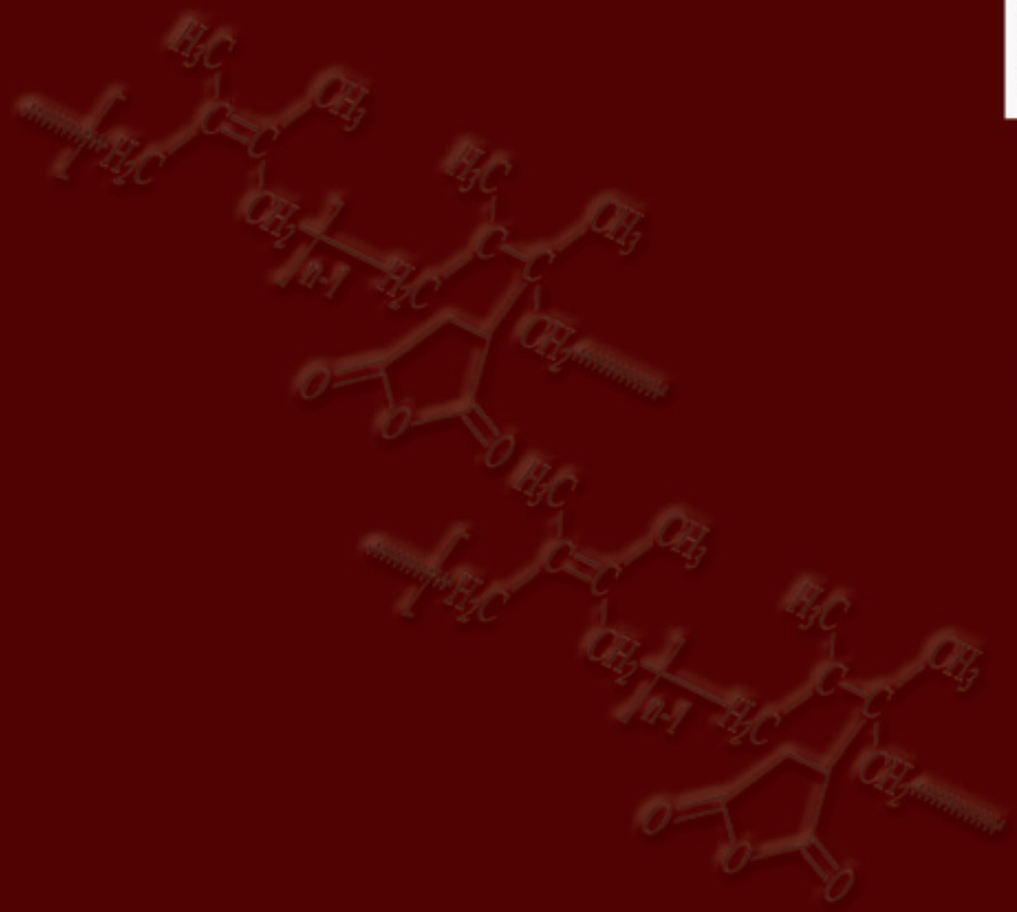

Ph.D Thesis
August 2009

Studies on Natural Rubber/Clay Nanocomposites: Effect of Maleic Anhydride Grafting of Rubber

Vijayalekshmi V

Department of Polymer Science & Rubber Technology
Cochin University of Science and Technology
Cochin-22

Ph.D Thesis

Studies on Natural Rubber/Clay Nanocomposites: Effect of Maleic Anhydride Grafting of Rubber

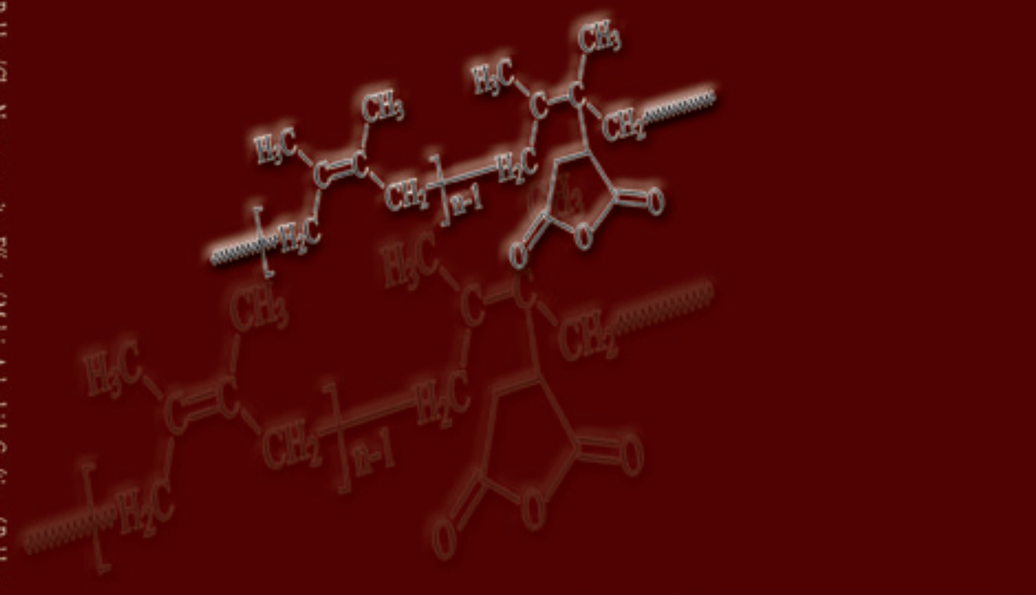

Vijayalekshmi V

Studies on Natural Rubber/Clay Nanocomposites: Effect of Maleic Anhydride Grafting of Rubber

Thesis submitted to the

Cochin University of Science and Technology

In the partial fulfillment
of the requirements for the award of the degree of

Doctor of Philosophy

in Polymer Science
Under the Faculty of Technology

By

Vijayalekshmi V

DEPARTMENT OF POLYMER SCIENCE AND RUBBER TECHNOLOGY

COCHIN UNIVERSITY OF SCIENCE AND TECHNOLOGY

KOCHI 22, KERALA, INDIA

DEPARTMENT OF POLYMER SCIENCE AND RUBBER TECHNOLOGY
COCHIN UNIVERSITY OF SCIENCE AND TECHNOLOGY
KOCHI 22, KERALA, INDIA

Dr. K.E GEORGE
Professor

Phone: 0484-2575723(Off)
0484-2577850(Res)
E mail: kegeorge@cusat.ac.in

Certificate

This is to certify that the thesis entitled **"Studies on Natural Rubber/Clay Nanocomposites: Effect of Maleic Anhydride Grafting of Rubber"** which is being submitted by Ms. Vijayalekshmi V in partial fulfillment of the requirements for the award of the degree of Doctor of Philosophy, to the Cochin University of Science and Technology, Kochi - 22 is a record of the bonafide research work carried out by her under my guidance and supervision, in the Department of Polymer Science and Rubber Technology, Kochi - 22 and no part of the work reported in the thesis has been presented for the award of any degree from any other institution.

Dr. K.E GEORGE
(Supervising Teacher)

Kochi 22
August 2009

DECLARATION

I hereby declare that the work presented in this thesis entitled **"Studies on Natural Rubber/Clay Nanocomposites: Effect of Maleic Anhydride Grafting of Rubber"** is based on the original research work carried out by me under the guidance and supervision of Dr. K.E George, Professor, Department of Polymer Science and Rubber Technology, Cochin University of Science and Technology, Kochi 22 and no part of the work reported in this thesis has been presented for the award of any degree from any other institution.

Vijayalekshmi V

Kochi - 22
August 2009

ACKNOWLEDGEMENTS

This work would not have become a reality had it not been for the blessings of the Almighty

I express my sincere and deep sense of gratitude to my supervising guide Dr. K.E George, Professor, Dept of Polymer Science and Rubber technology, Cochin University of Science and Technology for sound guidance, support, encouragement and understanding throughout the entire work.

I also wish to express my deep sense of gratitude to Dr. Pavithran C, Scientist, National Institute for Interdisciplinary Science and Technology (CSIR), Thiruvananthapuram for suggesting the topic for my research work, the invaluable guidance, fruitful suggestions and constant encouragement and motivation during the course of the investigation and preparation of the manuscript.

I am thankful to Dr. Thomas Kurian, Head, Department of Polymer Science and Rubber Technology, for his timely help and for providing the necessary facilities during the course of this study.

I wish to express my deep sense of gratitude to Prof. Dr. Rani Joseph, for the pertinent pieces of advice, especially during the preparation and finalization of the manuscript. I would like to express my sincere thanks to the other faculty members Dr. Eby Thomas, Dr. Philip Kurian, Dr. Sunil Narayanankutty and Ms. Jayalatha for their generous support and valuable tips, given during my days at PSRT. I also thank all the members of the non-teaching staff of the department, for their valuable assistance and co-operation.

I would like to express my heartfelt thanks to the entire FIP teachers Parameshwaran sir, Bhuvaneshwary teacher, Renjana teacher, Leny teacher, Dr. Joshy, Dr.Raju, Dr. Sreenivasan, Suma teacher, Dr Prema, Dr Maya, Dr Mary Alexander and Preetha teacher. I would like to thank Dr. Nisha, BipinBal,

Dr. Ansu, Dr. Saritha, Dr. Dhanya, Sinto, Abhilash, Jasmine, Julie, Zeena, Dennimol, Anna, Nimmi, Vidya, Vidhya, Sona, Nisha, Renchu and Zaisy for their love and support.

I am also grateful to Dr. Claramma N.M, Scientist, RRII, for her scholarly guidance and support in the radiation grafting studies. I also thank Dr. M.C.Sunny, Scientist, SCTIMST, Thiruvananthapuram, Prof. Anantharaman, Department of Physics, CUSAT for the help they have given the right for a few measurements made in their respective labs. I also thank Shri. John Britto, Technical Staff, RRII, Kottayam for his sincere help in Radiation Studies.

I take this opportunity to acknowledge the help received from my friend, Ms Vijutha. Department of Physics, CUSAT and Mr. Jobin Jose, IIT, Kharagpur for the TEM analysis.

I am greatly indebted to my parents, who inspired me a great deal to successfully complete my research project and, of course, my husband Dr Jayalal D, who supported me with all enthusiasm, making it possible for me to tide over the rough times. My son, Navaneethakrishnan J has been my inspiration through out the course of this work.

Vijayalekshmi V.

Contents

Page No

Chapter 6

PREFACE

Natural rubber (NR) is chemically cis 1,4 poly isoprene, which is non- polar in nature and is the only natural member in the rubber family. Maleated natural rubber (MA-g-NR) is one of the modified forms of natural rubber prepared by grafting maleic anhydride on to NR. Maleated natural rubber is polar in nature due to the presence of carboxyl group. This polar rubber can be mixed with NR to make the latter more polar to improve its solvent resistance and gas barrier properties. Fillers are incorporated into elastomers in order to modify properties, and to reduce cost. Commonly used fillers in rubber industry include carbon black, mineral fillers such as clay, silica and calcium carbonate. Nanofillers are the state of art and most interesting among the fillers because they offer exceptional reinforcement at very low filler loading.

The field of nanotechnology is one of the most popular areas for current research and development in virtually all technical disciplines. This obviously includes polymer science and technology. Polymer nanocomposites have received much attention due to its large surface area and very high aspect ratio. Polymer nanocomposites especially rubber based nanocomposites is one of the many composite materials in which researchers and engineers have shown great interest due to their potential to be used in critical applications. Polymer layered silicate (PLS) nanocomposites often exhibit remarkable improvement in materials properties when compared with the virgin polymer or conventional micro and macro composites. These improvements can include high moduli and tear strength, improved heat resistance and electrical properties, decreased gas permeability, swelling to solvents and flammability.

The grafting of maleic anhydride (MA) on natural rubber has been carried out by a novel technique: gamma (γ) radiation. The neat MA-g-NR thus obtained was used for the preparation of maleated natural rubber/clay nanocomposites using hydroxyethyl substituted tallow ammonium as the organo-modifier by direct and

by the master batch technique. The preparation and characterization of this new class of maleated natural rubber based nanocomposites is the topic of this study.

Contents of the thesis

The thesis is divided into nine chapters.

Chapter 1 is a brief introduction and literature survey covering the various fields connected to this study such as reinforcement of rubber, chemical modification of natural rubber, and modification of nanoclay, characterization of nanocomposites, polymer /clay nanocomposites and rubber/clay nanocomposites. At the end of this chapter the background and objectives of this study are also given.

Chapter 2 gives the specifications of the various materials used, and the details of experimental techniques employed for preparing and characterizing nanocomposites.

Grafting of maleic anhydride on to natural rubber by gamma radiation and its characterization of the product are discussed in **Chapter 3**. The radiation dosage and maleic anhydride concentration have been optimized and the grafting efficiency is determined. The tensile properties of the maleated gum vulcanisates are also presented.

The preparation of nanocomposites by direct method, characterization using XRD and TEM, the mechanical properties and cure characteristics of maleated natural rubber/organoclay nanocomposites are presented in **Chapter 4**. The comparison of maleated natural rubber/nanocomposites with unmodified natural rubber/ nanocomposites is also presented. The maleic anhydride concentration is varied for getting optimum mechanical properties.

The preparation of nanocomposites by masterbatch technique, characterization using XRD and TEM, cure characteristics and mechanical properties of maleated natural rubber/organoclay nanocomposites are presented in **Chapter 5**. 10% maleated rubber is used in this study. The properties of the nanocomposites prepared from different masterbatches (20, 30, 40 & 50 phr) at nanoclay loadings

of 1,3,5&7 weight percentages are compared with pure natural rubber gum vulcanisates.

The thermal stability and ageing behaviour of maleated natural rubber/organoclay nanocomposites prepared by direct and by masterbatch technique is presented in **Chapter 6**. The activation energy of the nanocomposites has been determined using thermal degradation kinetics. The flame retardant properties of the nanocomposites are also included in this chapter.

The transport properties of the maleated natural rubber nanocomposites are discussed in **Chapter 7**. The sorption, diffusion and permeation coefficients are measured. The oil resistance of maleated rubber nanocomposites is also determined.

The dynamic mechanical properties and dielectric properties of maleated natural rubber/ clay nanocomposites are presented in **Chapter 8**. The storage modulus, loss modulus and tan δ are studied by frequency sweep method. The heat build up and differential scanning calorimetry of the nanocomposites are also presented.

The summary and conclusions of the study are given in **Chapter 9**.

Chapter 1

Introduction

Polymer modification and blending of polymers have attained a prominent place in the field of polymer technology, as it is realized that synthesis of new polymers are not always necessary for applications requiring specific properties. It can be met by the modification of existing polymers or by blending of suitable polymers. So chemical modification and polymer blending have become a growing stimulation for research in the field of polymer chemistry and technology since the last few decades. Modification is attained by the incorporation of reactive functional groups on to the polymer chains. Functionalization of polymers results in new materials with wide spectrum of properties not available in parent polymer. Chemical modification of polymer backbone, grafting on to polymer chains, inter chain reactions and the formation of interpenetrating networks are the subject of many reviews [1-3]. Successful materials prepared by modification of natural rubber that have got a lot of commercial applications include cyclised rubber, chlorinated rubber, hydrochlorinated rubber, epoxidized and grafted natural rubber. In these products the degree of modification is extensive and the products no longer possess the high elasticity of the raw material.

Rubbers in their pristine form are seldom used. Because of the lack of hardness, strength, properties and wear resistance they are too weak to fulfill practical requirements. So they are used with a number of other components called compounding ingredients, which improve the possibility, performance properties and life of the final product. The selection of filler used in rubber formulation is made based on the property requirement of the end-product. Fillers are used to

enhance the performance related properties of rubbers. The fillers used in rubber compounding are characterized by their reinforcing effects, which ranges from inactive, semi active to very active fillers. Typically, carbon black would be used to enhance strength characteristics while mineral fillers provide a more modest strength enhancement at significantly reduced cost [4]. But due to its polluting nature, the ubiquitous black colour of the compounded rubber and its dependence on petroleum feedstock for the synthesis caused researchers to look out for other "white" reinforcing materials. Since silica is not quite reactive to rubber as carbon black, silane coupling agents are used for surface modification of silica particles. However, the curing time of rubber with silica is longer than with carbon black and thus the production time is extended resulting in reduced productivity. Clay, which has been used as cheap filler in the rubber industry, has poor reinforcing ability because of its large particle size and low surface activity.

Now, the layered silicates have attracted a great deal of interest as nanocomposites reinforcement in rubbers owing to their intrinsically anisotropic character and swelling capabilities. Moreover, these materials possess a high aspect ratio (500-2000) and plate-like morphology. Because of their nanometer size filler dispersion, nanocomposites exhibit markedly improved properties when compared to the pure polymers or their traditional composites. Most notable are increased modulus, increased gas barrier properties, increased heat distortion temperature, resistance to small molecule permeation, improved ablative resistance, increase in atomic oxygen resistance and retention of impact strength [5].

This thesis gives special emphasis on the grafting of maleic anhydride on natural rubber by gamma radiation and also for preparing maleated natural rubber (MA-g-NR)/clay nanocomposites. The effect of nanoclay on cure characteristics, mechanical, and physical properties of maleated natural rubber have also been investigated. Again the masterbatch technique is adopted for MA-g-NR/clay nanocomposites for reducing the cost and obtaining better mechanical properties.

Therefore, a general introduction is provided in the coming sections about filler characteristics, clay structure, grafting of natural rubber by maleic anhydride, rubber nanocomposites for the study. Finally, the objectives of the work are listed. The designation active or reinforcing refers to the influence of the filler on compound viscosity and failure properties such as tensile strength, abrasion and tear resistance. Structure as well as the surface properties of the filler is the main characteristics that determine the reinforcing effect. Active fillers are characterized by a large relative surface area and a high structure, both properties resulting in strong interparticle forces, which negatively influence the processing behavior due to agglomeration of filler particles during mixing and storage of the compound.

1.1 Rubber reinforcement

The particle size, structure and surface characteristics were the three factors that influence and help to decide the reinforcing ability of the reinforcing materials. From the above three characteristics the particle size of filler has the most significant influence [6-10]. The old concept is that, where reinforcement of polymer was not the main thing which was taken into account but different types of clay minerals have been used as fillers to reduce cost of the host polymer and provide some properties useful in rubber compounding. A wide range of non-black, particulate fillers is added to rubber compounds to improve the cured physical properties, reduced cost and impart colour to the rubber product. The chemical composition and its effect on physical properties of the rubber compound typically result in classifying particulate fillers into three broad divisions [8].

1.Non-reinforcing or degrading fillers
2.Semi-reinforcing or extending fillers
3.Reinforcing fillers

The term “reinforcement” refers to an improvement in end-use performance of the rubber compound associated with an increase in modulus and in the so-called ultimate properties including tensile strength, tear resistance and abrasion resistance. Reinforcing filler is a particulate material that is able to increase the tensile strength, the tear strength and abrasion resistance of natural/synthetic rubber. Semi-reinforcing filler is a particulate material that is able to moderately improve the tensile strength and tear strength, but does not improve abrasion resistance. Non reinforcing filler is unable to provide any increase on these properties and it function only as a diluents [6].

1.2 Characteristics of fillers

1.2.1 Particle size

The particle size of the filler has a great influence in improving the physical properties of the rubber vulcanisate. The increase of modulus and tensile strength is very much dependent on the particle size of the filler; smaller particle size fillers imparting greater reinforcement to the compound than the coarse ones. Since particle size is directly related to reciprocal of surface area per gram of filler, an increase in surface area that is in contact with the rubber phase which probably leads to the increase in reinforcement. Reducing particle size also simply results in a greater influence in polymer-filler interaction. In addition to average particle-size, the particle size distribution has also a significant effect on reinforcement. Particulate fillers with a broad particle-size distribution have better packing in the rubber matrix, which results in a lower viscosity than that provided by an equal volume of filler with a narrow particle-size distribution. Another important concern in reinforcement is the presence of large particles of agglomerates in the rubber. These agglomerates not only reduce the contact between rubber and filler matrix but function as failure initiation sites which would lead to premature failure of material.

1.2.2 Surface area

The most important single factor, which determines the degree of reinforcement, is the development of a large polymer-filler interface. It can be provided only by particle of colloidal dimensions. Spherical particles of 1μm diameter have a specific surface area of $6m^2/cm^3$. This constitutes approximately the lower limit for significant reinforcement. The upper limit of useful surface area is of the order of 300-400m^2/cm^3 and it is decided on the basis of considerations of dispensability and processability of the uncured compound and serious loss of rubbery characteristics of the composite [11]. The surface area of particulate solid is related to its particle size. If the entire particles are considered as spheres of the same size, the surface area A_S, per gram of a filler can be calculated from the equation,

$$A_S = 6/d\rho$$

where d is the diameter and ρ the density of the filler particle. In reality, particles have a distribution of size and are usually far from being spherical. Different fillers of the same particle size may not impart the same reinforcement, e.g., carbon black and silica. The shape of particle also may be different for different fillers, viz; spheroidal, cubic/ prismatic, tubular, flaky or elongated. Non-spherical particles can impart better reinforcement [12].

1.2.3 Porosity

Porosity is a characteristic property of carbon black and can be seen with other particulate type of fillers. Filler porosity can affect the vulcanizate properties. However, its effect on reinforcement is secondary. In most cases, the pores are too small for the polymers to enter although some smaller molecules in the compound may do so.

Particulate fillers used in rubber industry in general can be classified as “Black” and “Non-black”, depending on their origin, the former being mostly produced

from petroleum feed stock and the latter from mineral sources. The most important particulate fillers being used in rubber industry are carbon black and silica. Silicates, clays, whiting (calcium carbonate) and other mineral fillers are used extensively where a high degree of reinforcement is not essential [11].

1.2.4 Particle structure and anisometry of filler aggregate

In addition to the surface area the shape of the filler particle is an important factor that affects the performance of a rubber compound. In organic and mineral fillers possess considerable differences in particle geometry, depending on the crystal form of the mineral. The minimum anisotropy is found with materials that form crystals with approximately equal dimension in the three directions, i.e. isometric particles. More anisometric are particles in which one dimension is much smaller than two others, i.e. platelets. The most anisometric are particles which have two dimensions much smaller than the third, so that they are rod-shaped. In compounds containing fillers having identical surface area and chemical nature but differ in shape and modulus increases with increasing anisometry [13]. Particles with a high aspect ratio, such as platelets or fibrous particles have a higher surface to volume ratio, which results in higher reinforcement of the rubber compound. The greatest hardness is also provided by rod-shaped or plate-like particles, which can line up parallel to one another during processing, compared to spherical particles of similar diameter. Particle shape has a more pronounced effect on processing behavior than on reinforcement potential and provides important benefits in processing. It can also significantly increase modulus due to occlusion or shielding of some of the rubber phase in highly structured fillers such as structural aggregates of carbon black or silica [9].

1.3 Structure and properties of layered silicates

Clays are naturally occurring minerals with variability in their constitution depending on their groups and sources. The clays used for the preparation of nanoclays belong to smectite group clays which are also known as 2:1 phyllosilicates, the most common of which are montmorillonite [14]. The term-layered silicates also known as phyllosilicates include natural clays and synthesized layered silicates such as magadite, mica, laponite and fluorohectorite [15-17]. MMT is the most abundant and widely used naturally occurring clays. It is the determinative components in bentonite. The commonly used layered silicates for the preparation of PLS nanocomposites belong to the same general family of 2:1 layered or phyllosilicates. Their crystal structure consists of layers made up of two tetrahedrally coordinated silicon atoms fused to an edge-shared octahedral sheet of either aluminium or magnisium hydroxide [18-21]. The layer thickness is around 1nm, and the lateral dimensions of these layers may vary from 30nm to several microns or larger, depending on the particular layered silicate. Stacking of the layers leads to a regular Van der Waals gap between the layers called the interlayer or gallery. Isomorphic substitution within the layers (for example, Al^{3+} replaced by Mg^{2+} or Fe^{2+}, or Mg^{2+} replaced by Li^{1+}) generates negative charges that are counter balanced by alkali and alkaline earth cations (Na^{+}, K^{+}, Ca^{+}) situated inside the galleries [18]. This type of layered silicate is characterized by a moderate surface charge known as the cation exchange capacity (CEC), and generally expressed as meq/100gm. This charge is not locally constant, but varies from layer to layer, and must be considered as an average value over the whole crystal [22]

.

MMT, hectorite, and saponate are the most commonly used layered silicates. Layered silicates have two types of structure: tetrahedral-substituted and octahedral substituted. In case of tetrahedrally substituted layered silicate layers, and hence, the polymer matrices can interact more readily with these than with octahedrally-substituted material. Details regarding the structure and chemistry for these layered silicates are provided in figure1.1 and table 1.1 [23] respectively.

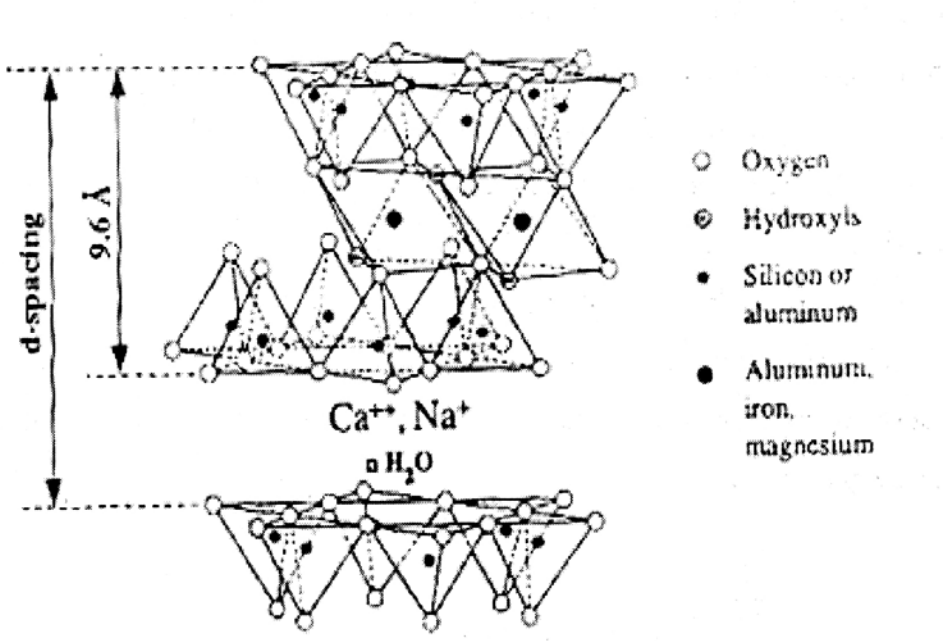

Figure 1.1 Structure of 2:1 phyllosilicates

Table 1.1 Chemical formula and characteristic parameter of commonly used 2:1 phyllosilicates

2:1Phyllosilicates	Chemical formula	CEC (meq/100g)
Montmorillonite	$M_x[Al_4\text{-}xMg_x](Si_8)O_{20}(OH)_4$	110
Hectorite	$M_x[Mg_6\text{-}xLix](Si_8)O_{20}(OH)_4$	120
Saponite	$M_x[Mg_6](Si_{8}\text{-}xAlx)\ O_{20}(OH)_4$	86.6

M, monovalent cation; x, degree of isomorphous substitution (between 0.5 and 1.3)

Two particular characteristics of layered silicates that are generally considered for PLS nanocomposites. The first is the ability of the silicate particles to disperse into individual layers. The secondary characteristic is the ability to fine-tune their surface chemistry through ion exchange reactions with organic and inorganic cations. These two characteristics are, of course, interrelated since the degree of dispersion of layered silicate in a particular polymer matrix depends on the interlayer cation [22].

1.4 Sturcture and properties of organically modified layered silicate (OMLS)

The physical mixture of a polymer and layered silicate may not form a nanocomposite. This situation is analogous to polymer blends, and in most cases separation into discrete phases takes place. In immiscible systems, which typically correspond to the more conventionally filled polymer, the poor physical interaction between the organic and the inorganic components leads to poor physical interaction between the organic and the inorganic components leads to

poor mechanical and thermal properties. In contrast, strong interactions between the polymer and the layered silicate in PLS nanocomposites lead to the organic and inorganic phases being dispersed in the nanometric level. As a result, nanocomposites exhibit unique properties not shared by their micro counter parts or conventionally filled polymers [24-29].

Pristine layered silicates usually contain hydrated Na^+ or K^+ ions [30]. Obviously, in this pristine state, layered silicates are only miscible with hydrophilic polymers, such as poly(ethylene oxide) (PEO) [31], or poly(vinyl alcohol) (PVA) [32]. To render the layered silicate miscible with other polymer matrices, one must convert the normally hydrophilic silicate surface to an organophilic one, making the intercalation of many engineering polymers possible. Generally, this can be done by ion-exchange reactions with cationic surfactants including primary, secondary, tertiary and quaternary alkylammonium or alkylphosphonium cations. Alkylammonium or alkylphosphonium cations in the organosilicates lower the surface energy of the inorganic host and improve the wetting characteristics of the polymer matrix, and results in a larger interlayer spacing. Additionally, the alkylammonium or alkylphosphonium cations can provide functional groups that can react with the polymer matrix, or in some cases initiate the polymerization of monomers to improve the strength of the interface between the inorganic and polymer matrix [33,34].

The basic formula is $[(CH_3\text{-}CH_2\text{-})n\ NH^{3+}]$, where n is in between 1and 18. It is interesting to note that the length of the ammonium ions has a strong influence on the resulting structure of nanocomposites. Lan *et al.* [35] observed that alkyl ammonium ions with chain length larger than eight carbon atoms were favoring the synthesis of exfoliated nanocomposites whereas ammonium ions with shorter chains lead to the formation of intercalated nanocomposites. Schematic representation of cation replacing from intergalleries by organic cation using alkyl ammonium ion is shown in figure 1.2.

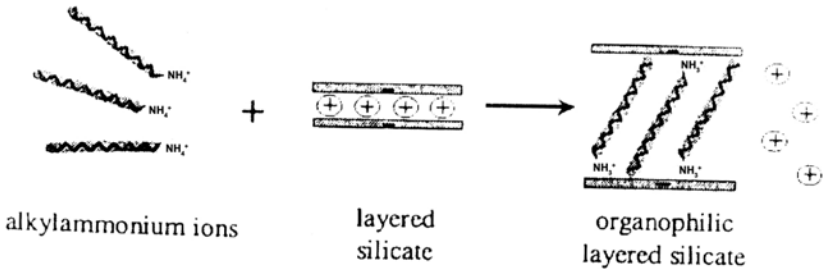

Figure 1.2 Schematic representation of cation-exchange from intergalleries

1.5 Natural rubber (NR)

Natural rubber remains the best choice of elastomer for many applications that require low heat build up such as, in large tires, carcasses of passenger car tires, vibration dampers, springs, engine mountings and bearings. Other products like hoses, conveyor belts, gaskets, seals, rollers, rubberized fabrics, elastic bands, latex foams, adhesives, pharmaceutical and medical products also consume a major part of natural rubber.

Natural rubber is a high molecular weight polymer of isoprene (2-methyl 1,3-butadiene) with a molecular weight of 200,000 to 600,000. It is the most widely used naturally occuring elastomer which is a homopolymer of isoprene having a cis 1,4 configuration as in figure 1.3 and is the only natural product in the rubber family. It has been identified in about 2000 plant species, but only the species Heava brasiliensis is of any commercial significance. From the tree the rubber collected in the form of latex by tapping. Rubber is separated from the latex by coagulation using acidification. The resultant coagulum is then processed into different marketable forms of NR such as, technically specified grades, sheets, crepes, etc. [36]. Most of the natural rubber based products are made from any of these forms. Also certain products are made from concentrated latex. The

molecular weight of polymer ranges from 200,000 to 600,000 with a relatively broad molecular weight distribution [37]. Today more than 80% of the total world production of natural rubber comes from Southeast Asia. Malaysia is the largest producer, followed by Indonesia. Thailand accounts for much of the remainder in this area [38]. NR vulcanizates have high tensile strength over a wide hardness range due to its "strain induced crystallization" [39]. It has the highest resilience (except BR) which is responsible for its very low heat build up. It shows very low compression set and stress relaxation, good electrical insulation and good resistance to abrasion, tear and fatigue. As an unsaturated elastomer, NR vulcanizates are susceptible to attack by atmospheric oxygen and ozone and hence its heat and weather resistance are very poor. It is not resistant to petroleum-based oils and fuels, as it contains no polar groups, but can be used with a wide range of organic and inorganic chemicals such as non-petroleum based automotive break fluids, silicone oils and greases, glycols, alcohols, water and non-oxidizing aqueous solutions of acids, alkalies and salts. The properties of NR can be improved by chemical modification such as grafting.

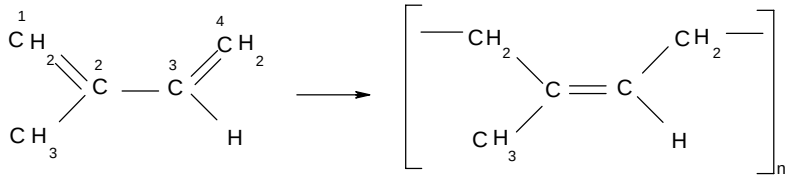

isoprene *cis* -1,4 - polyisoprene

Figure1.3 Structure of natural rubber (molecular weight of repeat unit: 68.12g/mol)

1.6 Modified forms of Natural rubber

NR can be modified by physical or chemical means and in some cases by a combination of the two [40]. Table 1.2 gives most of the different types of modifications in NR [41,42]. Physical methods involve incorporation of additives that do not chemically react with rubber. Examples are oil extension, blending

with other polymers, masterbatching, deproteinisation, prevulcanisation etc. NR is deprotonised to reduce water absorption and protein allergy which is affected by either enzymatic hydrolysis [43] or radiation process [44] or by multiple centrifugation. Deprotonised rubber (DPNR) is used in electrical and medical applications.

1.6.1 Chemical modification of NR

A chemical modification depends on the chemical reactivity of the NR molecule. Being unsaturated, NR is highly reactive and several chemical reactions could be carried out resulting in materials having entirely different properties. Depending on the extent of modification, four classes of products are identified [40] as in table 1.3. Low levels off modification have the object of retaining high elasticity while providing the means for altering specific properties to make the rubber suitable for particular application or conditions of use. For example, reactive site might be provided for new type of crosslinking for binding antioxidants or other materials or substrates. At moderate degree of modification, physical properties are altered due to the change in glass transition temperature (Tg) and a rubber with new properties is obtained. More drastic modifications lead to non-rubbery resinous or plastic materials. Finally modification only on the surface may be useful increasing adhesion to other surfaces or protection against hostile environments.

Table 1.2 Modification of NR

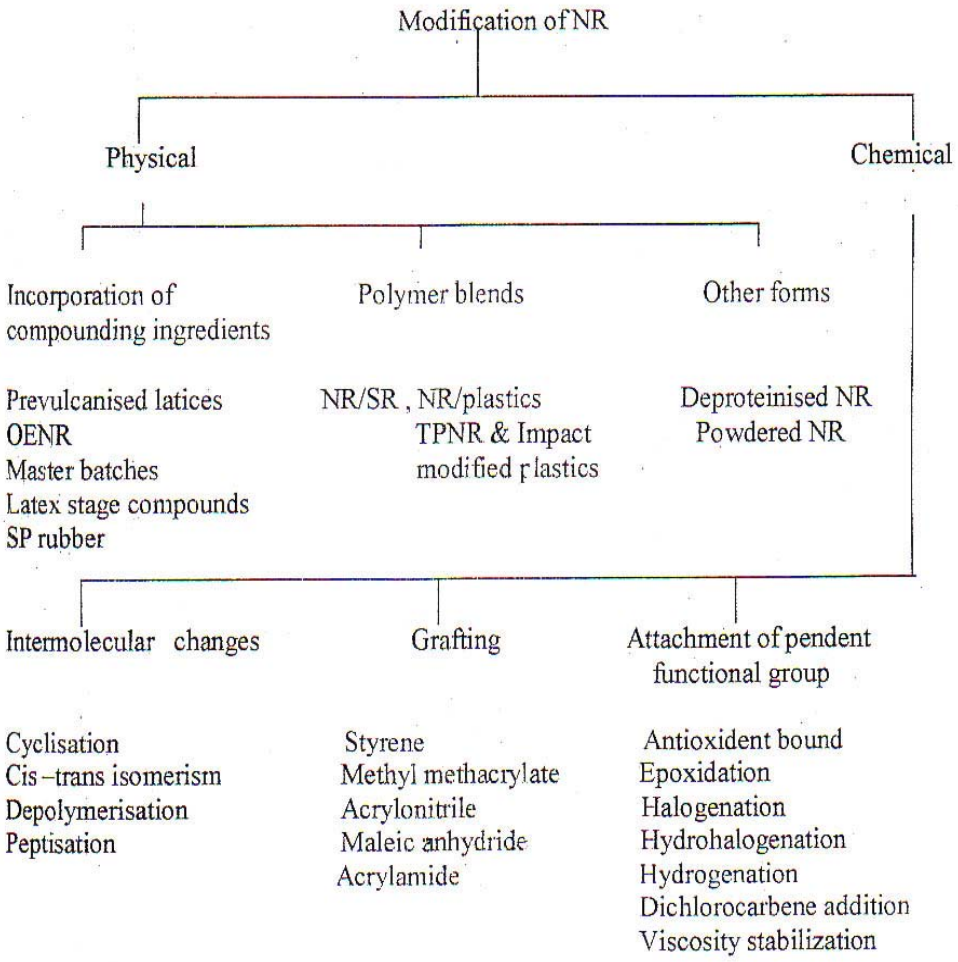

Table1. 3 Classification of modified forms of NR

Degree/type of modification	**Approximate extent of modification (mole%)**	**Effect on elastic properties**
Slight	<5	Essentially unchanged
Intermediate	5-25	Modified
Extensive	>25	Lost
Surface	<1	Bulk unchanged

Chemical modifications can be broadly grouped into

1) Attachment of a pendant functional group

2) Grafting of a different polymer at one or more points along the NR molecule

3) Inter molecular changes without the introduction of a new chemical group

1.6.1.1 Attachment of pendant functional group

1.6.1.1. A Chlorinated rubber

Chlorinated natural rubber (CNR) is one of the first forms of chemically modified NR which find use in many commercial applications [45]. Chlorination is carried out either in solution or latex [46] stage and the reaction involve substitution and cyclisation along with addition of chlorine [47]. For the industrial preparation, batch and continuous process are now available and in all cases carbon tetra chloride is used as solvent for NR to perform chlorination [48]. Recently liquid chlorine is reported to be used instead of carbon tetra chloride

[49]. Use of depolymerised NR as starting material is reported to give higher yield of product [50]. Chlorinated rubber of 65% chlorine content is a pale, cream coloured thermoplastic power which is non inflammable and highly resistant to ozone, weather and chemicals up to 100^0C. CNR is used in anticorrosive and heat resistant paints and coatings, adhesives, printing inks, paper coatings and textile finishes by mixing with an opportune solvent. The composition contains at least 10% of chlorinated rubber with plasticizers and pigments. It is also used to protect wood, steel, cement, etc. from the environmental attacks and has been recommended as traffic paints on roads. Commercial grades are available under several trade names like, Pergut, Alloprene etc.

1.6.1.1 B Epoxidised NR

Latex stage expoxidation of NR (ENR) with improved resistance to hydrocarbons and oils, low air permeability, increased damping and good bonding properties while retaining the high strength properties of NR [51-55]. Improvement of these properties depends on the degree of epoxidation. Two grades of epoxidised NR, ENR 25 and ENR 50 with 25 and 50 mole percent of epoxidation respectively have attained commercial importance. ENR can be used as cover compound for PVC core conveyor belting. The processing characteristics and physico chemical properties of thioglycolic acid modified low molecular weight ENR (ELMWNR-TGA) and its blend with NR is reported recently [56]. It is shown that ELMWNR-TGA exhibits lower tensile strength, higher elongation at break but better resistance to solvents and mineral oils.

1.6.1.1 C Constant viscosity and low viscosity NR

Increase in viscosity of NR during storage under ambient conditions known as storage hardening is caused by the cross linking reaction involving the randomly distributed carbonyl groups present on the main rubber chain and the amino acids present among the non-rubber consistuents [57]. This can be inhibited by the

addition of small amount of hydroxyl amine hydrochloride or hydroxyl amine neutral sulphate or semicarbazide to the latex before coagulation. These chemicals effectively block the carbonyl groups and preserve the Mooney viscosity of the rubber. Viscosity stabilized rubber is technically specified and is available in two forms. Indian Standards Natural Rubber, ISNR 5CV and ISNR 5LV as per Indian standards with Mooney viscosity range of 60-65 for CV and 50 ± for LV.

1.6.1.1 D Carbene addition

Carbenes (>C:) react readily with NR and is facilitated by the use of quaternary ammonium salts as phase transfer catalyst. The latter compounds bring the aqueous reagents into contact with the organic phase containing the polymer [58,59]. Treatment of cis poly isoprene in dilute aromatic solvent with dichlorocarbene prepared insitu from ethyltrichloro acetate with sodium methylate gives a white power. The double bonds are converted into gem dichlorocyclopropane rings [60]. Similarly reaction of polyisoprene with dibromocarbene formed insitu from bromoform give 70-75% saturation of polymer double bonds. Carbene derived from the photolytic or thermal decomposition of 3, 5 ditert butyl benzene-1, 4 diazoxide was used to introduce a polymer bound hindered phenol antioxidant on to NR [61].

1.6.1.1. D ENPCAF modification

Ethyl-N-Phenylcarbamoylazoformate (ENPCAF) modified NR shows the influence of bulky polar pendent groups on the physical properties of NR [62, 63]. This modification can be carried out in an internal mixer or mixing mill at 110^0C on dry rubber. The reaction can also be carried out in latex stage at 30^0C using deammoniated latex. The chemical modification results in the formation of hydroester pendent groups and is accompanied by an increase in Tg of the polymer along with high damping properties improved gas impermeability and solvent resistance. The highly polar group introduced has a dramatic effect on the

physical properties as shown by changes in stress relaxation and recovery of peroxide cured NR modified by ENPCAF [64].

1.6.1.1 F Hydrogenation

Hydrogenation of NR was first reported by Berthalot [65] and there had been a steady stream of research publications on this subject [68-68]. By using a reaction of hydrogen at 30-55 atmospheres with a 2% solution of pale crepe rubber in cyclohexane over Nickel-Kiesleguhr catalyst in an autoclave at 200^0C-220^0C for 12 hours lead to fully hydrogenated NR. More recently, homogeneous two component system based on a variety of Nickel and Cobalt compounds in combination with tri isobutylaluminium is reported to give complete hydrogenation in solution after 1 hour at 28^0C [69]. Hydrogenation of diene elastomers, their properties and applications are discussed by Singha *et al.* [70] in a recent review. Hydrogenated rubber is colorless and transparent. It is a plastic, elastic waxy solid with the peculiar characteristic of forming threads when stretched. Potential area of application is in cable industry, which would utilize its insulation properties.

1.6.1.1 G Hydrohalogenation

NR can be modified with hydrogen fluoride, hydrogen chloride, hydrogen bromide or hydrogen iodide to get the respective rubber hydrohalides [71-77]. The aim of this modification is same as that of halogenation, to reduce chemical reactivity of NR to oxygen and ozone by addition to the double bond. Bunn and Garner [75] reported that addition of HCl to poly isoprene obey Markownikov's rule. The rubber hydrochloride is a highly crystalline material. It is unaffected by dilute acids and bases at room temperature. NMR studies by Golub and Heller [71] have established that the cyclization reaction also occurs during hydrohalogenation.

1.6.1.2 Grafting

Grafting can be done by two methods:

1) Chemical grafting (using peroxides)

2) Radiation grafting (gamma radiation)

Advantages of gamma grafting over chemical grafting:

- Time saving (more output of grafted rubber can be obtained in a single mix.)
- Product quality can be controlled (grafting is done in a gamma chamber and it controls the over all reaction during the process of grafting)
- Clean process (contamination with chemicals can be avoided)

The chemical means of grafting maleic anhydride (MA) on to natural rubber was done on an internal mixer by the following procedure. The elastomer was mixed with 5% MA and 0.5% benzoyl peroxide in a Brabender torque rheometer at 100^0C and 50rpm speed for 10 minutes. The reaction of MA with elastomers was confirmed by FTIR spectroscopy and titration [78].

NR can be modified to graft copolymers by polymerizing vinyl monomers either in latex or solution. Methylmethacrylate (MMA), [79] styrene [80] and acrylonitrile [81] are the prominent monomers used for grafting on to NR. Among these polymethylmethacrylate grafted NR (PMMA-g-NR) is the most popular and has been commercialized since mid 1950's in Malaysia under the trade name Heveaplus MG. Generally grafting can be achieved by two methods viz., by use of chemicals or by irradiation with γ rays [82, 83]. The developments on this topic during the period of 1950-1990 had been recently reviewed by Blackly [84]. In later years, considerable efforts had been made to achieve thermoplastic elastomer characteristics to these graft polymers by controlling the

polymerization conditions [85,86]. Recently Schneider *et al.* reported that styrene and methylmethaccrylate can be graft polymerized on NR latex in two step emulsion polymerization and can be used as toughening agent for SAN and polystyrene [87,88]. Lehrle *et al.* [89] reported the effect of using small quantity of vinyl acetate on the efficiency of grafting methylmethacrylate in NR latex using AIBN as initiator. Fukushshima *et al.* [90] compared the grafting efficiency of styrene on to NR prepared from highly deproteinised latex and high ammonia concentrated latex using t-butyl hydroperoxide/TEPA redox system. The results are favorable towards high ammonia concentrated latex.

Polymethylmethacrylate is a hard plastic and when grafted on to NR, it increases the modulus of rubber depending on the percentage of methylmethacrylate grafted to it. Major use of Heveaplus MG is in adhesives [91]. In automotive industry for applications such as light shield, soft fronds, rear ends, rubbing strips and bumpers, blends of Heaveaplus MG49 with NR can be used. It can also function as a compatibilizer in rubber/plastic blends [92]. Styrene grafted NR (SG 50) can find application in micro cellular soleings in place of high styrene resin grade SBR [93].

Attempts to modify NR latex particle to produce NR interpenetrating networks was made by Hoursten *et al.* [94, 95]. Recently Subramanian *et al.* [96] reported NR latex seeded emulsion polymerization of a highly hydrophobic monomer, vinyl neo-deaconates, under carefully controlled conditions. The DSC studies of the particles so formed shows a 5^0C rise in Tg of the NR indicating the formation of a relatively homogenous semi interpenetrating network or graft microphase.

1.6.1.3 Intramolecular changes

1.6.1.3. A Liquid NR (LNR)

Liquid NR is prepared either by thermal or by chemical depolymerization of NR. In thermal depolymerization, rubber with 0.2 to 0.6phr peptizer is first masticated

to a Mooney viscosity of 25-30 and depolymerized by heating to 220-240^{0}C under stirring for 3-7hrs. LNR with viscosity average molecular weight (Mv) in the range of 5000-20000 is reported to be produced by this method [97]. Chemical depolymerisation is carried out in the latex stage by a redox reaction involving phenyl hydrazine by air to give phenyl radical which through addition or transfer reaction initiates the formation of hydroperoxides. These peroxides lead by chain breakage to liquid NR with molecular weight NR has been found to have similar properties with NR, for example affinity for ingredients during compounding, chemical behaviour and service life performance [98].

Liquid NR is used in elastic moulds, printing industry, as binder in grinding wheels, as reactive plasticizer [99] and as bulk viscosity modifier [100] in rubber compounds. Carboxy terminated liquid NR (CTNR) is reported as an adhesive in bonding rubber to rigid and non-rigid substrates.

1.6.1.3. B Cyclised NR

Cyclised NR is a resinous material, obtained by treating NR with acidic reagents like, sulphuric acid, p-toluene sulphonic acid and by Lewis acids like, $SnCl_4$, $TiCl_4$, BF_3 and $FeCl_3$. Cyclisation could be done in solid, solution or latex stage [101]. Cyclised NR is found to have increased softening point, density and refractive index than NR. The preparation of cyclised NR latex on commercial scale was well established as early as 1947 [102]. It is used in soleing compounds as on heating it changes to a hard thermoplastic material.

1. 7 Nanocomposites

Composites with more than one phase with a dimension in the range of 1-20nm are defined as nanocomposites [103,104-106]. Nanometer is an atomic dimension and hence the properties of nanoclusters or particles are reflective of atoms rather than bulk materials. More over adjusting the size can control the energy level spacing and other properties, but still large compared to the atomic limit. Recent

studies shows that it may be possible to combine the nanocrystal into nanocrystal molecules and nanocrystal solids in the same way as one does with real atoms; and these solids comprise tens to thousand of atoms and have dimensions in nanometer (10nm) range. Nanoscale materials have currently attracted a great deal of attention due to their interesting chemical and physical properties. The modified nano-sized systems are nanocomposites, nanocrystals, nanotubes, cluster assembled materials, quantum boxes, etc [107,108].

The three major advantages that nanocomposites have over conventional composites are as follows:

1. Low cost due to fewer amounts of filler use,

2. Lighter weight due to low filler loading and

3. Improved properties (includes mechanical, optical, electrical, barrier and thermal) compared to conventional composites at very low loading of filler.

Recently, polymer technologist show great interest in polymer/layered silicate nanocomposites, a new class of materials with enhanced properties compared to parent conventional micro composites and unfilled polymers. In contrast to various fibers and spherical mineral particles, such as silica, talc, and calcium carbonate, the layered silicates such as montmorillonite (MMT) have played an important role as effective reinforcement components in developing new nanocomposites. These materials have gained much interest due to the remarkable improvement in properties such as mechanical, thermal, electrical and gas barrier properties compared to pure organic polymers and microcomposite [109-124]. The enhancement in these properties depends on the uniformity, phase continuity, domain sizes and the molecular mixing at the phase boundaries [125].

1.7.1 Reinforcement with nanofillers

Nowadays, composite materials have replaced traditional ones in a variety of applications. Lightweight coupled with enhanced properties are the main reasons for their market acceptance and growth, and the optimization of their performance is a challenge worldwide. The high aspect ratio of reinforcing particle and its adhesion to the matrix are of great importance, because they control the final properties of the composites. Polymer/clay nanocomposites meet these requirements due to the shape (platelet, disc) and nanometer-scale dispersion of the clay layers in the polymeric matrix. This type of composites has raised significant scientific interest due to the improved physical properties that can be achieved by adding a small fraction of clay (<10wt %) into the polymer matrix [25, 26,116,126,127].

Best performance of the polymeric nanocomposites is achieved when the silicate layers are dispersed in the polymer matrix without agglomeration. An essential step in the preparation of a nanocomposite is the delamination of the layered silicates (LS), which is usually termed exfoliation in the literature. Both the layer thickness and the space (galleries) between the layers are of 1nm. The galleries are occupied by hydrated cations, which counterbalance the negative charge of the layers generated by the isomorphic substitution of some atoms in the silicate crystals. The environment of the galleries is hydrophilic and thus inappropriate for the hydrophobic macromolecular chains to penetrate therein. The replacement of the inorganic cations by organic onium ions (surfactant, intercalant, tenside) overcomes this inconvenience. The cationic head of, eg. an alkylammonium compound is tethered to the layers via coulombic interactions, leaving the aliphatic tail to hover between the layers. The longer the surfactant chain length and the higher the charge density of the clay, the further apart the clay layers will be forced [27]. The originally hydrophilic silicate renders organophilic due to the presence of these aliphatic chains in the galleries. A value that characterizes each LS is the cation exchange capacity (CEC), expressed in meq/100g, referring to

moderate negative charge of the clay layer surface. The effect of CEC has been checked for different types of clay [35]. It was claimed that a well exfoliated silicate structure can be obtained in polymers when layered silicates of optimum CEC (90meq/100g) are rendered organophilic.

Various models have been developed to trace the parameters forcing the macromolecular chain in the silicate layers and then causing their delamination. The interplay of entropic and energetic factors determines the outcome of polymer intercalation/exfoliation. The entropy decrease due to confinement of the polymer molecules when entering between the galleries is overcompensated by the increase in the entropy of the tethered chains of the surfactant while the silicate layers are moving apart prior to their final separation. In addition, energetically favored interactions between the surfactant and the polymer molecules may yield a negative mixing enthalpy. It should be noted that a molecular dispersion requires that the Gibb's free energy of mixing become negative.

Vulcanized rubbers are usually reinforced by carbon black and inorganic fillers. Carbon blacks are excellent in reinforcement owing to the strong interaction with rubbers, but their presence often reduces the processability of rubber compounds, especially at high volume loadings. On the other hand, minerals of various shapes (eg. fibrous, platy) are suitable for rubber filling, but they have a poor interaction with rubbers ("inactive fillers"). Therefore, it is of paramount interest to disperse LS in rubber on a nanometer level. The required level of reinforcement in rubbers can be achieved at very low LS loadings, which offers easier processing without any property deterioration compared to traditional "active" fillers.

1.7.2 Polymer layered silicate nanocomposites (PLSNs)

Polymer layered silicate nanocomposites (PLSNs) is a hybrid of an organic and an inorganic phase in which one of the phases has at least one dimension in the nanometer range. Some polymer/clay nanocomposites products have already

developed that being used commercially for certain applications. The first industrial application of polymer nanocomposites was provided by Okada *et al.* [128] at Toyota's Central Research Laboratories in Japan. They prepared Nylon-6 nanocomposites by polymerisation in presence of the inserted monomer. It was then marketed by UBE industries and Bayer, currently used to make the timing belt cover of Toyota's car engines and also for the production of packaging film. The theory and simulations addressing the preparation and properties of these materials [129-144] and they are also considered to be unique model systems to study the structure and dynamics of polymers in confined environments [145-152].

1.7.3 Classification of PLSNs

The clay or layered silicates are incorporated into a polymer matrix to form an organic/inorganic composite. Polymer/clay composites can be divided into four categories, depending on the clay concentration, degree of clay layer separation and distribution in the composites [152] as in figure 1.4.

In microcomposites or conventional composites the particles exist as aggregates with no insertion of polymer matrix. Hence it cannot impart any enhancement in properties. Intercalated nanocomposites consisting of a regular insertion of polymer in between the silicate layers in a crystallographic regular fashion [153-156]. In an exfoliated nanocomposite, the individual 1nm thick silicate layers are separated and dispersed in a continuous polymer matrix with average distances between layers depending on the clay concentration. Exfoliated nanocomposites exhibit better properties, because they maximize the polymer-layered silicate interactions, making the entire surface of the layers available for interactions with the polymer. The PLSNs commonly exhibit a mixed type of morphology where exfoliated and intercalated layers randomly distributed in the matrix.

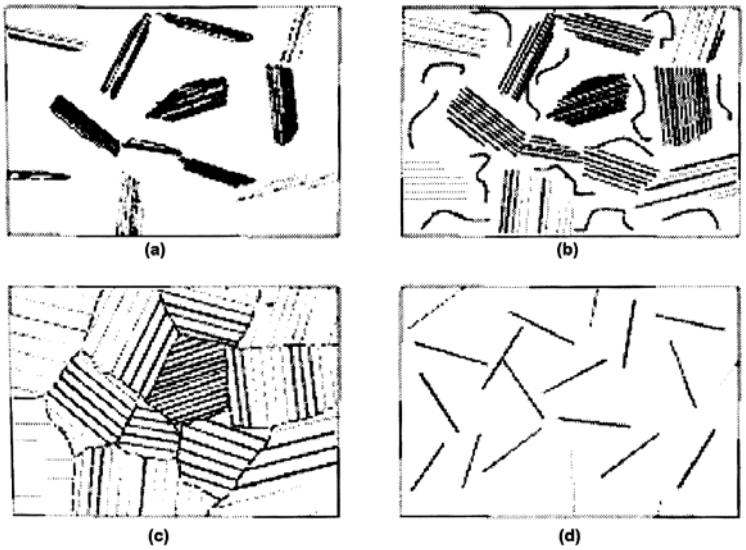

Figures 1.4 Types of polymer/clay composites (a) conventional (b) partially intercalated and exfoliated, (c) fully intercalated and dispersed and (d) fully exfoliated and dispersed

1.7.4 Preparation of PLSNs

PLSNs are currently prepared by three different methods:

(i) intercalation of monomers followed by in situ polymerisation

(ii) direct intercalation of polymer chains from solution

(iii) polymer melt intercation

As most of the rubbers are available in solid (dry) and latex (solution) forms, melt and latex intercalations are considered to be the industrially feasible methods for preparing rubber nanocomposites.

In case of in-situ polymeristion, the oxidizing properties of the host lattice induce polymerisation of suitable monomers. The resulting materials are intercalated systems in which the polymers are located between the layers. The disadvantages

of this method is that it only works with suitable monomers and the intercalation of polymer chains has a quite slow kinetics originating from diffusion phenomena [114,157-160]. The schematic representation of the process is given in figure 1.5

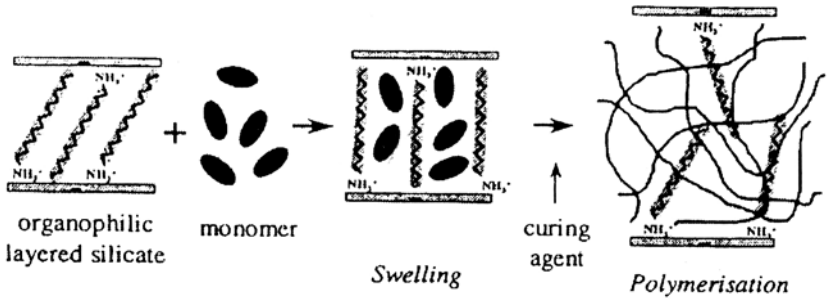

Figure 1. 5 The in-situ polymerisation method

Toyota CRDL group synthesised first polymer nanocomposite using Nylon-6 matrix by monomer intercalation method [161]. This method can be used for the preparation of nanocomposites based on thermosets [160,162-163] such as epoxies, unsaturated polyester and polyurethanes as well as for thermoplastic nanocomposites [164-165] based on poly (ethylene terephthalate) (PET), PS and PMMA.

Intercalation of polymer chains from solution is a two stage process in which the polymer is exchanged with intercalated solvent. The driving force for the polymer intercalation is the increase in entropy due to the desorption of solvent molecules, which can be nullified by the decrease in entropy caused by the intercalation of polymer chains [166]. Figure 1.6 shows the intercalation of polymer chains in silicates from solution.

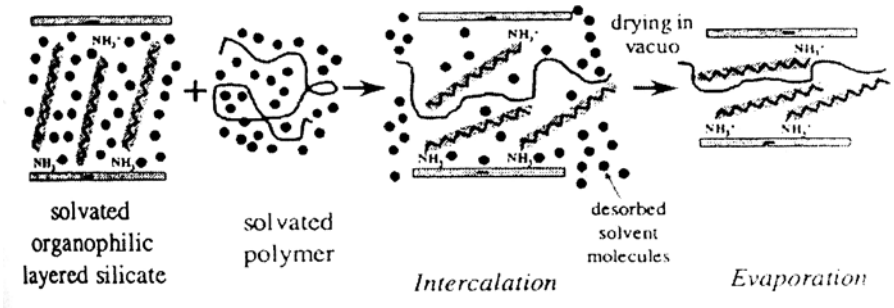

Figure 1.6 The solution method for the preparation of PLSNs

The major advantage of this method is that it offers the possibility to synthesize intercalated nanocomposites based on polymers with low or even no polarity. How ever, owing to high cost of solvents, their disposal and environment impact, this method is industrially impracticable. Another drawback is the requirement of a suitable solvent. Nanocomposites based on high-density poly(ethylene) (HDPE), poly(imide) and nematic liquid crystal polymers have been synthesized by this method [167-168].

The direct melt intercalation into layered host lattices is the preferred process for the formation of hybrid materials [169-175]. This process is based on the heating of a mixture of the polymer and the layered system above the Tg or the melting temperature Tm of the polymer, and the diffusion of the polymer between the galleries of the layers. The critical factor for this method is the enthalpic contribution of the polymer/organosilicate interactions during the blending and annealing steps. The melt intercalation process is shown in figure 1.7. This method was used for the synthesis of poly(styrene oxide) and non polar poly(styrene) nanocomposites [169,176]. Hasegawa *et al.* [177] found that maleic anhydride grafted PP (MA-PP) was able to intercalate into the inter-galleries of OMLS, similar to the functional oligomer, and described a facile approach for the preparation of PP clay nanocomposites by melt intercalation using a MA-PP and organically modified clay. The direct melt intercalation is highly specific for the polymer, leading to new hybrids that were previously inaccessible. In addition,

the absence of a solvent makes direct melt intercalation an environmentally sound and an economically favorable method for industries from a waste perspective.

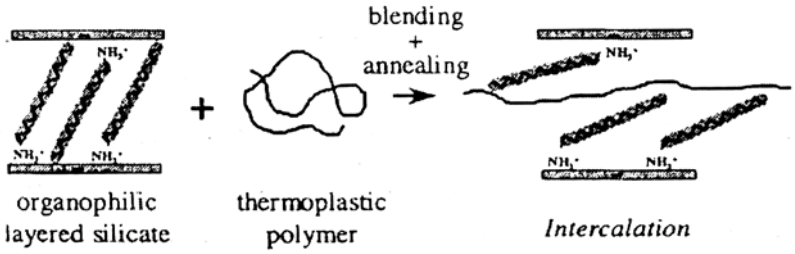

Figure 1.7 The melt intercalation method for the preparation of PLSNs

1.7.5 Characterization of PLSNs

The distinguishing feature of PLSNs and other polymer based nanostructured materials is their morphology, in which the size of inorganic particles is comparable to spacing between particles, both of which are nanoscopic (1-100nm). The detailed characterization of the nanoscale morphology of both the layered silicate and the polymer is critical to establish structure-property relationships of these materials. There are several techniques that are used to elucidate the nanostucture of polymer layered silicate nanocomposites including atomic force microscopy (AFM) [178], Nuclear magnetic resonance spectroscopy (NMR) [179,180], Neutron scattering method [181], Scanning electron microscopy (SEM), Transmission electron microscopy (TEM) and X-ray diffraction techniques (XRD). However TEM and XRD are the most commonly used techniques. By means of these techniques immiscible, intercalated, exfoliated and confined structures can be characterized.

XRD technique is one of the most widely used tools for the characterization of structure of PLSNs, and provides globally averaged information and potentially over six or more orders of magnitude. It is used to monitor the position and the intensity of the (001) basel reflection corresponding to the repeat distance

perpendicular to the layers. Figure 1.8 illustrates the diffractograms produced by different types of hybrids [174,175]. In the case of immiscible mixtures of polymer and OLMS, the basel reflection does not change upon blending with the polymer. Intercalated structures exhibited new basal reflection corresponding to the larger gallery height. A decrease in the degree of coherent layer stacking results in a peak broadening and intensity loss. Exfoliated structure does not result in a new observable basal reflection but leads to intensity loss and eventual disappearance of the unintercalated basel reflection. XRD method can also be successfully used to distinguish the intercalated and non-intercalated silicate fractions.

However, XRD's potential does not extend to the provision of information concerning the spacial distribution of the silicate in the polymer matrix, nor the shape of the hybrid, since all its data are averaged over the whole of the sample. Therefore, probability for the misinterpretation of nanocomposites structure is possible.

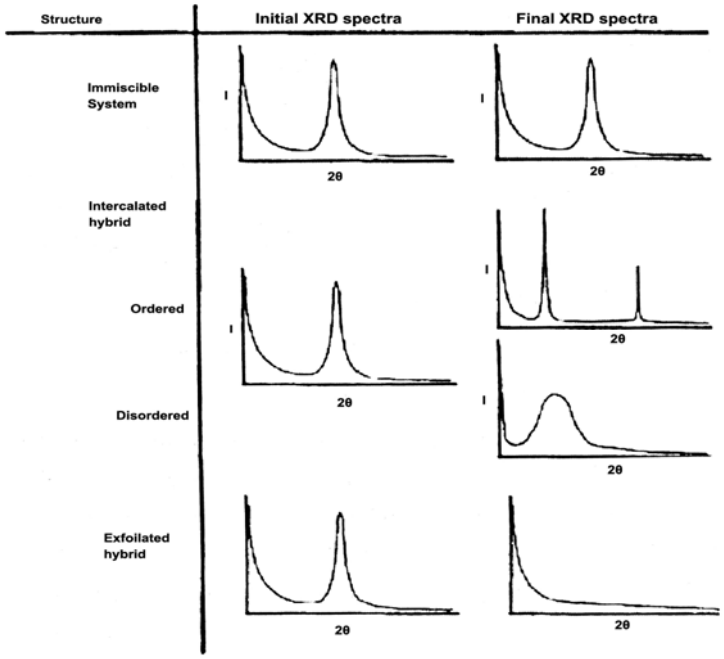

Figure 1.8 Schematic XRD Pattern of possible PLSNs Structures

TEM is the most powerful technique for the identification of structure of PLSNs. It gives a direct measure of the spatial distribution of silicate layers, morphology and structural defects of a selected area of the sample. But the lamination is that it requires substantial skill in specimen preparation and analysis.

1.7.6 Rubber-clay nanocomposites

Until recently research on layered silicates of synthetic and natural origin for the property modification of polymers was mostly concentrated in thermoplastics, [23,103,182-185] and thermosetting resins [23,103,182,186,187]. However, elastomers and rubbers are very promising polymeric matrices for the preparation of polymer clay nanocomposites because of the following reasons [188].

(i) It is well known that amine compounds act as curing reaction activators in sulphur containing rubber recipes [189]. Thus, PCNs intercalated by amine compounds may interact with the sulphur curatives thereby promoting thermodynamically favored interactions between the rubber chains and the silicate layers leading to increased intercalation/exfoliation.
(ii) Rubbers exhibit high melt viscosities during melt mixing because of their high molecular weight and this paves the path for generation of high shear stresses for the shearing and peeling apart of the silicate layers.
(iii) Further, the swelling of pristine and organophilic clays in both aqueous and organic solutions makes it amenable for the preparation of rubber clay nanocomposites via the latex and solution routes.
Nanocomposites have some unique outstanding mechanical property with respect to their conventional counterparts. Melt compounded and processing characteristics of natural rubber organoclay nanocomposites were studied by Varghese *et al.* [190,191]. Youping *et al.* studied the flame retardant properties of rubber/clay nanocomposites [192]. Thermal and barrier properties of NBR/organoclay were studied by Hwang *et al.* [193]. Stephan *et al.* studied the impact of layered silicates such as sodium bentonite and sodium flurohectorite on the rheological behaviour of NR, carboxylated SBR (XSBR) lattices, and their

blends with special reference to shear rate, temperature and filler loading [194]. Arroyo *et al.* reinforced NR with 10phr unmodified clay and octa deccaylamine modified MMT and compared the results loaded with 10 and 40phr carbon black [195]. The organoclay behaved as an effective reinforcement agent for NR and showed a stronger reinforcing effect than carbon black while retaining the elasticity of the elastomer. Joly *et al.* observed that organically modified galleries of MMT were easily penetrated by natural rubber (NR) chains and led to intercalated structures along with partial exfoliation [196]. Modulus increase comparable to that achieved by high loadings of conventional micrometer sized fillers was observed at 10wt% organically modified MMT loading demonstrating the advantages of high surface area of the filler and the better interface adhesion between the polymer and clay. Lopez- Manchado *et al.* studied the effect of incorporation of un modified and organically modified bentonite clay on the vulcanization kinetics of NR by Cure meter testing and Differential scanning calorimetry (DSC) under dynamic and isothermal conditions [197]. Gas transport through nano and micro composites of natural rubber (NR) and their blends with carboxylated styrene butadiene rubber (XSBR) latex membranes were studied by Stephen *et al.* [198].

1.8 Properties of PLSNs

PLSNs consisting of a polymer and layered silicate (modified or not) frequently exhibit remarkably improved properties when compared to those of pristine polymers containing a small amount (≤5 wt %) of layered silicate.

The great interest in the field of PLSNs arises due to the dramatic improvement in mechanical and physical properties of polymer nanocomposites. The findings of nanocomposites widely reported in the literature include an increased modulus, a lower thermal expansion coefficient, and reduced gas permeability, greater resistance to solvents, oils and ozone [22,122,155,158].

1.8.1 Mechanical properties

The improvement in mechanical properties such as tensile strength, tensile modulus and Young's modulus of PLSNs can be related to the degree of exfoliation of layered silicate in the polymer matrix. The enhancement in mechanical properties provided by the exfoliated nanocomposites structure on polyamide 6 (PA6)-clay hybrid was reported by the Toyota researches [199]. The modulus was increased by 90% and tensile strength by 55% with the addition of 4wt% of exfoliated clay. There are a lot of explanations on the reinforcement observed in polymer-layered silicate hybrids based on interfacial properties and restricted mobility of the chains.

Elastomers are filled with small and hard particles to improve the mechanical properties of polymeric material like elastic modulus or resistance to abrasion.

1.8.2 Dynamic mechanical properties

The dynamic mechanical properties of PLSNs depend highly on the extent of intercalation and exfoliation. In exfoliated and partially exfoliated structures, the interaction between the polymer and silicate layers are relatively high so that the change in the storage modulus with frequency and clay loading change substantially as compared with pristine polymer. Varghese *et al.* [200, 201] studied the damping behavior of layered silicates reinforced natural rubber nanocomposites. The frequency sweep of the NR and NR/ clay composites at 60^0C under 0.58 strains is reported [202]. The dynamic mechanical properties of NBR/clay [203], MA-g-EPDM/clay [204] have been studied. The dynamic properties are also of direct relevance to a range of unique polymer applications, concerned with the isolation of vibrations or dissipation of vibrational energy in engineering components.

1.8.3 Transport properties

Due to the large aspect ratio of the silicate layers, the permeability decreases drastically. The substantial decrease can be explained by the increase in tortuosity of the path of the gas as it diffuses into the nanocomposite. The tortuosity increases with the aspect ratio of the silicate layers [205]. Schematic representation of the tortuous path model is given in figure 1.9. From this it is clear that the gas molecules have to travel through a tortuous path in the presence of layered silicate.

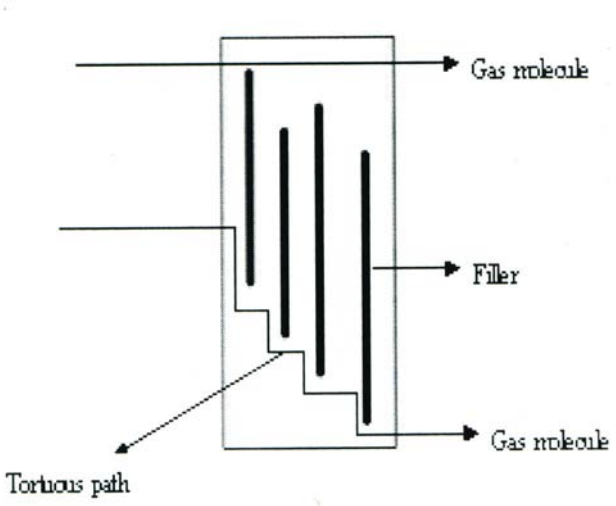

Figure 1.9 Schematic representation of tortuous path model

The barrier improvement is predicted by tortuous path model to be a function of the volume fraction of silicate layers, ϕ and a function of the aspect ratio of silicate layers, α with higher aspect ratios provide greater barrier improvement according to the following equation for permeability:

$$\frac{P}{P_0} = \frac{1-\phi_f}{1+\frac{L}{2W}\phi_f} \tag{1.1}$$

In the above equation, P is the permeability of the nanocomposites, P_0 is the permeability of the gum vulcanizate and ϕ_f is the volume fraction of the clay. L and W are length and width of the clay sheets, respectively, its ratio L/W, defines the aspect ratio α, of the fillers. The model assumes that the fillers are impermeable to the diffusing gas or liquid molecule and are oriented to the diffusion direction.

Toyota researches [199] reported that the water absorption of PA6-clay hydrid reduced by 40% as compared with the pristine polymer. Wang *et al.* [203] observed significant improvement in gas barrier properties of nanolayers incorporated SBR due to the tortuous diffusional path and lower fractional free volume. Utracki and Simha [206] shown that upon the addition of nanofillers to polymer matrix the free volume decreases considerably due to the increased polymer/filler interaction. The dispersed nanocomposites exhibit increased solvent resistance compared to immiscible hybrids. The exfoliated silicate layers prevent solvent molecules to diffuse and damage the polymer network [168,169].

1.8.4 Thermal stability

The thermal stability of nanocomposites is increased with the length and the content of silicate layers. It is due to the presence of a constrained region in the nanocomposites. There are large numbers of research papers on the improved themal stability of PLSNs [158,207-210]. Poly(ε-caprolactone) (PCL) based nanocomposites have a degradation temperature higher than neat PCL [177]. PCL nanocomposites are characterized by a single weight loss with the beginning of the degradation shifted to much higher temperature. This effect is explained by the fine dispersion of the clay layers, which decreases the polymer permeability to both oxygen and the volatile decomposition products.

1.9 Motivation for the study

Natural rubber (NR) is a naturally occurring material used in the manufacture of various rubber goods. The applications of NR depend mainly on its inherent soft and highly deformable nature, its excellent physical properties, low cost and easy availability. Maleated natural rubber (MA-g-NR), a potential polar form of NR, can be used for developing a host of value added forms of natural rubber and hence MA-g-NR is proposed to be prepared by grafting of maleic anhydride on NR by γ-radiation method. MA-g-NR has good weather resistance, high tensile strength, and is less permeable to gases and solvent molecules. The advantage of γ-radiation method is that contamination with chemicals is less when compared to the chemical method. Moreover, MA-g-NR is mechanically more stable than NR and can add fillers with out flocculation. The masterbatch technique of MA-g-NR has many potential advantages over direct method in which more through put of products is obtained in a single batch and less quantity of MA-g-NR is required for composite preparation.

Usually fillers are incorporated in elastomers to modify certain properties to an acceptable level. The type and optimum loading of filler vary from polymer to polymer. Generally, there are two classes of fillers, i.e., black and white fillers. Among black fillers carbon black is the most widely used filler in rubber industry. Clay and silica are the important white fillers used in rubber industry. It is well known that the particle size, structure and surface characteristics of reinforcing materials are the three factors, which influence the final properties of vulcanisates. The reinforcing capability of clay is poor owing to its large particle size and low surface activity. In the case of non-polar matrix, filler-filler interaction predominates which result in aggregation of filler.

During natural rubber/clay mixing the strength enhancement occurs due to the formation of active groups in organoclay and rubber. But the strength can be again improved by using modified rubber (maleated rubber) with organoclay. Here the rubber-filler interaction is comparatively higher when compared to that

of pure NR. This increase in rubber-filler interaction occurs as a result of polar nature of rubber. The 2:1 phyllosilicates have attracted a great attention as nanocomposite reinforcements in polymer owing to their high aspect ratio, intrinsically anisotropic character, swelling capabilities etc. Due to the nanometer level filler dispersion, nanocomposites exhibit markedly improved properties as compared to pristine polymer and traditional microcomposites. These properties include increased mechanical, gas barrier, solvent and thermal resistance.

Cloisite 30B, the layered silicate, is proposed to be used as the nanofiller for modifying NR. In present study the effect of nanoclay and the variation of maleic anhydride concentration on the mechanical properties of maleated natural rubber clay nanocomposites are also proposed to be investigated. Careful analysis of the literature clearly indicates that till date no systematic study has been performed on the effect of nanoclay on maleated natural rubber and its master batches.

1.10 Objectives of the work

The main objectives of the present study are the following:

- To study the effect of grafting of maleic anhydride on natural rubber through gamma radiation.
- To optimize dose of radiation for maleic anhydride grafting.
- To characterize grafted rubber and to determine the grafting efficiency through IR and titration method.
- To prepare and characterize 1,3,5 and 10% maleated natural rubber using the technique of gamma grafting.
- To prepare maleated natural rubber/clay nanocomposites and to characterize it using XRD and TEM.

- ❖ To study the effect of interlayer distance of layered clay on the mechanical properties of maleated natural rubber/clay nanocomposites.

- ❖ To study the effect of master batch technique on the mechanical properties of maleated natural rubber /clay nanocomposites.

- ❖ To investigate the thermal stability and ageing characteristics of maleated rubber/clay nanocomposites.

- ❖ To examine the barrier properties of maleated natural rubber/clay nanocomposites.

- ❖ To study the effect of nanofiller on the dynamic mechanical and dielectric properties of maleated natural rubber/clay nanocomposites.

References

1. Burlett D J, Lindt J T. Rubber Chem Technol 1993; 66: 411.
2. Singh R.P. Prog. Polym Sci 1992; 17:251.
3. Bergbeiter D E, Martin C R Functional Polymers Plenum Press New York 1989.
4. Katz HS, Milewski JV. Handbook of Fillers and Plastics,Van Nostrand Reinhold Co, New York 1987; p 459.
5. Messermith PB, Ginnaleis EP. J.Polym Chem 1995;33:1047.
6. Rothon R. Editor, Particulate- Filled Polymer Composites, Longman Scientific & Technical, New York, 1995; p371.
7. Blow CM, Editor, Rubber technology and Manufacture, The Chemical Rubber Co Ohio 1971; p509.
8. Dick JS, Editor, Rubber Technology: Compounding and testing for Performance, Hanser publishers, 2001; p523.
9. Eirich FR, Editor, Science and Technology of Rubber, Academic Press, New York, 1978; p633.

10. Franta I, Editor, Elastomers and Rubber Compounding Materials, Elsevier, New York, 1989; p588.
11. Medalia AI, Kraus G. In Science and Technology of Rubber, Eds, Mark JE, Erman B, Eirich RF, Acadamic Press, New York 1994;p 387.
12. Blow S, In: Handbook of Rubber Technology, Editor, Blow S, Galgotia Publication Ltd, New Delhi, 1998; p 483.
13. Wang MJ, Rubber Chem Technol 1998;71:520.
14. Patel HA, Rajesh SS, Hari CB, Raksh VJ. Bull. Mater. Sci 2006;29:133.
15. Lan T, Pinnavaia TJ. Mater Res Soc Symp Proc 1996 ;79 :435.
16. Wang Z, LanT, Pinnavaia TJ Chem Mater 1996;8:2200.
17. Munzy CD, Butler BD, Hanley HJM, Tsvetkov F, Pfeiffer DG Mater Lett 1996;28:379.
18. Yariv S, Cross H Eds Organo-Clay Complexes and Interactions, Marcel Dekker New York 2002.
19. Van Olphen H. An introduction to Clay Colloid Chemistry 2nd ed Wiley New York 1973.
20. Avena M, De Pauli C. Effect of Structural Charges on Proton Adsorption at Clay Surfaces, Geochemical and Hydrological Reactivity of Heavy Metals in Soils Eds Selim H, Kingery W, Lewis Publishers 2003;p 79.
21. Rohl W, Rybinski W, Schwuger M. (Adsorption of surfactants on low charged layer silicates Part I: Adsorption of cationic Surfactants) Prog Coll Polym Sci 1991;84:206.
22. Ray S. Okamoto M. Prog Polym Sci 2003;28:1539.
23. Glannelis EP.*et al*., Adv Polym Sci 1999;138:107.
24. Okada A, Kawasumi M, Usuki A, Kojima Y, Kurauchi T, Kamigatio O. Synthesis and properties of nylon-6/clay hybrids. In: Schaefer DW, Mark JE editors Polymer based molecular composites. MRS symposium Proceedings, Pittsburgh 1990;171:45.

25. Giannelis EP. Polymer layered silicate nanocomposites Adv Mater 1996;8:29.
26. Giannelis EP, Krishnamoorti R, Manias E. Polymer-silicate nanocomposites: model systems for confined polymers and polymer brushes Adv Polym Sci 1999;138:107.
27. LeBaron PC, Wang Z, Pinnavaia TJ Polymer-Layered silicate nanocomposites: an over view Appl Clay Sci 1999;15:11.
28. Vaia RA, Price G, Ruth PN, Nguyen HT, Lichtenhan J. Polymer/layered silicate nanocomposites as high performance ablative materials Appl Clay Sci 1999;15:67.
29. Biswas M, Sinha Ray S Recent progress in synthesis and evaluation of polymer-montmorillonite nanocomposites Adv Polym Sci 2002;155:167.
30. Brindly SW, Brown G. editors Crystal structure of clay minerals and their X-ray diffraction. London: Mineralogical society 1980.
31. Aranda P, Ruiz-Hitzky E. Poly (ethylene oxide) –silicate intercalation materials Chem mater 1992;4:1395.
32. Greenland DJ, Adsorption of Poly(vinyl alcohols) by montmorillonite J Colloid Sci 1963;18:647.
33. Blumstein A. Polymerization of adsorbed monolayers:II Thermal degradation of the inserted polymers J Polym Sci A 1965;3:2665.
34. Krishnamoorthi, Vaia RA, Giannelis EP. Structure and dynamics of polymer- layered silicate nanocomposites Chem Mater 1996;8:1728.
35. Lan T, Kaviratna PD, Pinnavaia TJ. Chem Mater 1995;7:2144.
36. George PJ, Kuruvilla Jacob C.Eds "Natural Rubber- Agromanagement and Crop Processing" RRII India (2000).
37. Williams CG. Proc Royal Soc 1860;10:516, J Chem Soc 1867;15:110.
38. Robert AD, Editor Natural Rubber science and Technology Oxford Science Publications 1988;p1078.
39. Gent AN, Zhang LQ. Rubber Chem Technol 2002;75:923.

40. Porter M. Chemical modification of NR, past, present and future Eur Rubb J 1977;13:159.
41. Campbell DS in "Natural Rubber:Biology, Cultivation and Technology", Sethuraj MR,Mathew NM(Eds), Elsevier Science Publishers Amsterdam 1992:p451.
42. George B, Alex R, Mathew NM. "Natural Rubber Agromanagement and Crop processing", George PJ, Kuruvilla Jacob C(Eds) RRII India, 2000;479.
43. George KM, Rajammal G, Peethambaran NR, Mathew NM, Ind J Nat Rubb Res 2001;14:7.
44. Varghese S, Katsumura Y, Makuuchi K, Yoshi F.Rubb Chem Technol 2000;73:80.
45. Fravel VH. US Pat 1955;2:716,669.
46. Zhong JP, Li SD, Wei YC, Yu HP, Peng Z J Appl Polym Sci 1999;62:2836.
47. Jien Pinzova, Proce Inter Rubb Conf IRC 97, Kulalumpur, Malaysia 1997; p297
48. Kraus G, Angrew. Macromolecular Chemistry 1977;60/61:215.
49. Fraco Cataldo. J Appl Polym Sci 1995;58;2063.
50. Veeralakshmanan B, Nair NR, Mathew NM, Sasimohan AL. Indian J Nat Rubb Res 1996 ;8 :85.
51. Baker CSL, Gellin IR, Newell R. Rubber Chem Technol 1985 ;58 :67.
52. Jacobi MM, Santin CK, Viganico ME, Alegre P, Schutzer RH, Kunststoffe GK 2004;57:82.
53. Gelling IR. Rubber Chem Technol 1985;58:86.
54. George B, Abraham SA, Mathew NM. Indian J Nat Rubb Res 1992;5:179.
55. Baker CSL, Gellin IR, Azemi S. J Nat Rubb Res 1986;1:135.
56. Okieimen PE, Akinabi AK, Aigbodion AJ,Bakare IO. J Polym Mater 2003;20:403.

57. Sekhar BC. J Polym Sci 1960;48:133.
58. Konietzny A, Beithan U, Ang Macromol Chem 1978;14;61.
59. Pande LM, Joshi GC Indian Pat 1974;132:396.
60. Pinazzi C, Levesque G. Compt Rend Part C 1967 ;246 :288.
61. Barnad D, Dawel K, Mente PG. Proce Inter Rubb Conf Vol 4 Rubber Res Inst of Malaysia 1975; 75:218.
62. Baker CSL, Barnad D, Peter MN Rubber Chem Technol 1970;43 501.
63. Cain ME, Knight GT, Lewis PM, Saville B J Rubb Res Inst Malaysia 1968;22:289.
64. Barnard D. Rubber developments 1975;28:58.
65. Berthalot PM. Bulletin de la Societe Chime de France 1869;11:33.
66. Pummerer R, Burkard PA, Chemische Berichte 1922 ;55 :3458.
67. Harris CD, Chemische Berichte.1923;56:1048.
68. Mango LA, Lenz RW. Macromolecular Chemistry 1973 ;163 ;13.
69. Burfield DR, Lion KL, Seow PK, Loo CT. Proc of International Rubb Conf Kuala Lumpur 1985;p247.
70. Singha NK, Battacharjee S,Sivaraman S. Rubber Chem Technol 1997;70:303.
71. Golub and Heller. J Poly Sci Poly Lett Edition 1984;2;723.
72. Harries CD, Chemische Berichte 1913;46;733.
73. Hinrichsen FW, Quensell H, Kindschen. Cheische Berichte 1913;46:1283.
74. Harries CD, Chemische Berichte 1923;56;1048.
75. Bunn CW, Garner EV. Journel of Chemical Society, 1942;654.
76. Weber CO. Chemische Berichte1900;33:779.
77. Tom DHE. J Appl Poly Sci 1956;20:381.
78. Gaylord N, Mehta M, Mehta R. Am Chem Soc Symp Ser 1988;364:438.
79. George KM, Claramma NM, Thomas EV. Radiation Phy & Chem 1987;30:189.

80. Cooper W, Sewell PR, Vaughan G. J Polym Sci 1959;41:167.
81. Claramma NM, Mathew NM, Thomas EV. Radiation Phy & Chem 1987;33:87.
82. Ono S, Yoshi F, Makuchi K, Ishigak I. Proce Second International Symp Radiation Vulcanization of Natural Rubber latex, Kula Lumpur 1996; p198.
83. Claramma NM, Varghese L, Thomas KT, Mathew NM. Proce 18th Rubb Confer Indian Rubb Manf Asso Mumbai 2000;p165.
84. Blackley DC. Polymer Lattices Chapman and Hall London 1997;2:ch-14.
85. Campell DS. Developments in Block Copolymers Goodman I Ed Elsevier Applied Science 1985;2;Ch-6.
86. Campell DS, Mente PG, Tinker AJ, Kautschuk Gummi Kunststoffe. 1981;3:636.
87. Schneider M, Pith T, Lambla MJ. J Appl Polym Sci 1996;62:273.
88. Schneider M, Pith T, Lambla MJ. Polymers for advanced Technologies 1996;p 245.
89. Lehrle RS, Willis SL. Polymer 1997;38:5937.
90. Fukushima X, Kawahara s Tanaka Y. J Rubb Res 1988;1:154.
91. Wheelans MA. Natural Rubber Science and Technology Ed Roberts Oxford University Press, Oxford 1998;p 235.
92. Suriyachi P, Kiathkamjornwong S, Prasassarakich P. Rubber Chem Technol 2004;77:914.
93. Ashalatha R, Kumaran MG, Thomas S. Rubber Chem Technol 1995;68:671.
94. Hourston DJ, Romanine JR. Eur Polym J 1989;25;695.
95. Hourston DJ, Romanine JR. J Appl Polym Sci 1991;43:2207.
96. Subramanian N, Balic R, Taylor JR, Griffiths M, Monteiro MJ, Gilbert RG, Ho CC, Abdullah I, Cacioli. J Nat Rubb Res 1997;12:223.

97. Claramma NM, Nair NR, Mathew NM. Indan J Nat Rubb Res 1991:4:1.
98. UNIDO, Development of Liquid NR, Project No. UF/ GLO/81/059, Institute de Researches Sur, Le Caoutchouc (IRCA), 1985 ;7.
99. Okieimen FE, Akinlabi AK. J Appli Polym Sci 2002 ;85 :1070.
100. Nair NR, Claramma NM Kuriakose B, Mathew NM. Indian J Nat Rubb Res 1989 ;2 :81.S
101. Kuriakose B, Gopalakrishnan KS, Thomas EV. Rubb Board Bulletin 1976 ;13 :55.
102. Tutroskii IA. Rubber Chem Technol 1963 ;36 :1019.
103. Alexandre M, Dubois P. Mater Sci Eng 2000 ;28 :1.
104. Komarneni SJ. J Mater Chem 1992 ;2 :1219.
105. Giannelis EP. Adv Mater 1996 ;8 :29.
106. Ziolo RF, Giannelis EP, Weinstein BA, Horo MP, Granguly BN, Mehrota V, Russell MW, Hoffman DR. Science 1992 ;257 :219.
107. Parson, Cupnik T, Davis J, M Phy Rev B 1988 ;38 ;282.
108. Gauthier C, Chazeau L, Prasse T, Cavaille JY. Comp Sci Tech 2005 ;65 :335.
109. Vaia RA, Benson T, Schmitt GF, Imeson D, Jones RJ. SAMPE Journal 2001 ;37 :6.
110. Okada A, Usuki A. Mater Sci Eng 1995;C3:109.
111. Gilman JW. Appl Clay Sci 1999;15:31.
112. Gilman JW, Jackson CL, Morgan AB, Harris R, Manias E, Giannelis EP, Wuthenow M, Hilton D, Philips SH. Chem Mater 2000;12:1866.
113. Porter D, Metcalfe E, Thomas MJK. Fire Mater 2000;24:45.
114. Zanetti M, Lomakin S, Camino G. Macromol Mater Eng 2000;279:1.
115. Ray SS, Okamoto M. Prog Polym Sci 2003;28:1539.
116. Kojima Y, Usuki A, Kawasumi M, Okada A. J Polym Sci Part A: Polym Chem 1993:31:983.

117. Krishnamoorthi RK, Vaia RA, Giannelis EP. Chem Mater 1996;8:1728.
118. Liao M, Zhu J, Xu H, Li Y, Shan W. J Appl Polym Sci 2004;92:3430.
119. The PL, Ishak ZAM, Hashim AS, Karger-Kocsis, Ishiaku US. Eur Polym J 2004;40:2513.
120. Lara TEB, Liu RYF, Hiltner A, Baer E. Polymer 2005;46:3043.
121. Osman MA, Rupp JEP, Suter UW. Polymer 2005;46:3043.
122. Chen Y, Zhou S, Yang H, Wu L. J Appl Polym Sci 2005 ;95 :1032.
123. Maiti M, Sadhu S, Bhowmic AK. J Appl polym Sci 2005;96:443.
124. Manchado MAL, Biagiotti J, Valentini L, Kenny JM, J Appl Polym Sci 2004;92:3394.
125. Sperling LH. Interpenetrating olymer Networks and Related Materials, Plenum Press, New York 1981.
126. Pinnavaia TJ, Beall GW. Polymer- Clay Nanocomposites Wiley, New York.
127. Utracki LA, Kamal MR. Clay-containing Polymer Nanocomposites Arab J Sci Eng 2002;27:43.
128. Okada A, Fukoshima Y, Inagaki S, Usuki A, Sugiyamma S, Kurashi T, Kamigaito O. 1998; US 4.739.007.
129. Dabrowski F, Bourbigot S, Delbel R, Bras ML. Eur Polym J 2000;36:273.
130. Vaia RA, Jandt KD, Karamer EJ, Giannelis EP. Macromolecules 1995;28:8080.
131. Vaia RA, Giannelis EP. Macromolecules 1997;30:7990.
132. Vaia RA, Giannelis EP. Macromolecules 1997;30:8000.
133. Lee JY, Baljon ARC, Loring RF, Panagiopoulos AZ. J Chem Phys 1998;109;10321.
134. Balazs AC, Singh C, Zhulina E. Macromolecules 1998;31:8370.
135. Balazs AC, Singh C, Zhulina E Acc Chem Res 1999;32:651.
136. Fredrickson GH, Bicerano J. J Chem Phys 1999;110:2181.

137. Ginzburg VV, Balazs AC. Macromolecules 1999;32:5681.
138. Baljon ARC, Lee JY, Loring RF. J Chem Phys 2000;111:9068.
139. Ginzburg VV, Singh C, Balazs AC. Macromolecules 2000;33:1089.
140. Kuznetsov D, Balazs AC. J Chem Phys 2000;112:4365.
141. Lee JY, Baljon ARC, Sogah DY, Loring RF. J Chem Phys 2000;112:9112.
142. Balazs AC, Singh C. Polym Int 2000; 49:469.
143. Manias E, Chen E, Krishnamoorthi R, Genzer J, Kramer EJ, Giannelis EP. Macromolecules 2000;33:7955.
144. Ginsburg VV, Balazs AC. Adv Mater 2000;12:1805.
145. Hackett E, Manias E, Giannelis EP. J Chem Phys 1998;108:7410.
146. Hackett E, Manias E, Giannelis EP. Chem Mater 2000;12:2161.
147. Anastasiadis SH, Karatasos K, Vlachos G, Manias E, Giannelis EP. Phys Rev Lett 2000;84:915.
148. Zax DB, Yang DK, Santos RA, Hegmann H, Giannelis EP, Manias E. J Chem Phys 2000; 112:2945.
149. Manias E, Kuppa V. In Vaia RA, Krishnamoorthi R Eds ACS symposium series 2002;804:193.
150. Kuppa V, Manias E. Chem Mater 2002;14:2117.
151. Kuppa V, Manias E. Colloids Surf A 2001;187:509.
152. Luo JJ, Dannial IM. Compo Sci Technol 2003;63:1607.
153. Komarneni S. Mater J Chem 1992;2:1219.
154. Giannelis EP. Adv Mater 1996;8;29.
155. Messermith PB, Giannelis EP. Chem Mater 1993;5:1064.
156. Ruiz –Hitzky E. Adv Mater 1993;5:334.
157. Kickelbick G. Prog Polym Sci 2003;28;83.
158. Yano K, Usuki A, Okada A, Kurauchi T, Kamigaito O. J Polym Sci Part A: Polym Chem 1993;31:2493.
159. Kojima Y, Usuki A, Kawasumi M, Okada A, Fukushima Y, Kurauchi T, Kamigaito O. J Mater Res 1993;8:1185.

160. Wang MS, Pinnavaia TJ. Chem Mater 1994;6:468.
161. Usuki A, Kojima Y, Kawasumi M, Okada A, Kurauchi T, Kamigaito O. J Mater Res 1993;8;1179.
162. Kornmann X. Ph.D Thesis Lulea University of Technology, Sweden, March;2001.
163. Lan T, Pinnavaia TJ. Chem. Mater 1994;6:2216.
164. Ke Y, Long C, Qi Z J appl Polym sci 1999; 71:1139.
165. Okamoto M, Morita S, Taguchi H, Kim YH, Kotaka T, Tateyama H. polymer 2000; 41:3887.
166. Theng BKG. Formation and Properties of Clay- Polymer complexes, Elsevier, Amsterdam 1979;p 133.
167. Jeon HG, Jung HT, Hudson SD. Polymer Bull 1998; 41:107.
168. Vaia RA, Ishii H, Giannelis EP. Chem Mater 1993;5:1694.
169. Burnside SD, Giannelis EP. Chem Mater 1995;7:1596.
170. Vaia RA, Vasudevan W, Krawiee LG, Scanlon G, Giannelis EP. Adv Mater 1995;7:154.
171. Vaia RA, Giannelis EP, Jandt KD, Kramer EJ. Macromolecules 1995;28;8080.
172. Vaia RA, Giannelis EP, Jandt KD, Kramer EJ. Chem Mater 1996; 8:2628.
173. Vaia RA, Giannelis EP. Macromolecules 1997;30:7990.
174. Vaia RA, Giannelis EP. Macromolecules 1997;30:8000.
175. Krawiec W, Scanlon LG, Fellner JP, Vaia RA, Vasudevan S, Giannelis EP. Power Sources 1995;54:310.
176. Vaia RA, Sauer BB, Tse O, Giannelis EP. J Polym Phys 1997;35:59.
177. Hasegawa N, Kawasumi M, Kato M, Usuki A, Okada a. J Appl Polym Sci 1998;67:87.
178. Gunter M, Recichert P, Mulhaupt R, Gronski W. Polym Mater Sci Eng 2000;82:228.
179. Davis RD, Jarrett WL, athias L J Polym Mater Sci Eng 2000;82:272.

180. Vander Hart DL, Asano A, Gilman JW Chem Mater 2001;13:3781.
181. Krishnamoorti R, Vaia RA, Giannelis EP. Chem. Mater 1996;8:1728.
182. Pinnavaia TJ,Beall GW Eds Polymer clay nanocomposites.Wiely New York 2000.
183. Dennis HR, Hunter DL, Chang L, Kim S White JL Cho JW, Paul DR. Polymer 2001;42:9513.
184. Fornes TD, Yoon PJ, Keskkula H, Paul DR. Polymer 2001;42:9929.
185. Kawassumi M, Hasegawa N Kato M, Usuki A. Okda A Macromolecules 1997;30:6333.
186. Biswas M, Sinha Ray S. Adv Polym sci 2001; 155:167.
187. Karger-Kocsis J, Gryshuchuk O, Frohlick J, Mulhaupt R. Compos Sci Technol 2003;63:2045.
188. Karger-Kocsis J, Wu CM. Polym Eng Sci 2004;44;1083.
189. Roberts AD, Editor, Natural Rubber Science and Technology, Oxford science Publishers, Oxford 1990.
190. Karger-Kocsis J, Varghese S. J Appl Polym Sci 2004;91:813.
191. Madhusoodanan KN, Varghese S. J Appl Polym Sci 2006;102:2537.
192. Wu Y, Huang H, Zhao W, Zhang H, Wang Y. 2008;107:3318.
193. Wei- Gwo Hwang, Kung- Hwa Wei. Polym Eng Sci 2004;44:2117.
194. Stephan R, Alex R, Cherian T, Varghese S, Joseph K, Thomas S. J Appl Polym Sci 2006;101:2355.
195. Arroyo M, Lopez- Manchado MA, Herrero B. Polymer 2003 ;44 :2447.
196. Joly S, Garnaud G, Ollitrault R, Bokobza L. Chem Mater 2002 ;14 :4202.
197. Arroyo M, Lopez- Manchado MA, Herrero B, Biagiotti J. J Appl Polym Sci 2003;89:1.
198. Stephan R, Ranganathaiah C, Varghese S, Joseph K, Sabu T. Polymer 2006;47:858.
199. Okada A, Kawasumi A, Usuki A, Kojima Y, Kurauchi T, Kamigatio O. Mater Res Soc Proc 1990;171;45.

200. Varghese S, Karger- Kocsis Polymer 2003;44:4921.
201. Varghese S, Karger- Kocsis, Gatos KG. Polymer 2003;44:3977.
202. Yuhai S, Yuanfang L, Demin J. J Appl Polym Sci 2008;107:2786.
203. Lan L, Demin J, Yuanfang L, Baochun G. J Appl Polym Sci 2006 ;100 :1905.
204. Gatos KG, Karger- Kocsis. Polymer 2005;46:3069.
205. Neilson LE. J. Macromol sci Chem 1967 ;A15 :929.
206. Utracki LA, Simha R. Macromolecules 2004 ;37 :10123.
207. Messersmith PB, Giannels EP. J Appl Polym Sci Part A: Polym Chem 1995;33:1047.
208. Wang S, Long C, Wang X, Li Q, Qi Z. J Appl Polym Sci 1998;69;1557.
209. Tyan HL, Liu YC, Wei KH. Polymer 1999;40;4877.
210. Doo JG, Cho I. Polymer Bull 1998;41:511.

Chapter 2

Experimental techniques and materials used

The specifications of the materials and details of the experimental techniques used in this study are given in this chapter.

2.1 Materials

2.1.1 Natural rubber (NR)

The natural rubber used in this study was ISNR-5 of Mooney viscosity (ML 1+4,100˚C) 85, obtained from the Rubber Research Institute of India, Kottayam. The Bureau of Indian standards specifications for the grade of rubber are given in Table 2.1 [1].

Table 2.1. BIS specifications of ISNR-5

SI.No	Parameters	Limit
1	Dirt content, % by mass, max	0.05
2	Volatile matter, % by mass, max	0.8
3	Nitrogen, % by mass, max	0.6
4	Ash, % by mass, max	0.6
5	Initial plasticity, Po, Min	30
6	Plasticity retention index (PRI), min	60

Rubber from the same lot has been used for the experimental since it is known that the molecular weight, molecular weight distribution and non rubber constituents of natural rubber are affected by clonal variation, season, and use of yield stimulants and method of preparation [2].

2.1.2 Compounding ingredients

2.1.2.1 Vulcanizing agent

Sulphur was the vulcanizing agent used throughout the investigation. It was obtained from M/s Bayer India Ltd., Mumbai, India

2.1.2.2 Accelerators

(a) N-Cyclohexyl benzthiazyl sulphenamide (CBS)

It is a fast accelerator and was supplied by M/s Bayer India Ltd., Mumbai, India.

(b) Tetra methyl thiuram disulphide (TMTD)

TMTD is used as a secondary accelerator and was supplied by M/s Bayer India Ltd., Mumbai, India

(c) Zinc oxide and stearic acid

Zinc oxide and stearic acid are used as an activator and co-activator respectively. It was collected from M/s CDH chemicals, Mumbai, India.

(d) Diethylene glycol (DEG)

DEG is used as an activator and was obtained from M/s CDH chemicals, Mumbai, India.

2.1.2.3 Filler

Organoclay (Cloisite 30B)

Organoclay is montmorillonite which is organically treated with methyl, tallow, bis-2-hydroxyethyl, quarternary ammonium chloride collected from Southern Clay Products Inc., USA.

Quaternary ammonium salt with the following structure is used as the modifier for cloisite 30B clay

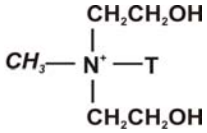

T : Tallow (~65% C18, ~30% C16, ~5% C14)

Anion : Chloride

MT2EtOH: methyl, tallow, bis 2 hydroxyethyl, quaternary ammonium

Table 2.2 Characteristics of Organoclay

Treatment/ Properties:	Organic modifier	Modifier concentration	% moisture	% Weight Loss on ignition	Layer distance
Cloisite®30B	MT2EtOT	90meq/100g clay	<2%	30%	18.5 A˚

2.1.3 Other chemicals

Toluene LR grade (E.Merck), maleic anhydride (MA) (Aldrich, 99% purity) and bromothymol blue (Sigma) were used.

2.2 Experimental methods

2.2.1 Preparation of maleic anhydride graft natural rubber (MA-g-NR)

MA-g-NR was prepared by the following procedure. NR was initially mixed with MA in a Brabender mixer at an rpm of 50 for 10minutes at 70^0C. This mix was then subjected to ^{60}Co gamma irradiation for a period of $1^1/_2$ hours for giving 2.5kGy in a gamma chamber. Trials were conducted by varying the radiation doses (0.5kGy, 2.5kGy, 5kGy, 7.5kGy and 10kGy). The maleic anhydride was

also added in various concentrations (1, 3, 5 and10). Grafted rubber was dissolved in 100ml of toluene at reflux temperature in order to separate unreacted MA. The polymer was then precipitated in acetone. Finally the recovered product was dried in a vacuum oven for 24hrs at 110^0 C.

2.2.2 Radiation grafting

Maleic anhydride mixed natural rubber was irradiated with gamma (γ) rays in a Gamma Chamber 5000 (figure 2.1). It is a compact self shielded cobalt-60 gamma irradiator providing an irradiation volume of approximately 5000cc. The material for irradiation is placed in an irradiation chamber located in the vertical drawer inside the flask. This drawer can be moved up and down with the help of a system of motorized drive, which enables precise positioning of the irradiation chamber at the center of the radiation field. Radiation field is provided by a set of stationary cobalt-60 sources placed in a cylindrical cage. The sources are doubly encapsulated in corrosion resistant stainless steel pencils and are tested in accordance with international standards. The samples were irradiated for different radiation doses at a dose rate of 2kGy per hour in air at room temperature.

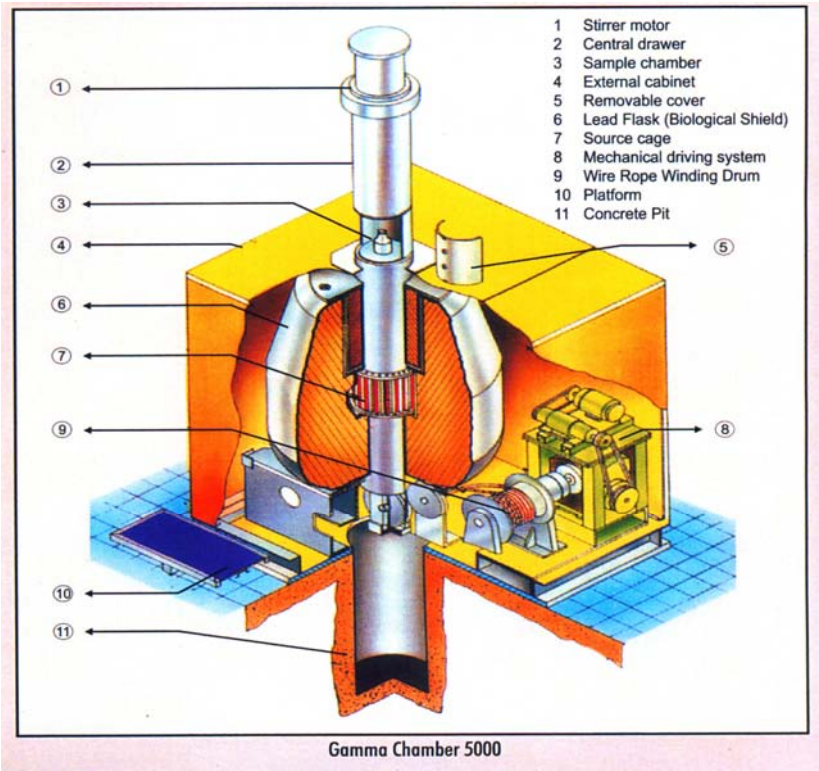

Figure 2.1 Gamma Chamber 5000

2.2.3 Characterization of MA-g-NR

2.2.3.1 Determination of grafting efficiency

The grafting efficiency (MA content in MA-g-NR) was determined by refluxing weighed amount of the grafted rubber in xylene saturated with water for 1hr to hydrolyze the anhydride and then titrating against a solution of 0.05N ethanolic KOH using 1% thymol blue as indicator [3]. The grafted MA content was calculated using the following equation: [4]

$$MA\ (wt\ \%) = [(N \times V \times 98)/ (2xW)]\ x100\ \% \qquad (2.1)$$

where N and V are respectively the concentration (mol/l) and volume (l) of potassium hydroxide-methanol standard solution and W is the weight (g) of the MA-g- NR sample.

2.2.3.2 FTIR spectroscopy

The FTIR spectra were recorded on a Bruker Tensor 27 IR spectrometer from 4000cm^{-1} to 400cm^{-1} with a 0.5cm^{-1} resolution and 14 scans were performed for each sample. Different functional groups and structural features in the molecules absorb energy at characteristic frequencies. The frequency and intensity of absorption are the indication of the bond strength and structural geometry in the molecule. A sample of maleated elastomer was extracted with diethyl ether for 24hrs to remove unreacted maleic anhydride. IR spectra of the sample after soxhlet extraction were recorded.

2.2.4 Mixing and homogenization of rubber clay nanocomposites

Incorporation of clay into maleated rubber was carried out by choosing an appropriate recipe and the mixing was carried out in a Brabender Plasticorder. It is a torque rheometer which is widely used for mixing, blending and to study processability of polymers such as mixing and extrusion and evaluation of the rheological properties of polymer melts [5]. It is used to measure the torque generated due to resistance offered by the material to mastication or flow under preselected conditions of shear and temperature. The heart of the torque rheometer is a jacked mixing chamber with horizontal rotors connected to a shaft. The volume of the chamber is approximately 40cm^3 for the model used (PL 3S). The resistance due to the mixing of the test material within the mixing chamber is measured with the help of dynometer balance. A dc thyrister controlled drive is used to control the speed of rotation of the rotors. The temperature of the mixing chamber can be varied up to 30^{0}C which can be controlled and measured with the aid of a temperature controller and a recorder. Different types of rotors can be employed depending upon the nature of the polymer used. After selecting the

temperature and the rotor speed, the rubber was charged into mixing chamber. When the nerve of the rubber had disappeared, compounding ingredients were added as per the sequence given in ASTM D 3182 (1982). Mixing was carried out at 60^0C and at rpm speed. Homogenization of the compound was carried out using a laboratory (15x 33cm) two roll mill at a friction ratio 1:1.25. The temperature of the roll was maintained at 60^0C and the compound was homogenized by passing the compound several times through the tight nip and finally made into a sheet at a nip gap of 3mm.

2.2.5 Determination of cure characteristics of the compounds

Cure characteristics of the mixes were determined as per ASTM D 2084-1995 using Rubber Process Analyser (RPA 2000-Alpha Technologies). It uses two directly heated, opposed biconical dies that are designed to achieve a constant shear gradient over the entire sample chamber. The sample of approximately 5g was placed in the lower die that oscillated through a small deformation angle (0.2^0) at a frequency of 50cpm. The torque transducer on the upper die senses the force being transmitted through the rubber. The torque was plotted as a function of time and the curve was called a cure graph. The important data that could be taken from the torque-time curve were minimum torque (M_L), maximum torque (M_H), and scorch time (T_{10}), optimum cure time (T_{90}) and cure rate. Optimum cure rate corresponds to achieve 90 percent of the cure calculated using the equation 2.2 [6].

Optimum cure time = time to achieve a torque of $0.9 (M_H-M_L) + M_L$ (2.2)

Cure rate index was calculated from the cure graph using equation 2.3

Cure rate index = $100/ t_{90} – t_2$ (2.3)

where t_{90} and t_2 are the times corresponding to the optimum cure and two units above minimum torque respectively.

2.2.6 Moulding of test specimens

Vulcanization of various test samples was carried out in an electrically heated hydraulic press having 45cm x 45cm platen at 150^0C at a pressure of 200kg/cm^2 on the mould up to optimum cure times. Moulded samples were conditioned for 24hrs before testing. For samples having thickness more than 6mm (compression set, abrasion resistance etc) additional curing time based on the sample thickness was given to obtain satisfactory moulding.

2.3 Tests on vulcanizates

For the tests described below at least three specimens per sample were tested for each property and mean values are reported.

2.3.1 Modulus, tensile strength and elongation at break

Tensile properties of the nanocomposites were determined according to ASTM D 412 (1980) using dumbbell specimens on a Shimadzu Universal Testing Machine (model-AG1) with a load cell of 10kN capacity. All the tests were carried out at ambient temperature. Samples were punched out from compression moulded sheets along the mill direction using a dumbbell die. A bench thickness gauge was used to measure the thickness of the narrow portion. The sample was held tight by the two grips, the upper grip of which was fixed. The gauge length between the jaws at the start of each test was adjusted to 30mm and the rate of separation of the power actuated upper grip was fixed at 500mm/min for elastomeric specimens. The tensile strength, elongation at break and modulus were evaluated and printed out after each measurement by the microprocessor. The modulus and tensile strength are reported in mega Pascal (Mpa) unit and elongation at break in percentage (%).

2.3.2 Tear resistance

Tear resistance of the samples was tested as per as ASTM D 624-1998, using unnicked 90^0 angle test specimens that were punched out from the moulded sheets, along the mill grain direction. The measurements were carried out at a crosshead speed of 500mm/m on a Shimadzu Model AG1 Universal Testing Machine according to ASTM standards, D 412-68 and D 624-54 respectively. The tear strength was reported in N/mm.

2.3.3 Hardness

The hardness of the moulded samples were tested using Zwick 3114 hardness tester in accordance with ASTM D 2240 (1981). The tests were performed on mechanically unstressed sample of 12mm diameter and 6 mm thickness. A load of 12.5Newton was applied and the readings were taken 10seconds after the intender made firm contact with the specimen. The mean value of three measurements is reported. The hardness values are reported in Shore A unit.

2.3.4 Compression set

The samples (6.5mm thick and 18mm diameter) in duplicate, compressed to constant deflection (25%) were kept 22hrs in an air oven at 70^0C. After the heating period, the samples were taken out, cooled to room temperature for half an hour and the final thickness was measured. The compression set was calculated using equation 2.4.

$$\text{Compression set (\%)} = \frac{(t_i - t_f)}{(t_i - t_s)} x100 \qquad (2.4)$$

where t_i and t_f are the initial and final thickness of the specimen respectively and t_s, thickness of the spacer bar used. The procedure used was ASTM D 395 (1982) method B.

2.3.5 Abrasion resistance

The abrasion resistance of the samples was measured using a DIN abrader. Sample having a diameter of 15mm and a length 20mm was kept on a rotating sample holder and 10Newton load was applied. Initially a pre-run was given for the sample and its weight was taken. The sample was then given a complete run and weight after final run was also noted. The difference in weight is the abrasion loss. It is expressed as the weight of the test piece getting abraded away by its travel through 42cm on a standard abrasive surface and expressed as the weight loss in gram (g). The abrasion loss was calculated using the equation 2.5,

$$V = \Delta m/\rho \qquad (2.5)$$

Where Δ m is the mass loss, ρ is the density of the sample and V is the abrasion loss in mm^3.

2.3.6 Rebound resilience

The rebound resilience of the samples was determined as per ASTM D 1054 (1974) using Scott Rebound Pendulum. This test is used for the determination of impact resilience of solid rubber from measurement of vertical rebound of a dropped mass. Resilience is determined as the ratio of rebound height to drop height of a metal plunger of prescribed weight and shape, which is allowed to fall on the rubber specimen. Resilience is a function of both dynamic modulus and internal friction of rubber. The test specimen should have a thickness of 12.5mm and the standard temperature is 23 ± 2^0C. Resilience is tested as follows. The instrument is leveled and the plunger is raised to the top of the guide rod. The resilience scale is positioned so that its full weight rests upon the specimen. It is locked in that position. The plunger is then released making sure it slides freely on its guide. The first three values are avoided. Record the next three values. Since the resilience scale is divided into 100 parts, the rebound height is equal to

the resilience in percentage. The rebound resilience was calculated as using the equation 2.6

$$\text{Rebound resilience \%} = \frac{1-\cos\theta_2}{1-\cos\theta_1} \times 100 \qquad (2.6)$$

where θ_1 and θ_2 are initial and rebound angles respectively, θ_1 was 45^0 in all cases.

2.3.7 Strain sweep studies

The stain sweep measurements on unvulcanized samples were conducted to study the rubber-filler interaction. Rubber Process Analyser (RPA 2000- Alpha Technologies) is a purposely modified commercial dynamic rheometer [7]. Such instrument was modified for capturing strain and torque signals, through appropriate software. Filled rubber compounds exhibit strong non-linear viscoelastic behaviour, the well- known Payne effect, i.e. the reduction of elastic modulus with increasing strain amplitude [8]. RPA can do strain sweep tests in which the variation of storage modulus (G'), loss modulus (G") and complex modulus (G*) with change in strain amplitude are measured. With respect to its measuring principle, the RPA cavity must be loaded with a volume excess of test material. In agreement with ASTM 5289, the manufacturers recommends to load samples of about 5.0g i.e.4.4cm^3 for a standard filled rubber compound with a specific gravity of 1.14g/cc. Samples for RPA testing were consequently prepared by die cutting 46mm diameter disks out of around 2mm thick sheets of materials. The testing temperature was selected as 100^0C; a temperature below the curing temperature and the shear strain was varied from 0.5% to 100% keeping the frequency measurements at 0.5Hz.

2.3.8 Dynamic mechanical analysis (DMA)

DMA works by applying an oscillating force to the material and the resultant displacement of the sample is measured. From this, the stiffness can be determined and tan δ can be calculated. Tan δ is the ratio of the loss component to the storage component. By measuring the phase lag in the displacement compared to the applied force it is possible to determine the damping properties of the material. Tan δ, storage modulus and loss modulus are plotted against frequency and clay loading. The dynamic mechanical thermal analysis was conducted using rectangular test specimens having a dimension of 30mm x 5mm x 2mm were tested under tension mode using a TA Instruments DMA Q-800 at a constant temperature of 60^0C. The frequency was varied from 1 to 50Hz under frequency sweep mode at a rate of 2Hz/min. The samples were subjected to dynamic tension strain amplitude of 0.1146 %.

2.3.9 Air permeability

The instrument consists of a gas cell divided into two chambers by the membrane to be tested. The gas under test is admitted at known pressure from one side. The permeability can be studied either by measuring the pressure decrease at the high pressure side or the pressure increase at the low pressure side. A highly sensitive heat conductivity cell with temperature compensation of the signal to standard conditions, a chart recorder, a water cooling/heating thermostat for maintaining constant temperature in the measuring chamber and a rotatory two stage vacuum pump are the remaining portions of the measuring instrument. Permeability measurements were carried out according to ASTM D 1434 (1982). Test specimens of thickness 0.25mm were moulded and used for measurements. The equipment used was Lyssy Manometric Gas Permeability Tester L 100-2402.

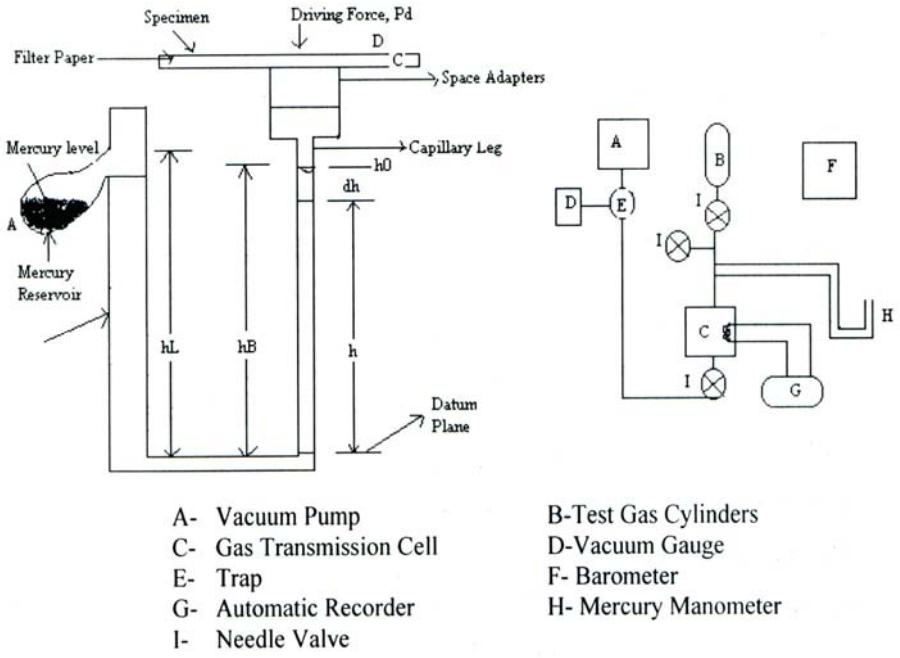

Figure 2.2 Experimental set up of gas permeability tester

The prepared film was used to divide the cell of the apparatus into chambers and air at a flow rate of 500ml/min was admitted from the upper compartment. The lower compartment was connected to a suction pump through a capillary U tube. The conditioning of the test specimen for a definite period is calculated from the equation 2.7.

$$T=b^2/2D \qquad (2.7)$$

where b is the thickness of the test piece in meter and D, the diffusion coefficient in meter square per second. The preconditioning times will vary from few minutes to several hours and even days depending on the type of the samples. In practice the preconditioning time is the time taken for attaining 10^{-4}torr pressure in the lowest compartment. Then mercury is poured into the capillary to a fixed mark. The level of mercury in the capillary steadily decreases as the air permeates through the membrane. This change is recorded in a chart moving at a

speed of 180cm/hour. From the distance traveled by the pointer in the chart, the time taken for the permeance of the sample (t_s) is determined. Permeability of the sample is then calculated by substituting the time taken by the standard PET sample (t_r) in the above chamber and under similar conditions using the equation 2.8.

$$\text{Permeability of the sample} \quad P_m = \frac{T_r \times P_r}{t_m} \tag{2.8}$$

where P_r is the permeability of the standard PET sample. If air is used the value of P_r is 30ml/m^2. day.

2.3.10 Heat build up

The Ektron flexometer conforming to ASTM D 623-1999 was used for measuring the heat build-up. A cylindrical sample of 25mm in height and 19mm in diameter was used for test. The oven temperature was maintained at 100^0C. The samples were placed in the preconditioning oven for 20minutes at 100^0C. Preconditioning the test samples were subjected to a flexing stroke of 4.45mm under a load of 10.9kg and the temperature rise at the end of 20minutes was taken as the heat build up.

2.3.11 Crosslink density and swelling studies

The crosslink density of vulcanized samples was determined by the equilibrium swelling method and using Florey-Rehner equation [9]. Approximately 0.3g samples were accurately weighed and kept in toluene solvent taken in an airtight container for 24hrs. The surface of the swollen samples was then gently wiped using filter paper and weighed. The samples were placed again in the solvent and weights were recorded at regular intervals, usually one hour, till equilibrium

weight was obtained. The swollen samples were heated at 60^0C for 24 hrs in an oven to remove the solvent. The deswollen weight was then determined. The volume fraction of rubber in the deswollen network was then calculated using the equation 2.9.

$$V_r = \frac{(D-FT)\rho_r^{-1}}{(D-FT)\rho_r^{-1} + A_0\,\rho_s^{-1}} \qquad (2.9)$$

where T = weight of test specimen, D = deswollen weight, F = weight fraction of insoluble component, A_0 = weight of the absorbed solvent corrected for the swelling increment,

ρ_r = density of the test specimen, ρ_s = density of the solvent.

A Swelling in toluene

In order to analyze the interaction between the components of the system, equilibrium swelling studies were carried out in toluene. Circular specimens of diameter 20mm were punched from the vulcanized elastomer sheet and were allowed to swell in toluene at room temperature. At different intervals, the amount of solvent entering the sample was assessed gravimetrically until equilibrium was reached, as evidenced by the constant weight of the sample. The mole% uptake of the solvent was calculated using the equation 2.10 [10].

$$Qt = \frac{\left[\frac{M_{c(m)}}{M_{r(m)}}\right]\times 100}{M_{i(s)}} \qquad (2.10)$$

where $M_c(m)$ is the mass of solvent at a given time, $M_r(m)$ is the molecular weight of the solvent and $M_i(s)$ is the initial weight of the specimen. At equilibrium swelling, Q_t was taken as Q_∞, the mole% uptake at infinite time. Sorption curves were obtained by plotting mole% uptake against square root of time. The effective diffusivity, D of the elastomer-solvent system was calculated from the initial portion of the sorption curves using the equation 2.11.

$$D = \pi \left[\frac{h\theta}{4Q_\infty} \right]^2 \qquad (2.11)$$

where θ is the slope of the initial portion of the sorption curve. Another parameter called sorption coefficient was calculated from the equilibrium swelling using the equation 2.12.

$$S = \frac{M_\infty}{M_0} \qquad (2.12)$$

where M_∞ is the mass of the penetrant sorbed at infinite time and M_0 is the initial weight of the polymer sample. Sorption coefficient describes both initial penetration and dispersal of the penetrant molecules into the elastomeric network.

The permeation coefficient which is a characteristic parameter reflecting the collective processes of diffusion and sorption was calculated using the equation 2.13 [11].

$$P = DS \qquad (2.13)$$

B Swelling in oils

The percentage weight change of the nanoclay filled composites in different oils was studied by swelling a cut sample in oil for constant weight. The swelling characteristics was determined as a change in weight calculated using equation (2.14)

$$\text{Change in weight (\%)} = \frac{W_t - W_0}{W_o} \times 100 \qquad (2.14)$$

where W_t is the weight after immersion and W_o is the original weight.

2.3.12 Thermal analysis

Thermogravimetric analysis

The thermogravimetric analyzer used for the studies was TGA Q-50 (TA Instruments). It is a computer-controlled instrument that permits the measurement of weight changes in the sample as a function of temperature or time. It is programmed in the required temperature range to measure the weight change resulting from chemical reaction, decomposition, solvent and water evolution, Curie point transitions and oxidation of the sample materials. The temperature is scanned at a linear rate. The instrument has two components, an ultra sensitive microbalance and a furnace element. The balance is sensitive to 0.1 microgram and the furnace could be heated from ambient to 800^0C at rates of 0.1 to 200^0C per minute. For purging platinum the sample holder, nitrogen gas is used so as to study the oxidation, burning and thermal stability of the materials. The purge gas flows directly over the sample. The recommended flow rate of the sample purge was kept less than the flow rate of the balance purge at all times.

Evaluation of kinetic parameters

The TGA data can also be used for studying the kinetics of decomposition, which provide an insight into the thermal stability of polymeric materials. There are many proposed methods to calculate the kinetic parameters of decomposition and the reported values depend not only on the experimental conditions, but also on the mathematical treatment of data.

Formulation of the rate equation

For many kinetic processes, rate of reaction may be expressed as a product of a temperature dependent function; *k(T)*, and a composition- or conversion-dependent term; *f(X)*:

$$r = dX / dt = k(T) f(X) \qquad (2.15)$$

where T is absolute temperature in Kelvin; X is conversion i.e. weight of polymer volatilized/initial weight of polymer and r is the rate of change of conversion or composition per unit time; t. The temperature dependent term in equation (2.15) is the reaction rate constant, which is assumed to obey the usual Arrhenius relationship:

$$k(T) = A \exp(-E_a / RT) \qquad (2.16)$$

where E_a is the activation energy of the kinetic process, A is the pre-exponential factor and R is the universal gas constant. The conversion-dependent function; $f(X)$, is generally very complicated. A particular term is usually valid only for a limited range of experimental conditions. If it is assumed that a simple n^{th} order kinetic relationship holds for the conversion-dependent term such that:

$$f(X) = (1-x)^n \qquad (2.17)$$

and that the quantity $(1-x)$ can be replaced by W, the weight fraction remaining in a TGA run, then:

$$r = dW / dt = AW^n \exp(-E_a / RT) \qquad (2.18)$$

$$\ln r = \ln(-dW / dt) = \ln A + n \ln W - E_a / RT \qquad (2.19)$$

Published methods of deriving the kinetic parameters from TGA data center about equation (2.19). They may be either differential i.e. involving the derivative term; $-dW/dt$ or integral i.e. based upon an integration of equation (2.19). The emphasis in these methods is on finding a way of plotting the data to

provide a rapid visual assessment of the order of the reaction and its activation energy.

Differential method for determining rate equation parameters

The difference form of equation (2.19) at different temperatures is:

$$\Delta \ln r = \Delta \ln(-dW / dt) = n\Delta \ln W - (E_a / R)\Delta(1/T) \tag{2.20}$$

Dividing (2.20) by Δ *(1/T)* gives

$$\left[\Delta \ln r / \Delta(1/T)\right] = n\left[\Delta \ln W / \Delta(1/T)\right] - (E_a / R) \tag{2.21}$$

A plot of *[*Δ *ln r/*Δ*(1/T)]* against *[*Δ *ln W/*Δ*(1/T)]* should be a straight line with slope equal to the order of reaction; *n*, and an intercept of $-E_a/R$.

Dividing (2.20) by Δ *ln W* gives

$$\Delta \ln r / \Delta \ln W = n + E_a\left[-\Delta(1/T) / R\Delta \ln W\right] \tag{2.22}$$

A plot of [Δ *ln r /*Δ *ln W]* versus *[-*Δ*(1/T)/R*Δ*ln W]* should also be a straight line of slope E_a and an intercept *n*. These two methods are generally attributed to Freeman and Carroll [12]. In spite of its limited precision, it is quite convenient for processing the acquired TGA data. This method may be used to obtain a rapid but rough estimate of the kinetic parameters when a limited number of data points are available.

Integral method

The integral methods involve the integration of equation (2.15) by separation of variables. By substituting equation (2.16) into this expression and defining $\beta = (dT/dt)$ as the heating rate, the following is obtained:

$$F(X) = \int_0^X dX \;/\; f(X) = \int_{T_0}^{T} (A/\beta)\exp(-E_a / RT)dT \qquad (2.23)$$

where T_0 is the initial temperature in the TGA analysis and T is the final temperature. For a constant heating rate β and if $T_0 \approx 0$, equation (2.23) becomes:

$$F(X) = (A/\beta)\int_0^T \exp(-E_a / RT)dT \qquad (2.24)$$

The different integral methods involve an approximation to the right-hand integral term in equation (2.24).

Among the integral methods, the Coats and Redfern approach [13] seems to be the most suitable from a practical point of view and is preferred over others and is applied here. The activation energy and the order of reaction were evaluated utilizing this equation for reaction order $n \neq 1$, which when linearized for a correctly chosen n yields the activation energy from the slope.

$$\log\left[1-(1-a)^{1-n} / T^2(1-n)\right] = \log\left[AR/\beta E\right] - E/2.303\,RT \qquad (2.25)$$

where α is the fraction decomposed, T is the temperature (K), n is the order of reaction, A is the Arrhenius constant, R is the universal gas constant, E_a is the activation energy and β is the heating rate. The plot of the left hand side of the equation (Y) against $1/T$ should be a straight line with slope = $-E_a/(2.303R)$ for the correct value of n.

Differential scanning calorimetry

The differential scanning calorimetry of maleated natural rubber gum and nanoclay loaded samples were recorded with a differential scanning calorimeter Q-100, TA instruments. The energy changes associated with transitions were recorded in a temperature range of -60 to 100^0C. Samples of known weight

encapsulated in standard aluminium pans placed in the sample holder were subjected to the analysis.

2.3.13 Thermal ageing studies

Tests were carried out as per ASTM D 573-1999 [6]. Specimens of vulcanized rubber were exposed to the deteriorating influence of air at specified elevated temperature in an air oven, for known periods of time, after which their physical properties determined. These were compared with the properties determined on the original specimens and the changes noted.

2.3.14 Ozone resistance

The ozone test chamber manufactured by MAST Development Company, USA was used to study ozone cracking as shown in figure 2.3. The chamber provided an atmosphere with a controlled concentration of ozone and temperature. Ozone concentration selected was 50pphm, which is generated by an UV quartz lamp.

The test was carried out as per ASTM D 1149-99 specifications at 38.5^0C. B type specimens were tested in duplicate and in the form of a bent loops. Rectangular strip of length 95mm, breadth 25mm and thickness 2 ± 0.2mm cut with the grain in the length direction from tensile sheets were folded and tied at 25mm length from the edges to get the required strain (20%). These were then conditioned for 24hrs. The conditioned samples were exposed to the ozonized air in the chamber. Periodic observations of the surface of the samples were made for crack initiation. Samples were exposed for longer time. Surfaces of the irradiated samples were scanned on a macro viewer of LEICA Q 500 IW image analyzer, images were acquired and the photo prints were taken.

Figure 2.3 Ozone chamber

2.3.15 Exposure to gamma radiation

Dumbbell shaped tensile test samples of 2 ± 0.2mm thickness were irradiated with gamma (γ) rays in a Gamma Chamber 5000 (figure2.1). The samples were irradiated for different radiation doses at a dose rate of 2kGy per hour in air at room temperature. The tensile strength was measured before and after irradiation and the percentage retention was calculated.

2.3.16 Dielectric measurements

Circular specimens of maleated rubber nanocomposite were used. The test samples were placed in between copper wires and are fixed on both sides of the

samples as electrodes. The capacitance, resistance and dielectric loss factor were measured in alternating current at room temperature using HP 4285 A LCR Hitester by varying the frequencies (0.1-8 MHz).

2.3.17 Test for Flammability

Flame resistance of vulcanisates of maleated natural rubber clay nanocomposites were evaluated as per UL 94 overview-test for flammability [14] of plastic materials for parts in devices and appliances. Method 94V, used for vertical burn test was applied. The test specimens were (strips of 12mm x 100mm and thickness 2.0mm cut from molded vulcanizates) held at one end in the vertical position. A burner flame was applied to the free end of the specimen for two ten seconds intervals, separated by the time it take for flaming combustion to cease after the first application. Two sets of three specimens were tested. The following were noted for each specimen.

Duration of flaming combustion after the first burner flame application.
Duration of flaming combustion after the second burner flame application.
Duration of glowing combustion after the second burner flame application.
Whether or not flaming drips ignite cotton placed below specimen.
Whether or not specimen burns up to holding clamp.

2.3.18 TEM analysis

The transmission electron microscopy was performed using a JEOL, JEM -2010 (Japan), TEM operating at an accelerating voltage of 200kV. The composite samples were cut by ultra-cyromicrotomy using a Leica Ultracut UCT. Freshly sharpned glass knives with cutting edge of 45^0 were used to get the cryosections of 50-70nm thickness. Since these samples were elastomeric in nature, the temperature during ultra cryomicrotomy was kept at -50^0C (which was will below the glass transition temperature of EVA) [15]. The cryosections were collected individually on sucrose solution and directly supported on copper grid of 300-mesh size.

2.3.19 X-ray diffraction technique (XRD)

X-ray diffraction (XRD) was used to study the nature and extent of dispersion of the clay in the nanocomposite. XRD patterns were obtained using Bruker, D8 advance diffractometer at the wavelength CuK_{α} =1.54^0, a tube voltage of 40kV and tube current of 25mA. Bragg's law defined as $n\lambda = 2d\sin\theta$, was used to compute the crystallographic spacing (d) for nanoclay. The samples were scanned in step mode by 1.0^0/min, scan rate in the range of 2 to 12^0.

The principle of X-ray diffraction technique is given in figure 2.4

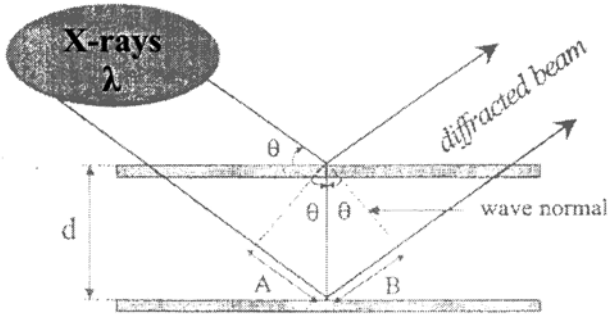

Figure 2.4 Principle of X-ray diffraction techniques

The diffraction from two consecutive silicate layers that are separated by a distance d and the intercept X-rays of wavelength λ at an incident angle θ. The experimental 2θ values are the angle between the diffracted and incoming X- ray waves. The change in d spacing of the rubber nanocomposites is observed from the peak position in the XRD graphs in accordance with the Bragg equation 2.26

$$n\lambda = 2d\sin\theta \qquad (2.26)$$

where n is the integer, λ is the wavelength and θ is the incident angle.

References

1. Babu PSS, Gopalakrishnan KS Jacob J. In: Natural Rubber: Agro mannagment and Crop Processing. Eds. George PJ, Jacob CK. Rubber Research Institute of India, Kottayam 2000; Ch. 24:434.
2. Subramanyam A. Proc. of R.R.LM. Planter's Conference 1971;Kuala Lumpur :255.
3. Gaylord N, Mehta M, Mehta R. Am. Che. Soc. Symp. Ser 1988;364:438.
4. Li HM, Chen HB, Shen ZG, Lin S. Polymer 2002;20:5455.
5. Lee GCN, Purdon JR. Polym Eng Sci 1969;9:360.
6. Annual Book of ASTMM Standards, 2000.
7. Jean L. Leblanc, Marie Cartault. J Appl Polym Sci 2001;80:2093.
8. Payne AR, Whittaker WE. Rubber Chem Technol 1971;44:440.
9. Blow CM, Hepburn C. Rubber Technology and Manufacture, 2nd Edn., Butterworth Publication1985.
10. Mathew G, Singh RP, Nair NR,Thomas S. Journal of Materials Science 2003;38:2469.
11. Harogoppad SB, Aminabhavi TM. Macromolecules 1991;24:2595.
12. Freeman ES, Carroll B. J Phys Chem 1958; 62:394.
13. Coats AW, Redfern JP. Nature 1964;201:68.
14. UL 94 Overview, Test for Flammability of Plastic Materials for Parts in Devices and Applications, U.K, Inc.
15. Hiroshi J, Spontak RJ. Polymer 2009;50:1067.

Chapter 3

Grafting of maleic anhydride onto natural rubber by gamma radiation

Grafting of polymeric materials under the influence of ionizing radiation has been known since the middle of the twentieth century as a versatile method for polymer modification [1-9]. Among other methods, radiation grafting has been considered for a longtime for the preparation of polymer electrolyte membranes for electrochemical applications [10].

Graft copolymers of maleic anhydride with synthetic and natural polymer have been widely studied in recent years. The copolymer products have been used extensively in the area of polymer reactive blending, as the main blend components [11-19], blend compatibilizers [12, 20-22, 23] or composite matrices [24]. Thermoplastic materials such as polypropylene [19,20,23,24,25,26] polyethylene [19,21,22,27,28,29] polystyrene [11,18] and polyester [30] are widely used as backbones of the graft copolymer. However, elastomeric backbones such as EPDM [14] EPR [11, 13, 15] and NR [12,16,17, 31-34] have also been studied. The graft copolymer of maleic anhydride onto the natural rubber molecules was generally carried out in the molten state [12,16,17]. The initiation system used in the graft copolymerization of MA onto NR was peroxide initiator [33] or the shearing action [12,16,17, 33,34] of the materials in an internal mixer at high temperature. Graft copolymer of MA onto the NR has also been prepared in the solution state [31,32]. However, there have been very limited data on preparation methods and material properties obtained from this technique. Natural rubber (STR 5L) was used as a polymer backbone for the grafting reaction with maleic anhydride in toluene solution.

Grafting with various functional monomers has been used as an effective tool for producing modified rubber with superior properties. Grafted rubber can be produced by chemical route or using gamma radiation (γ-ray). The chemical route is done in presence of peroxides. Irradiation of natural rubber swollen with methyl methacrylate was investigated by Angier and Turner [35]. A study on acrylonitrile graft NR prepared by γ-ray initiation was also reported [36]. Other functional monomers such as acrylic acid, methacrylic acid, glycidyl methacrylate sulfonic acid have also been successfully used for grafting modifications of natural rubber and olefins [37].

In this chapter the production of maleic anhydride grafted natural rubber (MA-g-NR) using gamma radiation and its characterization are proposed to be investigated.

3.1 Experimental

3.1.1 Preparation of MA-g-NR

Maleic anhydride grafted natural rubber (MA-g-NR) was prepared by the following procedure. NR was initially mixed with MA in a Brabender Plasticorder at 50rpm for 10 minutes at 70^0C**.** The mix was then subjected to ^{60}Co gamma irradiation for a period of 1½ hours in the gamma chamber. Trials were conducted by varying the radiation doses (0.5kGy, 2.5kGy, 5kGy, 7.5kGy and 10kGy) and maleic anhydride concentrations (1, 3, 5 and 10 percentage by weight). After irradiation, the unreacted MA was separated by dissolving the reaction products in toluene at reflux temperature and then precipitating the polymer by adding acetone. This was repeated until the recovered product was free from residual MA. The product was finally dried in a vacuum oven for 24hrs at 110^0C.

3.1.2 Maleic anhydride grafted natural rubber (MA-g-NR)

MA grafting reaction can be described as

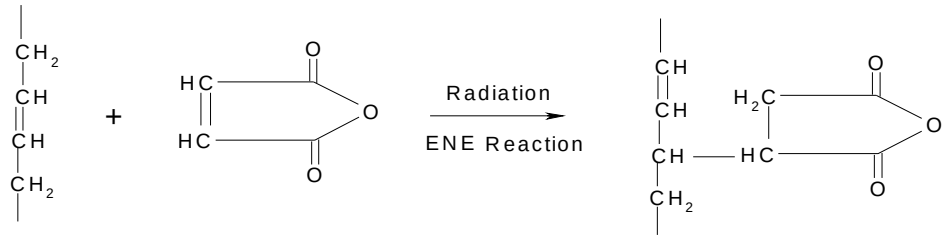

3.1.3 Characterization of MA-g-NR

3.1.3.1 Determination of grafting efficiency

The grafting efficiency was determined by titration method.

3.1.3.2 FTIR spectra

FTIR spectra are used for identifying the functional groups in maleated rubber.

3.1.3.3 Differential scanning calorimetry (DSC)

Grafting has been further confirmed from DSC data.

3.2 Results and discussion

3.2.1 Effect of radiation dosage on grafting efficiency

Figure 3.1 shows the variation of grafting efficiency (MA content) of MA-g-NR with different radiation dosages for 4.2% MA mixed NR. It can be seen that the MA grafting reaction is very much depended on the radiation dosage. The MA content increased sharply at radiation dose of 2.5kGy and then decreased on increasing the dose.

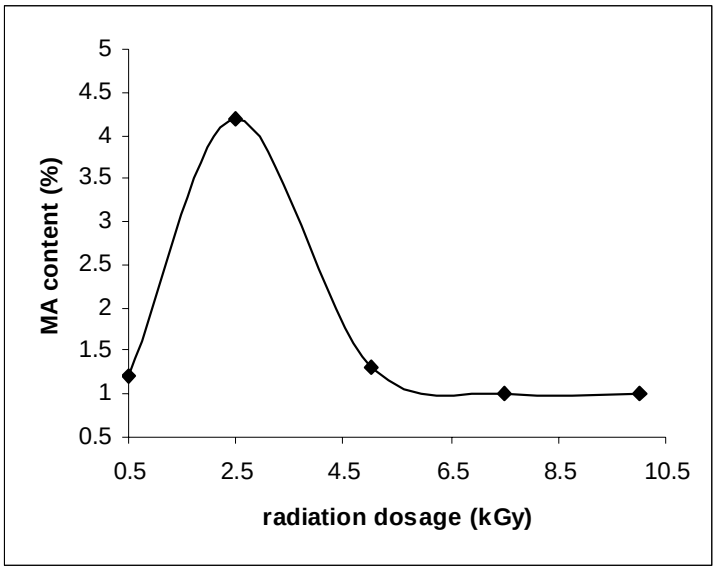

Figure3.1 Variation of MA content with radiation dose

The variation in the MA content with irradiation dose was also confirmed from the FTIR spectra of the grafted samples. Figure 3.2 shows the IR spectra of the pristine and maleated NR at different radiation dosages. In maleated rubber, the additional peak at 1738cm^{-1} which corresponds to the typical C=O stretching of anhydrides. The peaks at 1452cm^{-1} and 1375cm^{-1} correspond to the aliphatic CH_2 bending vibrations in NR. The peak at 800cm^{-1} corresponds to the CH_2 rocking. A comparison of the relative intensity of the peak at 1738cm^{-1} indicates that maximum grafting takes place at irradiation dose of 2.5kGy.

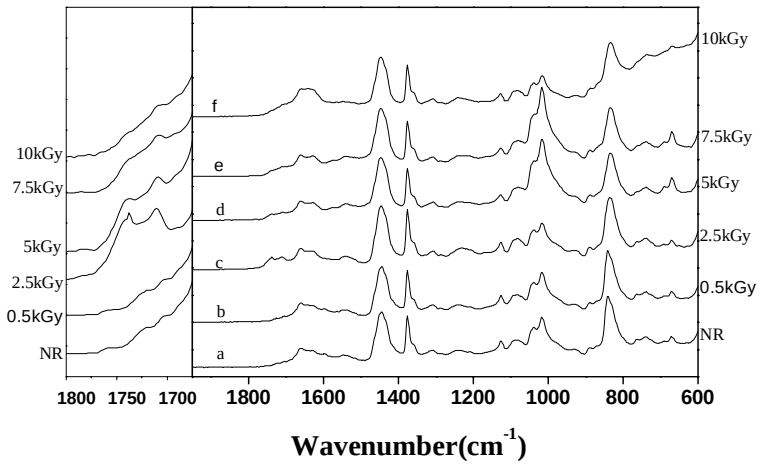

Figure 3.2 FTIR spectra of pristine and maleated NR.

The grafting of MA on NR takes place by ENE reaction [38, 39]. The joining of a double or triple bond to an alkene reactant having transferable allylic hydrogen is called ENE reaction. The reaction is reversible and the reverse is called retro-ENE reaction. In the present system, ENE reaction is promoted by irradiation dosage below 5kGy whereas the retro-ENE reaction becomes predominant at higher dosages.

3.2.2 Effect of MA concentration on grafting efficiency

Keeping 2.5kGy as the optimum radiation dosage for grafting, the grafting efficiency was also found to increase with MA concentration in the reaction mixture. Figure 3.3 shows the variation of MA content in MA-g-NR with MA concentration in the reaction mixture using the titration method according to the equation 2.1 in Chapter 2. The MA content proportionately increased from 0.7 % to 9.1 % on increasing the MA concentration from 1% to 10%.

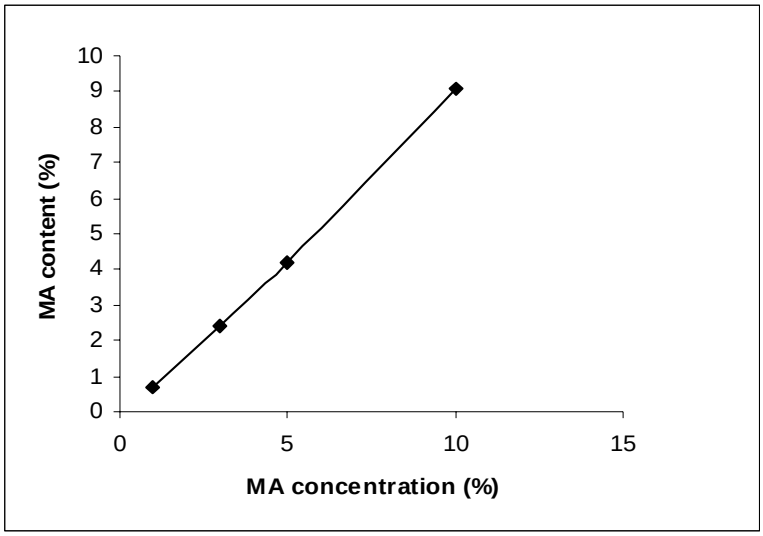

Figure 3.3 Variation of MA concentrations in MA-g-NR with MA concentration in the reaction mixture.

3.2.3 Effect of MA grafting on NR tensile properties

MA grafting was found to improve the tensile properties of the vulcanizates with out clay, possibly due to H-bond interactions. Figure 3.4 shows the variation of tensile strength of the vulcanizates with MA content. The tensile strength showed a sharp increase from 19.7MPa to 22.3MPa at an MA content of 0.7% and then showed gradual increase up to 23.4MPa with the increase of MA content to 4.2%. However, high MA content of 9.1% was found to retard the curing reactions of the rubber vulcanizates. So MA-g-NR with MA content of $\leq$ 4.2% was used for further studies. A 19% increase in tensile strength is obtained for 5MA-g-NR vulcanizates compared to NR gum.

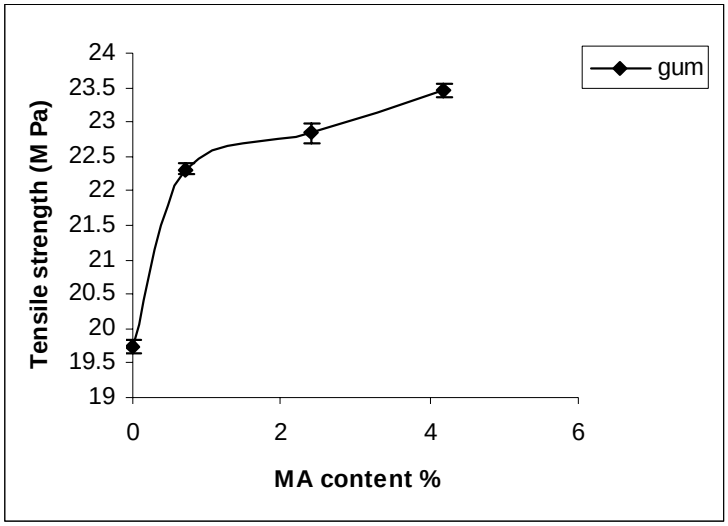

Figure 3 .4 MA content verses tensile strength of cured MA-g-NR with out clay.

3.2.4 Differential scanning calorimetry

The transition phenomena of the maleated natural rubber were studied by measuring the glass transition temperature (*T*g) which is seen in figure 3.5. 10MA-g-NR shows the maximum Tg value. As the grafting is increased the Tg value increases to higher values. Pure NR shows the lowest Tg value. The Tg value of pure NR is -63.36^{0}C. As the MA concentration is increased to 10% the Tg value is increased to -44.82^{0}C. Furthermore, the glass transition temperature increases with the increase of the MA concentration. This may be attributed to the restriction on chain mobility and flexibility because of the presence of the bulky grafted MA on the NR molecules. Increasing the grafted MA content also causes more inter chain interaction between polar groups of the graft copolymer. Hydrogen bonding is also more pronounced for the graft copolymer with the high grafted MA in the molecules. Higher the MA content the more stiffer will be the grafted rubber.

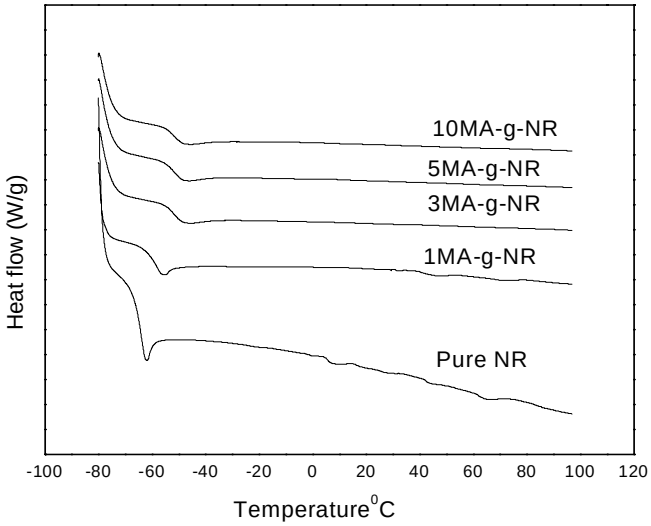

Figure 3.5 DSC thermograms of pure NR and MA-g-NR

3.3 Conclusions

This study shows that MA can be grafted to NR by the gamma radiation technique. MA concentration and radiation dose affect the grafting reaction significantly. Quantification of the grafted MA on the NR molecules can be determined using the titration method by determining the level of carboxylic acid which was determined by titration with standard KOH solution in methanol/benzyl alcohol. The estimation of the grafted MA level can also be performed using IR spectroscopy. It is found that MA grafting on NR molecules increases with MA concentration to a particular level with corresponding increase in the *T*g value.

References

1. Magat M. J Chim. Phys. 1955; 52: 709; Chapiro A, Magat M, Sebban J. to CNRS, brevet d'invention FR 1. 1957;130 099.
2. Ballantine D S, Glines A, Metz, D J, Behr J, Mesrobian R B,. Restaino A J, J Polym Sci. 1956; 19: 219; Chen W KW, Mesrobian R B, Ballantine D S, Metz D J, A. Glines A. J Polym Sci 1957;23:903.
3. Henglein A, Schnabel W, Heine K. Angew Chem 1958;70:461.
4. Chapiro A. Radiation chemistry of Polymeric systems, Interscience Publishers, New York, 1962.
5. Battaerd H A J, Tregear G W, −Graft Copolymers, Interscience, New York, 1967.
6. Wilson J E, −Radiation Chemistry of Monomers, Polymers and Plastics,Marcel Dekker, New York, 1974.
7. Huglin M B.Proc Roy Aust Chem Inst 1976;43:43.
8. Garnett J L, Radiat Phys Chem 1979 ;14 :79.
9. Ivanov VS. Radiation Chemistry of Polymers, VSP, Urtrecht, 1992.
10. Huslage J, Rager T, Schnyder B, Tsukada A Electrochim.Acta 2002;48:247.
11. Yang Z, Bhattacharya M, Vaiya UR. Polymer ;1996 :37 :2137.
12. Carone JR, Kipcak U, Goncalves MC, Nunes SP. Polymer 2000 ;41 :5929.
13. Mehrabzadeh M, Nia H. J Appl Polym Sci 1999;72:1257.
14. Phan TTM, DeNicola Jr A J, Schadler LS. J Appl Polym Sci 1998 ;68 :1451.
15. Oshinski AJ, Keskkula H, Paul DR. J Appl Polym Sci 1996 ;61 :623.
16. Nakason C, Kaesaman A, Samoh Z, Homsin S, Kiatkamjonwong S. Polym Test 2002;21:449.
17. Nakason C, Kaesaman A, Samoh Z, Homsin S, Kiatkamjonwong S. J Appl Polym Sci 2001;81:2803.

18. Lim J G, Baik JH, Zhang XQ, Son Y, Choi WM, Park OO. Polym Bull 2002;48:397.
19. Li C, Zhang Y, Zhang Y. Polym Test 2003;22:191.
20. Bohn CC, Manning SC, Moore RB. J Appl Polym Sci 2001;79:2398.
21. Sailaja RRN, Manda M. J Appl Polym Sci 2001;80:863.
22. Bikiaris D, Panayiotou C. J Appl Polym Sci 1998;70:1503.
23. Mi Y, Chen X, Guo Q. J Appl Polym Sci 1996 ;64 ;1267.
24. Li HM, Chen HB, Shen ZG, Lin S. Polymer 2002;43:5455.
25. Li TQ, Ng CN, Li RKY. J Appl Polym Sci 2001;81:1420.
26. Shi D, Yang J, Yao Z, Wang Y, Huang H, Jing W, Yin J, Costa G. Polymer 2001;42:5549.
27. Machado AV, Covas JA, Van Duin M. Polymer 2001;42:3649
28. Wang y, Ji D, Yang C, Zhang H, Qin B, Huang B. J Appl Polym Sci 1994;52:1411.
29. Deng JP, Yang WT, Ranby B. Eur Polym J 2002;38:1449.
30. Sen M, Bhattacharya M. Polymer 2002;41:9177.
31. Visconte LLY, Andrade CT, Azuma C. J Appl Polym Sci 1997:69:907.
32. Visconte LLY, Andrade CT, Azuma C. Polym Bull 1991;25:217.
33. Saedan M, Navarat T, Sombat A. Grafting o Maleic Anhydride on Natural rubber Molecules in a Molten state, The Nationall Research Council of Thailand (NRCT), Bangkok, 1997.
34. Pyke JB, Bauer RG, Cohen MP, Handa PK, US Patent no. 1991;4,996,263.
35. Angier, D.J.; and Turner ,D.T. J.Polym.Sci. 1958;39:419.
36. Claramma, N.M.; Thomas, E.V.; and Mathew, N.M. Radiat phys. Chem. 1989; 33: 87.
37. Sclavons, M.; Laurent, M. ; Devaux, J. ; Carlier V. Polymer 2005 ; 46 : 8062.
38. Lawson, D.F.; Hergenrother, W.L.; Matlock, M.G. J. Appl. Polym.Sci., 1990, 39, 2331.
39. Trivedi, B.C.; Culbertson, B.M. Maleic Anhydride Plenum, 1982 pp.172-3, NewYork.

Chapter 4

Mechanical properties of maleated natural rubber organoclay nanocomposites

In rubber industry, the elastomers filled with hard and soft particles are of great relevance, where the mechanical properties of polymeric material can be improved by the addition of fillers. The commonly used fillers for reinforcement of elastomers are silica and carbon black [1-3]. Polymer nanocomposites have been intensely researched in the last decade since the addition of a small quantity of reinforcing fillers, up to 5 weight percentage, such as nanoclays in the polymer matrix have led to improvements of mechanical, thermal, and barrier properties [4-7]. The preparations of various rubber clay nanocomposites by melt intercalation, solution blending and latex compounding and also its mechanical properties were reported. The simplest way to introduce nanoclay in a polymer matrix consists in the melt processing [8]. The enhancement of such properties is strongly influenced by the nanostructure of the dispersed clay and its interfacial interaction with the polymer. However, the larger specific surface area and smaller particle size of organoclay was believed to provide better rubber filler interaction [9]. The fundamental principle of polymer clay nanocomposite formation is that the polymer should penetrate into the intergalleries of the clay. The development of 'reactive' organoclays in which the intercalants, participate in the polymer building/crosslinking reactions [10,11] is a recent strategy to facilitate the nanocomposite. They include the modification of the surface of clay layers on the polymeric chains [12-16]. Further important factors are the length of the organophilic intercalant [17] and its number of alkyl tails [18], the molecular mass of the polymer matrix [19] and its polarity [20,21], as well as, the type of the layered silicate [22-23]. The layered silicates commonly used in

polymer nanocomposites belong to the structural family known as the 2:1 montmorillonite (MMT). In the pristine state, MMT is made up of stack of platelets resulting in a much smaller aspect ratio in the range of 50-200. A strong interaction between the matrix and filler is essential for enhanced properties of composites and this can be achieved by using fillers with high aspect ratio. Literature reveals that unprecedented improvement in properties has been observed in elastomers with nanofillers [24,25]. The layer thickness is around 1nm and lateral dimensions of the layers may vary from $300A^0$ to several microns and even more depending on the particular silicates. The startling property of montmorillonite is its ability to expand and contract its interlayer structure while maintaining two-dimensional crystallographic integrity. By this means, a large active surface area (700-800m^2/g) is potentially exposed, allowing an enormous range of guest molecules to be intercalated [26]. As the distance between the layers is less than 1nm, it does not allow the penetration of the polymer molecules therein. So the space between the platelets or layered galleries of the silicate should be made accessible for the polymer chains. To support intercalation and exfoliation, the interlayer distance should be greater than 1.5nm [27] and the layered structure should be broken down [28].

In this chapter, the mechanical properties and cure characteristics of layered silicate reinforced maleated natural rubber (MA-g-NR) nanocomposites are proposed to be investigated. The effects of nanofiller on the cure characteristics and mechanical properties are proposed to be analyzed with reference to filler loading and maleic anhydride concentration.

4.1 Experimental

4.1.1 Preparation of the maleated natural rubber-clay nanocomposites

Natural rubber of grade ISNR-5 obtained from Rubber Research Institute of India, Kottayam, India was used for preparing maleated natural rubber. The organically treated montmorillonite from Southern clay products, USA, was used

as the nanofiller for composite preparation. The nanoclay used was Cloisite 30B [MT2EtOH: methyl tallow, bis 2- hydroxyethyl, quaternary ammonium chloride] which has an interlayer distance of $18.4A^0$. Other chemicals used were of commercial grade. Compounds were prepared in a Brabender Plasticorder with various filler loadings from 1 to 7 weight percentages according to the recipe given in table 4.1. Maleic anhydride concentration was also varied from 1 to 5%.

The melt mixed compounds were matured for a period of 24hrs and the cure characteristics like cure time, scorch time, maximum and minimum torque were determined using rubber process analyzer at a temperature of 150^0C and a pressure of 200kg cm^{-2} pressure up to their respective cure times.

Table 4.1 Compound formulation

Ingredients	Sample Code		
	5MA-g-NR	3MA-g-NR	1MA-g-NR
Maleated natural rubber	100	100	100
ZnO	5	5	5
Stearic acid	2	2	2
Cloisite 30B	Y	Y	Y
Diethylene glycol	1	1	1
CBS	0.6	0.6	0.6
TMTD	0.2	0.2	0.2
Sulphur	2.5	2.5	2.5

Y= 1, 3, 5 & 7 parts of Cloisite 30B for hundred parts of rubber

4.1.2 X-ray diffraction

X-ray diffraction (XRD) was used to study the nature and extent of dispersion of the clay in the nanocomposite.

4.1.3 Transmission electron microscopy

The transmission electron microscopy was performed using a JEOL, JEM -2010 (Japan), TEM operating at an accelerating voltage of 200 kV.

4.1.4 Cure characteristics of the compounds

The processing characteristics of the compounds were monitored using a Rubber Process Analyzer. The die type used was biconical and the die gap was 0.487mm. The cure time; T_{90}, scorch time; T_{10}, maximum torque; T_{max} and minimum torque; T_{min} values were determined at 150^{O}C at a frequency of 50.0cpm and a strain of 0.20deg.

4.1.5 Mechanical properties

Mechanical properties of the nanocomposites are done according to the ASTM standards mentioned in Chapter 2

4.1.6 Strain sweep measurements

The strain sweep measurements on unvulcanized samples were conducted to study the rubber-filler interactions using the Rubber Process Analyzer (RPA 2000-Alpha Technologies).

4.2 Results and discussion

4.2.1 Characterisation of maleated natural rubber-clay nanocomposites using X-ray diffraction technique

Figure 4.1 (a), (b) &(c) shows the X-ray diffraction patterns of the cloisite 30B, pure natural rubber nanocomposite with 5wt% cloisite 30B and 5 MA-g-NR nanocomposite with 5wt% cloisite 30B respectively. The cloisite 30B clay shows a diffraction peak at $2\theta = 4.81A^0$ that is assigned to an interlayer platelet spacing (001 diffraction peak) of $18.4A^0$. In natural rubber based nanocomposite with 5wt% of cloisite 30B clay, the 2θ shifts to a lower value, 4.1^0 that is assigned to an interlayer spacing of 21.5 A^0. But for 5MA-g-NR nanocomposite with 5wt% of cloisite 30B clay, the 2θ shifts again to a lower value, 3.57^0 that is assigned to an interlayer spacing of $24.7A^0$ owing to the intercalation of rubber in the nanocomposites.

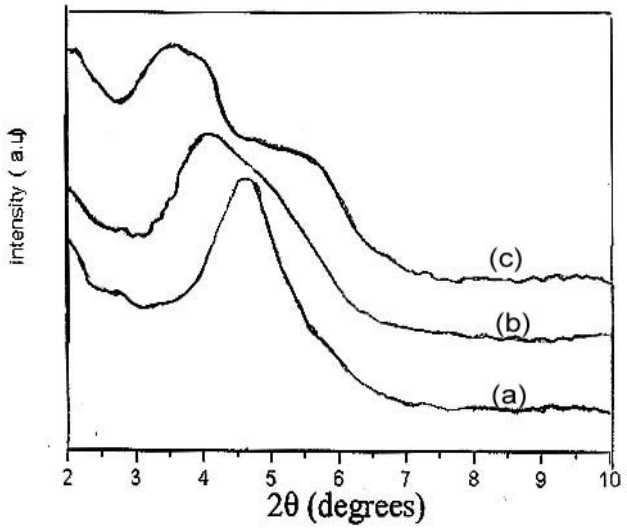

Figure 4.1 XRD patterns of: (a) cloisite 30B, (b) pure natural rubber nanocomposite with 5wt% cloisite 30B (c) 5MA-g-NR nanocomposite with 5wt% cloisite 30B.

4.2.2 Transmission electron microscopy

The Transmission electron microscopy (TEM) imaging for rubber nanocomposites was carried out using a Transmission Electron Microscope CM-200 of Philips Technology. TEM was used in order to visualize the morphology of the clay layers in the nanocomposites. A cockle- like dark objects in the micro graphs correspond to the clay layers [29]. Figure 4.2 (a), (b), (c) & (d) shows TEM micrographs for 5MA-g-NR, Pristine NR, 3MA-g-NR and 1MA-g-NR with 5wt% nanoclay loading with high interlayer distance. Even though, X-ray diffraction indicated all intercalated structures, exfoliated layers can also be observed in the TEM pictures.

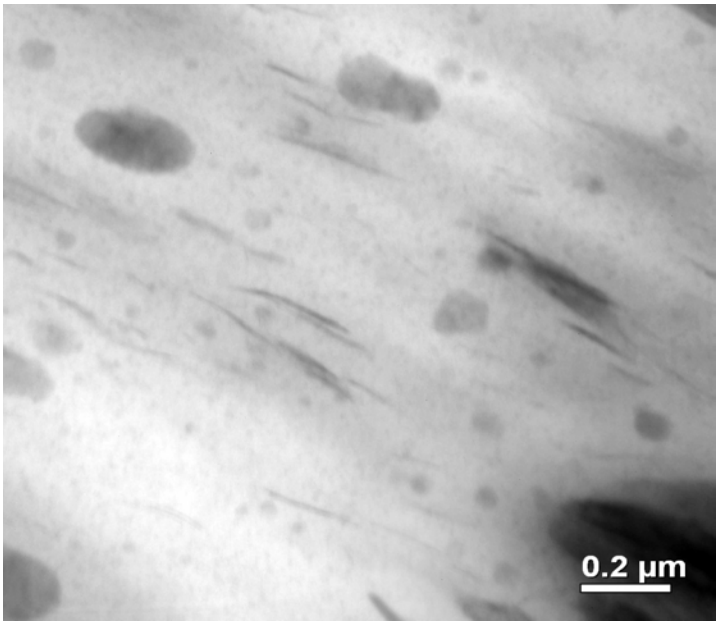

Figure 4.2 (a) TEM micrograph of 5MA-g-NR nanocomposite with 5wt% nanoclay loading.

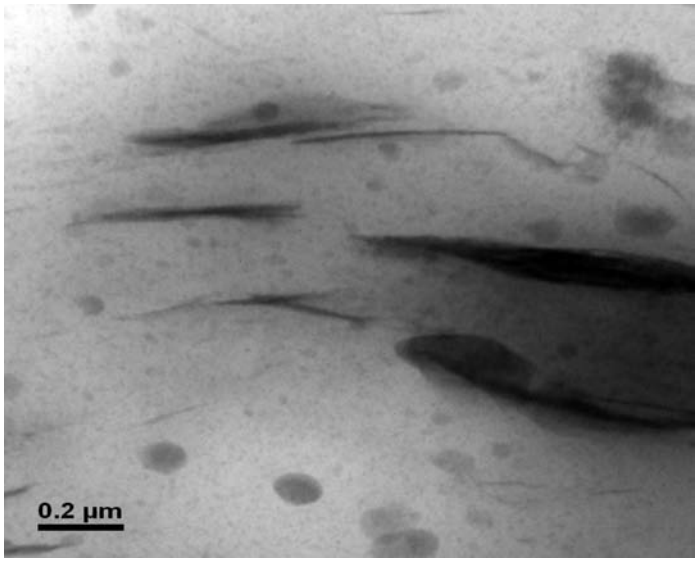

Figure 4.2 (b) TEM micrograph of pure NR nanocomposite with 5wt% nanoclay loading

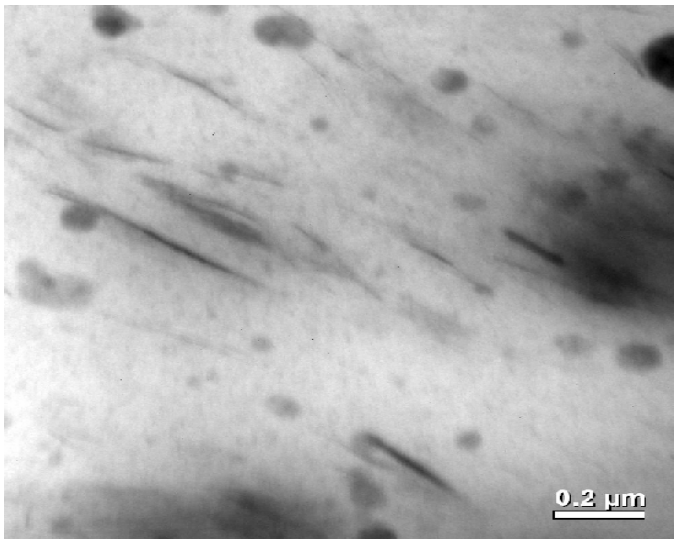

Figure 4.2 (c) TEM micrograph of 3MA-g-NR nanocomposite with 5wt% nanoclay loading.

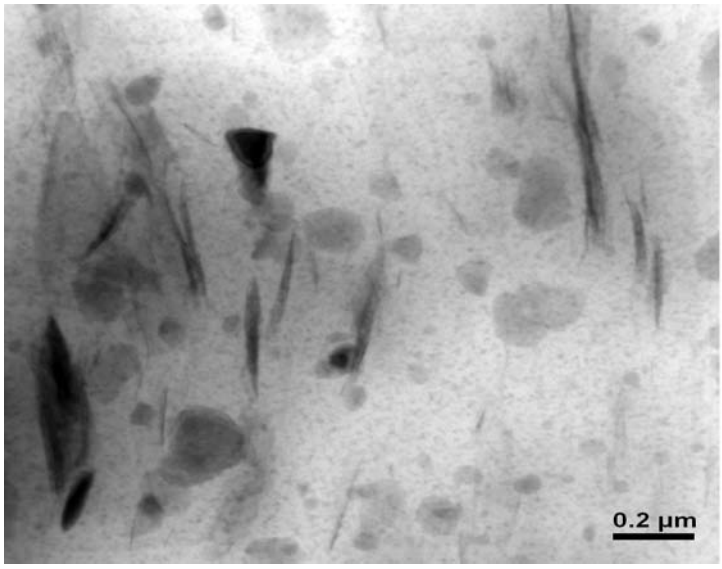

Figure 4.2 (d) TEM micrograph of 1MA-g-NR nanocomposite with 5wt% nanoclay loading.

4.2.3 Cure characteristics of the compounds

The use of rubber products always involves vulcanized materials because crosslinked elastomers present better mechanical properties. The cure characteristics of the mixes are given in figure 4.3(a) - 4.3(d). Rubber compounds with organoclay showed an accelerating effect on the cure characteristics. 5MA-g-NR compounds showed lower cure time compared to the NR compounds containing same amount of organoclay as seen in figure 4.3 (a).

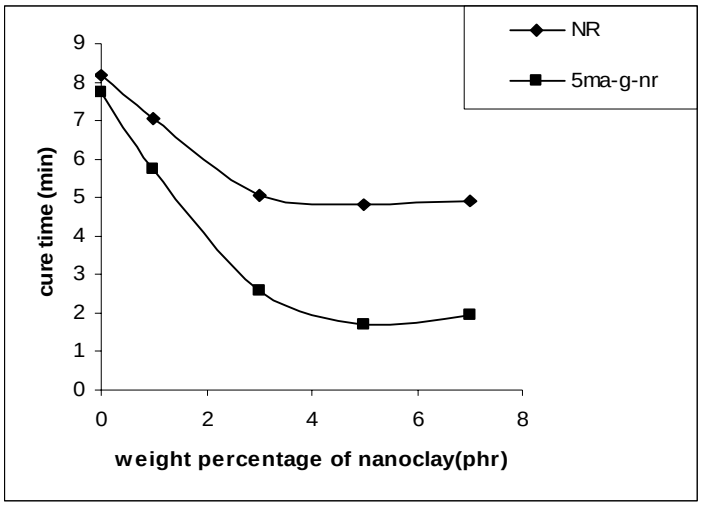

Figure 4.3(a) Variation of cure time with nanoclay loading

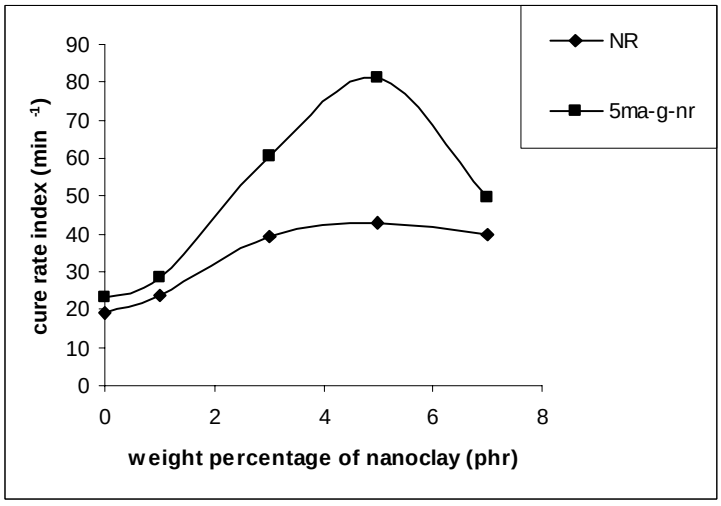

Figure 4.3 (b) Variation of cure rate index with nanoclay loading

The cure rate index is found to be high for 5MA-g-NR than NR with same amount of organoclay as seen in figure 4.3 (b). The cure time was reduced and cure rate index is increased. But for NR compounds, the cure time was reduced and cure rate index increased. This might have resulted in high rubber filler interaction through the anhydride group.

Scorch time is the time required for the torque value to reach 10% of maximum torque. It is a measure of the processing safety- the time available for safe processing before the onset of vulcanization reaction. Scorch time is lower for grafted rubber as shown in figure 4.3 (c) indicating better processing safety.

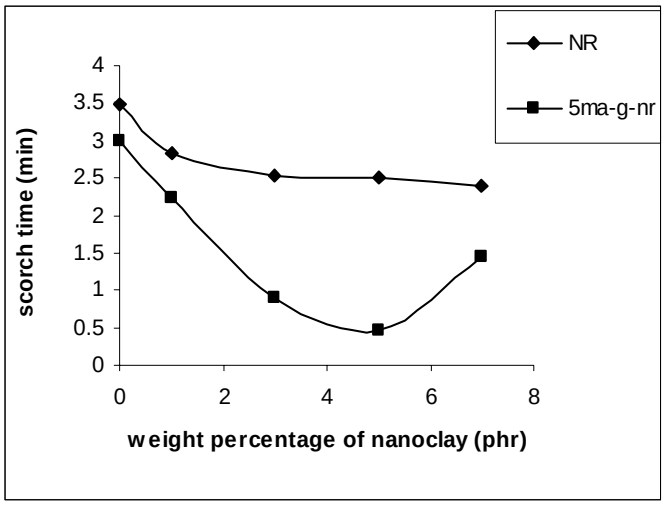

Figure 4.3 (c) Variation of scorch time with nanoclay loading

Figure 4.3 (d) shows that the torque development $T_{(max-min)}$ with filler loading is higher at 5wt % for MA-g-NR when compared to the NR system. The increased $T_{(max-min)}$ may be arising from the formation of more extensive crosslink. These results are attributed to the intercalation of the rubber with in the silicate galleries. Consequently, a better interaction between the rubber and the filler is obtained. The minimum torque; T_{min}, represents the effective viscosity of the mixtures before vulcanization. It is found to increase with filler loading for both grafted and ungrafted rubber. In the case of polymer nanocomposites filled with various particulate fillers the minimum torque in rheographs is considered to be a direct measure of the filler content. T_{min} can be considered as a measure of stiffness of the unvulcanized compound. The increase in viscosity with the addition of filler suggests a reduced mobility of the rubber chains caused by the incorporation of these fillers.

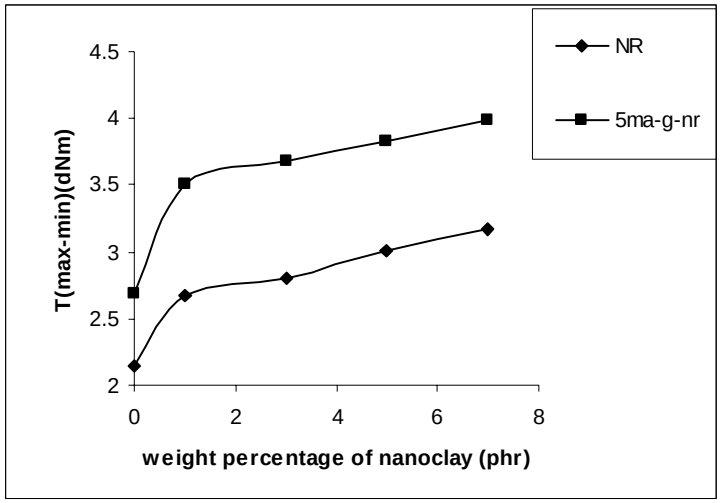

Figure 4.3 (d) Variation of $T_{(max-min)}$ with nanoclay loading.

4.2.4 Mechanical properties of nanocomposites

As the weight percentage of layered silicates increases the tensile strength also increases as evident from figure 4.4. The improvement in tensile properties is so pronounced in grafted rubber and an enhancement can be seen in both grafted and ungrafted rubber. Intercalation of rubber chains into the layers results in the increase in tensile strength. The enhancement in properties occurs because of the higher polymer-filler interactions than filler-filler interactions. 5MA-g-NR up to 5wt% nanoclay shows an increase in tensile strength and above that a decrease is noticed due to poor dispersion of filler in the polymer matrix. NR & 5MA-g-NR with 5wt% of nanoclay shows an improvement of 40.5 & 66.6% in tensile strength respectively.

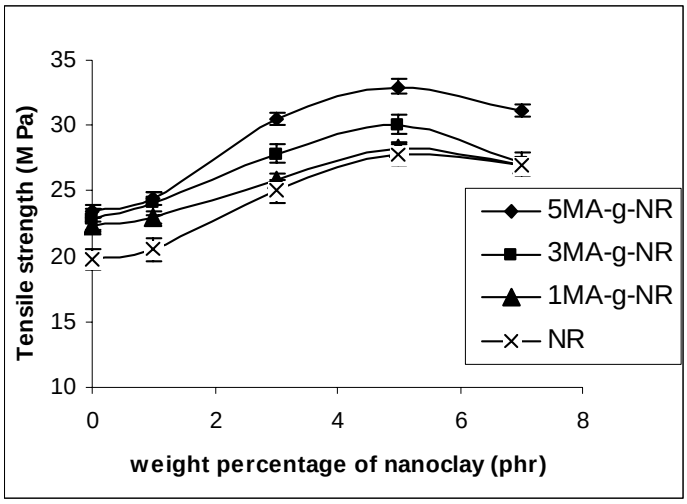

Figure 4.4 Tensile strength of nanocomposites with nanoclay loading

Figure 4.5 shows the elongation at break (%) curves of nanocomposites containing varying percentage of filler. The elongation at break of all systems decreases with increase in weight percentage of filler [30]. NR & 5MA-g-NR with 5wt% nanoclay shows a decrement of 25.47 & 32.83 % respectively. The decrease at higher loading is due to the enhancement in rigidity of the material. All the system shows the same trend. For most of the applications requiring a large initial reinforcement, the ultimate strain is not very crucial.

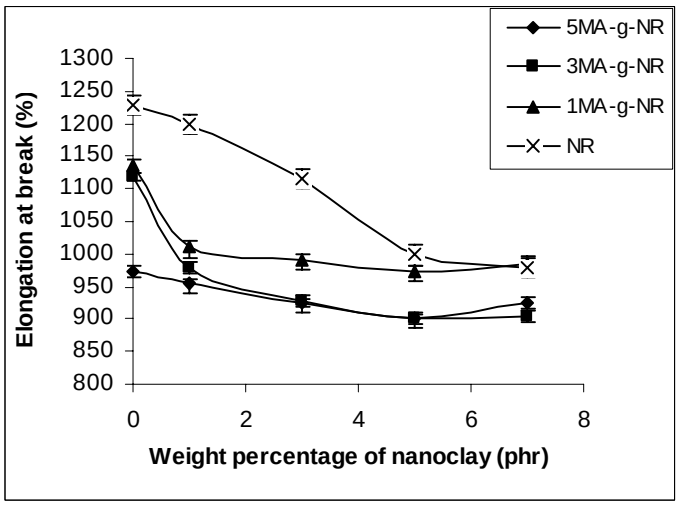

Figure 4.5 Elongation at break (%) of nanocomposites with nanoclay loading.

The dependence of modulus at 300% strain on nanoclay content is shown in figure 4.6. The modulus of all the samples is higher than the gum samples. NR & 5MA-g-NR with 5wt% nanoclay shows an increment in modulus of 45.63 & 76.88% respectively. From the results it is obvious that even with the addition of such a low loading (1-5wt%) of the layered silicates, the modulus increases considerably. The improvement in properties is due to the nanomeric dispersion of silicate layers resulting in efficient reinforcement leading to improved stiffness of the material. The clay platelet aspect ratio has a significant effect on the stiffness of the polymeric material. According to Daniel and co-workers [31] as the matrix modulus deceases there is a much higher relative stiffness enhancement in the rubbery state owing to the intercalation of the rubber into the layered silicates.

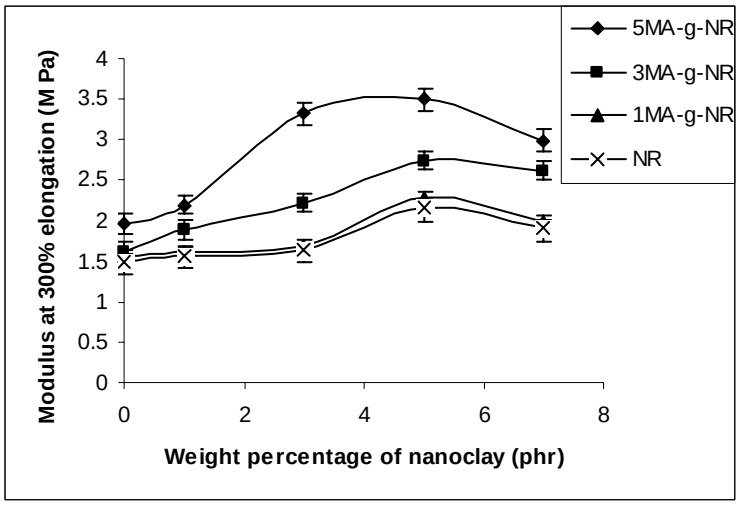

Figure 4.6 Modulus at 300% elongation of nanocomposites with nanoclay loading

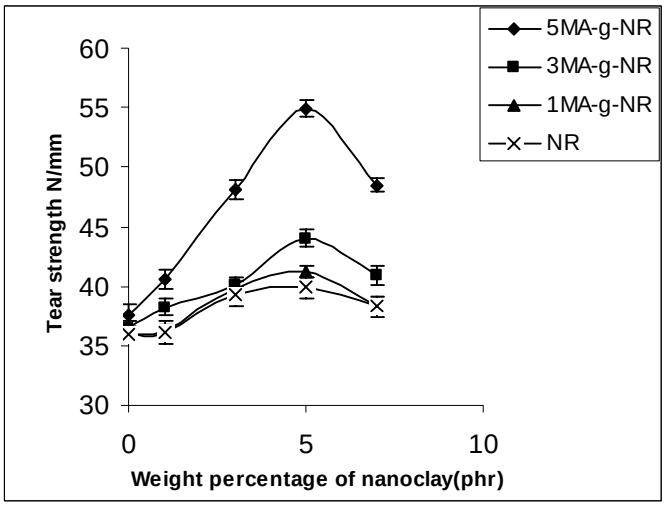

Figure 4.7 Tear strength of nanocomposites with nanoclay loading.

Figure 4.7 gives the tear strength curves of the system as a function of weight percentage of nanoclay loading. Layered silicate filled NR and maleated NR exhibit increase in tear strength up to 5wt% nanoclay loading and above that it shows a decrease. NR & 5MA-g-NR nanocomposites with 5wt% nanoclay shows an increment in tear strength of 11.4 & 97.92 % respectively, indicating the resistance offered in the silicates in order to enhance the crack propagation.

Hardness, a measure of low strain elastic modulus, is higher for grafted rubber, compared to the ungrafted rubber. From figure 4.8, it can be observed that 60 and 76% increase in hardness for NR and 5MA-g-NR respectively. This is expected because, as more nanofiller get into the rubber matrix, the elasticity of the rubber nanocomposite is reduced and the inter layer distance is increased resulting in more rigid vulcanizates. Here the tensile strength, modulus, tear strength and hardness show the same trend.

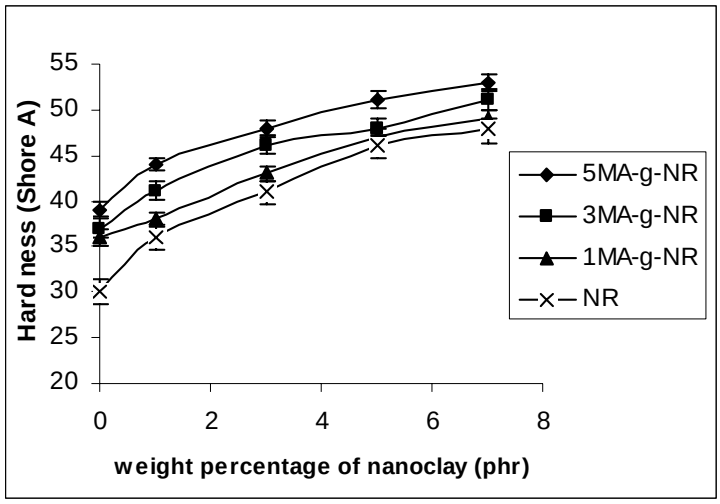

Figure 4.8 Hardness of nanocomposites with nanoclay loading

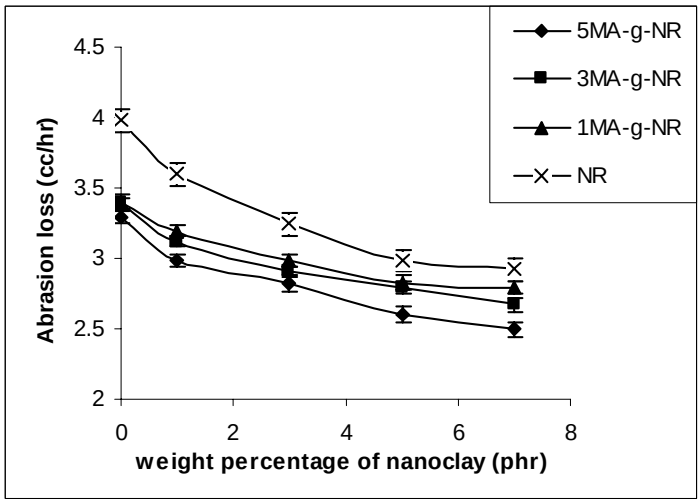

Figure 4.9 Abrasion loss of nanocomposites with nanoclay loading

As the hardness increases abrasion loss, which is a measure of reinforcement, should decrease and this is reflected in figure 4.9. A decrease of 12% in abrasion loss is observed for 5MA-g-NR nanocomoposites at 5wt% nanoclay loading when compared to NR nanocomposites at same clay loading. The increased crosslink density which results in increased hardness and modulus ultimately

gives rise to the enhancement of abrasion resistance. The abrasion resistance is a very important property for the application of tire and belt.

In addition to the reinforcing effect, the addition of organoclay in the maleated natural rubber nanocomposites led to improved elastic characteristics in the MA-g-NR, as deduced from the rebound resilience and compression set measurements. Compression set values depends strongly on the elastic recovery of the sample. Compression set values which is shown in figure 4.10 is lower for 5MA-g-NR when compared to NR. The compression set of the compounds loaded with nanoclay was significantly lower that the compression set of the reference compound [32-33]. A decrease of 14.4% in compression set value is observed for 5MA-g-NR nanocomoposites at 5wt% nanoclay loading when compared to NR nanocomposites at same nanoclay loading. This can be attributed to higher crosslink density. The lower compression set values indicate a more restrained matrix and elastic deformation is operational.

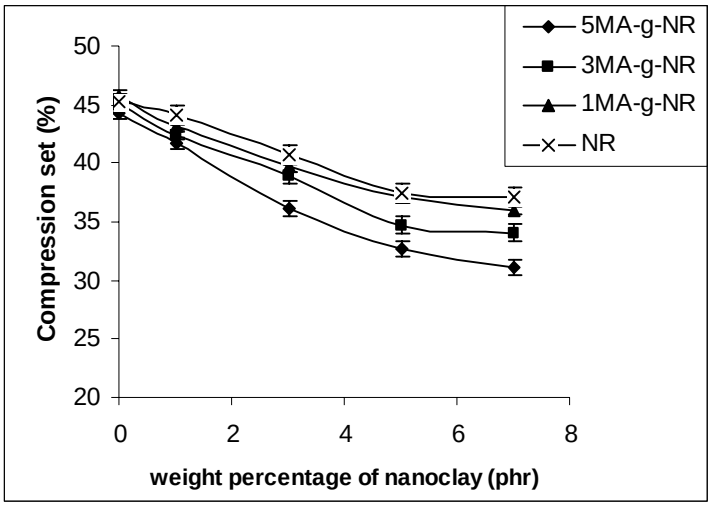

Figure 4.10 Compression set of nanocomposites with nanoclay loading

Resilience, a measure of the elastic component, was found to increase with increase in nanoclay loading as shown in figure 4.11. An increase of 20% in rebound resilience is observed for 5MA-g-NR nanocomoposites at 5wt% nanoclay loading when compared to NR nanocomposites at same nanoclay loading. The rebound resilience is increased by the increase in modulus. This is due to the high reinforcement between the filler and the elastomer which may be due to the larger specific surface area and small particle size of organoclay.

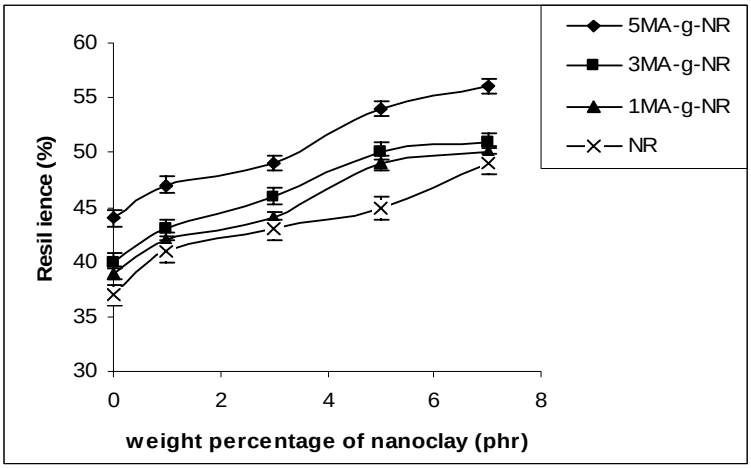

Figure 4.11 Resilience of nanocomposites with nanoclay loading

It is seen that the nanocomposite with the clay having higher interlayer distance shows better mechanical properties. This suggests that interlayer distance play a major role in the intercalation of the rubber matrix.

4.2.5 Strain sweep measurements of uncured compounds

The complex modulus (G*) values obtained for the uncured compounds are plotted and shown in figure 4.12. The elastic modulus of a filled rubber is strongly dependent on the deformation and decreases substantially at higher strains. This phenomenon is known as Payne effect and is attributed to the presence and breakdown of the filler network during deformation. But investigations performed with both experimental and theoretical approaches

shows that the decrease in G* with amplitude of deformation (strain) is attributed to the destruction-reformation of a percolating network of filler that can also involve polymer bonded filler [34] i.e. polymer filler links also. The complex modulus values at low strains (15%) are due to polymer networks and hydrodynamic interactions [35]. The limiting values at high strains are due to polymer networks and hydrodynamic effect. Polymer networks are the same for a fixed mass of rubber. But the hydrodynamic effect varies with the filler content and the nature of the filler. The theoretical meaning of hydrodynamic effect is given by the modified form of Guth and Gold equation [36, 37].

The addition of filler increases the shear modulus, G_f for the filled compound according to the equation

$$G_f = G_0 (1+0.67\ fs\phi +11.62\ fs^2\phi^2)$$

where ϕ is the volume fraction of the particles and the shape factor fs represents the ratio of the longest dimension to the shortest dimension of the particle. The modulus as calculated by the equation is independent of the applied strain [38]. The variation of complex modulus (G*) with strain for the composites with clay are presented in figure 4.12. The graph shows that the complex modulus values at low strain increases with filler concentration. As the complex modulus values of G* is due to higher filler-filler or filler-polymer interactions. Variation in mechanical properties of the composites explained earlier shows that the network formed are mainly between filler and polymer.

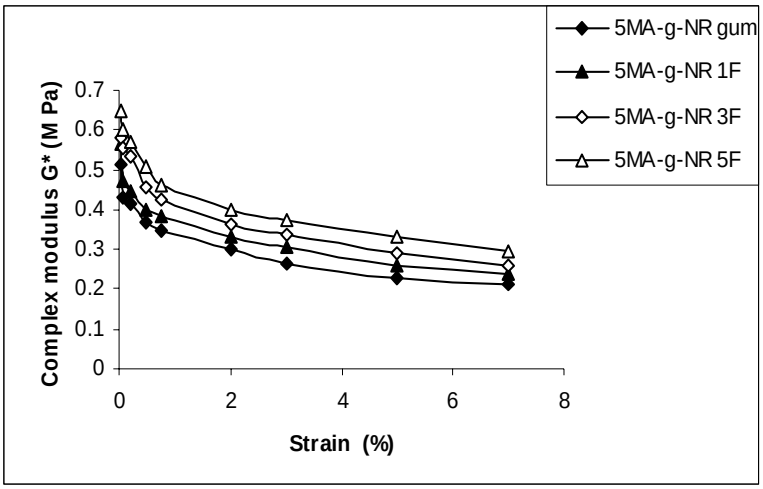

Figure 4.12 Variation of complex modulus with nanoclay content for 5MA-g-NR nanocomposites.

4.3 Conclusions

Maleated natural rubber-organoclay nanocomposites can be prepared successfully by a melt-compounding method. MA-g-NR nanocomposites can be prepared with nanoclay in varying clay loading and the clay content significantly affects the cure characteristics and mechanical properties. In presence of organoclay both the cure time and scorch time are considerably reduced. This reduction in cure time is boosted with the increase in interlayer distance of the clay. A dramatic increase in maximum torque value with increase in clay content is also observed for the nanocomposites. The mechanical properties of 5MA-g-NR nanocomposites are higher than NR nanocomposites. It is seen that the nanocomposites with the clay having interlayer distance shows better mechanical properties. The increase in d spacing for these layered clays evident from X-ray results and TEM photographs also confirmed the formation of partially intercalated and exfoliated structure.

References

1. Mark JE, Erman B, Eirich FR. Science and Technology of Rubber, Eds: Academic press, San Diego, CA, 1994.
2. Nielsen LE, Landel RF.Mechanical Properties of Polymers Composites,Eds: Marcel Dekker, New York,1994.
3. Edwards DC. J Mater Sci 1990;25:4175
4. Kojima Y, Kawasumi M, Usuki A, Fukushima Y, Kurachi T, Kamigaito, O. J Mater Res 1993;8(5):1185.
5. Fu X, Qutubuddin S. Polymer 2001;42:807.
6. Messersmith PB, Giannelis EP. Chem Mater 1996;6:1719.
7. Yano K, Usuki A,Okada A, Kurauchi T Kamigaito O. J Polym Sci A: Polym Chem 1993;31:2493.
8. Vaia RA, Wagner HD. Materials Today 2004;7:32.
9. Senguptha R, Chakraborty S, Bandyopadhyay S, Dasgupta S, Mukhopadhyay R, Auddy K and Deuri AS. Polym Eng Sci 2007;47: 1956.
10. Ma J, Yu ZZ, Zhang QX, Xie XL, Mai YW,Luck I. Chem Mater 2004;16:757.
11. Tyan HL, Liu YC, Wei KH. Chem Mater 1999;11:1942.
12. Ray SS, Okamoto M. Prog Polym Sci 2003;28:1539.
13. Kornmann X, Thomann R, Mulhaupt R, Finter J, Berglund L. J Appl Polm Sci 2002;86:2643.
14. Alexandre A, Dubois P.Mater Sci Eng 28 ;1 :2000.
15. Kawasumi M, Hasegawa N, Kato M, Usuki A, Okada A. Macromolecules 1997;30:6333.
16. Chow WS, Mohd Ishak ZA, Karger-Kosis J apostov AA Ishiaku US. Polymer 2003;44:7427.
17. Zilg C, Thomann R, Finter J Mulhaupt R. Macromol Mater Eng 2000;280/281:41.
18. Fornes TD, Hunder DL, Paul DR. Macromolecules 2004;37:1793.

19. Fornes TD, Yoon PJ, Keskkula H, Paul DR. Polymer 2001;42:9929.
20. Zheng H, Zhang Y, Peng Z, Zhang Y. J Appl Polym Sci 2004;92:638.
21. Li X, Ha CS. J Appl Polym Sci 2003 ;87 :1901.
22. Maiti P, Yamada K, Okamoto M, Ueda K, Okamoto K. Chem Mater 2002; 14:4654.
23. Lan T, Kaviratna D, Pinnavaia TJ Chem Mater 1995;7:2144.
24. Nah C, Ryu HJ, Han SH, Rhee JM, Lee MH.Polym Intl 2001;50:1265.
25. Zheng H, Zhang Y, Peng Z, Zhang Y. Polym Test 2004;23:217.
26. Theng BKG. Formation and Properties of Clay-Polymer Complexes,Elsevier Scientific Publishing Company, New York 1979; p 353
27. Wang Z,Pinnavaia TJ. Chem Mater 1998;10:1820.
28. Lan T Pinnavaia TJ,Chem SN,Lopez BH.J Appli Polym Sci 1992;44:1820.
29. Hiroshi J, Spontak RJ. Polymer 2009;50:1067.
30. Nielsen LE, Landel RF. Mechanical properties of Polymers and composites, 2nd ed., Marcel Dekker, Inc.,1994; p545.
31. Varghese S, Gatos KG, Apostolov AA, Karger-Kosis. J Appli Polym Sci 2004;92:543.
32. Franco Cataldo. Macromol Symp 2007;247:67.
33. Kim MS, Kim DW, Chowdhory SR, Kim GH. J Appli Polym Sci 2006 ;102 :2062.
34. Kluppel M, Schuster HR, Heinrich G. Rubber Chem Technol 1997; 70:243
35. Jean L, Leblanc MC. J Appli Polym Sci 2001; 80; 11: 2093
36. Guth E, Gold O. Phys Rev 1938;53:322
37. Smallwood HM. J Appli Phys 1944;15:758
38. Stickney PB, Falb RD. Rub Chem Technol 1964;37:1299

Chapter 5

Mechanical properties of maleated natural rubber organoclay nanocomposites developed through masterbatch technique

Exploiting the 'nanoreinforcement' effect of layered silicates (clays), property improvement can be achieved even by adding small amounts of organoclay [1-6]. Properties enhancement is a consequence of both higher specific surface area and higher aspect ratio, in comparison to conventional fillers [7–9]. Key aspect of the 'nano-concept' is to intercalate and exfoliate the layers of the silicate [10]. For that purpose, the inherent 'incompatibility' between the polymer and the clay has to be circumvented. In order to facilitate, the penetration of the chains in between the galleries and thus to form a nanocomposite, different strategies are followed. They include the modification of the surface of the clay layers and/or the polymeric chains [11–15]. Further important factors are the length of the organophilic intercalant [16] and its number of alkyl tails [17], the molecular mass of the polymer matrix [18] and its polarity [19,20], as well as, the type of the layered silicate [21,22]. Although systems with intercalated structures are also termed as nanocomposites, the ultimate goal is to reach full exfoliation of the clay. Intercalation is also shown to be affected by the type and content of clay [23–25] and the type of clay intercalant, i.e. clay organic modification [26]. In general, improved intercalation is obtained at relatively low clay loading and high coupling agent-to-clay ratio. To support intercalation and exfoliation, the interlayer distance should be greater than 1.5nm [27] and the layered structure should be broken down [28]. The most commonly used approach to further aid compatibilization and dispersion of organoclays in PP is by melt compounding with maleic anhydride grafted PP (MA-g-PP) [28–32]. This method is found to

be effective to a great extent, but leads to loss of properties, as a result of high concentrations of MA-g-PP required for complete exfoliation of nanoclays. It is believed that the polar character of the anhydride causes an affinity for the silicate surface such that the maleated polypropylene can serve as a compatibilizer between the matrix and filler. This approach has been well developed for polypropylene-based systems; however, only a few studies have reported how the ratio of MA-g-PP to organoclay affects morphology and the related performance of PP-based nanocomposites [33, 34]. Lopez-Manchado *et al.* [35-37] prepared organoclay nanocomposites based on natural rubber and noticed an increase in the crosslink density, degree of curing, structure, order and glass transition temperature. Cis-1,4-Polyisoprene and epoxidized natural rubber were studied by Vu and coworkers [38]. Masterbatch technique of PP/MA-PP cloisite 30B organoclay was also reported by Perrin-Sarazin *et al.* [39].

In this chapter, the mechanical properties and cure characteristics of layered silicate reinforced 10% maleated natural rubber (10MA-g-NR) nanocomposites developed through masterbatch technique are proposed to be investigated.

5.1 Experimental

5.1.1 Preparation of maleated natural rubber-clay nanocomposites developed through masterbatch technique

5.1.1 A Preparation of maleated natural rubber/clay masterbatch

Natural rubber of grade ISNR-5 obtained from Rubber Research Institute of India, Kottayam, India was used for preparing maleated natural rubber. The organically treated montmorillonite from Southern clay products, USA, was used as the nanofiller for composite preparation. The nanoclay used was Cloisite 30B [MT2EtOH: methyl tallow, bis 2- hydroxyethyl, quaternary ammonium chloride] which is having an interlayer distance of $18.4A^0$. Other chemicals used were of commercial grade. Nanoclay was blended using (10MA-g-NR) at a level of 20-

50phr to prepare a masterbatch. 10MA-g-NR nanocomposites cannot be prepared by direct method because there occurs retardation in cure due to the presence of the excess acid group in 10MA-g-NR. In order to overcome this problem and to obtain better strength and properties the masterbatch technique is preferred. The masterbatch is prepared by mixing 20-50phr nanoclay with 10MA-g-NR for 6 minutes in a Brabender Plasticorder in order to get a proper dispersion. Nanocomposites using different clay loading up to 7 weight percentage were prepared by mixing calculated amounts of the masterbatch and virgin NR. Then the above mix after 12hours is used for rubber compounding.

5.1.1 B Preparation of nanocomposites

The 10MA-g-NR clay masterbatch should be diluted with natural rubber in order to make the nanoclay loading in the range of 1, 3, 5&7 weight percentages. The ingredients were added to the masterbatch in the Brabender Plasticorder at 50 rpm for 10minutes according to the recipe given in table 5.1 for preparing nanocomposies. Maleic anhydride concentration of 10% was used through out the study in masterbatch technique. For10% MA concentration the masterbatch technique is preferred because; above 5% maleic anhydride concentration there occur retardation in cure due to the excess acid concentration of MA during nanocomposite preparation. The mixed compounds were matured for a period of 24hrs and the cure characteristics like cure time, scorch time, maximum and minimum torque were determined using rubber process analyzer at a temperature of 150^0C and a pressure of 200kg cm^{-2} pressure up to their respective cure times.

Table 5.1 Compound formulation

Ingredients	Sample Code			
	20 phr	30 phr	40 phr	50phr
10MA-g-NR+Y+NR	100	100	100	100
ZnO	5	5	5	5
Stearic acid	2	2	2	2
Diethylene glycol	1	1	1	1
CBS	0.6	0.6	0.6	0.6
TMTD	0.2	0.2	0.2	0.2
Sulphur	2.5	2.5	2.5	2.5

Y= 1, 3, 5 & 7 parts of Cloisite 30B for hundred parts of rubber

5.1.2 X-ray diffraction

X-ray diffraction (XRD) was used to study the nature and extent of dispersion of the clay in the nanocomposite.

5.1.3 Transmission electron microscopy

The transmission electron microscopy was performed using a JEOL, JEM -2010 (Japan), TEM operating at an accelerating voltage of 200 kV.

5.1.4 Cure characteristics of the compounds

The processing characteristics of the compounds were monitored using a Rubber Process Analyzer. The die type used was biconical and the die gap was 0.487mm. The cure time; T_{90}, scorch time; T_{10}, maximum torque; T_{max} and minimum torque;

T_{min} values were determined at 150^0C at a frequency of 50.0cpm and a strain of 0.20deg.

5.1.5 Mechanical properties

Mechanical properties of the nanocomposites are done according to the ASTM standards mentioned in Chapter 2

5.1.6 Strain sweep measurements

The strain sweep measurements on unvulcanized samples were conducted to study the rubber-filler interactions using the Rubber Process Analyzer (RPA 2000-Alpha Technologies).

5.2 Results and discussion

5.2.1 Characterisation of maleated natural rubber-clay nanocomposites using X-ray diffraction technique

Figure 5.1 (a),(b),(c),(d),&(e) shows the X-ray diffraction patterns of the cloisite 30B, nanocomposites with 1,3,5 and 7wt% cloisite 30B respectively for 40phr masterbatch which is having higher d-spacing among the mentioned masterbatches. For 20, 30 and 50phr loading also the XRD patterns shows the same trend and closer values with 40phr masterbatch. The cloisite 30B clay shows a diffraction peak at $2\theta = 4.81A^0$ that is assigned to an interlayer platelet spacing (001 diffraction peak) of $18.4A^0$. The first, second and third peak corresponds to the $d00_1$, $d00_2$ and $d00_3$ spacing respectively. It is also seen in figure 5.1 (b),(c),(d) and (e) that d-spacing is increased from $18.4A^0$ to 27, 27.56, 27.67 and $26.33A^0$ respectively owing to the intercalation of maleated natural rubber in the nanocomposites. This increase in interlayer distance of the clay by approximately $9.27A^0$ confirms the formation of intercalated nanocomposites.

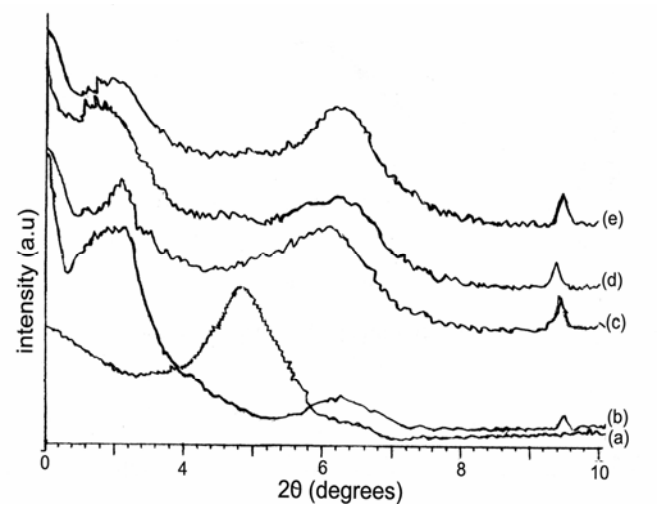

Figure 5.1 XRD patterns of: (a) cloisite 30B and (b),(c),(d) &(e) nanocomposites with 1,3,5 and 7wt% cloisite 30B loading respectively for 40phr masterbatch.

5.2.2 Transmission electron microscopy

The Transmission electron microscopy (TEM) imaging for rubber nanocomposites was carried out using a Trasmission Electron Microscope CM-200 of Philips Technology. TEM was used in order to visualize the morphology of the clay layers in the nanocomposites. Figure 5.2 (a), (b), (c) & (d) shows TEM micrographs of 10MA-g-NR at 5wt% nanoclay loading for 20, 30, 40 and 50phr masterbatch. Even though, X-ray diffraction indicated all intercalated structures, exfoliated layers can also be observed in the TEM pictures.

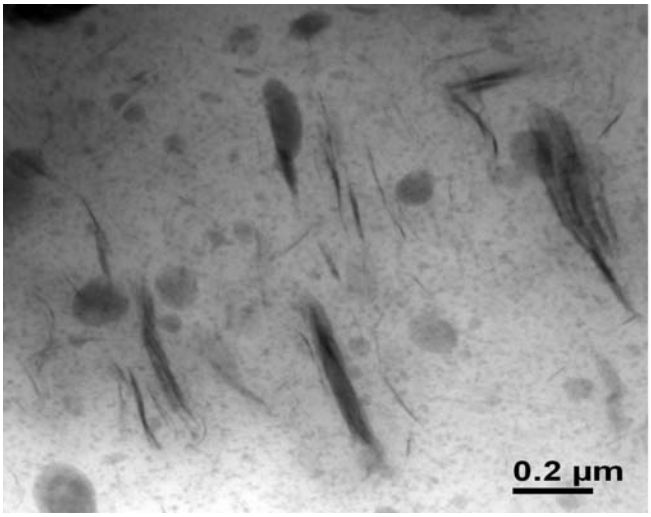

Figure 5.2 (a) TEM micrograph of 10MA-g-NR nanocomposites with 5wt% nanoclay loading for 20phr

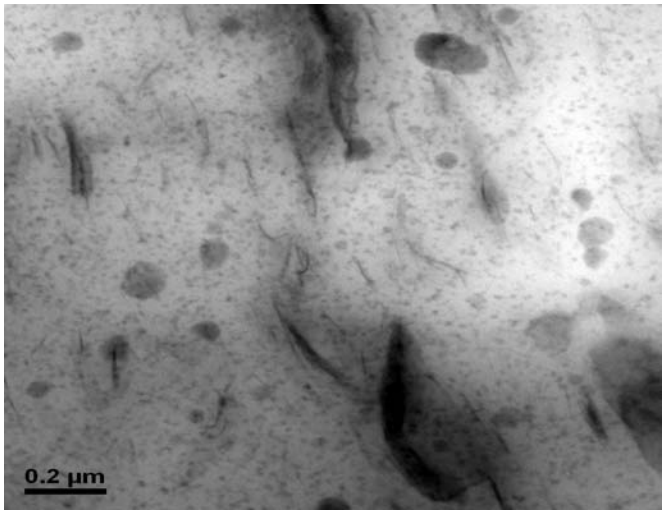

Figure 5.2 (b) TEM micrograph of 10MA-g-NR nanocomposites with 5wt% nanoclay loading for 30phr

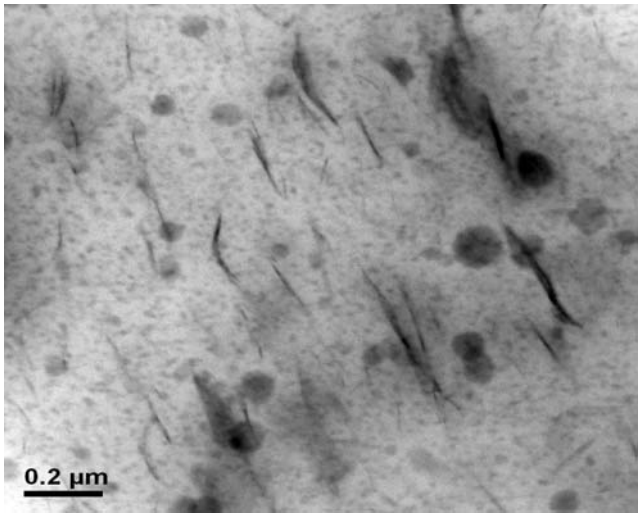

Figure 5.2 (c) TEM micrograph of 10MA-g-NR nanocomposites with 5wt% nanoclay loading for 40phr

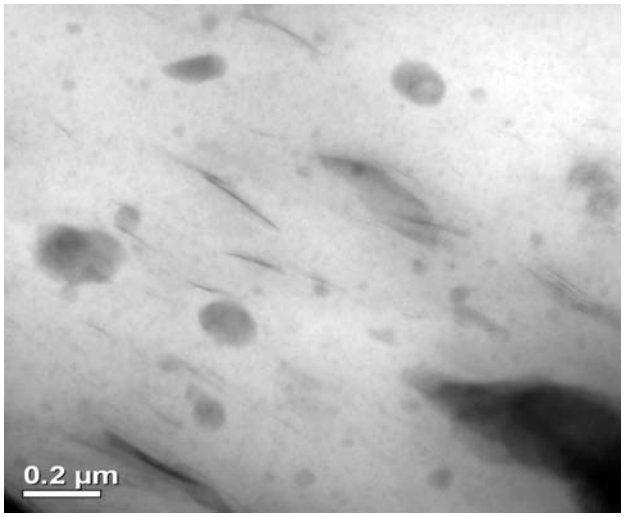

Figure 5.2 (d) TEM micrograph of 10MA-g-NR nanocomposites with 5wt% nanoclay loading for 50phr

5.2.3 Cure characteristics of the compounds

The use of rubber products always involves vulcanized materials because crosslinked elastomers present better mechanical properties. The cure characteristics of 5MA-g-NR compounds and NR compounds were discussed in the previous chapter. Here in this chapter the cure characteristics of 10MA-g-NR compounds developed through the masterbatch technique is discussed.

The cure characteristics of the mixes are given in figure 5.3(a) - 5.3(d). Rubber compounds with organoclay showed an accelerating effect on the cure characteristics [40,41].

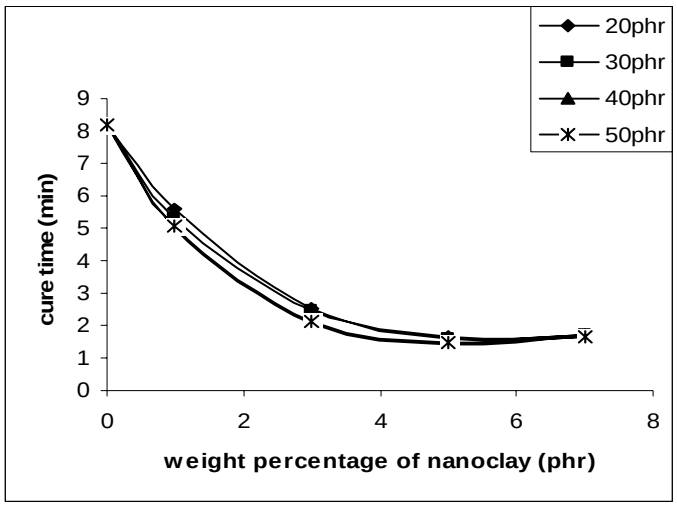

Figure 5.3(a) Variation of cure time with nanoclay loading

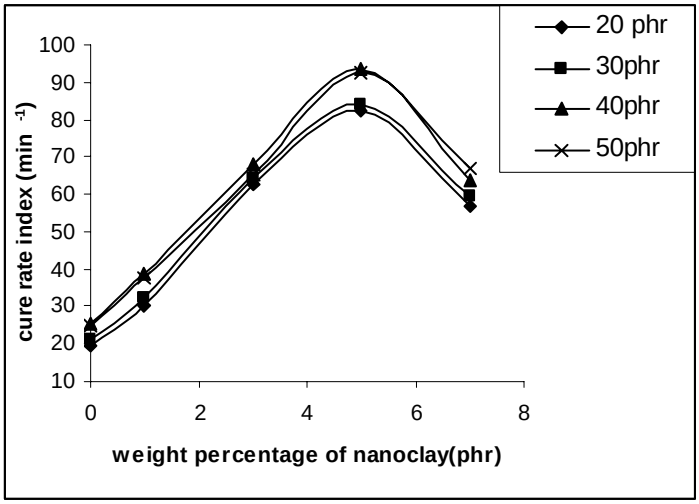

Figure 5.3 (b) Variation of cure rate index with nanoclay loading

The cure rate index is found to be high for 10MA-g-NR at 5wt% nanoclay loading in the case of 40phr than all other masterbatches with same amount of organoclay as seen in figure5.3 (b).The cure time was reduced and cure rate index is increased for 5 weight percentage filler loading for 10MA-g-NR compound in 40phr batch when compared with pure NR gum. But the cure time was reduced and cure rate index is increased when compared with 5MA-g-NR compound at 5 weight percentage filler loading. This might have resulted in high rubber filler interaction through the anhydride group and is very high in the case of master batch technique.

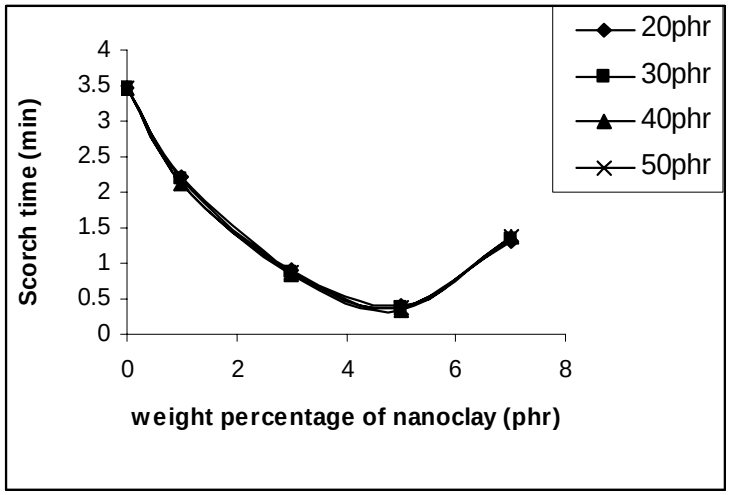

Figure 5.3 (c) Variation of scorch time with nanoclay loading

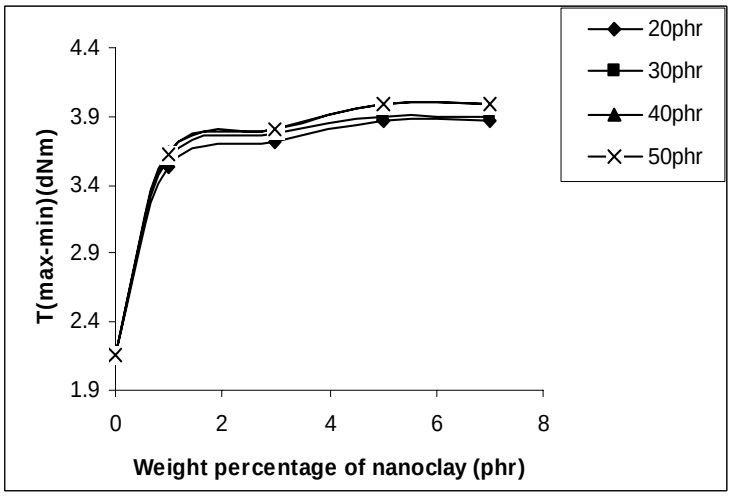

Figure 5.3 (d) Variation of $T_{(max-min)}$ with nanoclay loading

Scorch time is the time required for the torque value to reach 10% of maximum torque. It is a measure of the processing safety- the time available for safe processing before the onset of vulcanization reaction. Scorch time is lower for grafted rubber in the case of master batch as shown in figure 5.3 (c) indicating

better processing safety. The reduction in scorch time for organoclay is due to some catalytic effect of the silicates on the crosslinking reaction [40].

Figure 5.3 (d) shows that the torque development $T_{(max-min)}$ with filler content is higher at 5wt % for10 MA-g-NR when compared to the 5MA-g-NR system. The increased $T_{(max-min)}$ may be arising from the formation of more extensive crosslink. These results are attributed to the intercalation of the rubber with in the silicate galleries. Consequently, a better interaction between the rubber and the filler is obtained.The minimum torque; T_{min}, represents the effective viscosity of the mixtures before vulcanization. It is found to increase with filler loading for both grafted and ungrafted rubber. In the case of polymer nanocomposites filled with various particulate fillers the minimum torque in rheographs is considered to be a direct measure of the filler content. T_{min} can be considered as a measure of stiffness of the unvulcanized compound. The increase in viscosity with the addition of filler suggests a reduced mobility of the rubber chains caused by the incorporation of these fillers.

5.2.4 Mechanical properties of nanocomposites

As the weight percentage of layered silicates increases the tensile strength also increases as evident from figure 5.4. The improvement in tensile properties is so pronounced in10MA-g-NR nanocomposites in 40phr batch developed through master batch means when compare to 5MA-g-NR nanocomposites. After 40phr the enhancement in tensile strength is reduced by 3.23% (i.e. in the case of 50 phr). Intercalation of rubber chains into the layers resulted in increase in tensile strength. The enhancement in properties occurs because of the higher polymer-filler interactions than filler-filler interactions. The MA functional groups are incorporated into the polymer; the stress is much more efficiently transferred from the polymer matrix to the inorganic filler, resulting in a higher increase in tensile properties. The driving force for intercalation originates from the strong hydrogen bonding between the maleic anhydride group (COOH group generated from the hydrolysis of the maleic group) and the oxygen groups of the silicates

[42]. An increment of 87.33% in tensile strength is observed for 10MA-g-NR at 5wt% nanoclay in 40phr batch when compared to the pure NR gum sample. While on the other hand 10MA-g-NR nanocomposites when compared to the 5MA-g-NR at 5wt% nanoclay loading shows an increase in tensile strength of 12.14%.

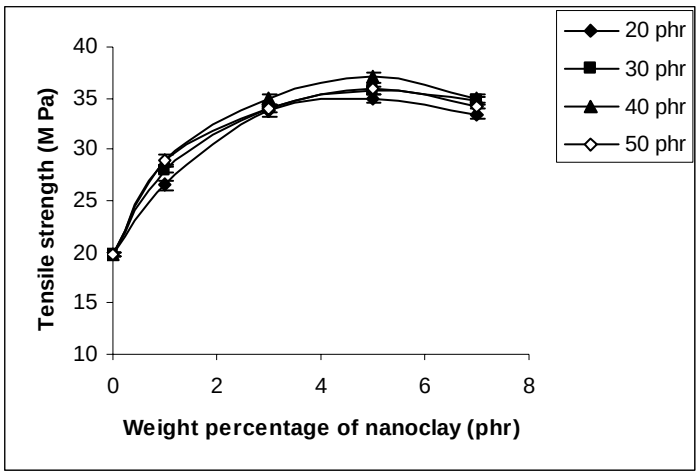

Figure 5.4 Tensile strength of nanocomposites with nanoclay loading

Figure 5.5 is the elongation at break (%) curves of nanocomposites containing varying percentage of nanoclay. The elongation at break of all systems decreases with increase in weight percentage of filler [43]. 10MA-g-NR for 40phr batch at 5wt% nanoclay & 5MA-g-NR with same nanoclay shows a decrement of 26.83 & 7.20% respectively. The decrease at higher loading is due to the enhancement in rigidity of the material and was possibly caused by the reduction in tensile crystallization. All the system shows the same trend. For most of the applications requiring a large initial reinforcement, the ultimate strain is not very crucial.

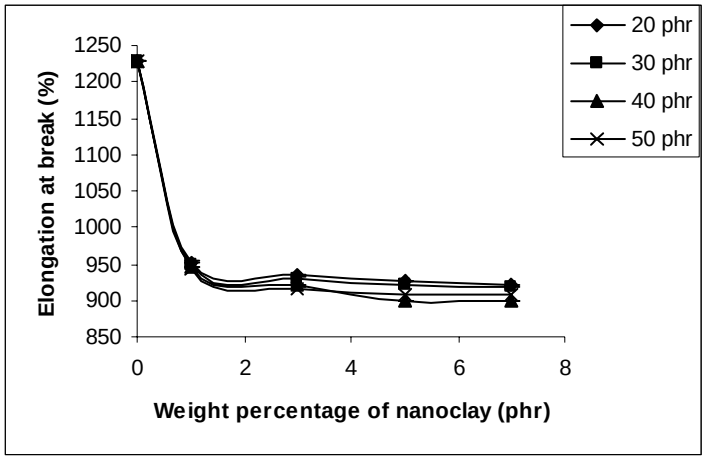

Figure 5.5 Elongation at break (%) of nanocomposites with nanoclay loading.

The dependence of modulus at 300% strain on filler content is shown in figure 5.6. The modulus of all the samples is higher than the gum samples. 10MA-g-NR for 40phr batch with 5wt% nanoclay & 5MA-g-NR with same loading shows an increment in modulus of 162.41 & 78.06% respectively. From the results it is obvious that even with the addition of such a low loading (1-5wt%) of the layered silicates, the modulus increases considerably. The improvement in properties is due to the nanomeric dispersion of silicate layers resulting in efficient reinforcement leading to improved stiffness of the material. The clay platelet aspect ratio has a significant effect on the stiffness of the polymeric material. According to Daniel and co-workers [44] as the matrix modulus increases there is a much higher relative stiffness enhancement in the rubbery state owing to the intercalation of the rubber into the layered silicates.

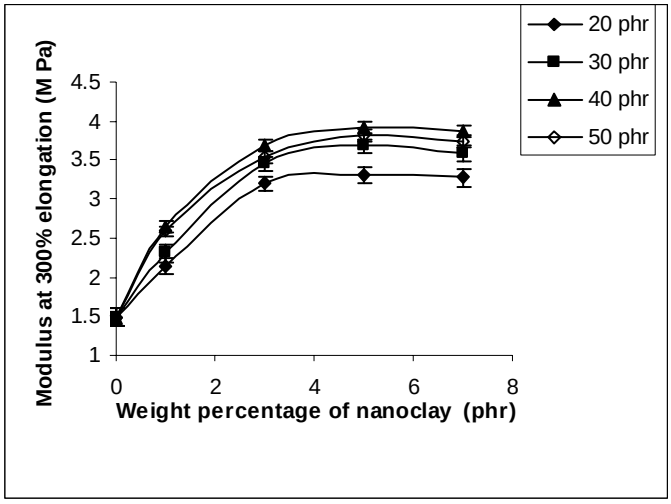

Figure 5.6 Modulus at 300% elongation of nanocomposites with nanoclay loading

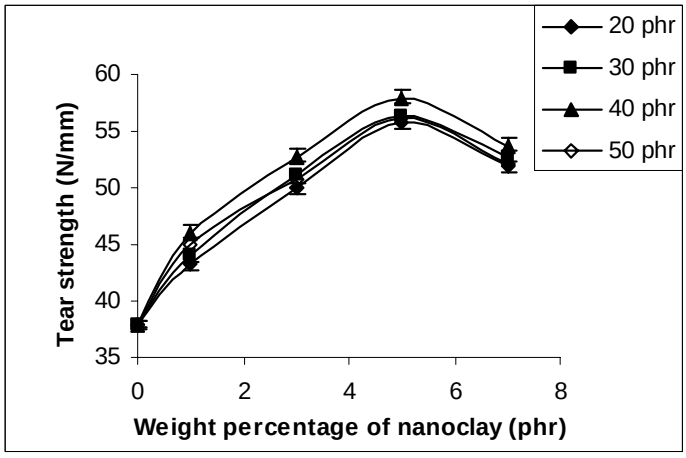

Figure 5.7 Tear strength of nanocomposites with nanoclay loading.

Figure 5.7 is the tear strength curves of the system as a function of weight percentage of nanoclay content. 10MA-g-NR and 5MA-g-NR filled layered silicate exhibit increase in tear strength up to 5wt% nanoclay loading and above that it shows a decrease. 10MA-g-NR for 40phr batch at 5wt% & 5MA-g-NR nanocomposites with 5wt% nanoclay shows an increment in tear strength of

52.57 & 46.32% respectively, indicating the resistance offered in the silicates in order to enhance the crack propagation and the super reinforcement of organoclay. Above all, the finely dispersed silicate layers divert the tear path, which in turn imparts high tear strength to nanocomposites.

Hardness, a measure of low strain elastic modulus, is higher for grafted rubber compared to the ungrafted rubber. From figure 5.8, shows the variation of hardness with nanoclay. 10MA-g-NR for 40phr batch with 5wt% nanoclay & 5MA-g-NR nanocomposites with same nanoclay loading shows an increase in hardness of 76.66% and 30.76% respectively. This is expected because, as more and more nanofiller get into the rubber matrix, the modulus increases and consequently hardness also increases. Here the tensile strength, modulus, tear strength and hardness show the same trend.

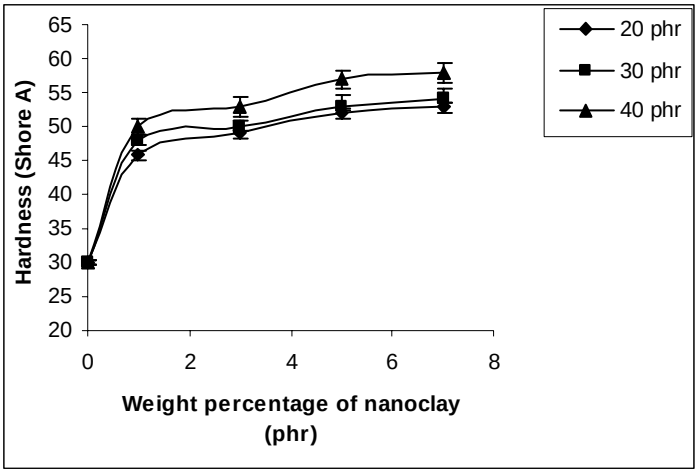

Figure5.8 Hardness of nanocomposites with nanoclay loading

As the hardness increases abrasion loss, which is a measure of reinforcement, should decrease and this is reflected in figure 5.9. The increased crosslink density which results in increased hardness and modulus ultimately gives rise to the enhancement of abrasion resistance. It can be observed that 12.5% decrease in

abrasion loss is observed for 10MA-g-NR nanocomposites at 5wt% for 40phr batch when compared to 5MA-g-NR nanocomposites at same nanoclay loading. This improved abrasion resistance in the organomodified silicate-filled composites is also due to the improved rubber-filler interaction. The intercalation and exfoliation of the modified silicate increased the surface area of the filler, leading to more interaction between the filler and the matrix.

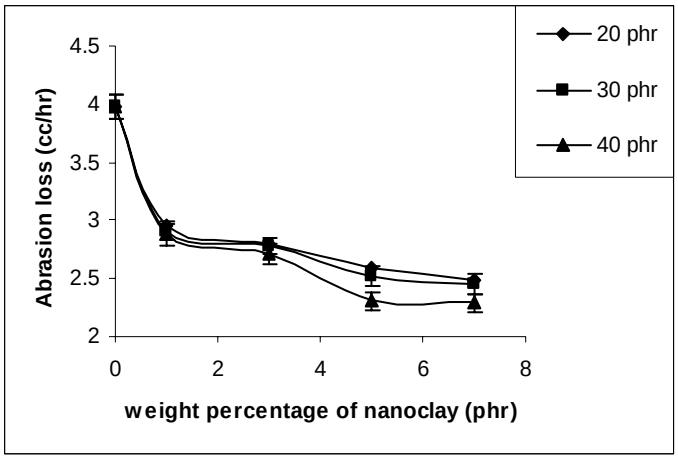

Figure 5.9 Abrasion loss of nanocomposites with nanoclay loading

Compression set values depends strongly on the elastic recovery of the sample. Compression set values which is shown in figure 5.10 is lower for 10MA-g-NR when compared to 5MA-g-NR nanocomposites. It can be observed that 7.2% decrease in compression set values is observed for 10MA-g-NR nanocomposites at 5wt% for 40phr batch when compared to 5MA-g-NR nanocomposites at same nanoclay loading. This can be attributed to higher crosslink density. The lower compression set values indicate a more restrained matrix and elastic deformation is operational.

Resilience, a measure of the elastic component, was found to increase with increase in nanoclay loading. An increase of 11.2% is observed for 10MA-g-NR nanocomposites at 5wt% for 40phr batch compared to 5MA-g-NR at same nanoclay loading. The rebound resilience is increased by the increase in modulus.

This is due to the high reinforcement between the filler and the elastomer as shown in figure 5.11.

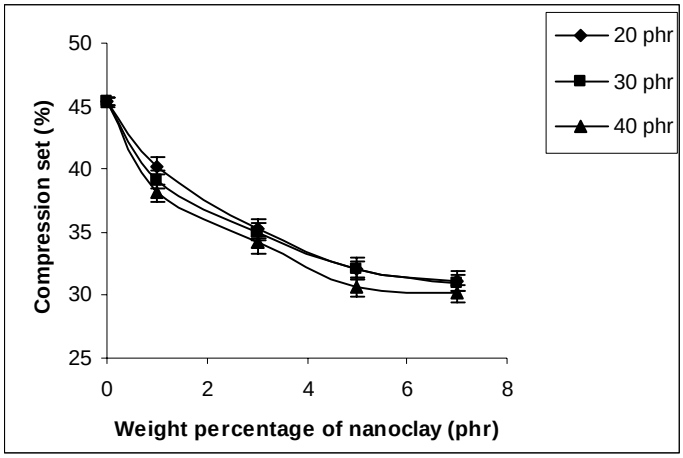

Figure 5.10 Compression set of nanocomposites with nanoclay loading

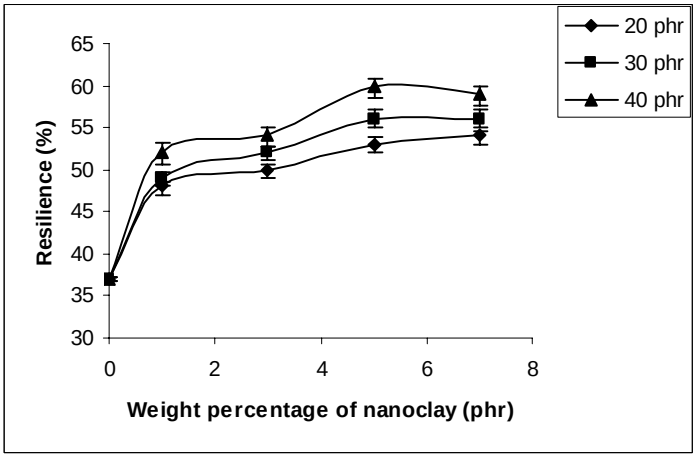

Figure 5.11 Resilience of nanocomposites with nanoclay loading

It is seen that the nanocomposite with the clay having higher interlayer distance shows better mechanical properties. This suggests that interlayer distance play a major role in the intercalation of the rubber matrix

5.2.5 Strain sweep measurements of uncured compounds

The complex modulus (G*) values obtained for the uncured compounds are plotted and shown in figure 5.12. The elastic modulus of a filled rubber is strongly dependent on the deformation and decreases substantially at higher strains. This phenomenon is known as Payne effect and is attributed to the presence and breakdown of the filler network during deformation. But investigations performed with both experimental and theoretical approaches shows that the decrease in G* with amplitude of deformation (strain) is attributed to the destruction-reformation of a percolating network of filler that can also involve polymer bonded filler [45] i.e. polymer filler links also. The complex modulus values at low strains (15%) are due to polymer networks and hydrodynamic interactions [46]. The limiting values at high strains are due to polymer networks and hydrodynamic effect. Polymer networks are the same for a fixed mass of rubber. But the hydrodynamic effect varies with the filler content and the nature of the filler. The theoritical meaning of hydrodynamic effect is given by the modified form of Guth and Gold equation [47, 48].

The addition of filler increases the shear modulus, G_f for the filled compound

$$G_f = G_0 (1+0.67\ fs\phi +11.62\ fs^2\phi^2)$$

Where ϕ is the volume fraction of the particles and the shape factor fs represents the ratio of the longest dimension to the shortest dimension of the particle. The modulus as calculated by the equation is independent of the applied strain [49]. The variation of complex modulus (G*) with strain for the composites with clay are presented in figure 5.12. The graph show that the complex modulus values at low strain increases with filler concentration. As the complex modulus values of G* is due to higher filler-filler or filler polymer interactions. Variation in mechanical properties of the composites explained earlier shows that the network formed are mainly between filler and polymer.

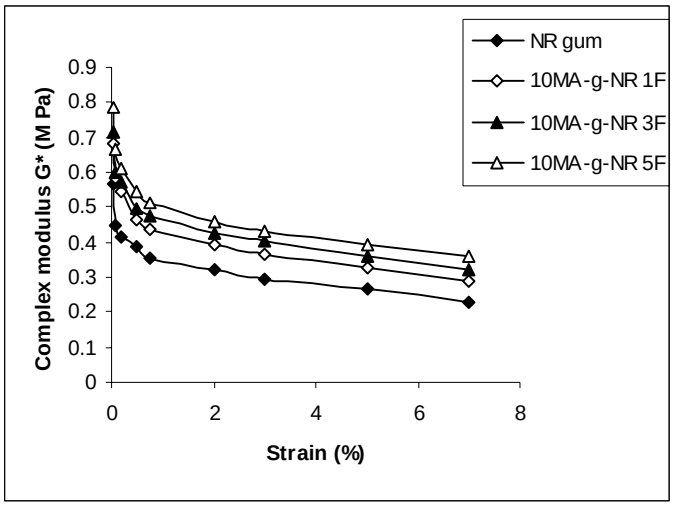

Figure 5.12 Variation of complex modulus with nanoclay content for10MA-g-NR nanocomposites at 40phr

5.3 Conclusions

Maleated natural rubber-organoclay nanocomposites can be prepared with nanoclay in varying clay loading and the clay content influences the cure characteristics and mechanical properties of maleated natural rubber. In presence of organoclay both the cure time and scorch time are considerably reduced. This reduction in cure time is boosted with the increase in interlayer distance of the clay. A dramatic increase in maximum torque value with increase in clay loading is also observed for the nanocomposites. The mechanical properties of 10MA-g-NR nanocomposites are higher than 5MA-g-NR nanocomposites which are obtained by direct method. Nanocomposites with the clay having higher interlayer distance shows better mechanical properties. The increase in d spacing for these layered clays evident from X-ray results and TEM photographs also confirmed the formation of partially intercalated and exfoliated structure.

References

1. Fornes TD, Yoon PJ, Hunter DL, Keskkula H, Paul DR. Polymer 2002;43:5915.
2. Gilman JW, Jackson CL, Morgan AB, Harris JR, Manias E, Giannelis EP, et al. Chem Mater 2000;12:1866.
3. Liu T, Tjiu C, He C, Na SS, Chung TS. Polym Int 2004;53:392.
4. Ma J, Yu ZZ, Zhang QX, Xie XL, Mai YW, Luck I. Chem Mater 2004;16:757.
5. Chang JH, An YU, Sur GS. J Polym Sci, Part B: Polym Phys 2003;41: 94.
6. Konstantinos G. G, Karger-Kocsis J. Polymer 2005;46:3069.
7. Cox HL. Br J Appl Phys 1952;3:72.
8. Hull D. An introduction to composite materials. London: Cambridge University Press; 1981.
9. Zanetti M, Lomakin S, Camino G. Macromol Mater Eng 2000;279:1.
10. LeBaron PC, Wang Z, Pinnavaia TJ. Appl Clay Sci 1999;15:11.
11. Ray SS, Okamoto M. Prog Polym Sci 2003;28:1539.
12. Kornmann X, Thomann R, Mu¨lhaupt R, Finter J, Berglund L. J Appl Polym Sci 2002;86:2643.
13. Alexandre A, Dubois P. Mater Sci Eng R 2000;28:1.
14. Kawasumi M, Hasegawa N, Kato M, Usuki A, Okada A Macromolecules1997;30:6333.
15. Chow WS, Mohd Ishak ZA, Karger-Kocsis J, Apostolov AA, Ishiaku US. Polymer 2003;44:7427.
16. Zilg C, Thomann R, Finter J, Mu¨lhaupt R. Macromol Mater Eng 2000; 280/281:41.
17. Fornes TD, Hunter DL, Paul DR. Macromolecules 2004;37:1793.
18. Fornes TD, Yoon PJ, Keskkula H, Paul DR. Polymer 2001;42: 9929.
19. Zheng H, Zhang Y, Peng Z, Zhang Y. J Appl Polym Sci 2004;92: 638.
20. Li X, Ha CS. J Appl Polym Sci 2003;87:1901.

21. Maiti P, Yamada K, Okamoto M, Ueda K, Okamoto K. Chem Mater 2002; 14:4654.
22. Lan T, Kaviratna D, Pinnavaia TJ. Chem Mater 1995;7:2144.
23. Svoboda P, Zeng C, Wang H, Lee LJ, Tomasko DL. J Appl Polym Sci 2002;85 :1562.
24. Maiti P, Nam PH, Okamoto M. Macromolecules 2002;35:2042.
25. Hambir S, Bulakh N, Jog JP. Polym Eng Sci 2002;(42):800.
26. Kalgaonkar RA, Jog JP. J Polym Sci, Part B: Polym Phys2003;41 :3120.
27. Wang Z,Pinnavaia TJ. Chem Mater 1998;10:1820.
28. Lan T Pinnavaia TJ,Chem SN,Lopez BH.J Appli Polym Sci 1992;44:1820.
29. Kawasumi M, Hasegawa N, Kato M, Usuki A, Okada A. Macromolecules1997;30:6333.
30. Garcı´a-Lo´ pez D, Picazo O, Merino JC, Pastor JM. Eur Polym J 2003;39:945.
31. Lertwimolnun W, Vergnes B. Polymer 2005;46:3462.
32. Preschilla N, Sivalingam G, Abdul Rasheed AS, Tyagi S, Biswas A, Jayesh RB. Polymer 2008;49:4285.
33. Reichert P, Nitz H, Klinke S, Brandsch R, Thomann R, Mulhaupt R. Macromol Mater Eng 2000;275:8.
34. Hasegawa N, Okamoto H, Kawasumi M, Kato M, Tsukigase A, Usuki A. Macromol Mater Eng 2000;280/281:76.
35. Lopez-Manchado MA, Herrero B, Arroyo M. Polym Int 2003;52:1070.
36. Arroyo M, Lopez-Manchado MA, Herrero B. Polymer 2003;44:2447.
37. Lopez-Manchado MA, Arroyo M, Herrero B, Biagiotti J. J Appl Polym Sci 2003;89:1.
38. Vu YT, Mark JE, Pham LH, Engelhardt M. J Appl Polym Sci 2001;82 :1391.
39. Perrin-Sarazin F, Ton-That MT, Bureau MN, Denault J Polymer 2005;46:1162.

40. Varghese S, Karger-Kocsis J, Gatos K. G. Polymer 2003;44:3069.
41. Varghese, S.; Karger-Kocsis, J. J Appl Polym Sci 2004;91:813.
42. Xiaohui L, Qiuju W. Polymer 2001;42:10013.
43. Nielsen LE, Landel RF. Mechanical properties of Polymers and composites, 2nd ed., Marcel Dekker, Inc.,1994; p545.
44. Varghese S, Gatos KG, Apostolov AA, Karger-Kosis. J Appl Polym Sci 2004;92:543.
45. Kluppel M, Schuster HR, Heinrich G. Rubber Chem Technol 1997; 70:243.
46. Jean L, Leblanc MC. J Appli Polym Sci 2001; 80; 11: 2093.
47. Guth E, Gold O. Phys Rev 1938;53:322.
48. Smallwood HM. J Appli Phys 1944;15:758.
49. Stickney PB, Falb RD. Rub Chem Technol 1964;37:1299.

Chapter 6

Thermal stability and ageing properties of maleated natural rubber organoclay nanocomposites

Thermogravimetric analysis of a polymeric material gives information about the stability and thermal degradation. A detailed understanding of the degradation characteristics of polymers on heating is essential for selecting materials with improved properties for specific application. It measures the change in weight of the material when it is heated against temperature in an inert atmosphere or in the presence of air or oxygen. When a compounded rubber is heated, the polymer part will get degraded first. Further heating will remove all organic matter, leaving inorganic components in the compound. The thermal degradation of polymer generally follow two paths, viz., unzipping and random. The unzipping mechanism gives the pure monomer while the random degradation leads to the formation of a host of products, depending on the structure of the polymer. Most of the polymers have carbon-carbon (C-C) chain as the backbone; hence their thermal stability depends on the stability of the C-C bond. The degradation of polymers is affected by the substituents in the backbone chain. The higher number of substituents usually decreases its thermal stability while the aromatic groups in a polymer backbone increase the thermal stability. The presence of oxygen atom and branching makes the polymer more susceptible to degradation. Thermal stability means the ability of a material to maintain the required properties such as strength, toughness, or elasticity at a given temperature. The assessment of thermal stability of polymeric materials can provide valuable technical information [1]. The demand for polymers, which could be used in high temperature applications, stimulated the investigations to unravel the relationship between thermal properties and chemical structure [2].

The addition of particulate fillers to elastomers resulting in enhancement in stiffness and resistance to fracture is one of the most important phenomena in material science and technology. The commonly used white fillers in rubber industry are clay and silica. The polymer/clay nanocomposites offer enhanced thermo mechanical properties. Bourbigot *et al.* [3] observed that the thermal stability of polystyrene (PS) is significantly increased in presence of nanoclay. Thermal and mechanical properties of clays multiwalled carbon nanotubes reinforced ethylene vinyl acetate (EVA) prepared through melt blending showed synergistic effect in properties [4]. Hu *et al.* [5] observed that as the chain length of alkyl group of the organically modified clay increased the thermal stability of the polymer. Thermal stability of nanofiller reinforced rubber composite has been analyzed by Varghese *et al.* [6]. Singh and co-workers [7] reviewed the thermal stability of different polymer nanocomposites. They found that the nanocomposites of all polymers showed higher thermal stability with dispersion of clay.

The thermal stability and ageing studies by thermal, radiation and ozone on maleated natural rubber nanocomposites and nanocomposites developed through masterbatch technique of different maleic anhydride (MA) content and filler loading is proposed to be investigated in this chapter.

6.1 Experimental

6.1.1 Maleated natural rubber clay nanocomposites

6.1.1.1 A Thermogravimetry

Thermogravimetric analysis measures the change in weight of the material when it is heated in the presence of inert atmosphere or in the presence of air/oxygen. When a rubber compound is heated at lower temperature the volatile components will move out. At 100^0C water present in the rubber will get evaporated. When heating, continues the polymer part will get degraded and converted into gaseous products, a corresponding loss in weight is reflected in the curve. Further heating

will remove all organic matter, giving the weight of inorganic fillers in the compound.

TG curves of MA-g-NR nanocomposites are presented in figure 6.1. The thermal stability of filled MA-g-NR samples is higher than unfilled system. At lower temperature there is no remarkable difference in thermal stability between unfilled and filled systems. At higher temperature nanofilled MA-g-NR shows enhanced thermal stability due to the barrier effect arising from the dispersion of clay platelets. As the filler content increases the thermal stability is less efficient due to the less optimal platelet dispersion. Filled samples show more residue than unfilled sample because of the presence of inorganic fillers, which is more thermally stable. Up to 5wt% nanoclay loading the thermal stability is increased and above it the thermal stability decreased due to the poor dispersion of clay platelets. Literature shows that the main products of thermal degradation of natural rubber (NR) are isoprene, dipentene and p- methane [8].

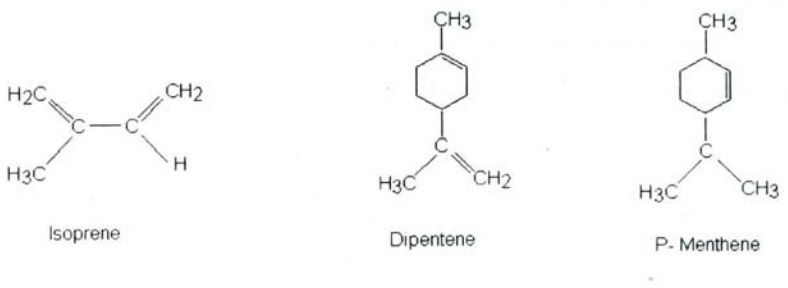

6.1.1.1 B Thermal degradation kinetics

Thermal degradation kinetics of MA-g-NR nanocomposites is studied by Coats Redfern and Freeman Carroll method.

6.1.1.2 Ageing resistance of maleated natural rubber clay nanocomposites

6.1.1.2 A Thermal ageing resistance

Thermal ageing was carried out at a temperature of 100^0C for 72hrs in a preheated oven. An understanding of the ageing behaviour of maleated natural rubber samples is essential for maintaining the physical properties of rubber goods during service. The vulcanized rubber may undergo chain scission reactions as well as crosslinking reactions during service life at elevated temperatures. The addition of fillers to rubber can improve the ageing resistance. The mechanical properties of thermally aged nanofilled samples have been investigated. During ageing, as a result of thermo-oxidative degradation; the properties of rubber get deteriorated. In presence of inorganic nanofillers the thermal stability of the rubber matrix does not decrease. This can be explained in terms of the enhancement in polymer-filler interaction due to the high aspect ratio of nanofillers.

6.1.1.2 B Radiation ageing

Dumbbell shaped tensile test samples of 2 ± 0.2mm thickness were irradiated with gamma (γ) rays in a Gamma Chamber 5000 (figure2.1 in chapter 2). The samples were irradiated for different radiation doses at a dose rate of 2kGy per hour in air at room temperature. The tensile strength was measured before and after irradiation and the percentage retention was calculated.

6.1.1.2 C Ozone ageing

The chamber provided an atmosphere with a controlled concentration of ozone and temperature. Ozone concentration selected was 50pphm, which is generated by an UV quartz lamp. The conditioned samples were exposed to the ozonized air in the chamber. Periodic observations of the surface of the samples were made for crack initiation. Samples were exposed for longer time. Surfaces of the irradiated samples were scanned on a macro viewer of LEICA Q 500 IW image analyzer, images were acquired and the photo prints were taken.

6.1.1.3 Test for flammability

Flame resistance of vulcanisates of maleated natural rubber clay nanocomposites were evaluated as per UL 94 overview-test for flammability

6.1.1.4 Differential scanning calorimetric analysis

The differential scanning calorimetry of maleated natural rubber gum and nanoclay loaded samples were recorded with a differential scanning calorimeter Q-100, TA instruments. The energy changes associated with transitions were recorded in a temperature range of -60 to 100^0C.

6.2 Results and Discussion

6.2.1 Maleated natural rubber clay nanocomposites

6.2.1.1 A Thermogravimetric analalysis

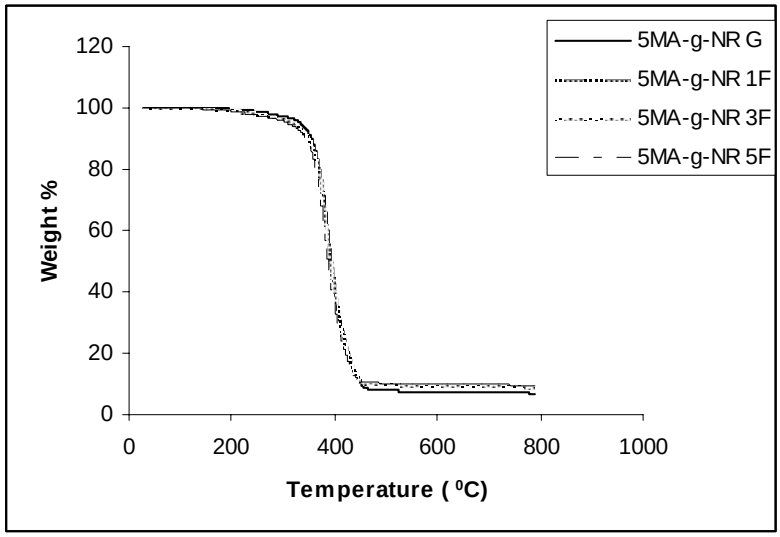

Figure 6.1 TGA curves of 5MA-g-NR nanocomposites

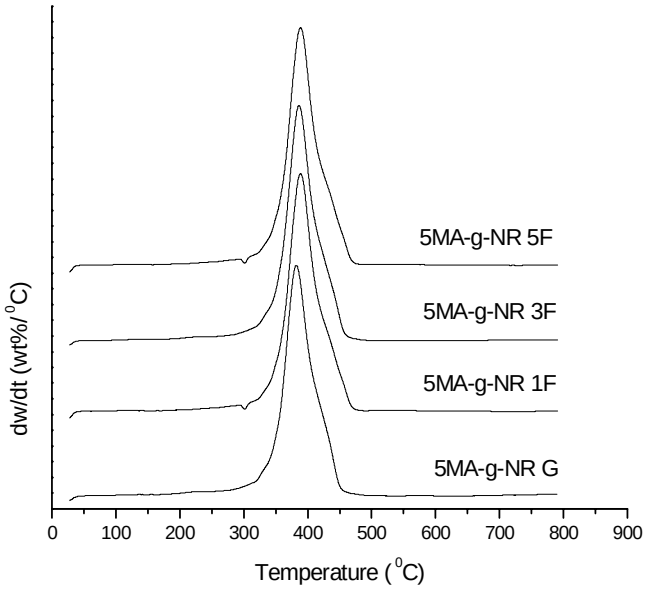

Figure 6.2 DTG curves of 5MA-g-NR nanocomposites

Table 6.1 shows the degradation temperature at different percentage of weight losses for 5MA-g-NR nanocomposites. It is found that thermal stabilization is higher for clay filled samples than the unfilled system and this is due to the better dispersion of rubber in between the silicate galleries.

Table 6.1 Degradation temperature at varying % of weight losses of 5MA-g-NR nanocomposites

Degradation temperature (^{0}C)				
Sample	$T_{5\%}$	$T_{10\%}$	$T_{50\%}$	$T_{90\%}$
5 MA-g-NR G	323	350	388	476
5 MA-g-NR 1F	325	352	391	478
5 MA-g-NR 3F	330	353	394	483
5 MA-g-NR 5F	334	350	389	485

The temperature at which maximum decomposition (T_{max}) occurred is shown in Table 6.2. How ever as compared to pristine polymer the temperature for maximum decomposition increases due to the higher extent of clay delamination in the polymer matrix. .

Table 6.2 Temperature at maximum degradation of 5MA-g-NR nanocomposites.

Sample	T_{max} (^{0}C)
5MA-g-NR G	383
5MA-g-NR 1F	385
5MA-g-NR 3F	386
5MA-g-NR 5F	389

The TG and DTG graph of 3MA-g-NR nanocomposites are shown in figure 6.3 & 6.4 respectively. Here with the addition of silicate the thermal stability of 3MA-g-NR nanocomposites shows the same trend as 5MA-g-NR nanocomposites.

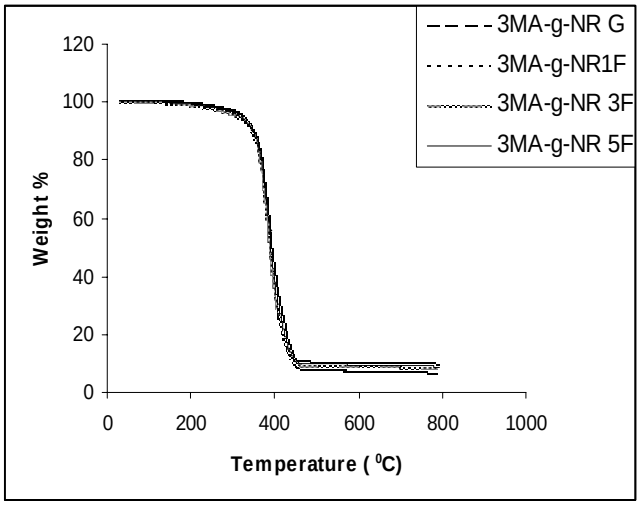

Figure 6.3 TG curves of 3MA-g-NR nanocomposites

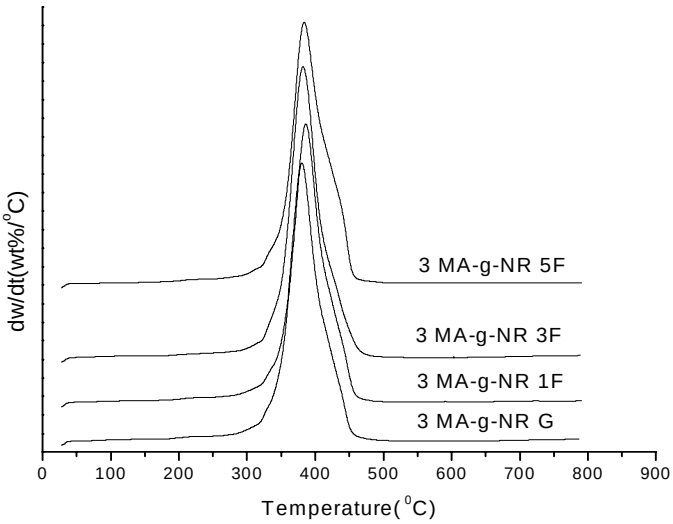

Figure 6.4 DTG curves of 3MA-g-NR nanocomposites

Table 6.3 Degradation temperature at varying % of weight losses of 3MA-g-NR nanocomposites

Degradation temperature(^{0}C)				
Sample	$T_{5\%}$	$T_{10\%}$	$T_{50\%}$	$T_{90\%}$
3 MA-g-NR G	320	345	385	456
3 MA-g-NR 1F	323	347	389	470
3 MA-g-NR 3F	326	350	390	480
3 MA-g-NR 5F	329	352	392	482

Table 6.4 Temperature at maximum degradation of 3MA-g-NR nanocomposites.

Sample	$T_{max}(^0C)$
3MA-g-NR G	379
3MA-g-NR 1F	380
3MA-g-NR 3F	380
3MA-g-NR 5F	385

At higher temperature nanofilled rubber shows enhanced thermal stability due to the barrier effect arising from the dispersion of clay. The decomposition temperature of 3MA-g-NR nanocomposites is shown in table 6.3. The temperature for maximum degradation also increases; it is given in table 6.4. The residue of both 5MA-g-NR & 3MA-g-NR nanocomposites are found to increase constantly as a function of clay loading. On comparison of the two maleic anhydride concentration of layered silicate reinforced sample the remaining is higher for 5MA-g-NR owing to its reinforcement in the polymer matrix. The residue of filled samples plotted against filler concentration is shown in figure 6.5. As the filler content increases the residue weight percentage for nanocomposite are found to increase. It is reported that the layered silicates filled polymer matrix can improve thermal stability and is explained to the hinderd diffusion of volatile decomposition products of the nanocomposite [9-13]. Qin *et al.* [14] reported that in oxygen atmosphere the degradation of samples mainly takes place through oxygenolysis. In this case, the barrier effect of the silicate layers is higher owing to the formation of carbonaceous silicate char on the surface of the nanocomposite resulting in the enhancement of thermal stability of nanocomposite. Sometimes, the thermal stability decreases at higher clay content

and has been explained in terms of the lower extent of clay delamination in the polymer matrix.

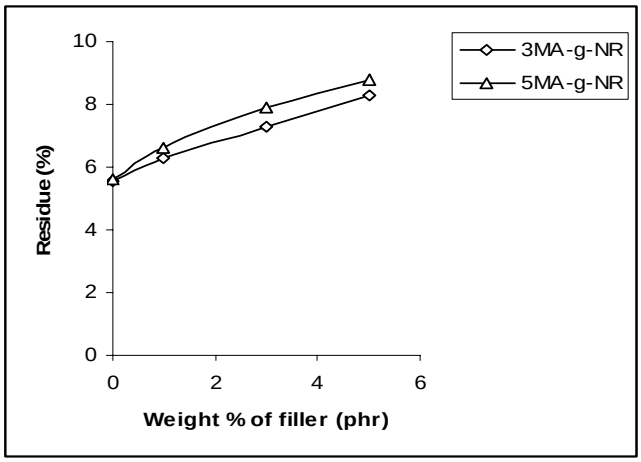

Figure 6.5 Residue (%) of MA-g-NR nanocomposites with filler loading

6.2.1.1 B Thermal degradation kinetics

The kinetics of the thermal degradation reaction was followed using TGA. The activation energy values for degradation can give an idea about the thermal stability of the system. The activation energy for degradation of MA-g-NR clay nanocomposites was determined by applying Coats-Redfern (CR) equation (equation 2.25) in Chapter 2. It is an integral method and the following equation is used for a first order reaction. Representative plots of each MA concentration for n = 1 are given in figure 6.6 and 6.7. The activation energies obtained from the corresponding plots are presented in table 6.5. It is found that the activation energy required for the thermal degradation of silicates filled samples is higher than pristine polymer. It indicates the enhanced thermal stability of nanofilled samples. The higher thermal stability of nanocomposites can be explained in terms of the barrier effect of the silicate layers on the surface of the polymer matrix.

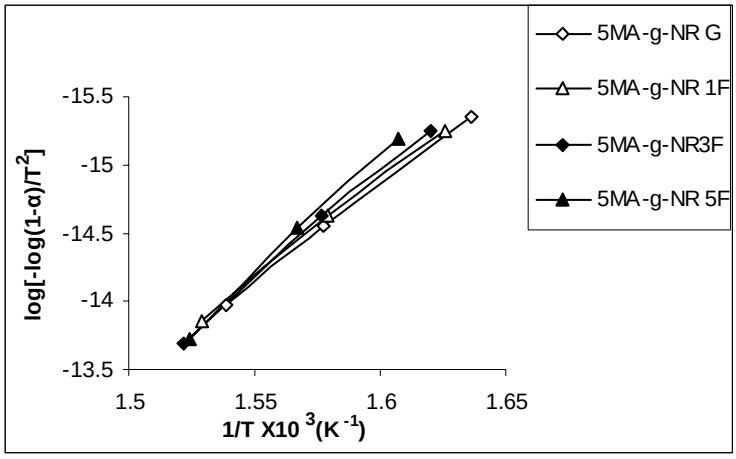

Figure 6.6 Coats-Redfern plots of 5MA-g-NR nanocomposites

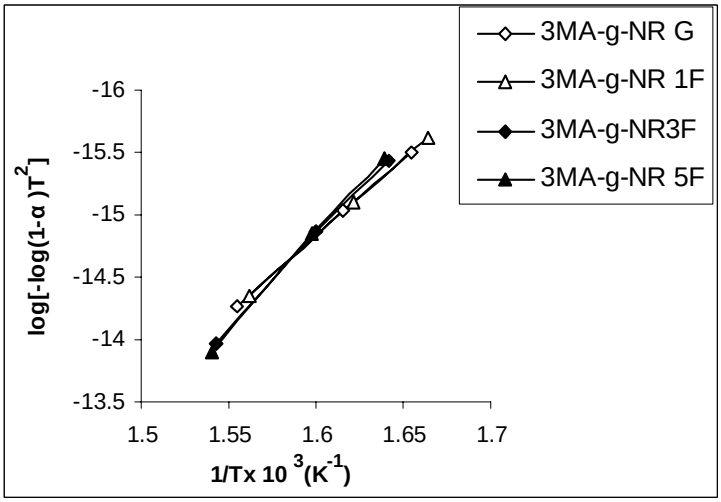

Figure 6.7 Coats-Redfern plots of 3MA-g-NR nanocomposites

The activation energy and order for the main stage of decomposition of MA-g-NR nanocomposites are determined using the Freeman and Carroll (FC) method (equation (2.22)) in Chapter 2. FC plots for the determination of activation energy of layered silicates reinforced nanocomposites are given in figures 6.8 and 6.9 respectively.

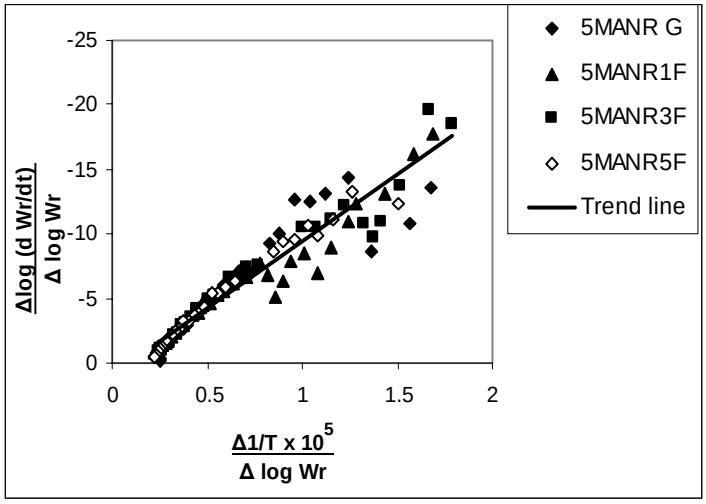

Figure 6.8 Freeman Carroll plots of 5MA-g-NR nanocomposites

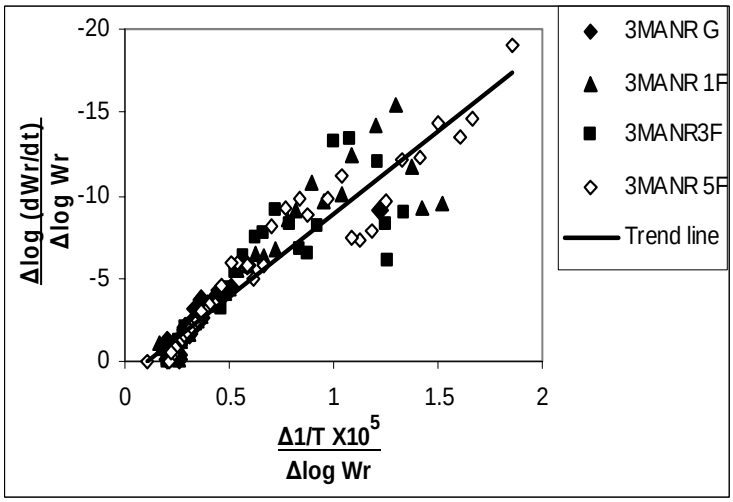

Figure 6.9 Freeman Carroll plots of 3MA-g-NR nanocomposites

In summary, both the methods indicate the order of the degradation reaction to be one.

Table 6.5 Kinetic parameters obtained from both methods

Sample	Coats Redfern	Freeman Carroll	
		Ea (kJ/mol)	n
5 MA-g-NR G	265.52	189.5	1.01
5 MA-g-NR 1F	277.70	196.4	1.03
5 MA-g-NR 3F	292.64	200.8	1.07
5 MA-g-NR 5F	343.39	203.3	1.07
3 MA-g-NR G	229.38	184	1.05
3 MA-g-NR 1F	235.97	188.4	1.02
3MA-g-NR 3F	281.48	190.1	1.02
3MA-g-NR 5F	296.60	197.9	1.06

6.2.2 Maleated natural rubber clay nanocomposites developed through masterbatch technique

6.2.2.1 A Thermogravimetry

10MA-g-NR at nanoclay loading of 20phr to 50phr was studied. From that it is understand that up to 40phr loading, most of the properties show an increasing trend and after which the property levels off. Here the 10MA-g-NR masterbatch is diluted with virgin NR to make the clay loading to 1, 3, 5 and 7 weight percentages. The properties of 10MA-g-NR nanocomposites are compared with pure NR gum sample in the masterbatch technique. 10MA-g-NR nanocomposites shows the same trend as 5MA-g-NR nancomposites but an increase in property is observed in the case of former.

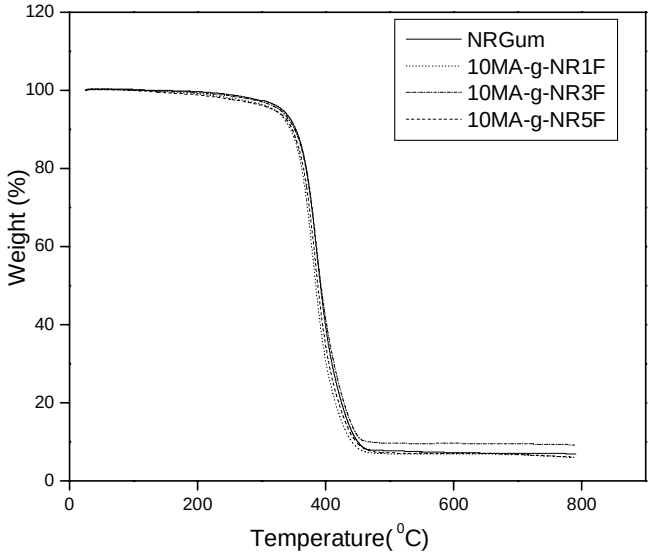

Figure 6.10 TG curves of 10MA-g-NR nanocomposites at 20phr masterbatch

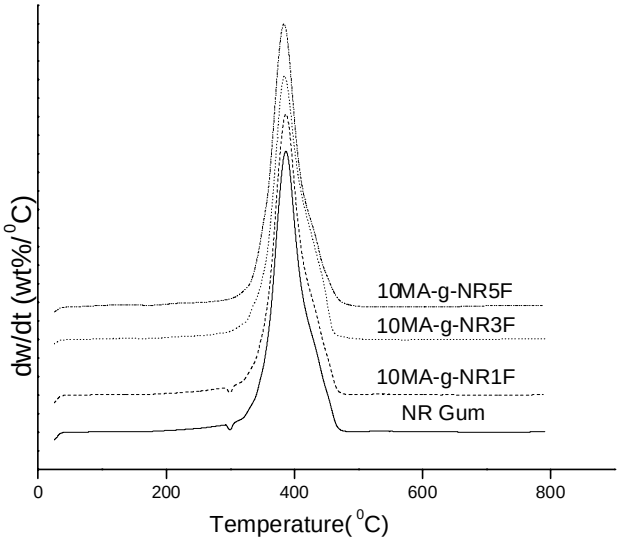

Figure 6.11 DTG curves of 10MA-g-NR nanocomposites at 20phr masterbatch

Maximum thermal stability is observed for 40 phr masterbatch when compared to the previous systems. This is due to the barrier effect which increases during volatilization owing to the reassembly of the reticular of the silicate on the surface. The incorporation of clay into the polymer matrix was found to enhance thermal stability by acting as a superior insulator and mass transport barrier to the volatile products generated during decomposition. Figure 6.10 and 6.11 shows the TG and DTG curves of 10MA-g-NR nanocomposites at 20phr masterbatch and figure 6.12 and 6.13 shows the TG and DTG curves of 10MA-g-NR nanocomposites at 40phr masterbatch. Table 6.6 and 6.8 degradation temperatures at varying % of weight losses of 10MA-g-NR nanocomposites at 20phr and 40phr clay loading. The temperature at maximum degradation of 20phr and 40phr are shown in tables 6.7 and 6.9 respectively. Residue (%) of 10MA-g-NR nanocomposites with filler loading is shown in figure 6.14.

Table 6.6 Degradation temperatures at varying % of weight losses of 10 MA-g-NR nanocomposites at 20phr clay loading

Degradation temperature (^{0}C)				
Sample	$T_{5\%}$	$T_{10\%}$	$T_{50\%}$	$T_{90\%}$
Pure NR Gum	321	350	374	449
10 MA-g-NR 1F	334	362	389	480
10 MA-g-NR 3F	338	369	394	485
10 MA-g-NR 5F	340	375	401	489

Table 6.7 Temperature at maximum degradation of 20phr MA-g-NR nanocomposites.

Sample	T_{max}(^{0}C)
Pure NR Gum	369
10 MA-g-NR 1F	386
10 MA-g-NR 3F	388
10 MA-g-NR 5F	391

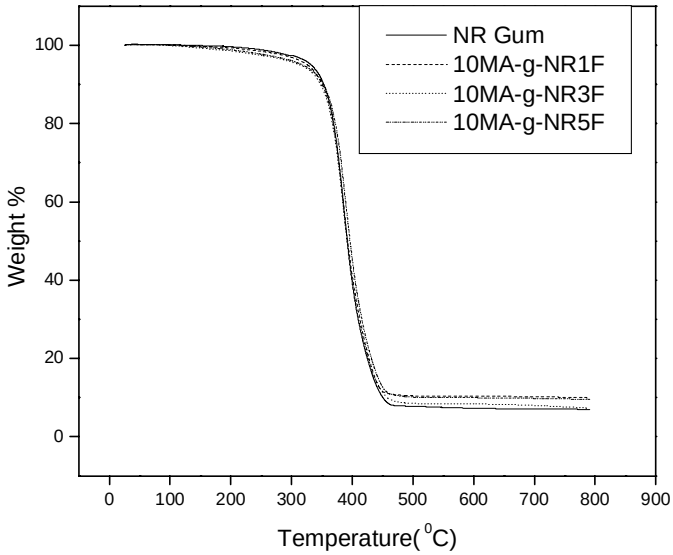

Figure 6.12 TG curves of 10MA-g-NR nanocomposites at 40phr masterbatch

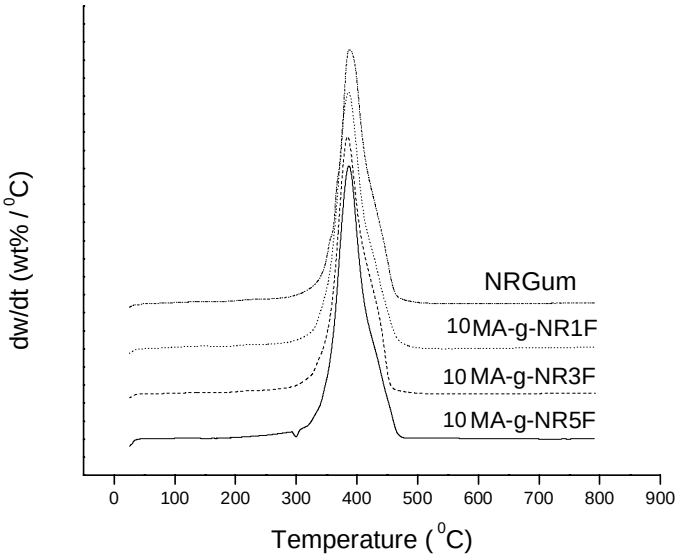

Figure 6.13 DTG curves of 10MA-g-NR nanocomposites at 40phr masterbatch

Table 6.8 Degradation temperature at varying % of weight losses of 40phr 10MA-g-NR nanocomposites

Degradation temperature (^{0}C)				
Sample	$T_{5\%}$	$T_{10\%}$	$T_{50\%}$	$T_{90\%}$
Pure NR Gum	321	350	374	449
10MA-g-NR 1F	337	366	394	463
10MA-g-NR 3F	341	373	398	493
10MA-g-NR 5F	344	381	409	494

Table 6.9 Temperature at maximum degradation of 40phr 10MA-g-NR nanocomposites.

Sample	$T_{max}(^0C)$
Pure NR Gum	369
10 MA-g-NR 1F	388
10 MA-g-NR 3F	391
10 MA-g-NR 5F	398

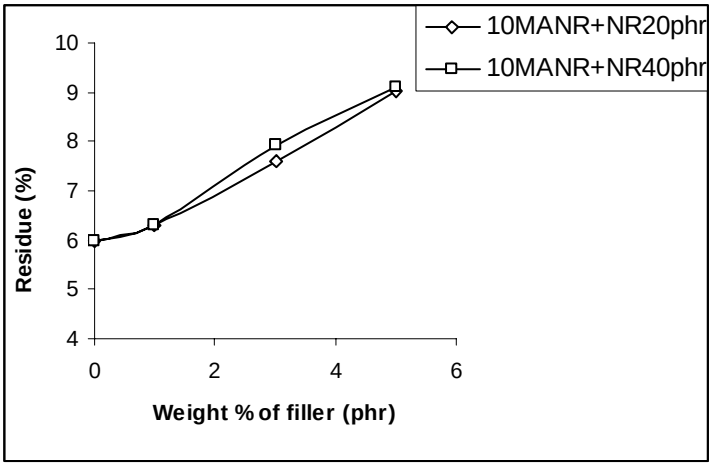

Figure 6.14 Residue (%) of 10MA-g-NR nanocomposites with filler loading

The clay acts as a heat barrier, which enhances the overall thermal stability of the system, as well as assist in the formation of char after thermal decomposition. In early stages of thermal decomposition, the clay would shift the decomposition to higher temperature. After that, this heat barrier effect would result in a reverse thermal stability. In other words, the stacked silicate layers could hold

accumulated heat that could be used as a heat source to accelerate the decomposition process, in conjugation with the heat flow supplied by the out side heat source [15].

6.2.2.1 B Thermal degradation kinetics

The activation energy values for degradation can give an idea about the thermal stability of the system. The activation energy for degradation of MA-g-NR clay nanocomposites was determined by applying Coats-Redfern (CR) equation (equation 2.25) in Chapter 2. It is an integral method and the following equation is used for a first order reaction. Representative plots of each masterbatch at 10MA concentration for $n = 1$ are given in figure 6.15 and 6.16. The activation energies obtained from the corresponding plots are presented in table 6.10. It is found that the activation energy required for the thermal degradation of silicate filled samples is higher than pristine polymer. It indicates the enhanced thermal stability of nanofilled samples. It is found that the activation energy required for thermal degradation of silicate filled samples is higher than pristine polymer. This also supports higher thermal stability.

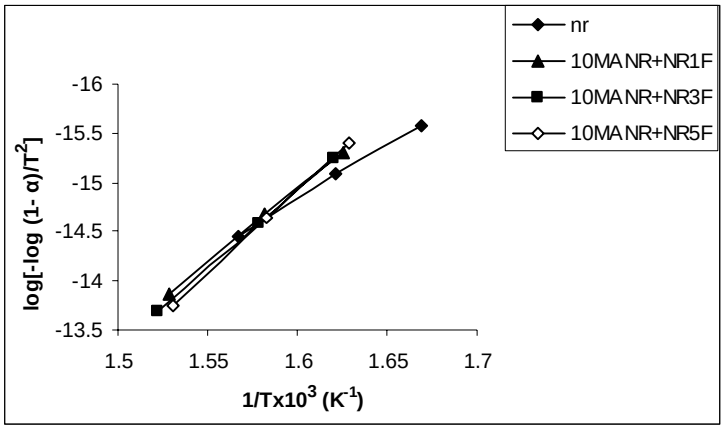

Figure 6.15 Coats-Redfern plots of 20phr nanoclay masterbatch

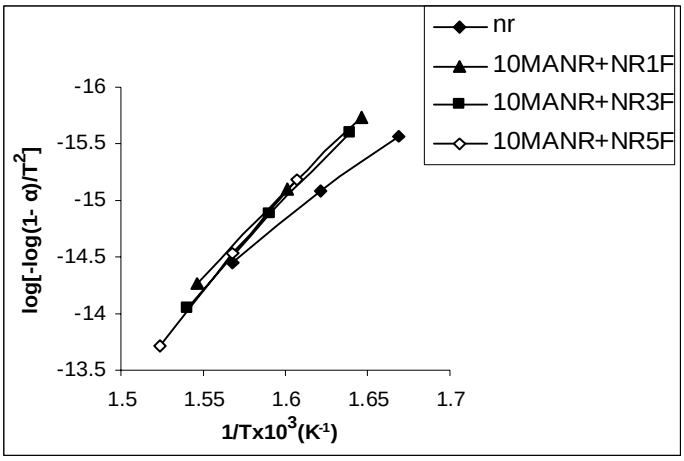

Figure 6.16 Coats-Redfern plots of 40phr nanoclay masterbatch

The activation energy and order for the main stage of decomposition of MA-g-NR nanocomposites are determined using the Freeman and Carroll (FC) method using the equation (2.22) in Chapter 2. FC plots for the determination of activation energy of layered silicate reinforced nanocomposites are given in figures 6.17 and 6.18 respectively.

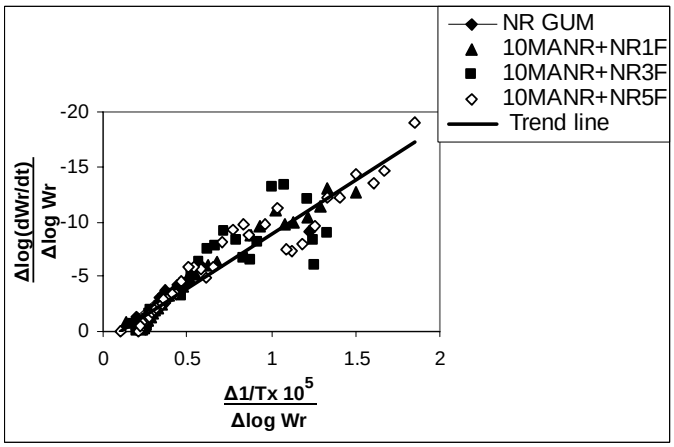

Figure 6.17 Freeman Carroll plots of 20phr nanoclay masterbatch

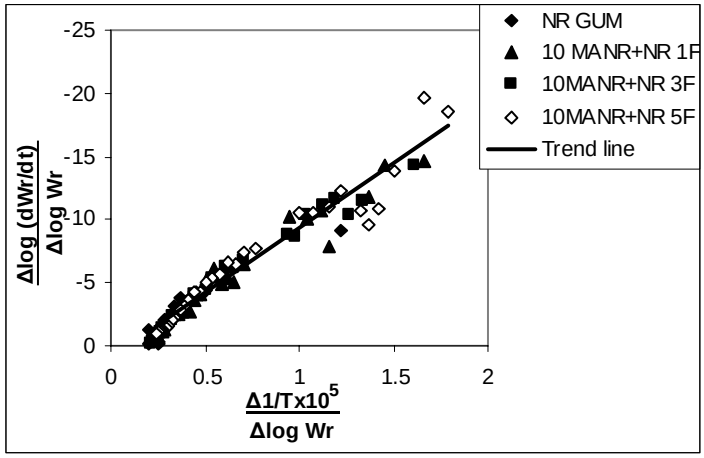

Figure 6.18 Freeman Carroll plots of 40phr nanoclay masterbatch

The order of reaction is one from both the CR and FC methods.

Table 6.10 Kinetic parameters obtained from CR and FC methods

Sample	Coats Redfern	Freeman Carroll	
		Ea (kJ/mol)	n
NR Gum	203.19	183.45	1.06
10MA-g-NR 1F, 20phr	279.66	187.38	1.07
10 MA-g-NR 3F, 20phr	296.79	187.99	1.02
10 MA-g-NR 5F, 20phr	329.34	189.50	1.06
NR Gum	203.19	183.45	1.06
10 MA-g-NR 1F, 40phr	280.56	190.58	1.09
10 MA-g-NR 3F, 40phr	299.23	193.64	1.06
10 MA-g-NR 5F, 40phr	343.39	198.89	1.07

6.2.3 Ageing studies of maleated natural rubber clay nanocomposites

6.2.3 A Thermal ageing

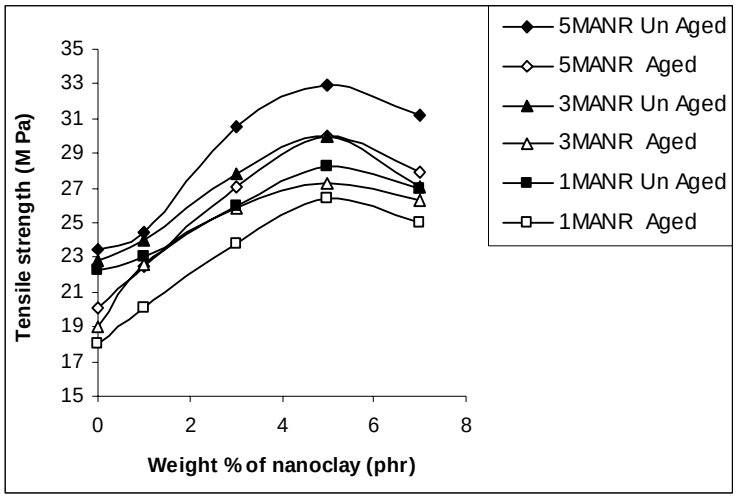

Figure 6.19 Variation of tensile strength with nanoclay loading

In the case of nanocomposites for 5,3 and 1 percentage MA concentration the tensile strength, tear strength and elongation at break showed a gradual decrease, while the tensile modulus at 300% elongation increases. The increase in tensile modulus is due to the formation of crosslinks during heating and subsequently the stiffness of the material increases. Variation of tensile strength, tensile modulus, elongation at break percentage and tear strength with nanoclay loading is shown in figures 6.19, 6.20, 6.21 and 6.22. Up to 72hrs the tensile and tear properties remains the same as that of unaged sample. This means that it is thermally stable upto 72hrs and after that the property is decreased.

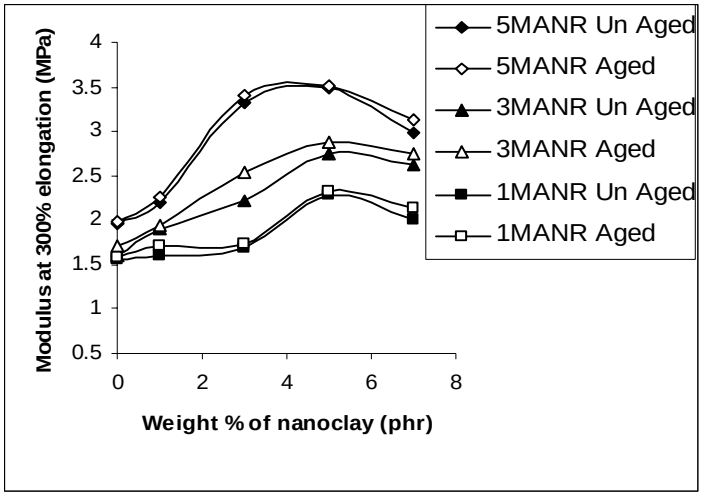

Figure 6.20 Variation of tensile modulus with nanoclay loading

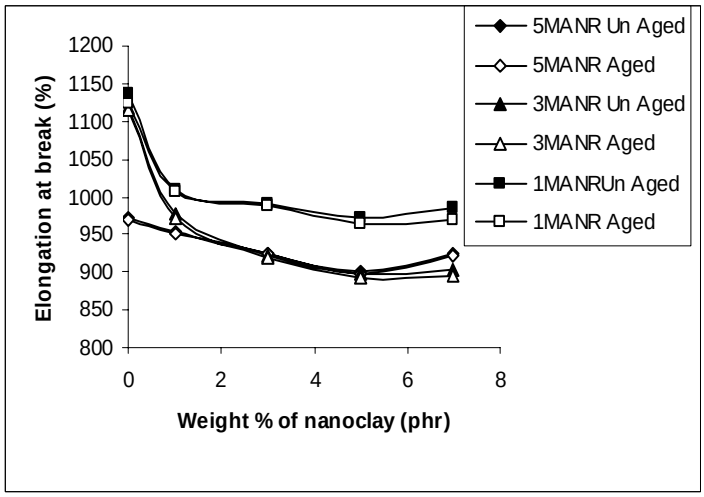

Figure 6.21 Variation of elongation at break with nanoclay loading

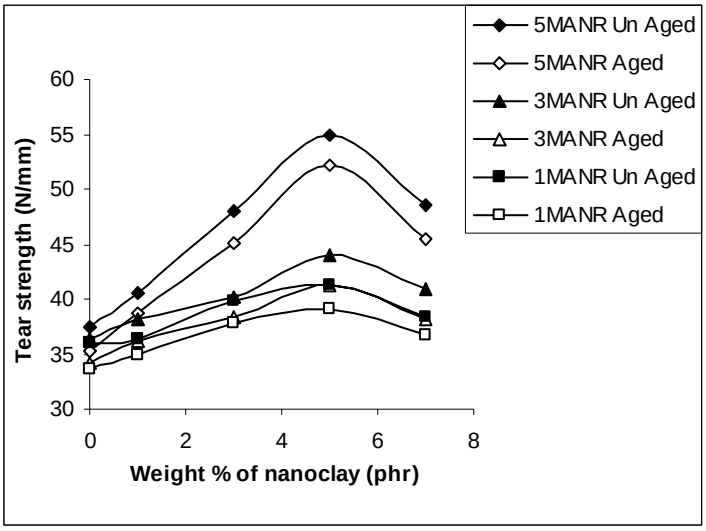

Figure 6.22 Variation of tear strength with nanoclay loading

6.2.3 B Radiation ageing

Application of elastomer components in nuclear plants, radiation therapy, medical equipments etc; have been increasing. Much work has been done on the effect of radiation on elastomers [16-17]. Radiation is a powerful method for crosslinking elastomers [18-19]. Reduction of tensile strength is a better measure of irradiation damage in rubber vulcanizates. Carbon black was found to protect rubber from degradation at lower levels of radiation [20]. The effects of radiation on polymeric materials and their blends and composites have been reported by researches [21-22]. The mechanical properties of the polymers changed considerably under the influence of high-energy radiations. This may be due to the cross-linking or can reduce the crystallinity by the degradation of polymer chain. Mechanical properties such as tensile strength, modulus, elongation etc; are reduced by chain degradation, while cross-linking enhances these properties. Figure 6.23 and 6.24 shows the variation of tensile strength and tensile modulus with radiation doze at 5wt% of nanoclay loading. The tensile properties showed a resistance to degradation up to 2.5kGy. For all loadings of nanoclay degradation

tendency starts only after 2.5kGy. This resistance may be due to the improved distribution of clay in the rubber matrix that holds the rubber together.

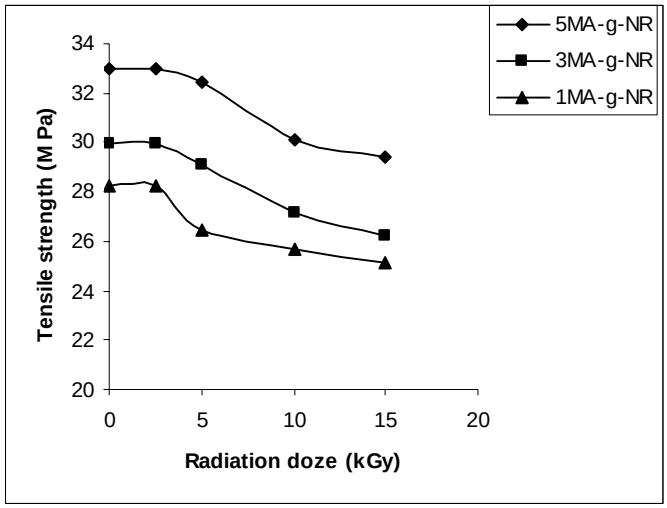

Figure 6.23 Variation of tensile strength with radiation dose at 5wt% nanoclay loading

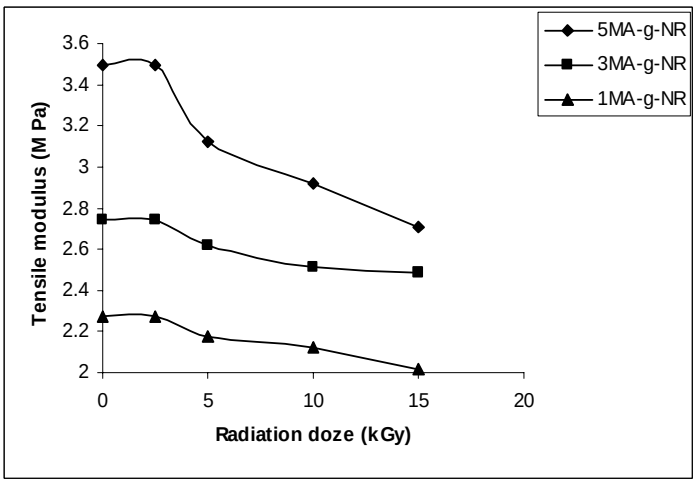

Figure 6.24 Variation of tensile modulus with radiation dose at 5wt% nanoclay loading

6.2.3 C Ozone ageing

One of the main types of degradation of elastomer products in service under natural conditions is caused by atmospheric ozone generated in nature by electrical discharge and also by solar radiation in the stratosphere [23]. Only a few pphm of ozone in air can cause cracking on surfaces which demolish the appearance and may destroy usefulness of the elastomer products. Ozonation and antioxidant efficiency of elastomers and blends has been extensively studied [24-27].

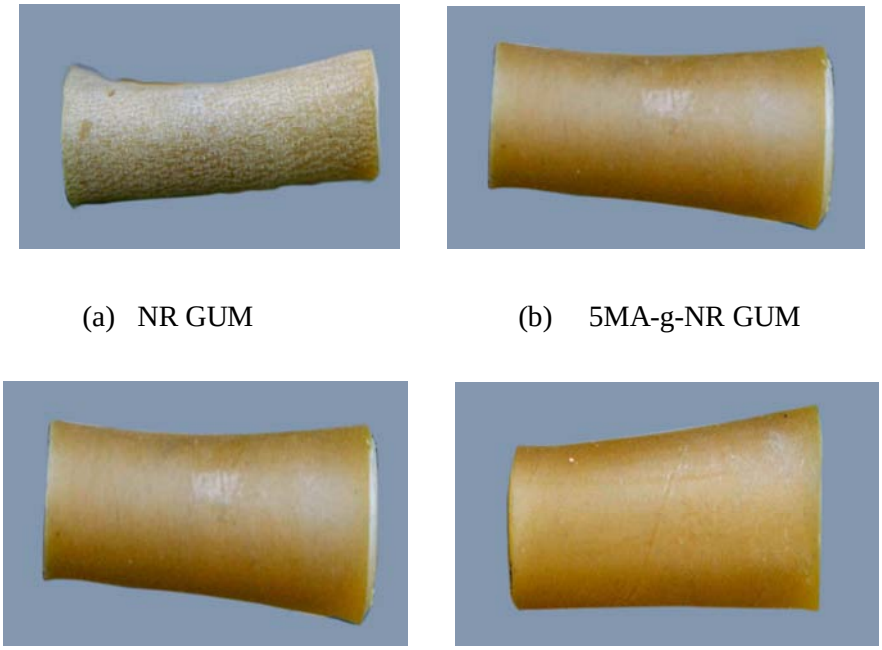

(a) NR GUM (b) 5MA-g-NR GUM

(c) 3MA-g-NR GUM (d) 1MA-g-NR GUM

Figure 6.25 Ozone irradiated surfaces of gum vulcanizates of NR, 5MA-g-NR, 3MA-g-NR and 1MA-g-NR after 4 hrs of exposure.

Figure 6.25 shows the photographs of ozone-irradiated surfaces of gum vulcanizates for 4hrs. It is observed that, NR samples cracked within 4hrs of irradiation and the propagation is also faster. Maleated rubber vulcanisates show

better resistance to ozone due to its polar nature. Figure 6.26 shows the optical photographs of the ozone irradiated surfaces of maleated natural rubber nanocomposites in an ozone chamber at 50pphm ozone concentrations at 38^0C. Within the first 4hrs itself cracks were formed on the surface of MA-g-NR gum samples. But it is seen that as the filler loading is increased up to 5wt% the time taken for the initiation of crack is increased. For 5MA-g-NR at 1, 3, 5 and 7wt% of nanoclay loading, the cracks were developed only after 5hrs, 6hrs, 8hrs and 7 hrs respectively.

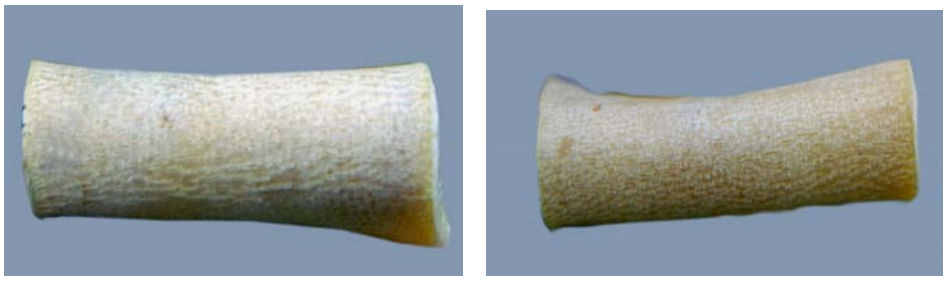

(a) 5MA-g-NR GUM (b) 5MA-g-NR 1F

(c) 5MA-g-NR 3F (d) 5MA-g-NR 5F

Figure 6.26 Ozone irradiated surfaces of 5MA-g-NR nanocomposites after 8hrs of exposure

It is understood that 5MA-g-NR nanocomposites up to particular clay content are less prone to ozone irradiation which indicates that the proper dispersion of clay in the rubber matrix is up to that level. The increase in clay loading showed a slower development and propagation of cracks.

6.2.4 Ageing resistance of maleated natural rubber clay nanocomposites developed through masterbatch technique

6.2.4 A Thermal ageing resistance

The vulcanized rubber may undergo chain scission reactions as well as crosslinking reactions during service life at elevated temperatures. The addition of fillers to rubber can improve the ageing resistance. Nanocomposites developed through masterbatch technique shows better thermal ageing resistance when compared to the maleated natural rubber by ordinary means. The slight retention in tensile strength, elongation at break and tear strength at 100^0C for 72hrs is shown in figures 6.27, 6.29 and 6.30. But the modulus shows an increase in all cases due to better crosslinking of chains as seen in 6.28.

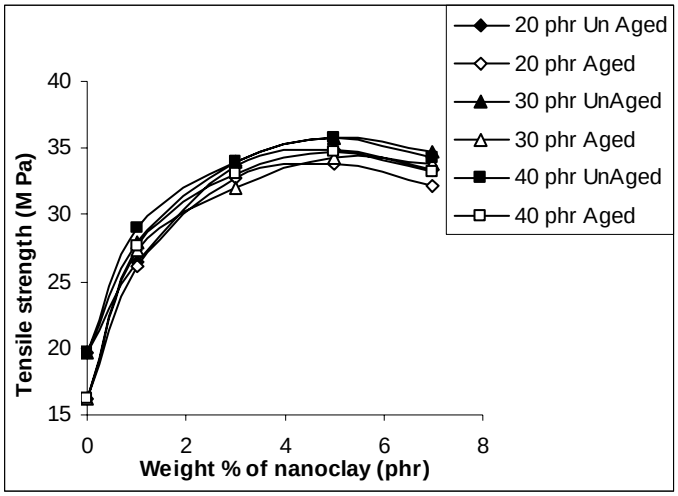

Figure 6.27 Variation of tensile strength with nanoclay loading

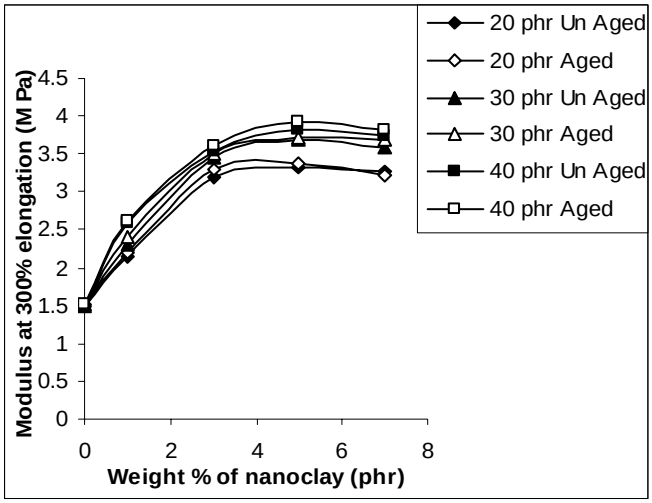

Figure 6.28 Variation of tensile modulus with nanoclay loading

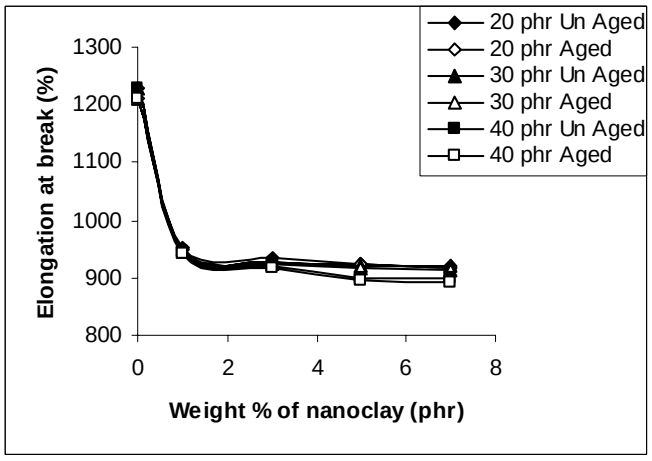

Figure 6.29 Variation of elongation at break with nanoclay loading

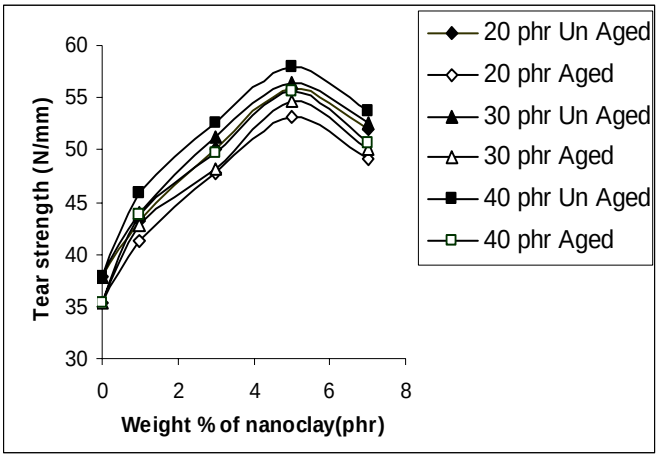

Figure 6.30 Variation of tear strength with nanoclay loading

6.2.4 B Radiation ageing

The mechanical properties of the polymers changed considerably under the influence of high-energy radiations. This may be due to the cross-linking or can reduce the crystallinity by the degradation of polymer chain. The tensile properties showed a resistance to degradation up to 2.5kGy. Figure 6.31 and 6.32 shows the effect of radiation verses tensile properties of nanocomposites. Here it is evident that 10MA-g-NR nanocomposites for 20phr, 30phr, 40phr shows the same trend as that of 5MA-g-NR nanocomposites.

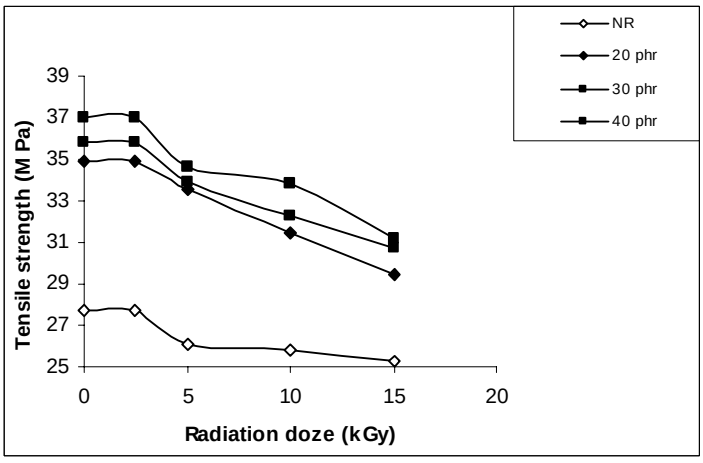

Figure 6.31 Variation of tensile strength with radiation dose of 10MA-g-NR at 5wt% nanoclay loading

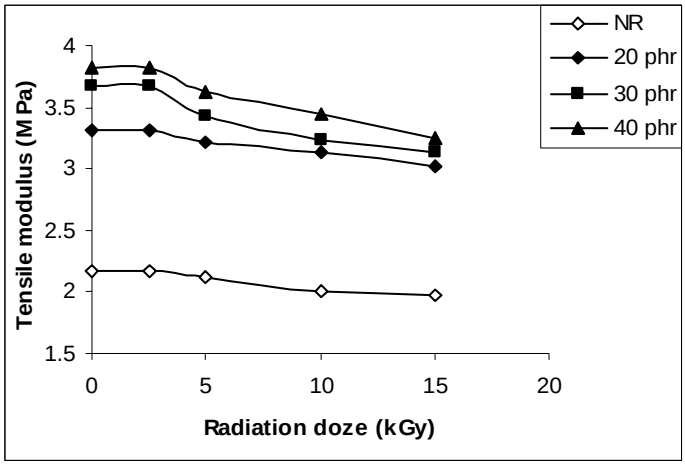

Figure 6.32 Variation of tensile strength with radiation dose of 10MA-g-NR at 5wt% nanoclay loading

6.2.4 C Ozone ageing

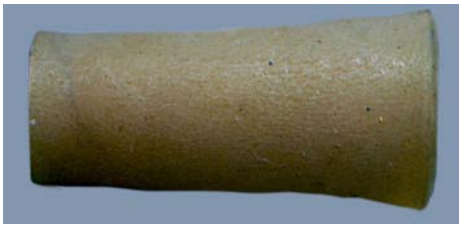

(a) NR GUM after 4hrs

(b) 10MA-g-NR 5F for 20phr after 7hrs

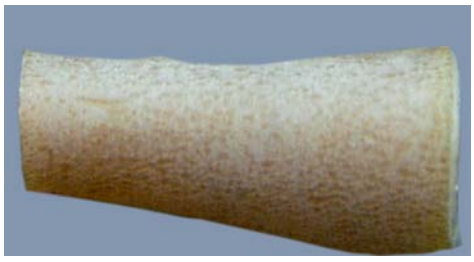

(c) 10MA-g-NR5F for 30phr after 7hrs (d) 10 MA-g-NR 5F for 40phr after 9hrs

Figure 6.33 shows the of photographs composites after exposure to ozone for 9 hrs

Unsaturated elastomers, especially those containing active double bonds in the main chain, are severely attacked by ozone resulting in deep cracks in a direction perpendicular to the applied stress. Protection against ozone attack can be achieved by the use of antiozonants. Several studies have been reported on the protection of rubber against ozone attack [28-29]. In the above samples i.e., in figure 6.33 (a), (b), (c) and (d) crack developed after 4hrs, 7 hrs, 7hrs and 9hrs respectively. The master batch samples shows better ozone resistance than the ordinary means due to greater hindrance to the progress of fracture front experienced due to the uniform distribution of clay in the rubber matrix and the improved rubber-filler interaction.

6.2.5 Flame resistance

Vulcanizates of varying nanoclay content and MA content were tested as per UL 94 by vertical burn test. 5MA-g-NR nanocomposites continued burning after the burner flame application and flaming drips ignited the cotton placed below the specimen, but took more time to complete burning than pure NR, indicating improvement in flame resistance [30]. If we want to utilize a system as a fire retardant, it must qualify under the UL-94 protocol. This is simply a test that measures the ease of extinction of a flame and four ratings are possible, depending upon the burning time and the presence of flaming drips. If a material extinguishes immediately, without dripping, it is afforded the rating V-0; a material that burns somewhat longer, but does not drip, is classified as V-1; a material that does not self-extinguish in a short time but drips is given the rating V-2; if a material burns longer than the protocol specifies, it is said to be not classified, NC. 5MA-g-NR and 3MA-g-NR at 5 and 3wt% nanoclay loading shows some what improved flammability property than its gum as given in table 6.11. But in the case of samples developed through masterbatch technique, good property obtained only for 5wt% nanoclay loading as given in table 6.12. This enhancement in property is due to the flame retardant property of organoclay.

Table 6.11 Dripping and burning characteristics, as well as the UL-94 classification for the systems here in studied.

Sample	Dripping	Burning	UL -94
5MA-g-NR Gum	Slow	Yes	NC
5MA-g-NR 1F	Slow	Yes	NC
5MA-g-NR 3F	Yes	Little	V-2
5MA-g-NR 5F	Yes	Little	V-2
3MA-g-NR Gum	Slow	Yes	NC
3MA-g-NR 1F	Slow	Yes	NC
3MA-g-NR 3F	Slow	Yes	NC
3MA-g-NR 5F	Yes	Little	V-2

Table 6.12 Dripping and burning characteristics, as well as the UL-94 classification for the systems here in studied.

Sample	Dripping	Burning	UL -94
NR Gum	Slow	Yes	NC
20 phr 10MA-g-NR 1F	Slow	Yes	NC
10MA-g-NR 3F	Slow	Yes	NC
10MA-g-NR 5F	Yes	Little	V-2
NR Gum	Slow	Yes	NC
40 phr 10MA-g-NR 1F	Slow	Yes	NC
10MA-g-NR 3F	Slow	Yes	NC
10MA-g-NR 5F	Yes	Little	V-2

6.2.6 Differential scanning calorimetry

6.2.6.1 Maleated Natural rubber clay nanocomposites by direct method

The Differential scanning calorimetric study of the gum rubber and the maleated rubber containing different clay loadings were done at low temperatures to study the change in glass transition temperature (Tg). The DSC thermogram of 5MA-g-NR at different clay loadings is shown in figure 6.34. The Tg value is increased as the clay is incorporated in the MA-g-NR matrix. Here 5MA-g-NR gum shows a Tg value of -62.25^{0}C and at 5wt% nanoclay loading the Tg value is increased to -56.42^{0}C. The Tg value of 3MA-g-NR gum is -64.56^{0}C and that of 5wt% nanoclay loading is -59.48^{0}C as shown in DSC thermogram figure 6.35. An increase in Tg value of 7^{0}C and 5^{0}C is observed in the case of 5MA-g-NR and 3MA-g-NR nanocomposites respectively at 5wt% nanoclay loading when compared to its gum.

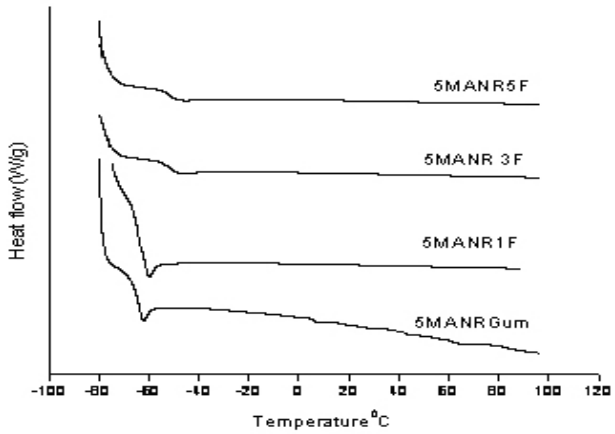

Figure 6.34 DSC curves of 5MA-g-NR nanocomposites

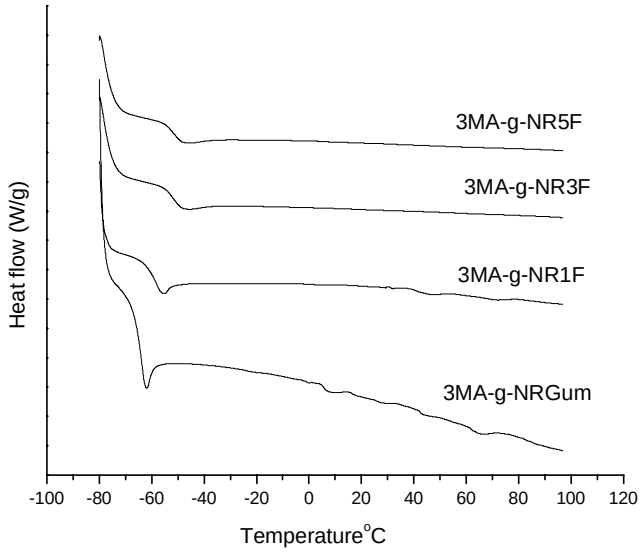

Figure 6.35 DSC curves of 3MA-g-NR nanocomposites

6.2.6.2 Maleated Natural rubber clay nanocomposites developed through masterbatch technique

Figure 6.36 and 6.37 shows the DSC thermograms of 10MA-g-NR nanocomposites at different clay loadings for 20phr and 40phr masterbatch. 40 phr batches shows higher Tg values when compared to 20phr and all other mixes. In the master batch technique NR gum is taken as the reference sample and it shows a Tg value of -68.24^0C. While at the same time NR at 5wt% clay loading shows a Tg value of -61.13^0C. In 40phr batch at 5wt% nanoclay loading shows a Tg value of -51.41^0C. In all the case the trend is same i.e. the clay loading increases the Tg value. This increase in Tg value is due to the better dispersion of clay in the MA-g-NR matrix and this can only be due to the confinement of the elastomer chains within the silicate layers with a restriction in the mobility of the polymer chains [31]. 40phr batch at 5wt% when compared to 5MA-g-NR at 5wt% nanoclay loading shows an increase in Tg value of 5.01^0C.

In general the maleated samples show better Tg values compared to NR nanocomposites.

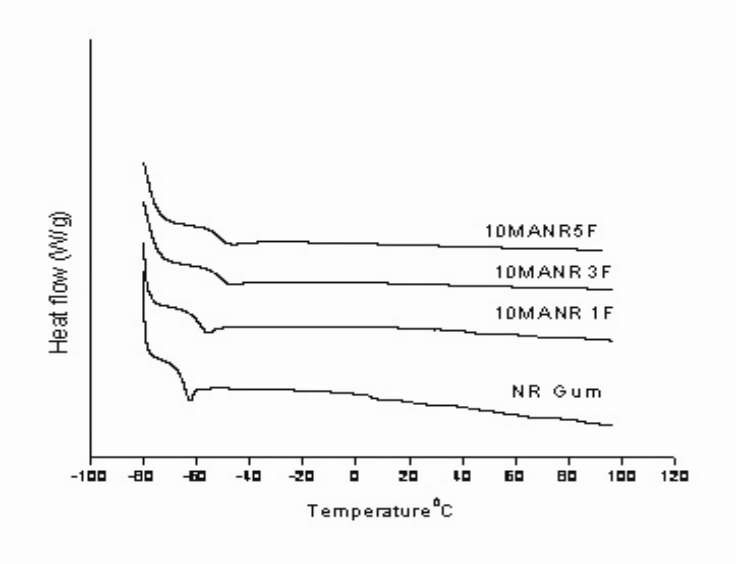

Figure 6.36 DSC curves of 10MA-g-NR nanocomposites for 20phr batch

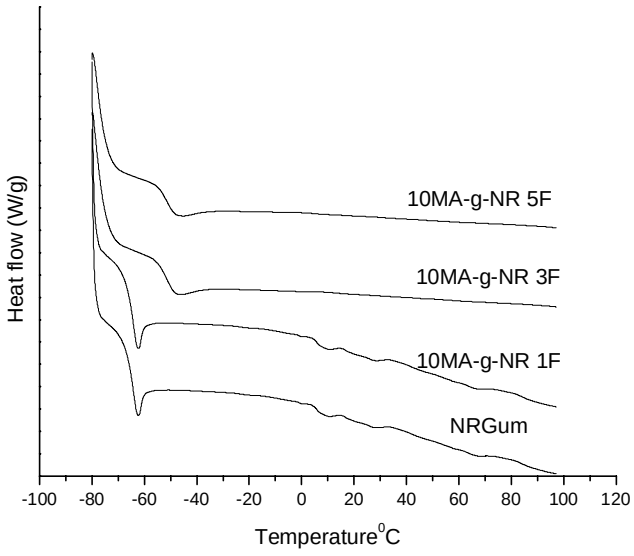

Figure 6.37 DSC curves of 10MA-g-NR nanocomposites for 40phr batch

6.3 Conclusions

The thermal stability of gum vulcanisates is lower than the nanocomposites irrespective of the matrix. In the direct method (5MA-g-NR, 3MA-g-NR&1MA-g-NR) the 5MA-g-NR at 5wt% nanoclay loading shows better thermal stability compared to others. While in the case of masterbatch technique (20phr, 30phr, 40phr, 50phr) the thermal stability is enhanced only up to 40phr batch. 40phr batch at 5wt% nanoclay shows better thermal stability compared to 5MA-g-NR at 5wt% nanoclay loading. The radiation ageing of the gum and nanoclay are studied at different radiation dozes (0, 2.5, 5, 10 &15kGy). In radiation ageing good resistance to degradation is observed up to 2.5kGy. For all loadings of nanoclay degradation tendency starts only after 2.5kGy. The masterbatch technique also shows the same trend. In the case of ozone ageing the intiation of crack occurs earlier with in 4hrs in the case of NR gum and propagation is also faster compared to maleated gum samples. Maleated rubber vulcanisates show better resistance to ozone due to its polar nature. In 5MA-g-NR nanocomposites, the initation of crack is developed only after 7hrs and also the crack is least for 5wt% nanoclay loading. It is understood that 5MA-g-NR nanocomposites up to 5wt% clay content are less prone to ozone irradiation which indicates that the proper dispersion of clay in the rubber matrix is up to that level. In the master batch technique 10MA-g-NR of 40phr batch with 5wt% nanoclay the crack initiation starts only after 9hrs and thus this has the maximum ozone resistant compared to all others. The flame retardant properties of 5MA-g-NR nanocomposites at 5wt% and 3wt% nanoclay shows V-2 rating according to U-L94 protocol, while in the case of masterbatch technique, the flame retardent properties of 20phr batch at 5wt% and 40phr at 5wt% nanoclay shows the same rating. From the DSC thermogram it is clear that the Tg value is increased as the clay loading is increased. High Tg value is observed for 40phr batch at 5wt% nanoclay when compared to 5MA-g-NR at 5wt% clay loading. In general the maleated samples show higher Tg values compared to NR nanocomposites.

References

1. Callum JRM. Comprehensive Polymer Science: The synthesis, Characterisation, Reactions and Applications of Polymers, Polymer Characterisation, 1st edn., Pergamon Press, 1989;1:903.
2. Still RH. Developments in Polymer Degradation, edn., Grassie N. Applied Science, London,1977;1:1.
3. Bourbigot S, Gilman JW, Wilkie CA. Polym Deg Stabi 2004;84:483.
4. Peeterbroeck S, Alexandre M, Nagy JB, Pirlot C, Fonseca A, Moreau N, Philippin G, Delhalle J, Mekhalif Z, Sporken R, Beyer G, Ph. Dubois, Compo Sci Technol, 2004;64:2317.
5. Hu YH, Chen CY, Wang CC. Polym Deg Stabi 2004;84:545
6. Varghese S, Karger-Kocsis J. Polymer 2003;44:4921.
7. Pandey JK, Eddy KR, Kumar AP, Singh RP. Polym Deg Stabi 2005;88:234.
8. Brandrup J, Immergut EH, Mc Dowell W. Polymer Hand book, 2nd edn., John Wiely & Son,1975.
9. Gilman JW, Jackson CL, Morgan AB, Harries R, Manias E, Giannelis EP, Wuthenow M. Chem Mater 2000;12;1866.
10. Burnside SD, Giannelis EP. Chem Mater 1995;7:1597.
11. Lee J, Takekoshi T, Giannelis EP. Mate Res Soc Symp Proc 1997;457:513.
12. Blumstein A. J Polym Sci 1965;A3;2665.
13. Zhu ZK, Yang Y,Yin J, Wang XY, Ke YC, Qi ZN. Appl Polym Sci 1999;73:2065.
14. Qin H, Su Q, Zhang S, Zhao B, Yang M. Polymer 2003 ;44 :7533.
15. SinhaRay S, Okamoto M. Prog. Polym.Sci.2003;28: 1539.
16. Ito M, Odaka S, Kuriyamma. J Mater Sci 1981;16:10.
17. Alex R, De PP, Kunststoffe KG. 1991;44:333.

18. Bik JM, Rzymskki Lordz WM, Gluszewski W, Zagorski ZPW, Kunststoffe KG. 2004 ;57 :651.
19. Makuuchi K. An Introduction to Radiation Vulcanisation of natural rubber Latex, T.R.I Global Co. Ltd., Thailand.2003:p28
20. Anderson HR. Rubber Chem Technol.1961;34:228.
21. Bohm GGA, Treekrem JO. Rubber Chem Technol 1982;55:575.
22. Charlesby A.Plast Rubb proc App. 1982;2:289.
23. Saito Y. Internat Polym Sci Technol 1995;22:47.
24. Subramamian R. Plast Ind 1980 ;5 :13.
25. Avirah S, Joseph R. J Appl Polym Sci 1995;57:1511.
26. Andrews EH. Rubber Chem Technl 1966;40:635.
27. Wilchinsky ZW, Kresge EN. Rubber Chem Technol 1974;47:895.
28. Ambelang JC, Kline RA. Rubber Chem Technol 1963;36:1497.
29. Layer RW, Lattimer RP. Rubber chem. Technol 1990;63:426.
30. Wang D, Echols K, Charls AW. Fire Mater 2005;29:283.
31. Lopez-Manchado MA, Herrero B, Arroyo M. Polym Int 2003;52:1070.

Chapter 7

Barrier properties of maleated natural rubber organoclay nanocomposites

The excellent gas barrier property of layered silicate/polymer nanocomposites is one of their most important advantages. The layered silicate sheets with high aspect ratio are believed to greatly reduce the gas permeability by creating a tortuous path that retards the progress of the gas molecules through the matrix [1-5]. The transport of gases through a membrane depends on various factors like permeant size and shape, permeant phase, polymer molecular weight, functional groups, density and polymer structure, crosslinking, crystallinity, orientation etc [6]. The wide application of membranes for gas separation has attracted polymer technologists to synthesize new polymeric membranes with good permeability and selectivity [7-9]. Paul and co-workers [10-14] have investigated the relationship between gas transport and polymeric structure. The introduction of functional groups in the polymer chain can alter the permeability and selectivity due to the variation in the existing free volume with in the polymer [15-16]. The selective transport of gases through polymeric membranes has been reviewed by Aminabhavi and co-workers [17]. Van Amerogen [18-19] has extensively studied the permeability of various gases through different elastomers. Several rubber/clay nanocomposites, such as isobutylene-isoprene rubber (IIR)/clay, natural rubber (NR)/clay, nitrile rubber (NBR)/clay, ethylene-propylene-diene rubber (EPDM)/clay and styrenebutadiene rubber (SBR)/clay, have been successfully prepared [20-24] and possess improved gas barrier properties. Thomas and co- workers [25] investigated the gas transport properties of rubber blends.

Among the layered silicates, MMT is the most widely used promising clay. There are numerous literature on the properties of polymers containing layered silicates [26-28]. The platelet structure of layered silicates has the ability to improve the barrier properties of polymer materials according to a tortuous path model in which a small amount of platelet particles significantly reduces permeant diffusion. In the exfoliated system the individual clay platelets will have very high aspect ratio and as a result the barrier properties get improved. Dufresne and co-workers [29] studied the swelling behaviour of waxy maize starch reinforced NR. They found that the solvent uptake of NR decreases upon the addition of starch nanocrystals. Swelling properties of ethylene propylene rubber (EPR)/clay based on maleic anhydride-modified EPR, natural rubber latex (NRL)/clay and organophilic clay are also reported [30-31].

7.1 Experimental

7.1.1 Gas permeability measurement

The air permeability of the natural rubber and maleated natural rubber layered silicate membranes were measured using Lyssy Manometric Gas Permeability Tester L100-2402. The test gas used was oxygen at a flow rate of 500ml/minute. Permeability of the samples is calculated using the equation, $Pm = (TrxPr)/t_m$, where P_m is the permeability of the test sample, tm is the interval time constant for the test sample, P_r is the permeability of the reference (standard PET) sample and T_r is the interval time constant for standard PET.

Gas barrier in polymer clay nanocomposites was traditionally explained in terms of Nielson model, originally adopted to describe the tortosity effect of plate like particulates on gas permeability of filled polymer composite structures [32].This model system consists of uniform platelets homogeneously dispersed in the polymer matrix and oriented parallel to the polymer film surface. The model can be applied using the equation (7.1), to obtain the clay aspect ratio from the permeability data of these nanocomposites.

$$\frac{P}{P_0} = \frac{1-\phi_f}{1+\frac{L}{2W}\phi_f} \tag{7.1}$$

In the above equation, P is the permeability of the nanocomposites, P_0 is the permeability of the gum vulcanizate and ϕ_f is the volume fraction of the clay. L and W are length and width of the clay sheets, respectively, its ratio L/W, defines the aspect ratio α, of the fillers.

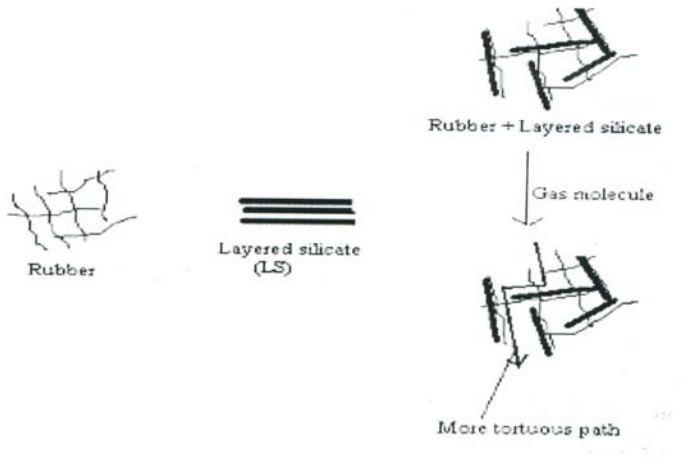

Figure 7.1 Schematic illustration of permeation of oxygen molecules through nanofilled rubber

7.1.2 Swelling studies

7.1.2A Swelling in toluene

A circular specimen of 20mm diameter and 2mm thickness were cut using a sharp edged circular disc from the vulcanised samples. The samples were immersed in airtight test bottles containing about 15-20ml of toluene maintained at constant temperature. Samples were removed periodically and the surface

adhered solvent drops were wiped off carefully by pressing them between the filter wraps. The mass of the sorbed sample was determined immediately on a digital balance with an accuracy of ±0.01mg. As the weighing was done within 30-40sec, the error due to evaporation of other than surface adsorbed liquid is considered insignificant. Desorbed weights of the samples were also taken after complete removal of solvent.

The mole percent uptake of the sample is calculated from the diffusion data. The Q_t values are determined using the equation, (7.2)

$$Q_t = \frac{(Wt.of\ the\ solvent\ sorbed\ \ at\ a\ given\ time)/(Mol.wt.of\ \ the\ solvent)}{(Intial\ Wt.\ of\ \ the\ rubber\ \ specimen \times 100)} \quad (7.2)$$

7.1.2 B Swelling in oils

The percentage weight change of the nanoclay filled composites in different oils was studied by swelling a cut sample in oil for constant weight.

7.1.3 Crosslink density measurements

Swelling studies of the composites were conducted in toluene to find their crosslink densites using Flory-Rehner equation.

7.2 Results and discussion

7.2.1 Gas permeability

The oxygen permeability of the maleated natural rubber and maleated natural rubber masterbatch with gum and nanoclay filled vulcanisate having 2mm thickness are given in table 7.1 and 7.2. It is clearly seen that the oxygen permeability decreased substantially (21.63%) by the incorporation of 1wt% of layered silicate. As the silicate loading is increased to 5wt%, the permeation resistance increased to 36%. Higher permeation resistance is offered by the nanoclay having higher interlayer distance. This supports the better exfoliation,

which resulted in the permeation resistance obtained by the incorporation of lower silicate loadings.

The model assumes that the fillers are impermeable to the diffusing gas or liquid molecule and are oriented to the diffusion direction. Aspect ratios calculated are given in tables 7.1 and 7.2. The samples with better dispersion presented the highest aspect ratio suggested by the permeability data. Thus, the presence of the filler particles creates tortuous path for the permeant to travel through the composites. The denominator on the right hand side of the equation is also referred to as the tortouosity factor, τ, defined as the distance a molecule must travel to get through the film divided by the thickness of the film. From tables 7.1 and 7.2, it is seen that with the increase in clay content the aspect ratio is decreasing and thus the tortuousity factor increases. Permeability data (table7.1 and 7.2) of the nanocomposites also suggests the same and thus the permeation of oxygen molecules through the nanocomposites fits the Nielsen model. Sample with lower clay content presents the higher aspect ratio due to the better dispersion of clay in the rubber matrix, thus only a slight decrease in the permeability is observed with the increase in clay content.

Table 7.1 Oxygen Permeability of the maleated rubber vulcanisates and aspect ratio of clay from Nielson's model.

Sample code	Oxygen Permeability (mL /m^2 day)	Aspect ratio from Nielson's model
5MA-g-NR gum	450.85	_
1F	370.65	87.72
3F	368.14	48.09
5F	330.14	39.87
3MA-g-NR gum	526.05	_
1F	498.57	8 .91
3F	481.91	3.92
5F	467.58	2.76

Table 7.2 Oxygen Permeability of pure NR nanocomposite and maleated rubber vulcanisates through master batch technique and aspect ratio of clay from Nielson's model.

Sample code	Oxygen Permeability (mL/m^2 day)	Aspect ratio from Nielson's model
NR gum	590.52	—
NR 5F	569.37	1.034
10MA-g-NR(20phr)		
1F	360.65	262.13
3F	220.86	227.12
5F	180.24	183.96
10MA-g-NR(40phr)		
1F	358.92	265.69
3F	219.24	229.81
5F	178.73	186.19

The 10MA-g-NR nanocomposites developed through masterbatch technique shows higher aspect ratio when compared to 5MA-g-NR clay nanocomposites. Up to 40phr better properties are obtained. About 227.62% and 80.19% reduction in permeability values is obtained for 10MA-g-NR nanocomposite developed through masterbatch and 5MA-g-NR nanocomposites respectively.

7.2.2 Swelling studies in toluene

7.2.2.1 Swelling behaviour of maleated natural rubber nanocomposites

Swelling studies of the vulcanisates prepared with different MA concentration and filler loading were done in toluene at 303 K. Sorption curves of 5MA-g-NR, 3MA-g-NR and 1MA-g-NR vulcanisates that are obtained by plotting Q_t (mole% uptake per 100g of the solvent) against time as shown in figures 7.1, 7.2 and 7.3. For all compositions, the uptake is rapid in the intial zone. After this, the sorption rate decreases leading to a plateau corresponding to equilibrium swelling. Note that the gum has maximum toluene uptake at equilibrium swelling. The swelling of the material is strongly reduced in presence of clay with in MA-g-NR matrix. The presence of impermeable clay layers decreases the rate of transport by increasing the average diffusion path length in the specimen. The decrease in solvent uptake in nanocomposites can also be associated with the tortuosity of the path and the reduced transport area in polymeric matrix in presence of nanofillers.

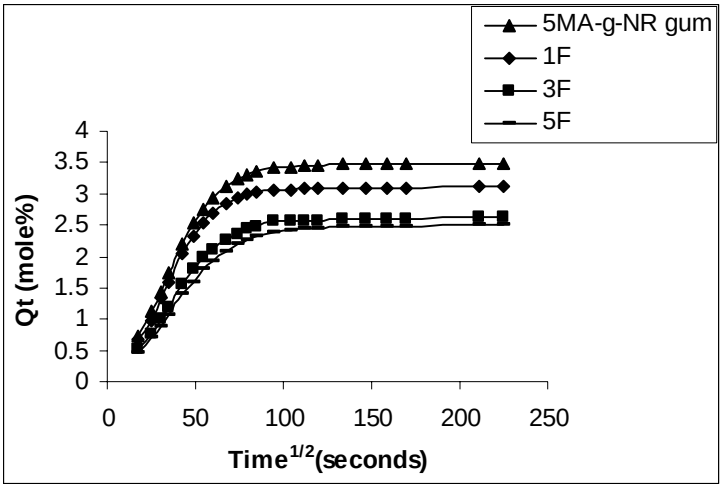

Figure7.1 Soption curves of 5MA-g- NR nanoclay vulcanisates at 303K

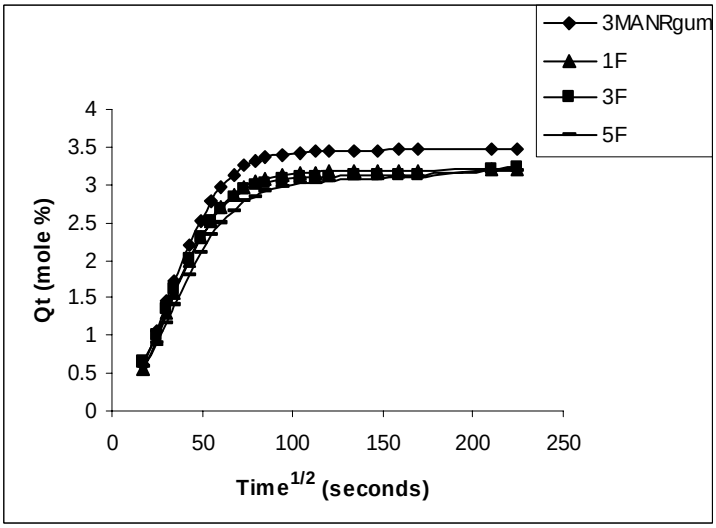

Figure7.2 Soption curves of 3MA-g- NR nanoclay vulcanisates at 303K

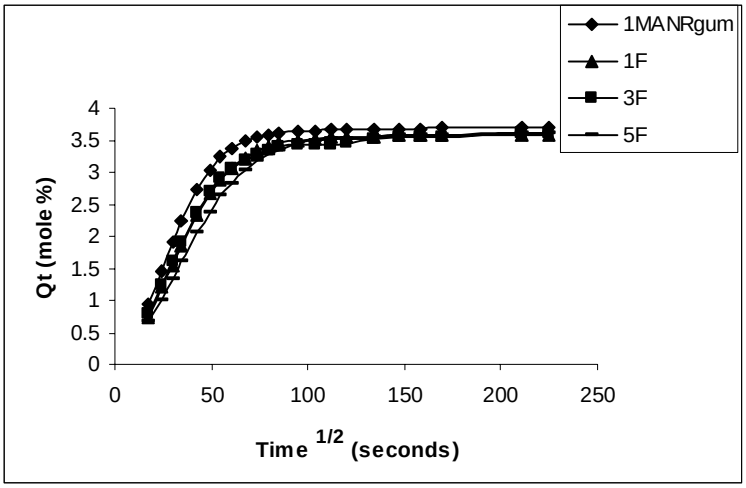

Figure.7.3 Soption curves of 1MA-g- NR nanoclay vulcanisates at 303K

In order to determine how the clay content affects the permeability, the transport properties like diffusion coefficient, permeation coefficient and sorption coefficient of the samples were calculated as given below. The mechanism of diffusion was investigated using the equation (7.3) [33,34,35]

$$\log Qt / Q\infty = \log k + n \log t \qquad (7.3)$$

The value of k depends on the structural features of the polymer, whereas the value of n determines diffusion mechanism.

The swelling of polymer is also affected by solvent transport. As swelling increases, free volume increases due to chain mobility, which facilitates transport process. The diffusion coefficient, D can be determined using the relation (7.4) [36,37]

$$D = \pi \left[\frac{h\,\theta}{4\,Q_{\infty}} \right] \qquad (7.4)$$

where h is the intial thickness of rubber sample, θ the slope of the linear portion

of the sorption curve and Q_∞ is obtained from the Q_t verses $t^{1/2}$ graph (figures 7.1, 7.2,7.3).

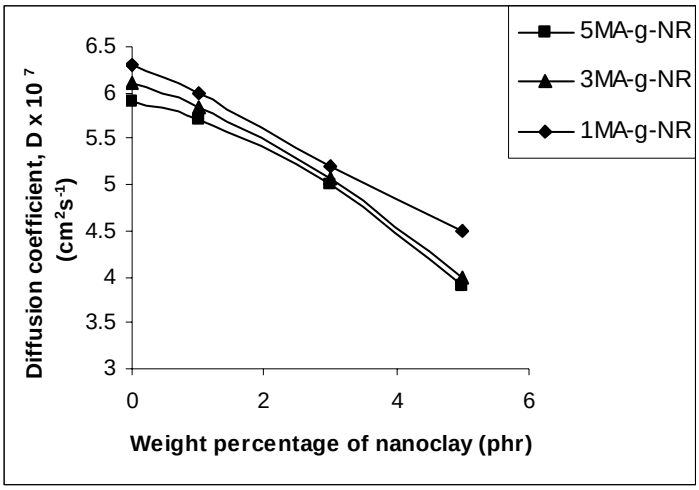

Figure 7.4 Variation of Diffusion coefficients (D) with nanoclay content

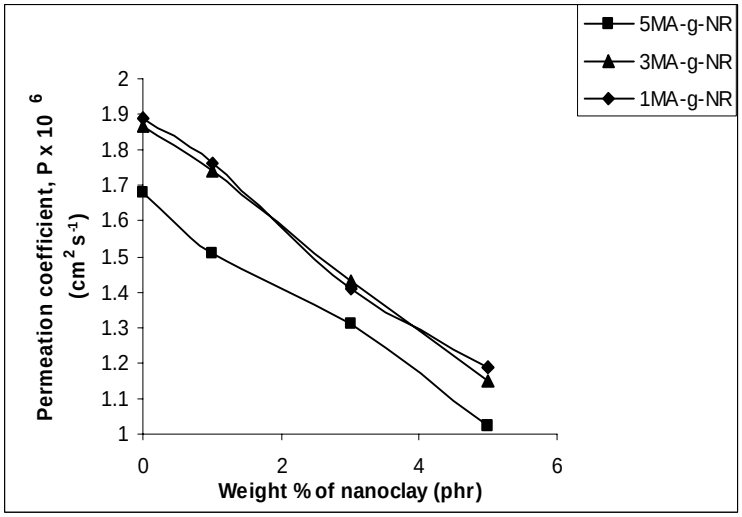

Figure 7.5 Variation of Permeation coefficients (P) with nanoclay content

The values of D are given in table 7.3. The variation of D depends on the solvent uptake, which is maximum for gum vulcanisate (figure 7.4). Adding clay within the MA-g-NR matrix results in a progressive decrease of D value and a substantial decrease with increase in clay content. This may be due to the reduced availability of space for solvent molecules in the intercalated structure of the nanocomposites. This also shows the strong interaction between the filler and the matrix, which limits the toluene diffusivity within the entangled polymer matrix.

Table 7.3 Variation of Diffusion coefficient (D), Sorption coefficient (S) and Permeation coefficient (P) with loading of nanoclay

Sample code	Diffusion coefficient, D $\times 10^7$ (cm^2 s^{-1})	Sorption coefficient, S	Permeation coefficient, P $\times 10^6$ (cm^2 s^{-1})
5MA-g-NR gum	5.9	2.85	1.68
1F	5.7	2.65	1.51
3F	5	2.62	1.31
5F	3.9	2.61	1.02
3MA-g-NR gum	6.1	3.06	1.84
1F	5.84	3 .01	1.74
3F	5	2.9	1.43
5F	4	2.8	1.15
1MA-g-NR gum	6.32	3.01	1.89
1F	6.01	2.93	1.76
3F	5.01	2.8	1.4
5F	4.5	2.64	1.19

The permeation of a solvent into a polymer membrane will also depend on the sorptivity of the penetrant in the membrane. Hence sorption coefficient, S has been calculated using the relation (7.5) [38]

$$S = \frac{W_s}{W} \tag{7.5}$$

where W_S is the weight of the solvent at equilibrium swelling and W, the intial weight of the polymer sample. The numerical values of sorption coefficient are also given in table 7.3. The values are slightly higher for the gum than in the nanocomposites because of the higher contribution of the layered silicates. Since the permeability depends on both diffusivity and soptivity, the permeation coefficient has determined using the relation (7.6) [38]

$$P = D \times S \tag{7.6}$$

The permeation coefficient, the net effect of sorption and diffusion process is also found to be decreased (figure 7.5). The values obtained for P are given in tables 7.3. It is seen that the decreasing value of the permeability of the nanocomposites is largely dominated by the diffusion phenomenon, as shown by the respective values of sorption and diffusion reported in the table 7.3.

7.2.2.2 Swelling behaviour of maleated natural rubber nanocomposites developed through masterbatch technique

Swelling studies of the vulcanisates prepared with 10 MA concentration and filler loading were done in toluene at 303K. Sorption curves of 10MA-g-NR for 20, 30 and 40phr masterbatch vulcanisates that are obtained by plotting Q_t (mole% uptake per 100g of the solvent) against time as shown in figures 7.6, 7.7 and 7.8. For all compositions, the uptake is rapid in the intial zone. After this, the sorption rate decreases leading to a plateau corresponding to equilibrium swelling. Note that the gum (pure NR gum) has maximum toluene uptake at equilibrium swelling. 40phr batch at 5wt% clay loading shows the maximum

swelling resistance when compared to all other mixes. The swelling of the material is strongly reduced in presence of clay with in MA-g-NR matrix. The presence of impermeable clay layers decreases the rate of transport by increasing the average diffusion path length in the specimen. The decrease in solvent uptake in nanocomposites can also be associated with the tortuosity of the path and the reduced transport area in polymeric matrix in presence of nanofillers.

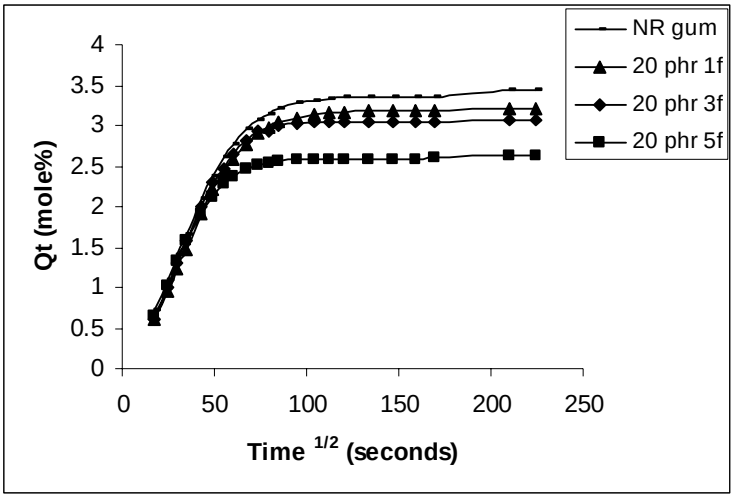

Figure 7.6 Soption curves of 10 MA-g-NR nanoclay vulcanisates at 303K

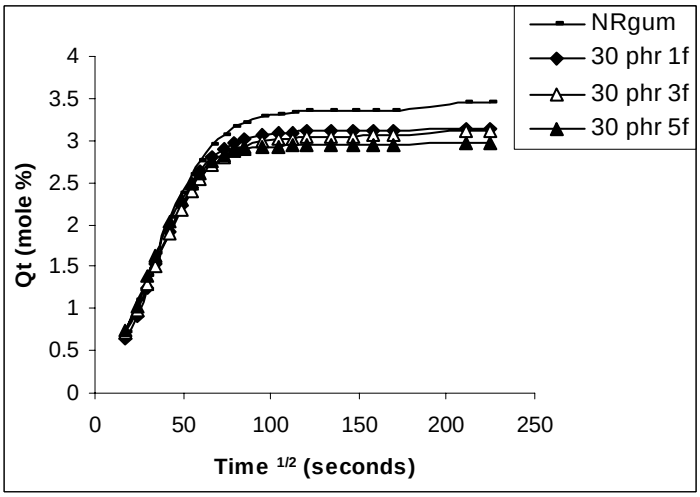

Figure 7.7 Soption curves of 10MA-g- NR nanoclay vulcanisates at 303K

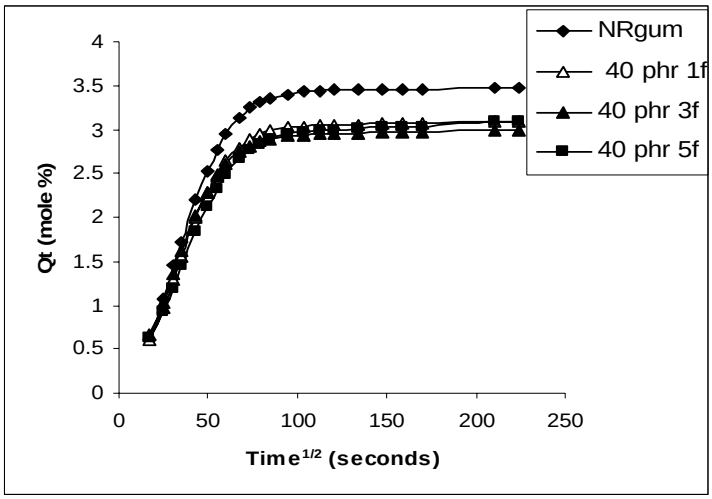

Figure 7.8 Soption curves of 10MA-g- NR nanoclay vulcanisates at 303K

The diffusion coefficient and permeation coefficient of the samples are shown in figures 7.9 and 7.10. These coefficients show the same trend as that of 5MA-g-NR nanocomposites.

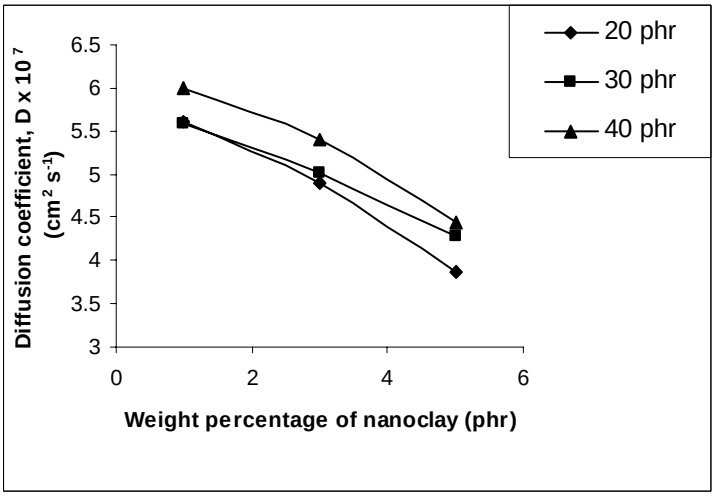

Figure 7.9 Variation of Diffusion coefficients (D) with nanoclay loading for 10MA-g-NR

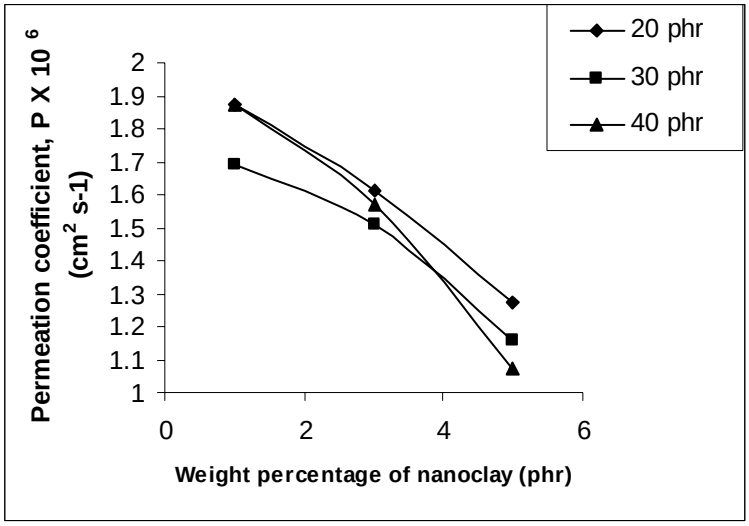

Figure 7.10 Variation of Permeation coefficients (P) with nanoclay loading for 10MA-g-NR

Table 7.4 Variation of Diffusion coefficient (D), Sorption coefficient (S) and Permeation coefficient (P) with loading of nanoclay

Sample code	Diffusion coefficient, D $\times 10^7$ ($cm^2\ s^{-1}$)	Sorption coefficient, S	Permeation coefficient, P $\times 10^6$ ($cm^2\ s^{-1}$)
10MA-g-NR 20phr			
1F	5.6	3.34	1.87
3F	4.9	3.3	1.61
5F	3.86	3.21	1.27
10MA-g-NR 30phr			
1F	5.58	3 .03	1.69
3F	5.02	2.8	1.51
5F	4.29	2.7	1.16
10MA-g-NR40phr			
1F	6	3.11	1.86
3F	5.4	2.8	1.57
5F	4.45	2.4	1.07

7.2.3 Swelling in oils

7.2.3.1 Swelling behaviour of maleated natural rubber nanocomposites

The percentage weight change of the nanoclay filled composites in different oils was studied by swelling a cut sample in oil for constant weight. The swelling characteristics was determined as a change in weight [39,40] calculated using equation 2.14 which is given in Chapter 2

Figure 7.11, 7.12 and 7.13 shows the percentage mass of oil absorbed with nanoclay for 5, 3 and 1% MA-g-NR nanocomposites respectively. It is observed that the swelling values of 5MA-g-NR nanocomposites are found to be much less when compared to 3MA-g-NR and 1MA-g-NR nanocomposites. This can be explained in terms of the polar-polar interaction between the polymer and filler. The increase in filler content (1-7wt%) also shows reduced swelling index values (Figure 7.11, 7.12 & 7.13). In 5MA-g-NR nanocomposites at 5wt% nanoclay loading, the transformer oil, hydraulic oil and engine oil decreases the swelling index by 28.02, 22.44 and 20.23% respectively. The reduction of swelling upon the addition of layered silicates is due to the enhanced rubber/filler interaction. This can also be explained in terms of the more tortouosity of path and the reduced transport area in the rubber matrix in presence of nanoclay. It is observed that swelling index values is lower for transformer oil and higher for engine oil.

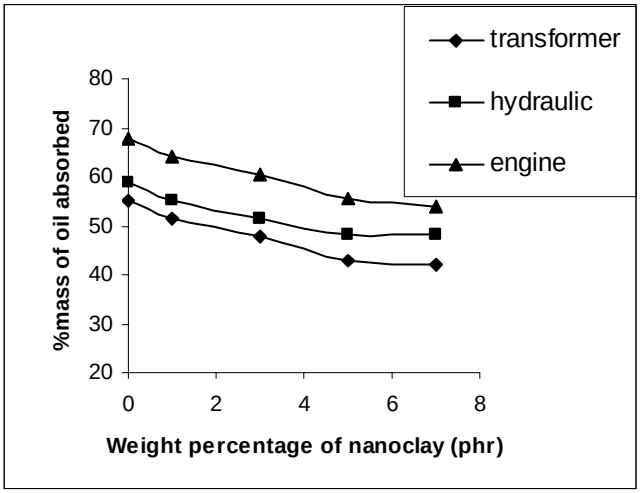

Figure 7.11 % mass of oil absorbed with nanoclay content for 5MA-g-NR

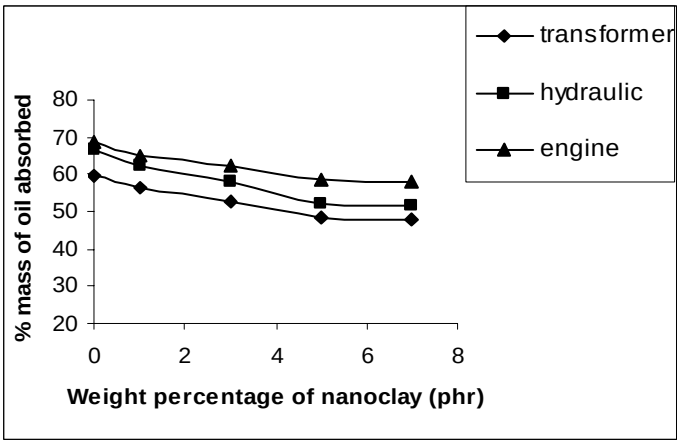

Figure 7.12 % mass of oil absorbed with nanoclay content for 3MA-g-NR

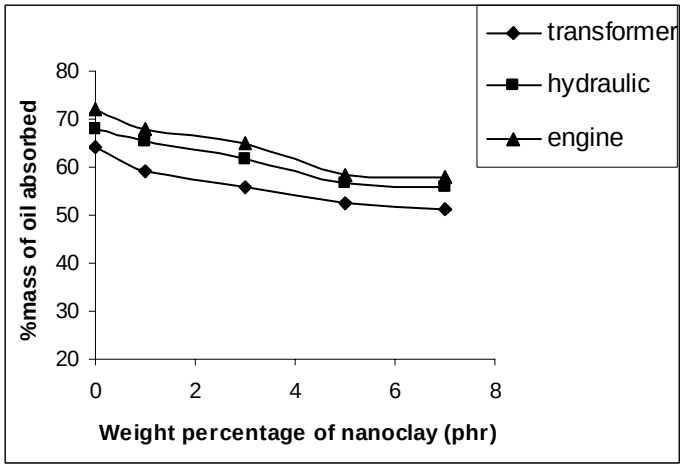

Figure 7.13 % mass of oil absorbed with nanoclay content for 1MA-g-NR

7.2.3.2 Swelling behaviour of maleated natural rubber nanocomposites developed through masterbatch technique

Figure 7.14, 7.15, and 7.16 shows the percentage mass of oil absorbed with nanoclay for 10MA-g-NR nanocomposites at 1-7wt% for 20, 30, and 40phr batches respectively. The first point in the below graphs corresponds to the swelling index values of pure NR gum in the respective oils. It is observed that the swelling values of 10MA-g-NR nanocomposites are found to be much less when compared to pure NR nanocomposites. A 57%, 54% and 37% decrease in swelling index is observed for transformer oil, hydraulic oil and engine oil for 40phr 10MA-g-NR when the clay content is increased from 1-5wt%. The same trend is observed in the case of 20 and 30 masterbatches too. If we compare 5MA-g-NR and 10MA-g-NR nanocomposites which is developed through masterbatch technique the reduction in swelling index percentage is higher for the 10MA-g-NR masterbatch nanocomposites due to better dispersion and crosslinking of clay in the rubber matrix.

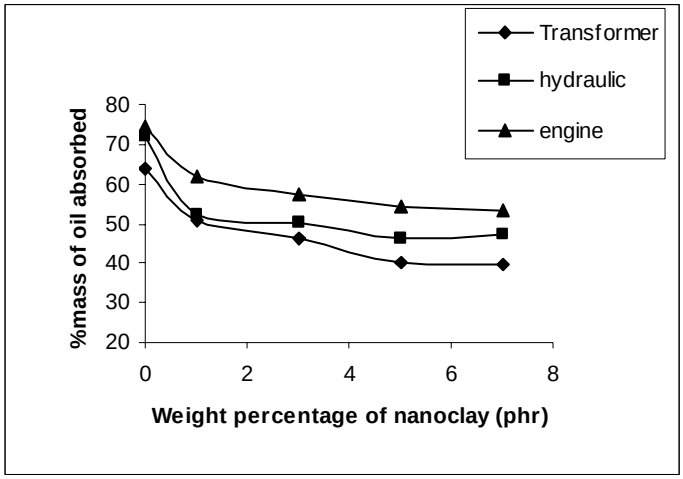

Figure 7.14 % mass of oil absorbed with nanoclay content for 20phr10MA-g-NR

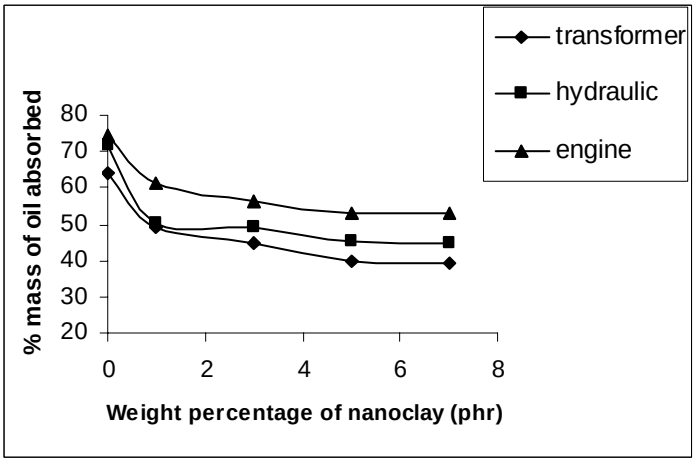

Figure 7.15 % mass of oil absorbed with nanoclay content for 30phr10MA-g-NR

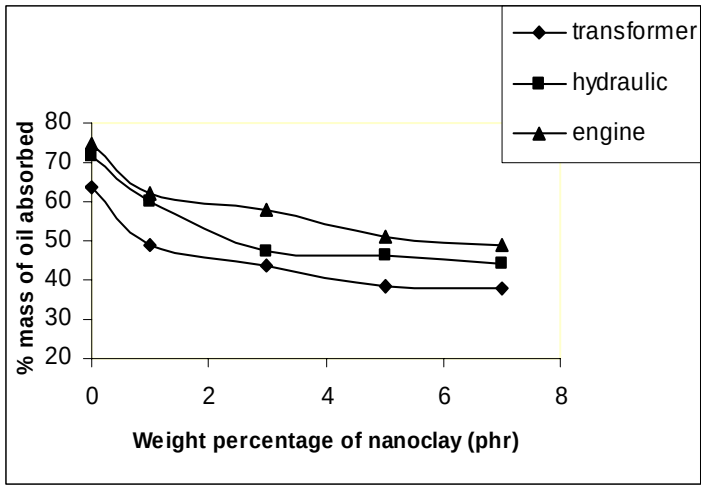

Figure 7.16 % mass of oil absorbed with nanoclay content for 40phr10MA-g-NR

7.2.5 Crosslink density measurements

Swelling studies of the composites were conducted in toluene to find their crosslink densities using Flory-Rehner equation [41]. Figure 7.17 & 7.18 shows the crosslink density values of composites obtained through two different techniques (direct & masterbatch). In the second set i.e. 10MA-g-NR developed through masterbatch technique, reference sample is the crosslink density of pure NR gum vulcanisates. It is found that the crosslink density values of 10MA-g-NR nanocomposites (20, 30 and 40phr) is higher than 5MA-g-NR nanocomposites. An increase of 4.8% in crosslink density is observed for 10MA-g-NR at 5wt% for 40phr batch when compared to 5MA-g-NR nanocomposites at same clay loading. 5MA-g-NR nanocomposites at 5wt% loading shows an increase of 24.5% in crosslink density values when compared to NR nanocomposites at same loading. The cross link density values of 30 and 40phr shows the same trend and some what closer values to that of 20phr master batch. Here cross link density values increases up to 5wt% filler loading and above it no further increment is noticed due to the poor dispersion of clay. The swelling of rubber in a solvent is affected by the incorporation of filler. In the case of reinforcing filler, strong

rubber-filler interaction will have some effect on the apparent crosslink density of the system. Ratio of restriction of swelling of the filled rubber vulcanisate to that of the gum rubber is used as a means for evaluating the reinforcing ability of filler in rubber. The high value of crosslink density confirms the presence of improved rubber-filler interaction in composites.

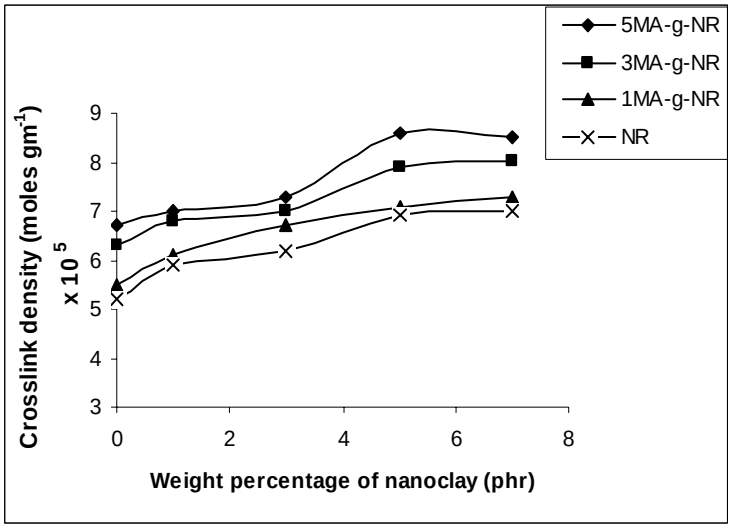

Figure 7.17 Variation of crosslink density with nanoclay loading

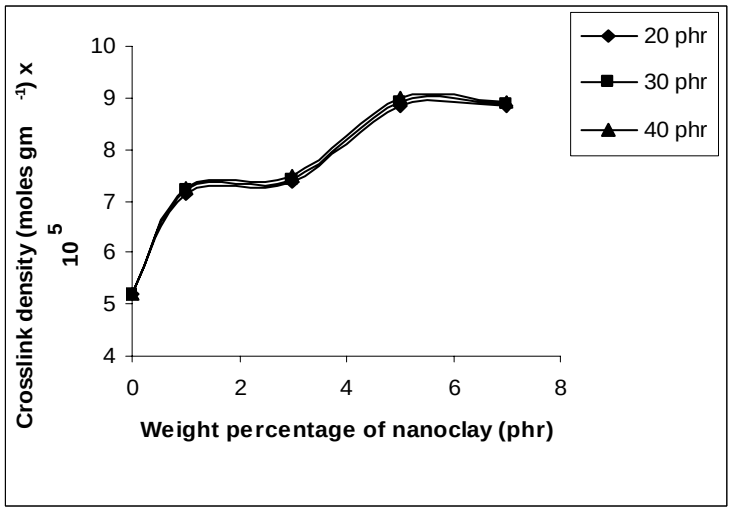

Figure 7.18 Variation of crosslink density with nanoclay loading

7.3 Conclusions

Transport properties of the nanocomposites were studied. The sorption, diffusion and permeation coefficients were measured using toluene at 303K. The percentage mass of oil absorbed by the rubber matrix was also studied in different oils at room temperature. Due to the tortous path these solvent molecule have to take in the intercalated nanocomposites, a considerable decrease in diffusion, permeation and sorption coefficients were observed. It is observed that decreasing value of permeability of nanocomposites is largely dominated by the diffusion phenomenon. The permeation resistance of the nanocomposite is confirmed from the gas permeability values which fit with the Nielson's model. The crosslink density increases with increase in the clay loading up to a particular level.

References

1. Wang Y, Zhang H, Wu Y, Yang W, Zhang L. European Polymer Journal 2005 ;41 :2776
2. Sinha ray S, Yamada K, Okamoto M, Ogami A, Ueda K. Chem Mater 2003;15:1456.
3. Zhang HF, Feng YX, Wu YP,et al. China Rubber Industry 2001 ;48 :587.
4. Wu YP, Wang YQ, Zhang H F, Wang, YZ, Yu DS, Zhang LQ, Yang, J. Compos Sci Technol 2005 ;65 :1195.
5. Li P, Wang L, Song G, Yin L, Qi F, Sun L. J Appl Polm Sci 2008;109:3831.
6. Naylor T. Permeation properties in Handbook of comprehensive polymer science, 1989; Vol.2, edn, 1:643, Pergamon Press Plc, UK.
7. Compan V, Zanuy D, Andrio A, Morillo M, Aleman C, Guerra SM. Macromolecules, 2002;35:4521
8. Arnold ME, Nagai K, Freeman BD, Spontak RJ, Betts DE, De Simone JM, Pinnau I. Macromolecules 2001;34:5611.
9. Barbi V, Funari SS, Gehrke R, Scharnal N Stribeck N Macromolecules. 2003;36:749.
10. Pixton MR, Paul DR. Macromolecules 1995;28:8277.
11. Vega MA, Paul DR. J.Polym. Sci, Part B: Polym.Phys.Edn,1993;31:1599 and 1993;31:1577.
12. Aitken CL, Koros WJ, Paul DR. Macromolecules 1992 ;25:3651.
13. Mc Hattie JS, Koros WJ, Paul DR. Polymer.1992;33:1701.
14. Mc Hattie JS, Koros WJ, Paul DR. Polymer.1991;32:2618.
15. Tiemblo P,Guzman J, Riande E, Mijangos C, Reinecke H. Macromolecules 2002;35:420.

16. Neilson PW, Xu GF. Macromolecules 1996 ;29 :3457.
17. Aithal US, Balundgi RH, Aminahavi TM, Shukla SS. Polym Plast. Technol. Eng 1991;30:299.
18. van Amerongen GJ. J Appl Phy. 1946;17:972 Rubber Chem Technol 1947;20:494.
19. Van Amerongen GJ. J Appl Polym sci. 1950;5:307 Rubber Chem Technol 1951;24:109.
20. Liang Y, Wang Y, Wu Y, Lu Y, Zhang H, Zhang L. Polymer Testing 2005;24:12.
21. Usuki A, Tukigase A, Kato M. Polymer 2002; 43:2185.
22. Varghese S, Karger-Kocsis. J.Polymer 2003; 44:4921.
23. Alexandre M, Dubois P. Materials Science and Engineering 2000;28:1
24. Zhang LQ, Wang YZ, Wang et al, YQ. J Appl Polym sci.2000 ;78 : 1873.
25. Johnson T, Thomas S. Polymer 1999;40:3223.
26. Hasegawa N, Okamoto H, KatoM, Usuki A, Sato N. Polymer 2003;44:2933.
27. Giannelis EP.Adv.Mater.1996;8:29.
28. Weiner MW, Giannelis EP, Sogah DY, Sogah. J Am Chem Soc.1999;122:1615.
29. Angellier H, Molina-Boisseau S, Lebrun L, Dufresne. Macromolecules 2005;38:3783.
30. Hasegawa N, Okamoto H, Usuki A. J Appl Polym sci 2004;93:758.
31. Valadares LF, Leite CAP, Galembeck F. Polymer 2006; 47: 672.
32. Nielsen L. J Macromol Sci Chem A1 1967: 929.
33. Aithal US, Aminabhavi TM, Cassidy PE. J Memb Sci 1990;50:22.
34. Franson NM, Peppas NA. J Appl Polym Sci 1983;28;1299.
35. Chiou JS, Paul DR. Polym Eng Sci 1986;26:1228.
36. Crank J. IN: The Mathematics of diffusion. 2nd Ed. Ox: Clarendon Press, 1975; p244.

37. Britton LN, Ashman RB, Aminabhavi TM, Cassidy PE. J Chem Educ 1988; 55:368.
38. Aprem AS, Joseph K, Mathew AP, Thomas S. J Appl Polym Sci 2000;78:941.
39. Tanrattanakul V, Wattanathai B, Tiangjunya A, Muhamud P. J Appl Polym Sci 2003;90:261.
40. Mousa A, Ishiaku US, Mohd ishak Z A.J Appl Polym Sci 1998;69:1357.
41. Flory PJ, Rehner J. Chem Phys 1943;11:512.

Chapter 8

Dynamic mechanical and dielectric properties of maleated natural rubber organoclay nanocomposites

Dynamic mechanical analysis is a useful technique for characterization of polymer layered silicate nanocomposites. The extend of intercalation and exfoliation of layered silicates in polymer can be obtained from the storage modulus and glass transition temperature. A large number of rubber articles like automobile tyres, springs and dampers are subjected to cyclic deformation or loading during their service life. Rubber is used as the base material in a product if it requires rubber-like elasticity and flexibility. Since rubber products generally undergo dynamic loading during service, their dynamic mechanical analysis is very important. Thus it is particularly useful for evaluating the mechanical properties of viscoelastic materials like polymeric composites whose properties exhibit time, temperature and frequency dependence. The dynamic mechanical properties of polymer layered silicate nanocomposites depend highly on the separation of the silicate layers. As the spacing between the silicate layers increases the storage modulus (E') increases and the damping peak corresponding to the glass transition temperature broadens. The viscoelastic behaviour of polymer nanocomposites has been studied by many scientists for analyzing the change in glass transition temperature, damping behaviour (tan δ), storage and loss modulus (E") with addition of nanofillers [1-9]. Arrighi *et al.* [7] observed a second relaxation dynamics due to interaction of the polymer with filler surface. Varghese *et al.* [10, 11] studied the damping behavior of layered silicates reinforced natural rubber nanocomposites. The frequency sweep of the

NR and NR/clay composite at 60^0C under 0.58 strain is reported [12]. The dynamic mechanical properties of NBR/clay [13], MA-g-EPDM/clay [14] have been studied. Dynamic mechanical studies have considerable practical significance for several reasons, particularly if they are analyzed over a wide range of frequencies and temperatures. The dynamic properties are also of direct relevance to a range of unique polymer applications, concerned with the isolation of vibrations or dissipation of vibrational energy in engineering components.

Dielectric property analysis of filled polymers and polymer-polymer blend contribute to a better understanding of the structure-property relationships at the morphological level [15-18]. The dielectric properties of polymeric material depend on the additives, fillers and impurities present in it. The effect of filler on the electrical properties of polymeric material has been investigated by many researches [19, 20-24]. The most widely used fillers in polymeric material are carbon black, graphite particles and conducting fibers. The properties of these composites depend on three phases, namely, the phase of organic polymer, the phase of filler content and the phase of interaction between the polymer and the blend.

The dynamic mechanical analysis and dielectric properties of nanoclay reinforced maleated natural rubber nanocomposites by direct method and masterbatch technique are proposed to be investigated with reference to the maleic anhydride content, organoclay content and frequency using the frequency sweep method.

8.1 Experimental

8.1.1 Dynamic mechanical analysis

In dynamic mechanical analysis the frequency is proposed to be varied from 1 to 50Hz under frequency sweep mode at a rate of 2Hz/min and at a temperature of 60^0C.

8.1.2 Dielectric studies

The dielectric permittivity was measured in alternating current at room temperature using HP 4285 A LCR Hitester by varying the frequencies (0.1-8 MHz).

8.1.3 Heat build-up

The Ektron flexometer conforming to ASTM D 623-1999 was used for measuring the heat build-up.

8.2 Results and discussion

8.2.1 Dynamic mechanical properties (DMA)

8.2.1.1 Maleated natural rubber clay nanocomposites

The dynamic mechanical response of the maleated natural rubber (MA-g-NR) containing layered silicate is measured to examine the degree of filler-matrix interaction. Maleic anhydride concentration in direct method is taken as 1, 3, 5 percentages. The elastomer chains get intercalated into the layered structures of silicate resulting in the change in modulus and damping behaviour. The interaction of polymer chain into silicate layers will enhance the contact surface area of filler and matrix. Figure 8.1 is the E' vs weight percentage of nanoclay curves at different frequency of 5MA-g-NR. The E' connects with the elastic modulus of the material. The E' of nanocomposite is higher than unfilled system. Due to the aggregation of filler at higher concentration, the clay filled MA-g-NR shows reduced modulus. The enhancement in modulus with the addition of filler is associated with the stiffness of the material. Up to 5 weight percentage nanoclay there shows an enhancement in storage modulus and this may be due to better interaction between the polar rubber and polar filler. Figure 8.2 is the E' verses weight percentage of nanoclay curves at different frequency of 3MA-g-NR. For 3MA-g-NR system, the E' is higher for filled system. 3MA-g-NR nanocomposites show the same trend as that of 5MA-g-NR. But the storage modulus is decreased by 18% in the case of 3MA-g-NR nanocomposites. From

this it is evident that by increasing the maleic anhydride concentration the storage modulus can be improved and may be due to the better polarity of the matrix. Higher storage modulus indicates better dispersed and more exfoliated system. In case of intercalated structures, the contact surface area between polymer and the silicate layers are relatively low and as a result the change in E' with frequency are not very predominant as compared to virgin polymers.

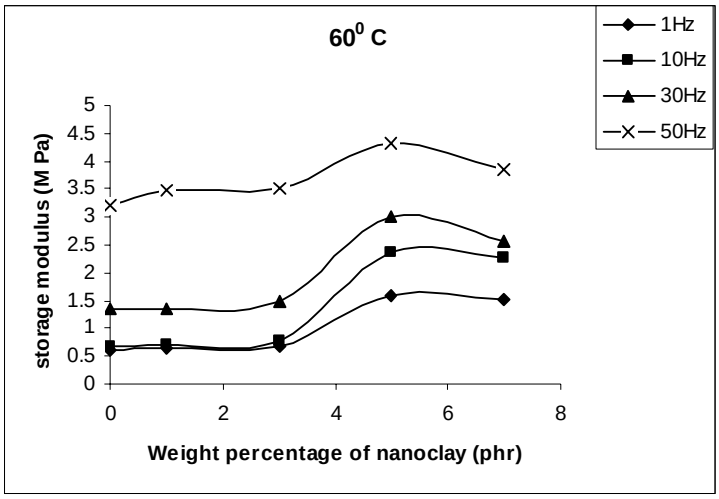

Figure 8.1 Storage modulus vs nanoclay curves of 5MA-g-NR nanocomposites

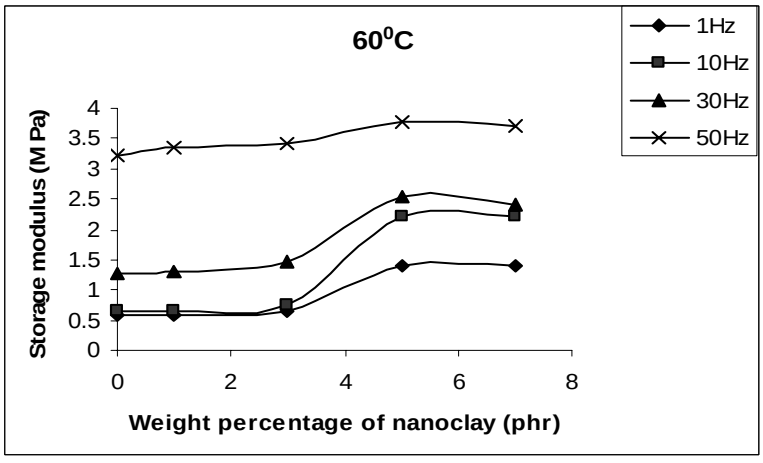

Figure 8.2 Storage modulus vs nanoclay curves of 3MA-g-NR nanocomposites

Up to 30Hz the storage modulus gradually increases at 5 weight percentage nanoclay but at 50Hz the increase is very fast. For 1MA-g-NR nanocomposites the storage modulus shows the same trend as that 5MA-g-NR and 3MA-g-NR. But the storage modulus is very low compared to the above two matrices.

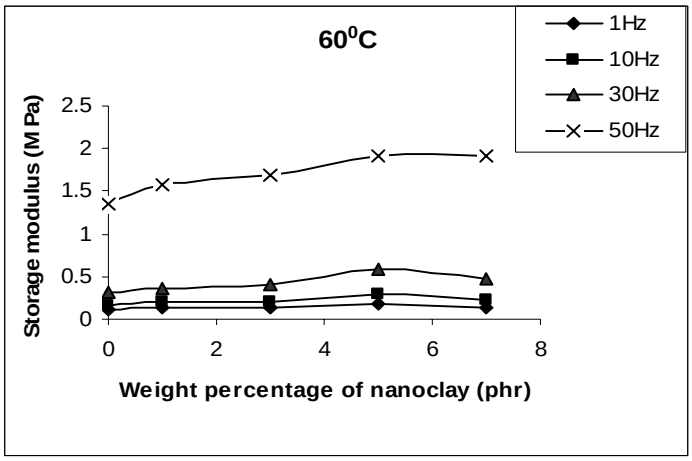

Figure 8.3 Storage modulus vs nanoclay curves of NR nanocomposites

The dynamic mechanical properties of pristine natural rubber and its composites with clay were investigated over a wide frequency range as shown in figure 8.3. A 400% increase in storage modulus is observed for 5MA-g-NR at 5wt% compared to pure NR at 5wt% nanoclay loading for a frequency of 30Hz. Storage modulus E' shows linear increase with frequency for all the composites irrespective of the matrix.

Figures 8.4-8.6 shows the E" vs nanoclay curves of layered silicate filled 5MA-g-NR, 3MA-g-NR and NR. At lower concentration of filler the E" increases. The E" relates to the energy loss due to viscous dissipation. It is the viscous modulus of polymeric material. E" shows a high value for gum sample compared to the filled nanocomposites. Up to 5wt% of nanoclay loading the loss modulus shows a decreasing trend and above that the loss modulus is increased. The E" is decreased by 11.09% by the addition of 5wt% nanoclay in 30Hz for 5MA-g-NR when compared to the NR nanocomposite. It was seen that, E" of the

composite at any frequency is lower than that of gum compound. Clay incorporation decreases the E", which indicates the lower heat dissipation (heat build-up) in the clay reinforced MA-g-NR nanocomposites compared to that of gum compound. But an increment in loss modulus is observed at 7wt% nanoclay loading irrespective of the frequency. At 50Hz the loss modulus is increased which means high heat dissipation which may be explained in terms of the friction between the filler particles and the matrix. The nanoclay loading have also a significant effect on the frequency-dependency of the E' and E".

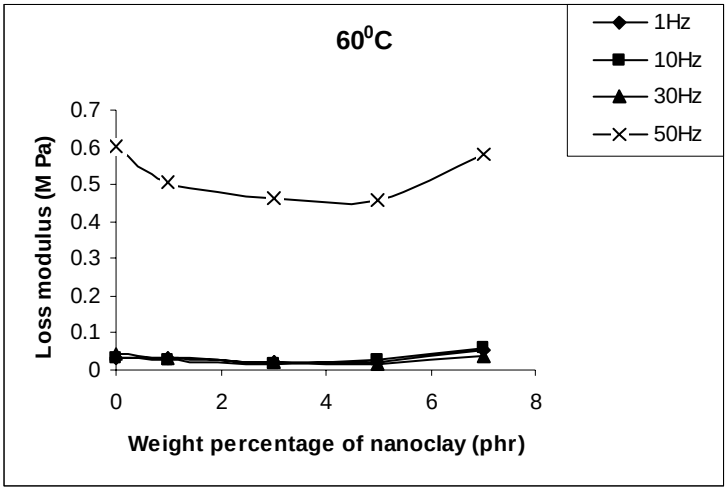

Figure 8.4 Loss modulus vs nanoclay curves of 5MA-g-NR nanocomposites

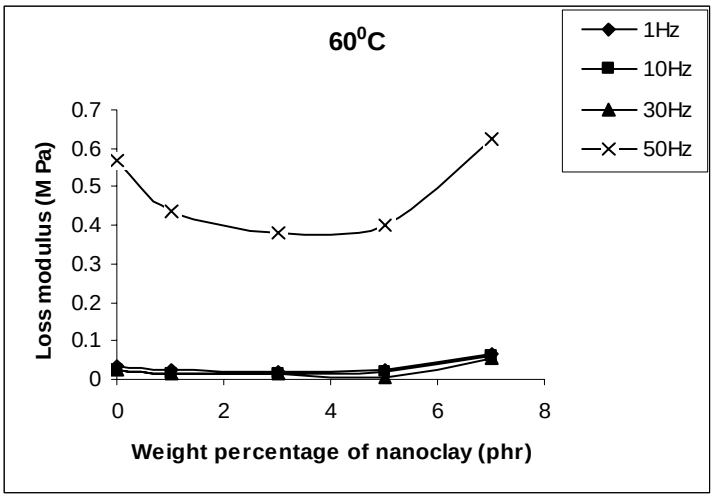

Figure 8.5 Loss modulus vs nanoclay curves of 3MA-g-NR nanocomposites

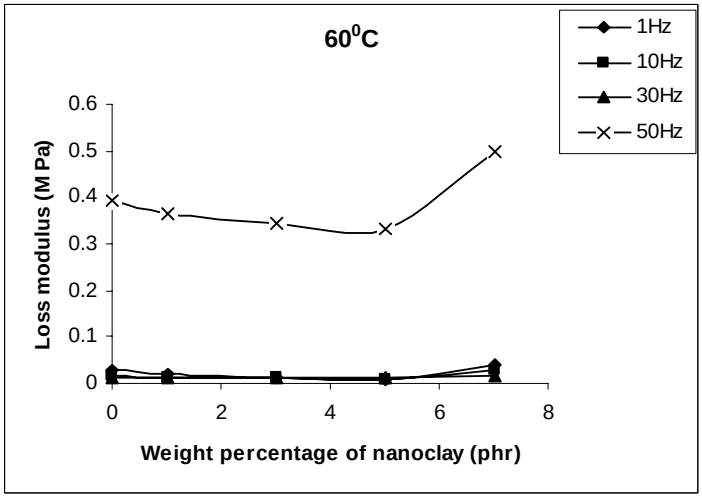

Figure 8.6 Loss modulus vs nanoclay curves of NR nanocomposites

The damping behaviour of nanocomposites is displayed in figures 8.7-8.9. It is seen that the nanofiller reinforcement caused a decrease in tan δ value; increase in concentration of layered silicate results in a consistent decrease in loss tangent. This can be interpreted in terms of the restricted mobility of polymer chains due to their confinement in the layers of the silicates.

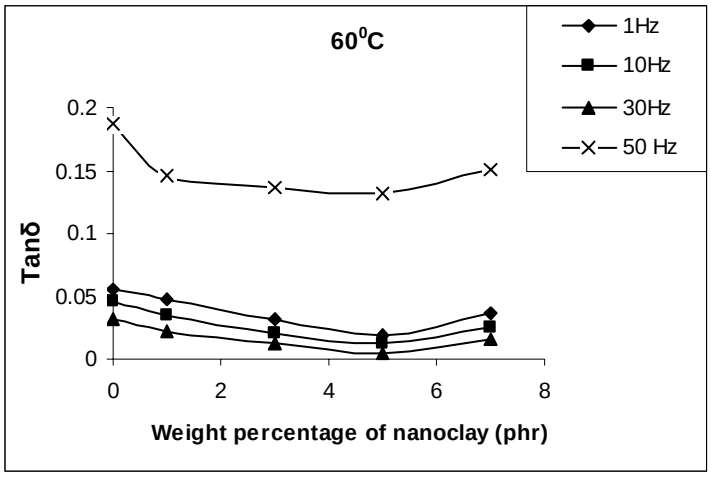

Figure 8.7 Tan δ vs nanoclay curves of 5MA-g-NR nanocomposites

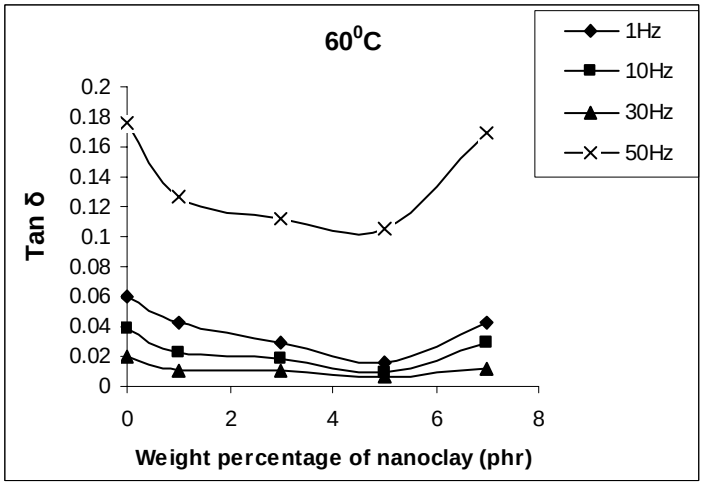

Figure 8.8 Tan δ vs nanoclay curves of 3MA-g-NR nanocomposites

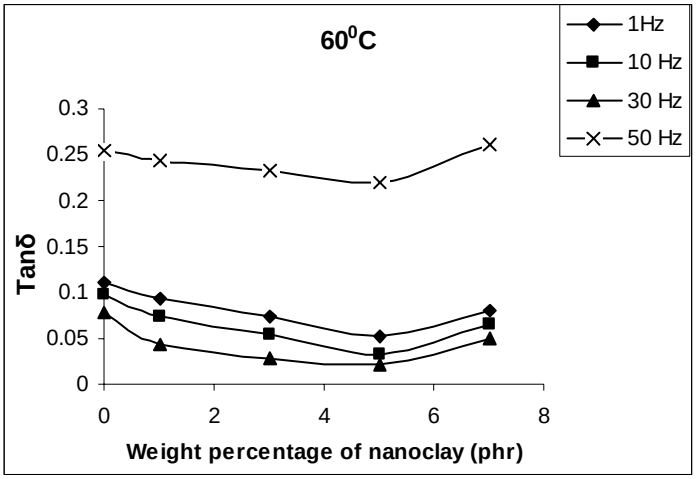

Figure 8.9 Tan δ vs nanoclay curves of NR nanocomposites

By the addition of clay, the tan δ becomes smaller. It is known that the height of the dynamic transition of a composite apparently reflects the relative quantity of the component itself. The decrease in tan δ is the result of the reduction of the amount of polymer being deformed during strain oscillation and thus reduces the amount of dissipated energy in the dynamic transition and this may be due to the greater amount of polymer in the intercalated stacks. It is often believed that the mechanical loss factor at 60^0C has apparent relation with rolling resistance when the rubber is used for tire. The lower value of mechanical loss factor at 60^0C indicates lower rolling resistant. The frequency sweep of the NR and MA-g-NR/clay composites at 60^0C under 0.5146 strains is studied. The results show that pure NR [12] slightly decreases the mechanical loss factor under experimental conditions because of the weak interaction between the clay and matrix. In 5MA-g-NR organoclay nanocomposites decrease in the mechanical loss factor is high compared to pure NR nanocomposites due to the better interaction between the filler and polar matrix. It is interesting to point out that the decrement is much more in the case of 5wt% organoclay and when more clay is incorporated the storage modulus increases again, but still lower than 5MA-g-NR vulcanizate. A decrement of 351% and 223% in tan δ by the addition of

5wt% nanoclay in 30Hz for 5MA-g-NR and 3MA-g-NR when compared to the NR nanocomposites. From these results, it can be deduced that 5MA-g-NR reinforced with 5wt% organoclay has the lowest rolling resistant. It is assumed that at the experiment conditions the organoclay gets the best dispersion and morphology in the rubber matrix, which lead to best dynamic mechanical properties. When adding more inorganic fillers in the matrix, the dynamic mechanical properties become worse because the superabundant filler cannot deform and absorb energy during strain oscillation.

8.2.1.2 Maleated natural rubber clay nanocomposites developed through masterbatch technique

10MA-g-NR masterbatches with 20, 30, 40 and 50phr loading were studied. The maximum property improvement is only up to 40phr and above that a decrement is noticed. So 20phr and 40phr is taken for the study. The mechanical property shows a maximum value at 40phr batch at 5wt% loading for10MA-g-NR which is mentioned in chapter 5. Figure 8.10 and 8.11 shows the storage modulus verses nanoclay loading of 10MA-g-NR at a frequency of 1, 10, 30 and 50Hz for 20phr and 40phr batch.

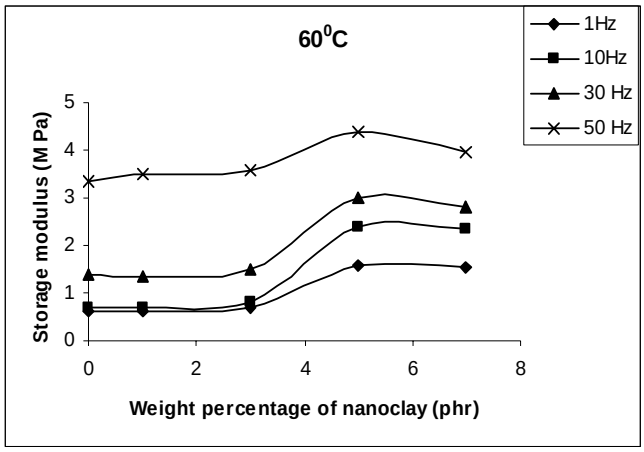

Figure 8.10 Storage modulus vs nanoclay of 10MA-g-NR nanocomposites at 20phr masterbatch.

It is seen that the storage modulus increased up to 5wt% nanoclay loading and above that a decreasing trend is observed. At higher levels of clay loading this decrease is due to the poor dispersion of clay. The increase in storage modulus may be due to the stiffness of the material. This is due to the confinement of the macromolecular segments into the organoclay nanolayers and the strong interaction between the filler and rubber matrix. 40phr masterbatch shows the maximum storage modulus when compared to 20phr batch and 5MA-g-NR nanocomposites developed by direct method. An increase of 405% and 519% in storage modulus is observed for 10MA-g-NR at 5wt% nanoclay for 20phr and 40phr batch respectively compared to pure NR nanocomposite at 5wt% loading. And also an increase of 23.52% in storage modulus is observed for 40phr batches when compared to 5MA-g-NR at 5wt% clay loading.

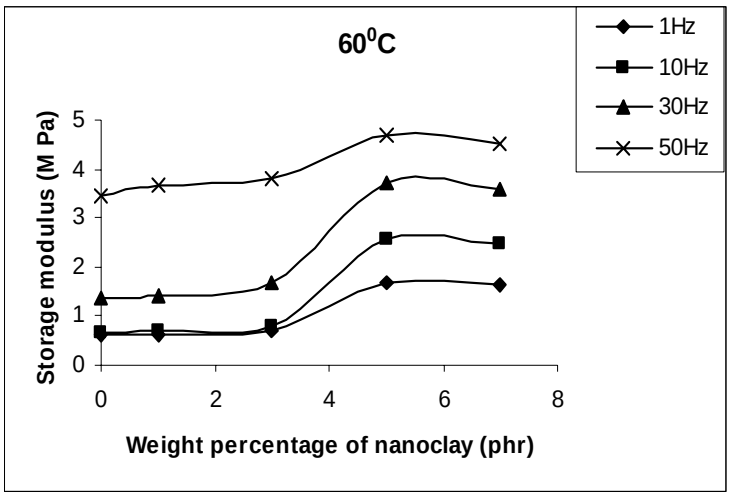

Figure 8.11 Storage modulus vs nanoclay of 10MA-g-NR nanocomposites at 40phr masterbatch

Figure 8.12 and 8.13 shows the loss modulus verses nanoclay loading of 10MA-g-NR at a frequency of 1, 10, 30 and 50Hz for 20phr and 40phr. The E" relates to the energy loss due to viscous dissipation. It is the viscous modulus of a polymeric material. Decrease in loss modulus is observed for all nanocomposites irrespective of the matrix. This is due to low heat dissipation (heat build up) in nanocomposites. Decrement is higher for 40phr batch at 5wt% clay loading which means low heat built up.

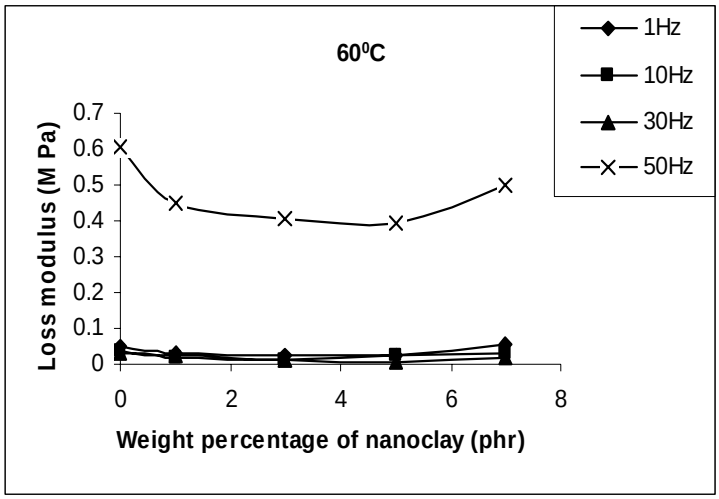

Figure 8.12 Loss modulus vs nanoclay of 10MA-g-NR nanocomposites at 20phr masterbatch

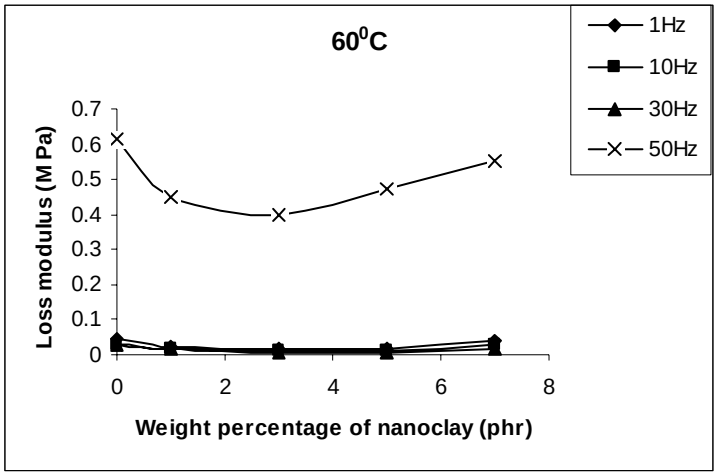

Figure 8.13 Loss modulus vs nanoclay of 10MA-g-NR nanocomposites at 40phr masterbatch

Figure 8.14 and 8.15 shows the tan δ verses nanoclay loading of 10MA-g-NR at a frequency of 1, 10, 30 and 50Hz. The damping behaviour of nanocomposites is lower compared to the gum sample. All matrixes show the same trend. The 40phr batch at 5wt% loading show the lower value in loss tangent compared to all other matrix. The increase in concentration of layered silicates results in a consistent decrease in loss tangent. This can be interpreted in terms of the restricted mobility of polymer chains due to the confinement in the layers of silicates. The decrease in tan δ suggests a strong adhesion between the rubber and filler.

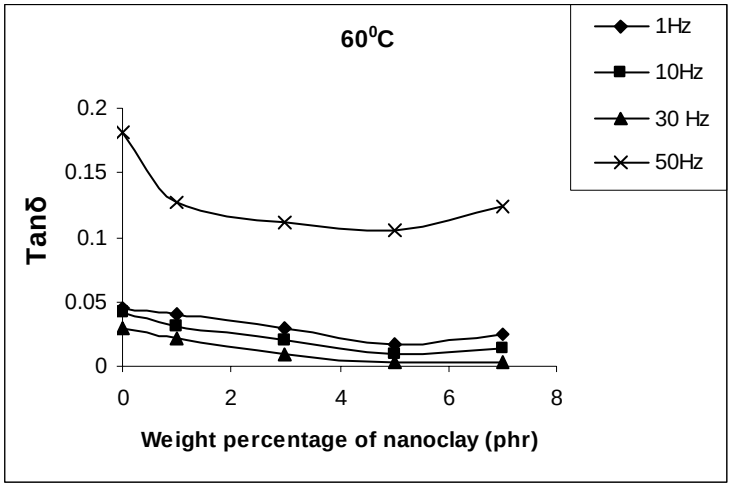

Figure 8.14 Tan δ vs nanoclay of 10MA-g-NR nanocomposites at 20phr masterbatch

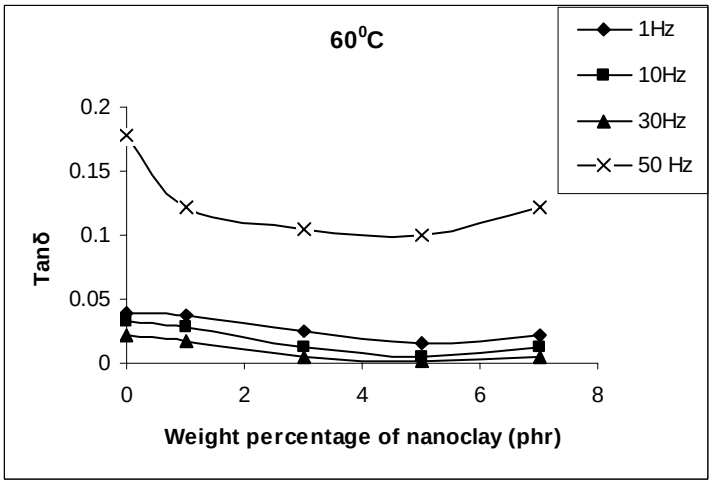

Figure 8.15 Tan δ vs nanoclay of 10MA-g-NR nanocomposites at 40phr masterbatch

8.2.2 Heat Build up

Effect of nanoclay in NR and maleated NR nanocomposites were also studied at certain dynamic properties such as the generation of heat under cyclic deformation. We have used the classic test of the Ektron flexometer and the temperature increase was then divided by the hardness of the sample to have a heat index. All the data of this study are reported in figure 8.16-8.19. It can be observed that the heat build up decreases by the addition of nanoclay and the best results are already achieved at 5wt% nanoclay level. The further addition of nanoclay does not affect anymore the heat index. Thus, the nanoclay offers also the beneficial effect of being able to reduce the hysteresis of a rubber compound [25].

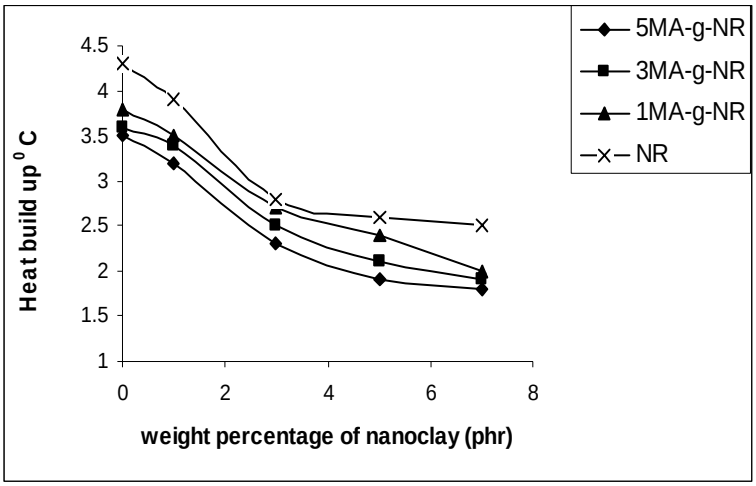

Figure 8.16 Heat build up verses nanoclay loading of nanocomposites

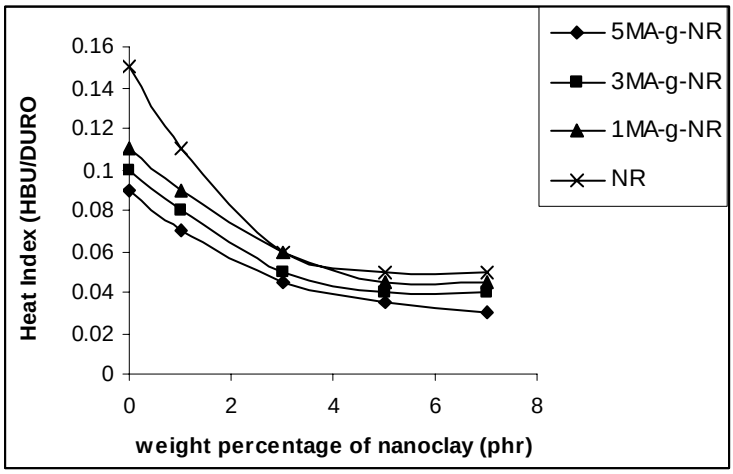

Figure 8.17 Heat index verses nanoclay loading of nanocomposites

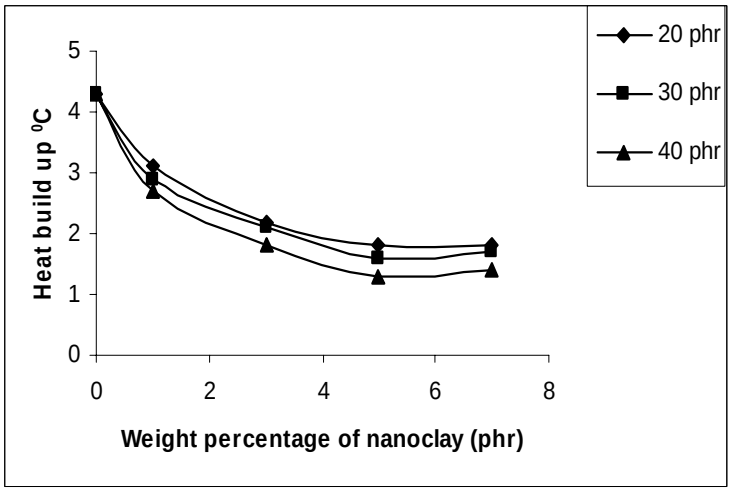

Figure 8.18 Heat build up verses nanoclay loading of 10MA-g-NR nanocomposites

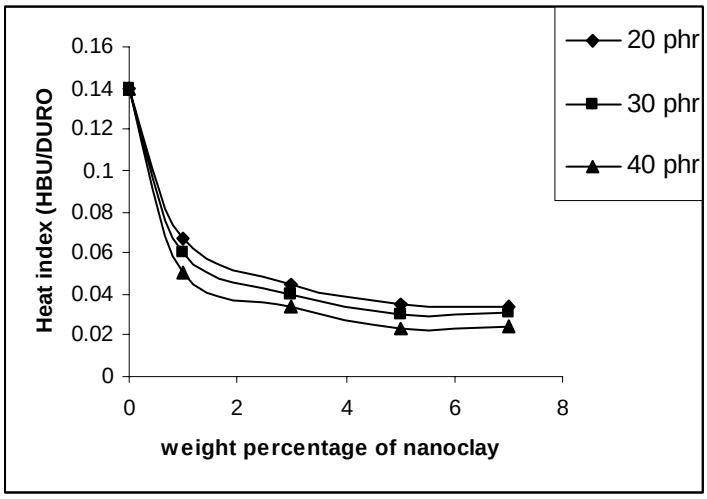

Figure 8.19 Heat index verses nanoclay loading of 10MA-g-NR nanocomposites

The heat build up and heat index of 10MA-g-NR nanocomposites developed through masterbatch technique is lower than the 5MA-g-NR nanocomposites developed by direct method. The first point in the graph of masterbatch method corresponds to the values of pure NR gum. Pure NR gum is taken as the reference material for 10MA-g-NR masterbatch. A decrease in heat build up of 508% is observed for 40phr batch at 5wt% nanoclay loading when compared to pure NR gum. While in the case of 5MA-g-NR nanocomposites at 5wt% nanoclay loading shows a decrease of 200% in heat built up when compared to 5MA-g-NR gum samples. 5MA-g-NR gives lower heat build up values when compared to 3MA-g-NR and 1MA-g-NR nanocomposites. Low heat generated samples are used in tires of automobiles. At the Ektron flexometer the compounds filled with nanoclay show lower heat build up and hence shows lower hysteresis than the reference compound without nanoclay under dynamic conditions. The heat index calculated as the ratio between the temperature jump at the Ektron flexometer and the hardness confirms the trend to lower hysteresis for the nanoclay filled compounds.

8.2.3 Dielectric properties

Figure 8.20 is the dielectric permittivity (ε') verses frequencies of 5MA-g-NR gum and its organoclay filled nanocomposites at 30^0C. It is observed that the filled systems show lower ε' than pristine polymers. A decrease of 12.19% and 9.21% in ε' respectively is observed for 5MA-g-NR and 3MA-g-NR at 5wt% nanoclay loading when compared to its gum. This may be due to the formation of ester as result of reaction between OH group of clay and COOH group of maleic anhydride which shows that better interaction at 5wt% of nanoclay loading. At 7wt% of nanoclay loading a noticeable change is not observed and this means that there are no more groups to interact with the OH groups of clay. But when compared to pure NR nanocomposites, the maleated nanocomposites show higher values.

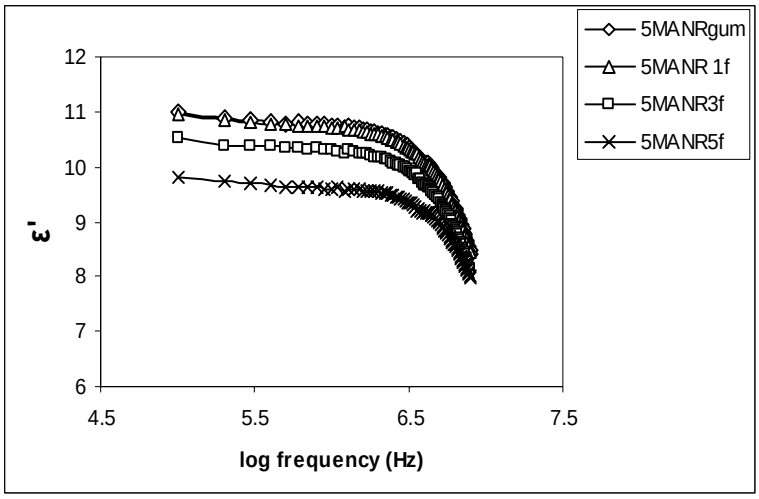

Figure 8.20 Dielectric permittivity vs frequency plots of nanocomposites at 30^0C

In the case of 3MA-g-NR gum and its nanocomposites the ε' is lower when compared to 5MA-g-NR nanocomposites and which is shown in figure 8.21. In all systems ε' decreases with increase in frequency. 3MA-g-NR at 7wt% shows

the same trend as seen in 5MA-g-NR at 7wt% nanoclay loading. 1MA-g-NR shows again lower values of ε' when compared to the above two maleated matrices. This may be due to the low polarity of 1MA-g-NR and its nanocomposites.

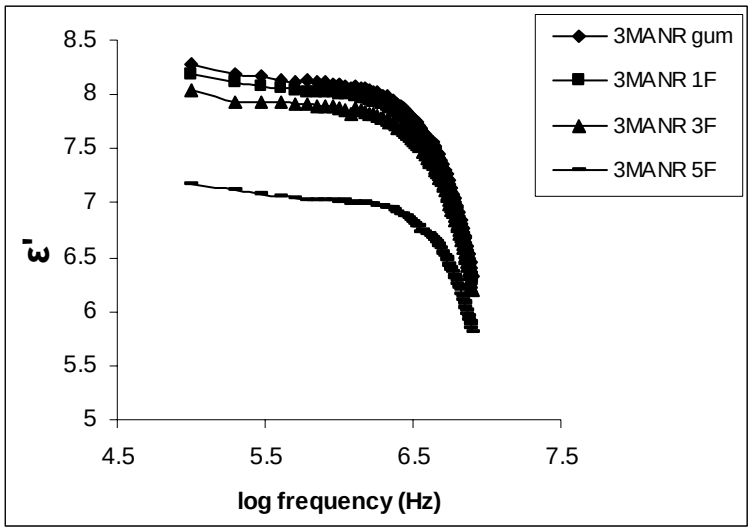

Figure 8.21 Dielectric permittivity vs frequency plots of nanocomposites at 30^0C

ε' decreased up to 5wt% of nanoclay loading in all the case and after that the decrease is not so pronounced as shown in figure 8.22. This shows that further interaction is not possible even after the addition of excess clay and this may be due to the poor interaction between the filler and the matrix which arises due to the lack of acid groups in the maleated rubber matrix for further interaction.

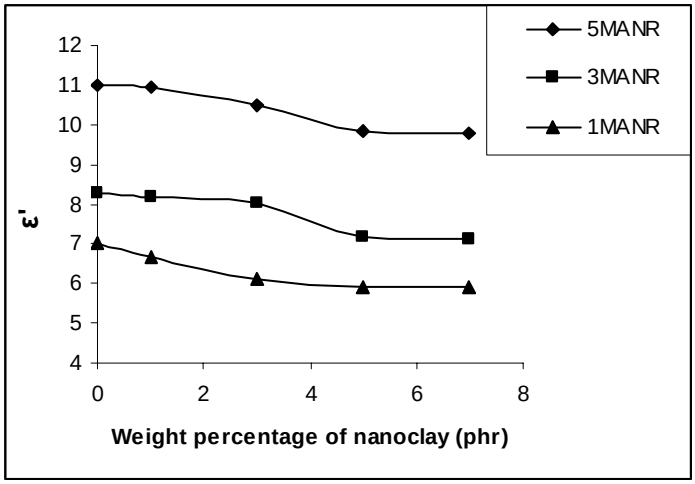

Figure 8.22 Dielectric permittivity vs nanoclay loading at 30^0C

Figure 8.23 and 8.24 shows the dielectric permittivity vs frequency plots of 10MA-g-NR nanocomposites at 30^0C for 20phr and 40phr batch respectively. Here also ε' decreases with increase in frequency as that of 5MA-g-NR nanocomposites which is obtained by direct method. And also ε' shows a decrement as the clay content is increased as shown in 8.25. 40phr batch shows lower ε' compared to 20phr batch at 5wt% nanoclay loading. This is due to the better dispersion of clay in the matrix. NR nanocomposites show lower ε' values when compared to the maleated nanocomposites which shows that conductivity is higher in maleated nanocomposites due to the polar nature. A slight increasing trend (23.38%) is observed in the case of NR nanocomposites as the clay content is increased but still lower than the maleated sample which is due to the polar nature of nanoclay.

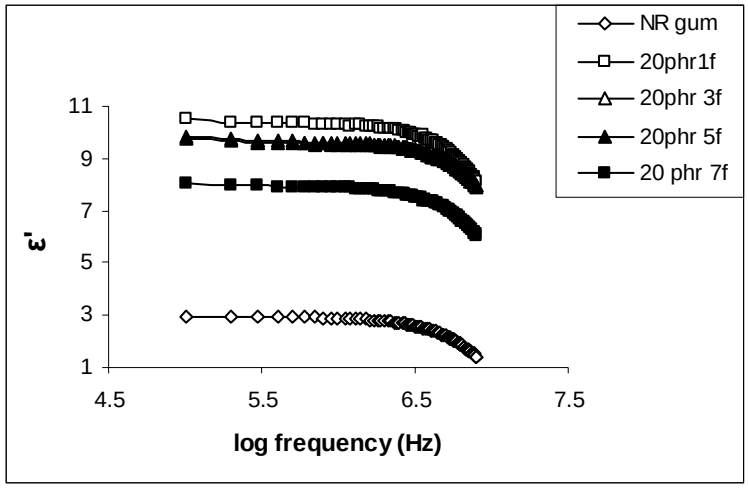

Figure 8.23 Dielectric permittivity vs frequency plots of 10MA-g-NR nanocomposites at 30^0C

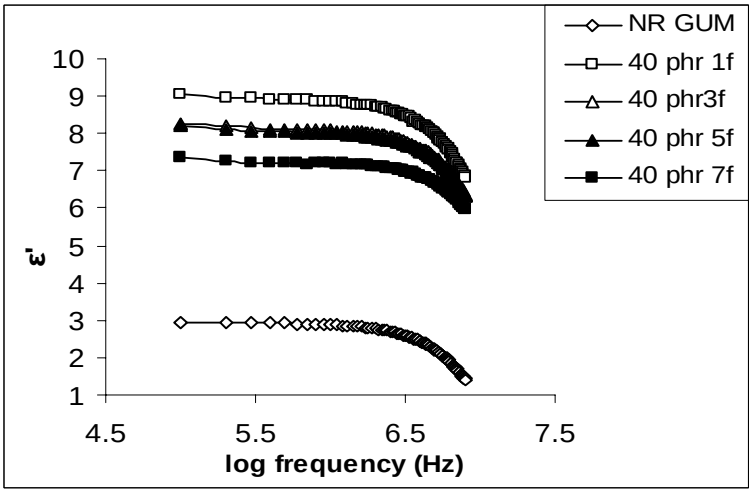

Figure 8.24 Dielectric permittivity vs frequency plots of 10MA-g-NR nanocomposites at 30^0C

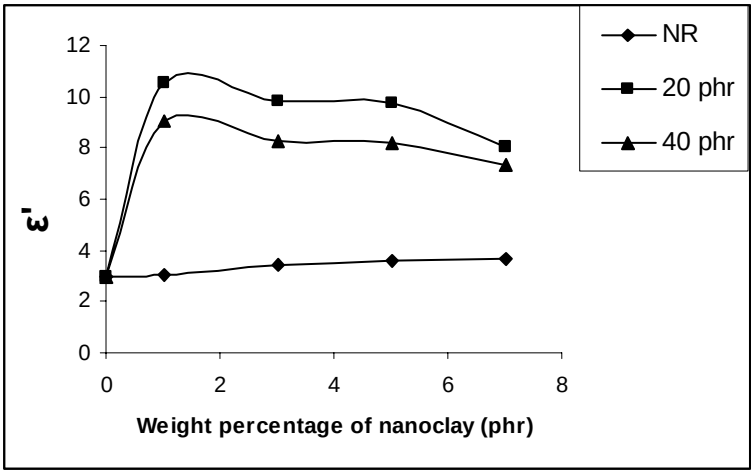

Figure 8.25 Dielectric permittivity vs nanoclay loading of 10MA-g-NR at 30^0C

8.3 Conclusions

Storage modulus increases while loss modulus and tan δ decrease with increase in the frequency in frequency sweep method. The storage modulus of nanocomposite is higher than unfilled system up to 5weight percentage clay loading. This is due to the aggregation of filler at higher concentration, the clay filled MA-g-NR shows reduced modulus. 3MA-g-NR shows the same trend as that of 5MA-g-NR. But the storage modulus is decreased by 18% in the case of 3MA-g-NR nanocomposites. The storage modulus increases as the maleic anhydride concentration in the matrix increases. The loss modulus and damping behaviour is decreased by increasing the clay loading to a particular level. The heat build up is decreased by the addition of nanoclay to a particular loading in all the mixes. The dielectric permittivity is higher for maleated gum samples compared to filled samples. Maleated samples show better dielectric permittivity compared to NR nanocomposites due to hydrogen bonding. In MA-g-NR nanocomposites the dielectric permittivity is decreased by the addition of nanoclay even though the values are higher than that of pure NR nanocomposites.

References

1. Zheng H, Zhang Y, Peng Z, Zhang Y. Polym.Test 2004;23:217.
2. Xiong J, Liu X, Yang X, Wang X Polym Deg Stabi 2004;86:549
3. Lopez- Manchado MA, Biagiotti J, Valentini L, Kenny JM. J Appl Polym Sci 2004;92:2004.
4. Wan C, Qiao X, Zhang Y, ZhangY. Polym Test 2003;22:453.
5. Teh PL, Mohd Ishak ZA, Hashim AS, Karger- Kocsis J, Ishiaku US. Eur Polym.J 2004; 40:2513.
6. Chabert E, Bornert M, Bourgeat-Lami E, Cavaille JY, Cavaille R, Daniel C, Gauthier C, Putaux JL, Zaoui A. Mater Sci Eng 2004;381:320.
7. Arrighi A, Mc Ewen IJ, Qian H, Prieto MBS. Polymer 2003;44:6259.
8. Hu YH, Chen CY, Wang CC Polym Deg Stabi 2004;84:545.
9. Zheng H, Zhang Y, Peng Z, Zhang Y. Polym Test 2004 ;23:217.
10. Varghese S, Karger- Kocsis Polymer 2003;44:4921.
11. Varghese S, Karger- Kocsis, Gatos KG. Polymer 2003;44:3977.
12. Yuhai S, Yuanfang L, Demin J. J Appl Polym Sci 2008;107:2786.
13. Lan L, Demin J, Yuanfang L, Baochun G. J Appl Polym Sci 2006 ;100 :1905.
14. Gatos KG, Karger- Kocsis. Polymer 2005;46:3069.
15. Chung KT, Sabo A, Pica A. J Appl Polym Sci 1982;53:6867.
16. Taipalus R, Harmia T, Zhang MQ, Friedrich K, Compo Sci Technol 2001;61:801.
17. Mamunya EP, Davidenko VV, Lebedve EV. Polym Compos 1995 ;16 :319.
18. Zois H, Apekis L, Mamunya YP. Macromol Symp 2003;194;351.
19. Varghese S, Varghese KT, Thomas S. J Appl Polym Sci 1999;73;255.
20. Zois H, Apekis L, Mamunya YP. J Appl Polym Sci 2003; 88:3013.

21. Zois H, Kanapitsas A, Pissis P, Apekis L, Lebedev E, Mamunya YP. Macromol Symp 2004; 205:263.
22. Cendoya I, Lopez D, Alegria A, Mijangos C. J Appl Polym Sci 2001;39:1968.
23. Mamunya Y, Kanapitsas A, Pissis P, Lebedev E,Bioteux G. Macromol Symp 2003;198:449.
24. Chand N, Jain D. Compos Part A: Appl Sci Manuf 2005;36:594.
25. Franco Cataldo. Macromol Symp 2007;247:67.

Chapter 9

Summary and Conclusions

A novel route for preparing maleated natural rubber (MA-g-NR) was developed by grafting maleic anhydride onto natural rubber (NR) by γ-radiation. This route is cleaner (avoids the use of chemicals), faster (higher throughput in a single batch) and versatile (product quality can be controlled by the radiation dosage). The maleated natural rubber thus produced has very attractive properties due its polarity compared to unmodified natural rubber and can be utilized for a variety of applications. The major finding of the study is that the maleated natural rubber can be successfully utilized for developing nanocomposites based on nanoclay.

The field of nanotechnology is one of the most popular areas for current research and development in basically all technical disciplines. This obviously includes polymer science and technology. Polymer nanocomposites have received much attention due to the nanoscale dispersion and very high aspect ratio of nanofillers. Polymer layered silicate (PLS) nanocomposites often exhibit remarkable improvement in material properties when compared with the virgin polymer or conventional micro-and macro-composites. These improvements can include high moduli and electrical properties, increased tensile strength, heat resistance, tear strength, decreased gas permeability, swelling to sovents and flammability.

A key factor in the polymer-organoclay interaction is the affinity polymer segments have for the silicate surface. The degree of dispersion of layered silicate in a particular polymer matrix depends on the inter layer cation. To support intercalation and exfoliation the inter layer distance should be greater than 1.5nm and the layered structure should be broken down. Thus the polymer interaction might be made more effective by increasing the interlayer distance. A

detailed and systematic study of maleated natural rubber clay nanocomposites by direct and masterbatch technique varying the maleic anhydride content and clay content in order to optimize its properties is presented in the thesis.

The grafting of maleic anhydride (MA) on natural rubber by gamma (γ) radiation has been the first part of this investigation. The modification of rubber using maleic anhydride improves its compatibility with different types of fillers. The effect of radiation dosage (0.5-10kGy) and MA concentration on grafting efficiency was evaluated. The MA content in MA-g-NR increased from 0.7% to 9.1% on increasing the MA concentration (from 1 to 10% of NR) in the reaction mixture. But high MA content retards the curing reactions of the rubber compositions. The MA grafted polymers also have been used extensively in the area of polymer reactive blending, as blend components or as compatibilizers. Grafted rubber can also be produced through chemical route. When compared to chemical routes, the novel radiation route adopted in this study is pollution free and adaptable for bulk production. It is observed that the MA grafting reaction strongly dependant on the radiation dosage. The MA content increases sharply up to a radiation dose of 2.5kGy and then decreases on further increasing the dosage. Highest grafting efficiency was observed at a dosage of 2.5kGy from IR and titration method. When concentrations of 1, 3 ,5 and 10percentages were taken the MA content proportionately increased from 0.7% to 9.1%.

Even though maleated natural rubber can be utilized for a variety of applications, this study mainly focused on the preparation and characterization of maleated natural rubber organoclay nanocomposites using hydroxyethyl substituted tallow ammonium as the organo-modifier. Effect of inter layer distance of the layered clay on the cure characteristics, mechanical properties and transport properties of natural rubber and maleated natural rubber by direct and master batch method were investigated. The improvement in properties were in the order NR <MA-g-NR direct <MA-g-NR master batch. Maximum torque of nanoclay filled compounds increased with increase in clay content while the cure time

reduced, which shows the accelerating effect of organoclays in the curing of rubber. This reduction in cure time marginally increased with the increase in interlayer distance of clay. It is seen that the nanocomposite with clay having higher interlayer distance show better mechanical properties. This shows that as the interlayer distance increases, the polymer chains penetrate more easily into the clay layers, which make the formation of intercalated structure. The morphology of filler dispersion in rubber matrix was analyzed using the transmission electron microscopy.

The mechanical properties such as tensile strength, elongation at break, modulus at 300% elongation, and tear strength of the nanocomposites were analyzed. The tensile strength increased with the concentration of clay for MA-g-NR and NR systems.

10% MA concentration was taken in the masterbatch technique. An increment of 87.33% in tensile strength is observed for 10MA-g-NR at 5wt% nanoclay in 40phr batch when compared to the pure NR gum sample. While on the other hand 10MA-g-NR nanocomposites when compared to the 5MA-g-NR at 5wt% nanoclay loading shows an increase in tensile strength of 12.14%. 10MA-g-NR in 40phr batch & 5MA-g-NR with 5wt% nanoclay shows a decrement of 26.83 & 7.20% respectively in the case of elongation at break. The decrease at higher loading is due to the enhancement in rigidity of the material and is possibly caused by the reduction in tensile crystallization. All the systems show the same trend. The increase in d-spacing for these layered clays is evident from X-ray results. TEM photographs also confirm the formation of an intercalated structure.

The thermal stability of nanofilled samples was higher due to the obstructed diffusion of volatile decomposition products within the nanocomposite. However, for a few samples at higher concentration of nanofiller, thermal stability decreased due to the reduced degree of delamination of clay in the matrix. The nanofillers act as a barrier by forming a coating on the surface of the polymer. As a result the thermal stability of the polymer nanocomposite

increases. The activation energy required for thermal degradation of MA-g-NR nanocomposites was determined by Coats-Redfern and Freeman Carroll plots. The activation energy required for thermal degradation of nanofilled samples was found to be higher than that of unfilled systems. Higher the activation energy the greater was the thermal stability. The ageing resistance of MA-g-NR nanocomposites was found to be higher than the unfilled system. The flame retardency of MA-g-NR nanocomposites is not much improved when compared to unfilled sample.

The transport properties of MA-g-NR nanocomposites with a low level of filler loading were studied in detail. A considerable decrease in diffusion, permeation and sorption coefficients were observed for nanocomposites. The permeation resistance of the nanocomposites was confirmed by the gas permeability testing and it fits with the Nielson's model, which describes the tortousity effect of plate like particulates on the gas permeability of polymer composite structures. The percentage mass of oil absorbed with nanoclay for 5, 3, and 1% MA in MA-g-NR nanocomposites were studied in transformer oil, hydraulic oil and engine oil. It is observed that the swelling values of 5MA-g-NR nanocomposites are found to be much less when compared to 3MA-g-NR and 1MA-g-NR nanocomposites and also the swelling index values is lower for transformer oil and higher for engine oil. This can be explained in terms of the polar-polar interaction between the polymer and filler. The increase in filler content (1-7wt%) also shows reduced swelling index values. The reduction of swelling upon the addition of layered silicates is due to the enhanced rubber/filler interaction. This can also be explained in terms of the higher tortuosity of path and the reduced transport area in the rubber matrix in presence of nanoclay.

The dielectric property for MA-g-NR nanocomposites is higher for unfilled system when compared to gum in all cases. The dielectric property of maleated NR gum is higher than pure NR gum due to the polar nature of maleated rubber. When nanoclay is added to maleated system the polarity is reduced due to the

interaction of OH group of organoclay with acid group of maleated rubber. The hydrogen bonding takes place here and this directs to the interaction between the maleated rubber and filler. Filled MA-g-NR nanocomposites show increased storage modulus. Here the tan δ value is reduced owing to the better dispersion of clay layers in the matrix. The loss modulus also shows the same trend as tan δ.

List of Abbreviations and Symbols

α	Aspect ratio
A^0	Angstrom
ASTM	American Society for Testing and Materials
As	Surface area
BF_3	Boron tri fluoride
BIS	Bureau of Indian Standards
BR	Poly butadiene rubber
^0C	Degree celsius
CBS	N-cyclohexyl-2-benzothiazyl sulphenamide
CEC	Cation exchange capacity
cm	Centimetre
CP	Centi poise
cpm	Cycles per minute
CR	Coats Redfern
D	Diffusion coefficient
d	Diameter
DEG	Di ethylene glycol
deg	Degree
DMA	Dynamic mechanical analysis
dNm	Deci Newton meter
DSC	Differential scanning calorimetry
DTG	Differential thermogram
E’	Storage modulus
E”	Loss modulus
Ea	Activation energy
EB	Elongation at break
ENR	Epoxidised Natural Rubber
ϕ_f	Volume fraction of the clay

$Fecl_3$	Ferric chloride
FC	Freeman carroll
FTIR	Fourier transform infrared
G’	Storage modulus
G”	Loss modulus
G*	Complex modulus
g	Gram
γ	Gamma
HCl	Hydrochloric acid
hrs	Hours
Hz	Hertz
IR	Infrared
ISNR	Indian Standard Natural Rubber
K	Kelvin
kg/cm^2	Kilogram per square centimeter
kGy	Kilo gray
kJ/mol	Kilo joule per mol
kN	Kilo newton
KOH	Potassium hydroxide
kV	Kilo volt
LS	Layered silicate
µ	Micro meter
MA	Maleic anhydride
MA-g-NR	Maleic anhydride graft natural rubber
Mc	Molar mass between crosslinks
meq	Molar equivalent
M_H	Maximum torque
MHz	Mega Hertz
min	Minutes
M_L	Minimum torque
MMT	Montmorillonite

MPa	Mega pascal
n	Order
NC	not classified
nm	Nano meter
N/mm	Newton per millimeter
NMR	Nuclear magnetic resonance
NR	Natural rubber
OMLS	Organo modified layered silicate
P	Permeation coefficient
ρ	Density
%	Percentage
PCN	Polymer clay nanocomposites
PET	Polyethylene terephthalate
phr	Parts per hundred
PLS	Polymer layered silicate
PLSNs	Polymer layered silicate nanocomposites
pphm	Parts per hundred million
PRI	Plasticity retention index
PS	Polystyrene
R	Universal gas constant
rad	Radiation
RPA	Rubber process analyzer
rpm	Rotations per minute
S	Sorption coefficient
sec	Seconds
SEM	Scanning electron microscope
θ	Theta
T	Absolute temperature
t_{10}	Scorch time
t_{90}	Optimum cure time

tan δ	Loss factor
TEM	Transmission electron microscope
Tg	Glass transition temperature
TG	Thermogravimetry
$TiCl_4$	Titanium tetra chloride
Tm	Melting temperature
TMTD	Tetramethyl thiuram disulphide
T max	Maximum decomposition temperature
T min	Minimum decomposition temperature
UTM	Universal testing machine
Vs	Molar volume of solvent
wt %	Weight percentage
XRD	X-ray diffraction
ZnO	Zinc Oxide

Publications and Presentations

1) Maleation of natural rubber by radiation grafting and its use in developing layered clay nanocomposites, *Vijayalekshmi V, George K.E, Pavithran C,* Journal of Applied Polymer Science, John Wiley & sons. (under revision)

2) Studies on maleated natural rubber/ organoclay nanocomposites, *Vijayalekshmi V, George K.E, Pavithran C,* Progress in Rubber Plastics and Recycling Technology. (communicated)

3) Maleated Natural Rubber/Clay Nanocomposites Developed through Masterbatch Technique, *Vijayalekshmi V, George K.E, Pavithran C,* Journal of elstomers and plastics. (communicated)

4) Use of maleated natural rubber for developing natural rubber-clay nanocomposites *Vijayalekshmi V, George K.E, Pavithran C,* POLYCHAR- 16, Lucknow, 2008.

5) Effect of the effect of cure, mechanical and swelling characteristics of maleated natural rubber/ clay nanocomposites *Vijayalekshmi V, George K.E, Pavithran C* International Conference on Materials Science Research and Nanotechnology (ICMSRN), Kodikanal, 2008.

6) Barrier properties of Maleated naturalrubber/clay nanocomposites *Vijayalekshmi V, George K.E, Pavithran C,* Polymers-Prospects and Challenges, NIT, Calicut, 2008.

7) Barrier properties of maleated naturalrubber/clay nanocomposites developed through masterbatch technique *Vijayalekshmi V, George K.E, Pavithran C,* APT, Cochi, 2008.